TECHNISCHE UNIVERSITÄT WIEN

Dissertation

Polycyclic aromatic hydrocarbons in different environmentally important matrices

A thesis submitted for the degree of

Doctor of Technical Sciences (Dr. techn.)

at

Technische Universität Wien

Faculty of Technical Chemistry

Institute of Chemical Technologies and Analytics

E164-02-2

under the supervision of

Ao. Univ. Prof. Dr. techn. Anne Kasper-Giebl

defended by

DI Bernadette Kirchsteiger

Mat.Nr.: 01305620

Wien, Oktober 2022

"Science is not a boy's game, it's not a girl's game.
It's everyone's game.
It's about where we are and where we are going."

- Nichelle Nichols

Abstract

Combustion processes have been identified as major contributors to the local air pollution across Europe, negatively impacting climate and human health. Additionally to the emission of particulate matter (PM), incomplete combustion processes emit various (semi-) volatile, toxic substances such as polycyclic aromatic hydrocarbons (PAHs). Benzo(a)pyrene (BaP) is a known carcinogen and used as the common PAH guiding substance. To improve air quality and to protect human health, limit values for PM and BaP were set by the European Union (EU) (i.e. EU limit value of 1 ng/m^3 for the annual BaP concentration in PM samples, and 40 µg/m^3 for the annual PM_{10} concentration), while stricter air quality guidance (AQG) levels are recommended by the World Health Organization (WHO) (i.e. 15 µg/m^3 for the annual PM_{10} concentration). Most analytical procedures are optimized for the quantification of one single PAH, namely BaP. PAHs are, however, widespread and ubiquitous substances, which are always emitted as a complex mixture of different congeners. Therefore, analytical techniques to selectively quantify a large range of PAHs will always need refinement.

This thesis focusses on the quantification of polycyclic aromatic hydrocarbons derived from samples representing different atmospheric matrices, i.e. particulate matter, snow and cloud water. Results presented in this work span the scope from PAH quantification at the emission source itself, i.e. small scale combustion devices, to their contribution in ambient PM and additionally present novel methods for the quantification of PAHs in snow and cloud water samples.

In Austria combustion activities for residential heating have been identified as one of the major contributors to the overall PM and PAH load. The implementation of dedicated reduction strategies relies on up to date emission measurements. PAH emissions using total suspended particle (TSP) samples during operational extreme cases representing real-life operations were investigated, e.g. increased fuel load, decreased air supply, improper ignition method, poor fuel quality to burning waste material. In order to evaluate the impact of the users' habit two types of combustion experiments were performed, one representing the diversity of possible maloperations and another one realized under optimized combustion conditions following a strict optimization protocol. The quantitative determination of 12 PAH congeners was performed according to EN 15549:2008 using a GC-MS setup. Thereby, a clear decrease in PAH emissions (to a maximum of 1% of TSP emissions) and a shift towards low molecular weight PAHs reflected by lower toxicity equivalents could be observed.

Ambient PAH concentrations were quantified from $PM_{2.5}$ samples from an urban sampling station in Graz Don Bosco within a time line covering an episode influenced by high PM burdens in early 2017. These high PM levels were observed across mid-Europe and thus also in Austria. Up to 23 individual PAH congeners were quantified using a modified GC-MS method according to EN 15549:2008. Ambient PAH levels decreased following a seasonal pattern and with proceeding time also a shift in PAH patterns could be observed and additionally, the ratio of PAH/$PM_{2.5}$ changed.

PAH concentrations show a gradient trend in different compartments, with highest contributions found in emission samples followed by a decrease moving from more to less polluted environments like atmospheric samples, snow or cloud water. Shifting the focus from atmospheric

PAH concentrations to the quantification of PAHs in the liquid phase is challenging and requires the development of novel quantification methods.

A method based on SPE extraction and GC-MS/MS analysis was developed to investigate PAH concentrations from surface snow samples derived from different sampling locations across Austria. For that, bi-functional SPE columns were used to extract PAHs from melted snow samples with volumes larger than 1000 mL. The two-layered column furthermore allows the separation of PAHs from structurally similar compounds (e.g. humic like substances) and thus also served as a purification step. Quantification was realized using a dedicated GC-MS/MS method, which allows the simultaneous quantification of up to 37 different PAH congeners including substituted and non-substituted PAHs.

To understand in which extent PAHs are dispersed and transported from one region to another, the focus of PAH contributions was enlarged to cloud water. The combination of low concentration and limited sample volume refused the application of typically used analytical methods for PAH quantification. Thus a novel method based on a multimethod approach using a highly sensitive instrument coupled with high mass selectivity was developed: PAH contributions in cloud water samples were analyzed using thermal desorption - proton transfer reaction - time of flight - mass spectrometry (TD-PTR-ToF-MS). The use of this analytical technique also allowed to investigate the interaction of PAHs with other emerging pollutants like microplastics and nanoplastics. For the first time, measurements of ultrafine microplastics and nanoplastics on the single polymer level in ambient particulate matter ($PM_{2.5}$) were performed for an urban sampling site in Austria. Additionally, possible carrier activities of two polymer types with selected, highly toxic and carcinogenic PAH congeners were identified.

Keywords: air quality • emerging contaminants • environmental analytics • GC-MS/MS • polycyclic aromatic hydrocarbons • toxicity equivalents

Kurzfassung

Verbrennungsprozesse tragen einen wesentlichen Teil zur lokalen Luftverschmutzung bei. Dies hat negative Auswirkungen auf das Klima, die Umwelt und die menschliche Gesundheit. Neben der Emission von Feinstaub (PM) werden bei unvollständigen Verbrennungsprozessen auch verschiedene flüchtige und teilweise kanzerogene Substanzen wie beispielweise polyzyklische aromatische Kohlenwasserstoffe (PAKs) freigesetzt. Benzo(a)pyren (BaP) ist ein nachgewiesenes Kanzerogen und wird daher als gängige PAK Leitsubstanz verwendet. Zur Verbesserung der Luftqualität und zum Schutz der menschlichen Gesundheit wurden daher von der Europäischen Union (EU) Grenzwerte für PM und BaP festgelegt. Seit 2013 gilt EU-weit ein Grenzwert für BaP von 1 ng/m³ (Jahresmittelwert), stellvertretend für die gesamte Gruppe der teilweise hoch kanzerogenen polyzyklischen aromatischen Kohlenwasserstoffe. Der Grenzwert für den Jahresmittelwert der PM_{10} Fraktion liegt EU-weit bei 40 µg/m^3. Die Weltgesundheitsorganisation (WHO) empfiehlt die Einhaltung strengerer Richtwerte (AQG), i.e. 15 µg/m^3 für den Jahresmittelwert der PM_{10} Konzentration. Die meisten analytischen Methoden sind auf die Quantifizierung von BaP optimiert. PAKs sind jedoch ubiquitäre und persistente Stoffe, die stets als komplexe Mischung verschiedener Kongenere emittiert werden. Analytische Methoden zur selektiven Quantifizierung eines breiten Spektrums von PAKs werden daher stets modifiziert und weiterentwickelt.

Diese Dissertation konzentriert sich auf die Entwicklung und Modifizierung analytischer Methoden zur simultanen Quantifizierung von bis zu 37 PAKs aus verschiedenen umweltrelevanten Matrices. Die, in dieser Arbeit präsentierten, Ergebnisse umfassen PAK Konzentrationen direkt an der Emissionsquelle bis hin zu ihren atmosphärischen Konzentrationen. Darüber hinaus werden neu entwickelte Methoden zur simultanen Quantifizierung von PAKs in Schnee- und Wolkenwasserproben vorgestellt.

In Österreich zählen Heizungsanlagen in Privathaushalten zu den Hauptverursachern erhöhter PM und PAK Belastungen. Um dies zu reduzieren sind insbesondere aktuelle Emissionsmessungen, welche das reale Heizverhalten widerspiegeln, von großer Bedeutung. Im Rahmen dieser Dissertation wurden die PAK Emissionen anhand von Gesamtschwebstaubproben (TSP) direkt an der Emissionsquelle untersucht. Um die Auswirkungen der Benutzergewohnheiten zu bewerten, wurden zwei Arten von Verbrennungsexperimenten durchgeführt. Ein Satz von Experimenten beschreibt dabei die Vielfalt möglicher Fehlbedienungen während extremer Betriebszustände (i.e. erhöhte Brennstofflast, verringerte Luftzufuhr, unsachgemäße Anzündmethode, schlechte Brennstoffqualität bis hin zur Verbrennung von Abfall), wobei der Zweite die Emissionen unter optimierten Verbrennungsbedingungen darstellt. Die quantitative Bestimmung von 12 PAK Kongeneren wurde gemäß EN 15549:2008 unter der Verwendung eines GC-MS Systems durchgeführt. Durch die Optimierung der Verbrennungsbedingungen konnte eine deutliche Reduktion der PAK Emissionen (auf einen Maximalgehalt von 1% der TSP Emissionen) und Weiters eine Verschiebung zu höheren Konzentrationen niedermolekularer PAKs beobachtet werden.

Atmosphärische PAK Konzentrationen wurden von Immissionsproben ($PM_{2.5}$) einer städtischen Probenahmestation (Graz Don Bosco) quantifiziert. Ausgangspunkt dieser Probenahme war eine

Episode mit erhöhter PM Belastung zum Jahresbeginn 2017, welche in ganz Mitteleuropa beobachtet werden konnte. Die Erweiterung der standardisierten Methode (EN 15549:2008) ermöglichte die Quantifizierung von bis zu 23 PAKs. Neben der Abnahme der atmosphärischen PAK Konzentrationen, welche einem generellen saisonalen Trend folgt, wurden Unterschiede zwischen Zeiträumen, die durch lokale Emissionen oder auf regionaler Ebene beeinflusst wurden, nachgewiesen. Mit fortschreitender Zeit konnten auch eine Verschiebung der PAK Muster und eine Veränderung des PAK/$PM_{2.5}$ Verhältnisses beobachtet werden.

Die Beiträge von PAKs unterscheiden sich in umweltrelevanten Kompartimenten. Die höchsten Beiträge werden nahe an Emissionsquellen beobachtet, gefolgt von atmosphärischen Proben und geringere PAK Konzentrationen werden in Schnee- und Wolkenwasserproben beobachtet. Die Verlagerung des Fokus von der Bestimmung von PAKs aus atmosphärischen Proben hin zur Quantifizierung von PAKs in der flüssigen Phase stellt eine analytische Herausforderung dar und erfordert die Entwicklung neuer Quantifizierungsmethoden.

Im Rahmen dieser Dissertation, wurde eine Methode, basierend auf dem Prinzip der Festphasenextraktion (SPE) und einer darauffolgenden GC-MS/MS Analyse zur Quantifizierung von PAKs in Oberflächenschneeproben, entwickelt. Zur Extraktion wurden PAK spezifische bifunktionelle SPE Säulen verwendet, welche die Extraktion von PAKs aus Oberflächenschneeproben mit Volumina größer 1000 mL ermöglichten. Die Anwendung der bifunktionelle Säulen ermöglicht zudem die Abtrennung der PAKs von strukturell ähnlichen Verbindungen, wie beispielweise Huminsäure ähnliche Substanzen, und dient somit auch als Aufreinigungsstufe. Die Quantifizierung wurde mit einer eigens dafür entwickelten GC-MS/MS Methode durchgeführt, welche die simultane Quantifizierung einer breiten PAK Palette, einschließlich substituierter und nicht-substituierter PAKs, ermöglicht.

Um die Verteilung von PAKs in unterschiedlichen Kompartimenten zu untersuchen wurde der Schwerpunkt der PAK Beiträge auf die Bestimmung dieser in Wolkenwasser ausgeweitet. Die Kombination aus niedriger Konzentration und die Limitierung des verfügbaren Probenvolumens verhinderte jedoch die Anwendung gängiger analytischer Methoden. Daher wurde eine Methode basierend auf einem Multimethodenansatzes erarbeitet: PAK Beiträge in Wolkenwasser proben wurden mit Hilfe eines TD-PTR-ToF-MS Instrumentes analysiert. Die Verwendung der TD-PTR-ToF-MS Methode ermöglichte zudem die Untersuchung der Wechselwirkung von PAKs mit anderen wichtigen Umweltschadstoffen, wie Mikro- und Nanoplastik. Im Rahmen dieser Arbeit werden zum ersten Mal atmosphärische Konzentrationen einzelner Polymertypen präsentiert und die Interaktion dieser mit 23 verschiedeneren PAKs, gewonnen aus urbanen $PM_{2.5}$ Proben, untersucht, um so etwaige Transportaktivitäten der Polymere feststellen zu können. Aus den Ergebnissen wird deutlich, dass nicht jeder quantifizierte Polymertyp als Vehikel für den atmosphärischen PAK Transport fungiert.

Schlagworte: Luftqualität • Umweltschadstoffe • Umweltanalytik • GC-MS/MS • polyzyklische Kohlenwasserstoffe • Toxizitätsequivalente

Acknowledgements

Ever since I was a kid, I am impressed by how things are built up by the assembly of particles, cells or molecules. This fascination also may have been the catalytic force, why I decided to move to Vienna for school at the age of 14. During the last years I have gained so much more than a profound knowledge in environmental or analytical chemistry and method development, this journey also promoted my personal growth. Especially the last 4ish years have been the most challenging of my life so far. As *'anybody achieves anything alone'* the following words are devoted to those people who supported me endlessly.

Firstly, I would like to thank my supervisor Anne Kasper-Giebl for giving me the opportunity to work in your research group and for the scientific and personal guidance. Thanks, for supporting me with all your knowledge and patience and for providing me the environment that allowed me to experience many different perspectives of working in a scientific community including the opportunity to attend international conferences and summer schools.

I would also like to thank Erwin Rosenberg and Rupert Holzinger, for not only taking the time to read my thesis and being part in my examination committee, but also for all the valuable scientific discussions we had and for answering all my questions.

Furthermore I wanted to thank all collaboration partners. Thanks to…

…all colleagues from *BEST - Bioenergy Sustainable Technologies GmbH*. Especially to Manuel, Rita and Franziska. It was a pleasure to work on different research projects.

…all colleagues from *BOKU Wien*, especially to Harald, Christian and Christoph. It was a pleasure to be part of this interdisciplinary team.

…all colleagues from the *IMAU* research group at *Utrecht University*. It was an amazing time at home away from home. Special thanks to Rupert, Dušan and Hanne for the warm welcome and support during the entire last year.

Big thanks to all people from BB03 and 02. Especially to all *aerosoul* members, you made long lab days so much more enjoyable. Thanks to all my former and present colleagues in the *aerosoul* group, for all the support I received and valuable discussions we had. Special thanks to Daniela, Michaela and Hong for proof reading parts of this thesis.

A rather simple thank you is not enough for the support I received and the friendship which evolved from that. Thank you, Bettina, Jakob and Stephan for all those coffee talks, beers, boat trips and good times. Special thanks to Bettina, for your scientific and emotional support throughout the last months!

After almost 10 years at university with lastly 4ish years working on my PhD, I reached the end of my journey at TU Wien. It was a journey full of amazing moments, full of ups and downs and one of steady growth. I am sure, I would not have been able to keep on going without the support of a loving circle of friends. Special hugs to my forever friends Raffaela, Mario, Astrid, Katharina, Sabine, Johannes– and many more.

Ein ganz besonderes Danke gilt meiner Familie:

…allen voran meinen Eltern Astrid und Werner. Ihr habt mich mit jenen Eigenschaften ausgestattet, die mich (fast) täglich an meine Grenzen bringen, mir aber auch immer wieder den Mut und die Neugier verleihen diese zu überschreiten. Ich wünschte jede/r hätte das Glück in so einem Zuhause aufwachsen zu können – frei von Geschlechterstereotypen und mit viel Platz zum Träumen.

…meinem ganz persönlichen Trio Infernale – Lukas, Oliver und David – ihr seid die besten Geschenke, die ich niemals missen möchte!

…Theresa, für den emotionalen und graphischen Support, ganz egal in welchem Sektor.

…meinen Großeltern, Erni und Karl, mitunter fürs versorgen mit den weltbesten Kipferln und viel Kaffee, aber eigentlich für noch ganz viel mehr.

…und auch meinem Opa Anton, der mir gezeigt hat, wie flexibel die eigenen Grenzen sind.

…to Lisa and David. Thank you for always believing in me and making me the proudest auntie on earth – this is a true honor!

Isolation, spending most of my time in the lab and being a ruthless perfectionist did not only take a lot of me. Getting to know each other during chaotic times like these makes a special kind of understanding indispensable. Thank you Erik for the emotional support, all your love and patience and for keeping the earth below my feet – you made this time so special to me!

Lastly, I wanted to thank all the people, I met throughout this journey. Meeting people from all over the world, understanding different cultures, perspectives and passions, enriched my life and for sure made me a better human being.

Content

Abbreviations

WHO	World Health Organization
EU	European Union
US EPA	United States Environmental Protecting Agency
SDG	Sustainable Development Goals
IARC	International Agency for Research on Cancer
PM	Particulate matter (general term)
PM_{10}	Particulate matter having particle size 10 micrometers or smaller
$PM_{2.5}$	Particulate matter having particle size 2.5 micrometers or smaller
POPs	Persistent organic pollutants
PAH	Polycyclic aromatic hydrocarbons
NO_x	Oxides of nitrogen
SO_2	Sulfur dioxide
NH_3	ammonia
VOCs	Volatile organic compounds
ppb	parts per billion
ppt	parts per trillion
ecdf	Empirical cumulative distribution function
LD	Lockdown
Pre-LD	Pre lockdown
WLK C733	European Cooperation in Science and Technology Action 733 weather classification scheme
p-PAHs	Parent PAHs
N-PAHs	Nitro-PAHs
O-PAHs	Oxy-PAHs
OH-PAHs	Hydroxy-PAHs
LMW PAHs	low molecular weight PAHs
HMW PAHs	High molecular weight PAHs
CYP450	microsomal cytochrome systems P450
BaP_{eq}	BaP equivalent
TEF	toxic equivalency factor
GC	Gas chromatography
MS	Mass spectrometry
GLC	Gas-liquid-chromatography
GSC	Gas-solid-chromatography
EI	Electron ionization
CI	Chemical ionization
PTR	Proton transfer reaction
ToF	Time of flight
TD	Thermal desorption
SD	Source drift region
DT	Drift tube

H_3O^+	Hydronium ions (primary ions)
E/N	Reduced electric field
E	Electric field strength
N	Gas number density
RP	Repeller plate
EG	Extractor grid
oa-ToF-MS	Orthogonal acceleration ToF-MS
MCP	Microchannel plate
ppbV	Part per billion by volume
m/z	Mass over charge ratio
DCM	Dichloromethane
cHex	Cyclohexane
i-prop	Iso-propanol
IST	Internal standard
RST	Recovery standard
HVS	High volume sampler
PUF foam	Polyurethane foam
SPE	Solid phase extraction
LLE	Liquid-liquid-extraction
HULIS	Humic like substances
LPE system	Low pressure evaporation system
EF	Emission factor
OC	Organic carbon
OM	Organic matter (OC converted by applying a conversion factor of 1.5)
EC	Elemental carbon
HPAE-PAD	High-performance anion-exchange chromatography with pulsed amperometric detection
SNR	Signal to noise ratio
MRM	Multiple reaction monitoring
UFMNP	Ultra-fine microplastics and nanoplastics
MP	Microplastics
NP	Nanoplastics
PET	Polyethylene terephthalate
PP	Polypropylene
PE	Polyethylene
asl	above sea level

Symbols

K_p	gas-particle partitioning coefficient
c_{ig}	Concentrations of compound *i* in the gaseous phase
c_{ip}	Concentrations of compound *i* in the particulate phase
c_m	mass concentration of particulate matter
T	Ambient temperature
N_s	surface concentration of sorption sites
A_m	specific surface area of PM
Q_l	enthalpy of desorption from a surface
Q_v	Enthalpy of vaporization of the super-cooled liquid
p_L^0	vapor pressure of the super-cooled liquid
K_{OA}	octanol-air partitioning coefficient
f_{OM}	mass fraction of organic matter
ρ_{oct}	density of octanol
MW_{oct}	mean molecular weight of octanol
MW_{OM}	mean molecular weight of organic matter
γ_{oct}	activity coefficient of the absorbing component in octanol
γ_{OM}	activity coefficient of the absorbing component on organic matter
f_{BC}	mass fraction of black carbon
ρ_{BC}	density of black carbon
$A_{atm\text{-}BC}$	for absorption available surfaces of atmospheric black carbon
a_{soot}	for absorption available surfaces of diesel soot
$K_{soot\text{-}air}$	partitioning coefficient between diesel soot and air
K	Equilibrium constant
$c_{i,s}$	molar concentrations of the analyte *i* in the stationary phase *s*
$c_{i,m}$	molar concentrations of the analyte *i* in the mobile phase *m*
α	selectivity factor
K_B	partitioning ratio of the stronger retained analyte *B*
K_A	partitioning ratio of the faster eluted analyte *A*
t_{TOF}	Time of flight
l	Length of the flight path
e	Elementary charge (= 1.6022 * 10^{-19} C)
V	Potential between repeller plate and extactor grid
t_{int}	Time of mass spectra integration (=10 min)
$F_{zero\ air}$	Flow of zero air used to transfer molecules into PTR system (= 100 mL/min)
V_M	molar volume (= 22.4 L/mol)
$MH^+/(ABCD)H^+$	protonated molecular ion

Introduction

Clean air is a human right (United Nations General Assembly 2019). Still most of the global population is exposed to hazardous air pollutants negatively impacting human health and climate. The World Health Organization (WHO) named ambient air pollution as *the single largest environmental health risk in Europe* (WHO 2021), causing a wide range of diseases including inflammation, respiratory and cardiovascular diseases. The attempt of the European Union to reduce the carbon footprint along with pollutants from burning fossil fuels and replacing them with biomass must be implemented thoughtfully: Emissions from residential wood combustion have been identified as a major contributor to the local air pollution in Europe (Cincinelli et al. 2019) and thus also in Austria (Caseiro et al. 2009). Particulate matter (PM) is also generated upon burning biomass and comprises particles in air in the size range larger than 10 µm to the sub-nanometer range. PM is listed as one of the key components for the estimation of air pollution levels. The United Nations targets the reduction of PM in their Sustainable Development Goals (SDGs) defined by the United Nations to achieve a better and more sustainable future for the whole globe by 2030 (WHO 2022). Besides particulate emissions, wood combustion is responsible for the emission of a variety of toxic and carcinogenic substances, amongst others polycyclic aromatic hydrocarbons (PAHs). PAHs are persistent and widespread compounds and comprise a group of several hundred congeners including unsubstituted and substituted congeners (IARC 2010), which are emitted as by-products during incomplete combustion processes (e.g. Bjørseth 1983, Patel et al. 2020, Manzetti 2013) and the combustion of biomass always results in the emission of PAHs. As PAHs are ubiquitous, they are found in all environmental compartments ranging from urban to remote and even pristine areas such as the Arctica and Antarctica (Xie et al. 2022).

To understand the accumulation of PAHs in different compartments, it is necessary to expand the effort of PAH quantification and perceive different matrices as interacting and agile. PAHs are usually present in very small amounts (ppb to ppt – parts per billion to parts per trillion) and in

complex matrices (as it is the case for every environmental compartment) specific and accurate analytical techniques are still evolving:

In the framework of this thesis different analytical methods and procedures were developed allowing to quantify PAHs from different environmentally important matrices. Generally, PAH concentrations show a gradient trend in different matrices, with highest contributions found close to the emission source and lower ones expected in particulate matter, snow or cloud water. Applying the modified and developed procedures provide tools to tackle the description of the 'PAH cycle' presented in this wok: from the emission source, ambient contributions and contributions in snow and cloud water samples far from the emitter.

Chapter 1 introduces the basics of ambient air quality, including the legislative situation in the European Union and the situation in Austria. As ambient air quality is not solely determined by local emissions, this chapter further highlights the importance of meteorological factors and the effect of abrupt changes of emissions, as experienced during the COVID-19 pandemic. In addition, it introduces the special role of polycyclic aromatic hydrocarbons spanning the scope from their sources and formation to atmospheric reactivity and mechanism of toxicity. In **Chapter 2** the fundamentals for gas chromatographic separation, mass selective detection and proton transfer reaction - time of flight - mass spectrometry are summarized. The experimental details for the dedicated quantification methods and the PAHs of interested, as well as the modified and developed sample preparation techniques are given in **Chapter 3**. Within **Chapter 4**, the quantification of PAHs derived from particulate matter samples is presented. The first subchapter 4.1. presents the results obtained during a field measurement campaign including real-life emission factors for 12 different PAH congeners and the toxic risk assessment. The second subchapter 4.2. presents PAH concentrations retrieved from ambient PM samples of an urban sampling station in Graz, Austria. This study aimed to investigate differences among two subgroups of PM based on a macro-tracer source apportionment and the toxic risk assessment of ambient PAH concentrations. **Chapter 5** presents the interaction and relationships of PAHs with newly emerging pollutants, i.e. ultrafine microplastics and nanoplastics. The first subchapter highlights the emerging situation of microplastics and nanoplastics in the environment and discusses the sorption ability of PAHs to different polymer types amplifying their combined environmental threat. The following subchapters present the quantification of polymers and PAHs down to the single polymer/PAH congener level. We identified significantly high Spearman rank correlations among two polymer types and 7 highly toxic and carcinogenic PAH congeners indicating possible carrier activities. To understand in which extend PAHs are dispersed and transported from one region to another, we enlarged the common focus of PAH contributions to other vehicles for atmospheric transport, which is discussed in **Chapter 6 and 7**. In general, lower PAH contributions are expected in snow and cloud water samples, they, however, significantly differ in the available sample volume. **Chapter 6** presents an in-house developed quantification method and the obstacles we had to face during method development. Within this chapter we present a novel method for the quantification of up to 37 different PAH congeners, including substituted and unsubstituted ones. Snow sample preparation is realized using a bi-functional solid-phase extraction followed by a highly sensitive quantification method (down to the sub-ppb level). Cloud water samples present a different picture as the combination of low sample volume and analyte concentration prevents the use of standard analytical methods for PAH quantification. **Chapter 7** presents the development a novel method based on thermal desorption- proton transfer

reaction – time of flight - mass spectrometry (TD-PTR-ToF-MS) to tackle the demand in analysis of cloud water samples. The first subchapter gives insights in the development of a qualification and quantification method for PAHs, while this method was then applied to cloud water samples derived from the remote sampling station at Sonnblick Observatory.

This thesis written as a monograph to extend already published scientific articles (see Appendix A), and thereby explains the challenges faced during method development and discusses the obtained results in a broader perspective, e.g. additional information about source apportionment, toxic risk assessment or the interaction with other chemical compounds.

Chapter 1 Fundamentals of ambient air quality and polycyclic aromatic hydrocarbons

Polycyclic aromatic hydrocarbons (PAHs) are ubiquitous compounds, generated by incomplete combustion processes and often adsorbed on particulate matter. The following chapter summarizes a broad spectrum covering air quality aspects and the role of PAHs and is therefore divided into two main subjects: **Section 1.1.** addresses the fundamentals of ambient air pollution with special focus on the situation in Europe and Austria. It further highlights the role of biomass combustion as a major contributor to ambient air pollution. **Section 1.2.** introduces the compounds of interests and gives an overview of the physical and chemical properties of PAHs, their sampling methods and aspects about the impact on human health as well as toxicology and risk assessment.

1.1. Ambient air pollution and the role of particulate matter

Anthropogenic air pollution states one of the greatest environmental risks in modern times, with multiple facets related to economic, political and social concerns (e.g. Manisalidis et al. 2020, WHO 2020, Tomlin 2021). Air pollution and climate change are highly related and it is well known that anthropogenic activities significantly contribute to the emission of various pollutants. Besides that, air pollution also influences various environmental compartments like soil or water bodies (Manisalidis et al. 2020). Among gaseous compounds, i.e. CO, O_3, NO_2, SO_2, the particulate matter (PM) fractions PM_{10} and $PM_{2.5}$ have been listed as *`major health-damaging air pollutants'* by the World Health organization (WHO) (WHO 2021).

Particulate matter is one of the key components for the estimation of air pollution levels explicitly mentioned as one target of the Sustainable Development Goals (SDGs) defined by the United Nations to achieve a better and more sustainable future for the whole globe by 2030 (WHO 2022). Ambient PM is a complex mixture of solid particles and liquid droplets, varying in chemical

composition, shape and size (EPA 2019). The term PM refers to all particles suspended in the atmosphere, encompassing multiple size fractions. While the amount of total suspended particles is referred to as TSP, the terms of PM_{10} and $PM_{2.5}$ comprise subsets, i.e. all particles with a nominal mean aerodynamic diameter smaller or equal to 10 µm or 2.5 µm, respectively. The chemically and physically diverse properties of PM may be partly attributed to different formation processes, i.e. particles are either emitted directly by the emission source (primary PM) or formed during atmospheric reactions involving precursor gases such as NO_x, SO_2, NH_3 and VOCs (secondary PM). Due to standardized and widely implemented sampling procedures, but also because of their known negative health effects, PM_{10} and $PM_{2.5}$ are the most studied size fractions of PM. PM_{10} includes a notable amount of particles emitted directly, while $PM_{2.5}$ particles are mainly formed via secondary formation mechanisms (EPA 2019). Both size fractions, i.e. PM_{10} and $PM_{2.5}$, characterize the overall PM load, and epidemiological and toxicological studies link the exposure of elevated PM concentrations to mortality, respiratory and cardiovascular diseases and even cancer (e.g. Salvi and Holgate 1999, WHO 2013, Guarnieri and Balmes 2014, Pandolfi et al. 2014, EEA 2019, 2020). The effects on human health are strongly related to the deposition and retention of those particles in the human lung and consequently depending on their aerodynamic properties (i.e. size, shape and density), physico-chemical properties (i.e. surface area and water solubility) and chemical composition (Salvi and Holgate 1999, Bolling et al. 2009). TSP and PM_{10} fractions are mainly deposited in the head and upper respiratory tract (i.e. large conducting airways), whereas $PM_{2.5}$ particles penetrate deeper leading to depositions throughout the respiratory tract, particularly in the smaller airways (Guarnieri and Balmes 2014). While even smaller subsets of particles, i.e. PM_1 (nominal mean aerodynamic diameter smaller or equal to 1 µm) and ultrafine particles (UFP, nominal mean aerodynamic diameter <0.1 µm) reach the alveoli (Guarnieri and Balmes 2014).

1.1.1. Air quality standards and limit values in Europe and the situation in Austria

In order to improve air quality and to protect human health, limit values were implemented by both, the European Union and WHO. The European Ambient Air Quality Directive 2008/50/CE sets annual limit values for PM_{10} and $PM_{2.5}$, i.e. 40 µg/m^3 and 20 µg/m^3 respectively (EC 2008). Even lower annual air quality guidance (AQG) levels are recommended by the World Health Organization (WHO 2021), i.e. 15 µg/m^3 for PM_{10} and 5 µg/m^3 for $PM_{2.5}$. In 2018, ten EU member states reported PM_{10} concentrations violating the EU annual limit value (EEA 2020). The $PM_{2.5}$ concentration is monitored at 1438 stations within 33 European countries (EEA 2020). In 2018, six European member states reported violations of the annual $PM_{2.5}$ limit value, primarily occurring in urban or suburban areas (EEA 2020).

A similar situation can be observed at Austrian air quality monitoring sites. In Austria, limit values for certain air pollutions are set within the national legislation, i.e. Immissionsschutzgesetz – Luft (IG-L). This legal document permits an annual maximum of 25 days of exceedance of the daily limit value of 50 g/m^3 for PM_{10}. Since 2004 a decreasing trend of PM_{10} concentration could be observed in Austria (Spangl and Nagl 2019), however, some hotspots are still flawed with enhanced PM burdens. According to the IG-L no violation of the European annual limit value for PM_{10} was reported at any of the Austrian monitoring sites in 2020 (Spangl and Nagl 2021). The daily limit value however, was exceeded on 17 out of 25 days at maximum within the same time

period in 2020 (Spangl and Nagl 2021). The highest annual average PM_{10} concentration (24 µg/m^3) was observed at one monitoring site in the city of Graz, i.e. Graz Don Bosco (Spangl and Nagl 2021). The same holds true for $PM_{2.5}$, whereas, according to the permissions set within the IG-L, no violation of the European annual limit value was registered at any Austrian monitoring site in 2020. The highest annual $PM_{2.5}$ concentration was also observed at monitoring stations in the city of Graz, i.e. Don Bosco (16.5 µg/m^3) and Graz Süd (15.8 µg/m^3) (Spangl and Nagl 2021). Due to the fact that the city of Graz repeatedly registers violations of the daily and annual limit values, it is a known hotspot for air quality monitoring. Because of its special orographic situation, located in a basin in the mountainous region, the region of Graz is prone to temperature inversions allowing air pollutants to accumulate. In January and February 2017 high pollution of PM occurred in mid-Europe (EEA 2019), which markedly influenced PM concentrations in Graz as well. During January to March 2017 the EU short time limit value for the PM_{10} concentration (50 µg/m^3 as daily mean) was exceeded several times in Graz, with peak abundances exceeding 100 µg/m^3. During the time period of 02.01. – 31.03.2017, 34 days with a PM_{10} concentration exceeding 50 µg/m^3 and thus violating the EU short time PM_{10} limit value were observed. In total 54 days violating the EU short time PM_{10} limit value occurred during that short time period, which showed a marked change to the general decreasing trend of annually occurring days of exceedances (Amt der Steiermärkischen Landesregierung 2018). Findings presented in Kirchsteiger et al. (2020) indicate, that local inversion was not the dominant driver of the elevated PM pollution period in 2017 (Kirchsteiger et al. 2020). In fact widespread increases in PM abundance have been reported on larger scale due to enhanced European pollution backgrounds (EEA 2019), which can be traced back to long-range transport of pollutants. Besides that, also naturally occurring events such as dust outbreaks, as it occurred later in 2017 and also in 2020 lead to elevated PM burdens (Spangl and Nagl 2021).

1.1.2. The importance of meteorological factors and the effect of abrupt changes of emissions to the local PM burden

It is well known that ambient meteorological conditions strongly modulate PM burdens and determine particulate accumulation and decay (e.g. De Hartog et al. 2005, Barmpadimos et al. 2011, Pandolfi et al. 2014, Ailish et al. 2020, Glojek et al. 2022). At given emission scenarios high PM levels coincide with one or multiple of the following meteorological variables: stagnant weather conditions, calm winds and limited ventilation, cold ambient temperatures leading to a shallow boundary layer and temperature inversions inhibiting vertical mixing. These enumerated only demonstrate the variety of meteorological key variables to ambient PM concentrations and highlight the importance of comparing time periods with consistent meteorological parameters. If emissions of PM are considered, primary and secondary sources have to be taken into account. This makes the evaluation of abrupt changes in emissions even more complex as secondary formation in the atmosphere needs not be related to local emissions. One of those abrupt changes in emissions happened in spring 2020, with the outbreak of the SARS-CoV-2 pandemic. PM concentrations were effected during the respective COVID-19 lockdown periods in many European cities, caused by the drastic decline in anthropogenic emissions i.e. traffic and industry (EEA 2020). Briz-Redón et al. (2021) reported a decrease of PM_{10} concentrations during lockdown period at three cities in Spain, i.e. Barcelona, Sevilla and Valencia (Briz-Redon, Belenguer-

Sapina, and Serrano-Aroca 2021). In Barcelona, this decrease of PM_{10} concentrations could be observed at both, traffic influenced and background stations (Toscano and Murena 2020). Also other European regions, like the Po Valley, which is a densely populated and highly industrialized area in Northern Italy, reported decreasing PM_{10} concentrations during lockdown periods (Toscano and Murena 2020). Although, PM concentrations change related to abrupt changes in emissions associated to industrial activities and mobility, those changes seem to be highly inconsistent and quite variable as different station types experience different source contributions (Ropkins and Tate 2021).

In Austria, the first nationwide lockdown occurred during the time period of 16.03. – 14.04.2020 and strongly affected emissions associated to transport and industrial activities (Anderl et al. 2021). The reduction of traffic emissions lead to a reduction of NO_x ($NO_X = NO + NO_2$) (Staehle et al. 2022). Besides its importance as an air pollutant, NO_x is known to be a precursor of PM emission which consequently affected the PM burdens as well, but resulting changes were expected to be much smaller than those observed directly for NO_x (for more detailed information see Stähle et al. (2022) (Staehle et al. 2022)). In Austria, residential heating is the major contributor to the Austrian PM_{10} burdens (Spangl and Nagl 2021), and thus PM_{10} was expected to be less influenced by these abrupt changes in precursor pollutants, compared to the NO_x emissions. To evaluate even small changes attributed to lockdown restrictions, it is necessary to disentangle PM concentrations from its various influencing factors. For that, a dedicated meteorological filtering approach has been presented by Stähle et al. (2022) (Staehle et al. 2022). This method discriminates pollution levels from the impact of emission changes by applying the following: (1) geographical grouping of regions with similar climatological characteristics in order to consider different orographic situations, (2) definition of weather categories in order to compare time periods impacted by similar meteorological parameters (i.e. conditions favoring high pollution concentrations are preferred, as they show higher local influence), (3) comparison of an equal number of sampling days between the lockdown and pre-lockdown period and (4) comparison of changes observed within the lockdown period with those observed within a defined reference period, to consider the already declining trend of PM and precursor emissions. Specific details regarding the meteorological key variables used for filtering are given in Stähle et al. (2022) (Staehle et al. 2022).

Applying the meteorological filtering method to PM_{10} and $PM_{2.5}$ concentrations observed at the urban sampling site Graz Don Bosco and to PM concentrations observed at the respective background station pointed to changes in PM concentrations. As expected, changes were less pronounced than those observed for NO_x emissions in the respective region (Staehle et al. 2022). In Austria, only a small fraction of PM_{10} emission can be attributed to traffic related sources (on average 16% of total PM_{10} concentration (Anderl et al. 2021), however, the reduced road emissions also affected PM concentrations. Changes in PM concentrations were evaluated on the basis of empirical cumulative distribution functions (ecdf) for the corresponding lockdown (LD) and pre-lockdown (pre-LD) periods. This allows the investigation of relative changes in emission considering many sampling locations situated in the same climatological region and corresponding to the meteorological filtering. **Figure 1** presents the empirical cumulative distribution functions (ecdf) for the corresponding lockdown (LD) and pre-lockdown (pre-LD) periods for PM concentrations observed at urban sites situated in the south of Austria and the respective background stations. Results for the already mentioned hot spot location (Graz Don Bosco,

hereinafter referred to as GDB) are highlighted by dark blue lines while the respective concentrations observed at the background station (Bockberg, hereinafter referred to as BB) are highlighted by a grey line. Relative changes of emissions regarding all sampling locations in the south of Austria (blue shadings) varied in a narrower sense during lockdown period compared to the same time periods of previous years (grey shading). Also distributions during lockdown periods become steeper than those compared to the same time period of previous years. This is caused by the lack of peak PM concentrations during the LD period. Besides that, PM concentrations observed at GDB seem to become more similar to the ones observed at the respective background station BB during the LD period. The extend of harmonization of PM_{10} data based on the evaluation of percentiles is presented by Stähle et al. (2022) (Staehle et al. 2022). $PM_{2.5}$ concentrations seem to be affected to a lower extent by the partial curfews policies, which may be caused by the much lower number of sampling sites investigated (n=3) than those for PM_{10} (n=28).

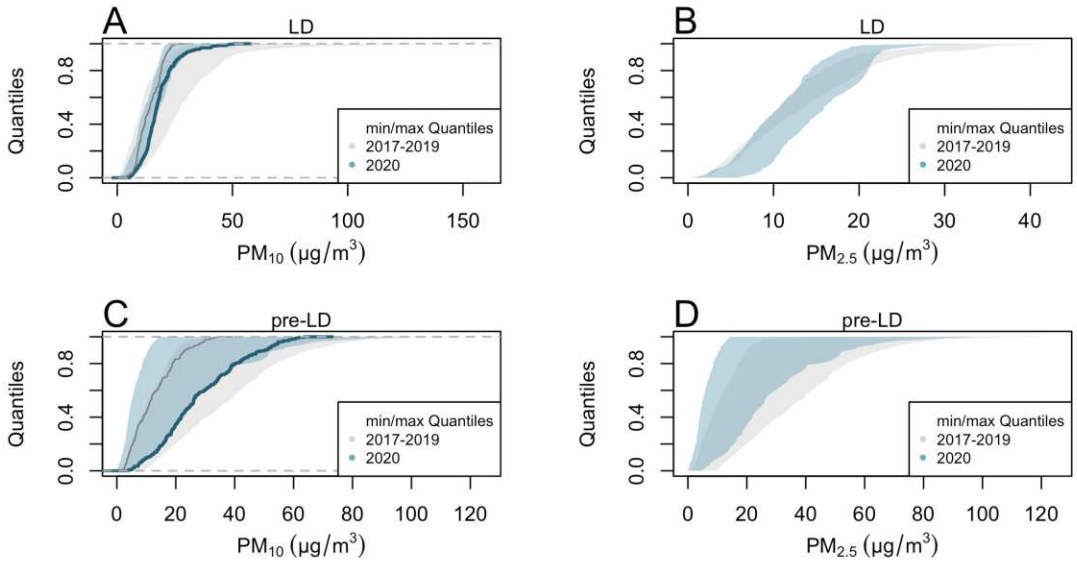

Figure 1 A-D. Empirical cumulative distribution functions (ecdf) based on half-hourly data for the corresponding lockdown period (LD, sampled days within 16.03. – 10.04.) and pre-lockdown period (pre-LD, sampled days within 15.01. – 29.02.) for PM_{10} (**A** and **C**, respectively) and $PM_{2.5}$ (**B** and **D**, respectively). Colored shadings (grey: previous years 2017- 2019, and blue: 2020) indicate the range of individual quantiles (max/min) of 28 selected stations (PM_{10}) and three selected stations ($PM_{2.5}$), all stations are situated in the south of Austria. The dark blue line provides the ecdf distribution of the PM concentration observed at the sampling station Graz Don Bosco (GDB), while thin grey line provides the ecdf distributions of the respective PM concentration observed at the background station Bockberg (BB). Note, that for GDB and BB only PM_{10} data were available. The situation of $PM_{2.5}$ is given by the remaining sampling stations situated in the same region.

1.1.3. PM sources and the role of biomass combustion on ambient air quality

PM is a complex mixture and the ambient PM concentration at one specific location depends on the proximity to the emission sources, emission and dispersion conditions and topography of the surrounding. The interaction of local emissions and transport of PM from more distant sources is of special importance (Lenschow et al. 2001, Puxbaum et al. 2004). To reduce ambient air pollution it is necessary to understand the emitter-receptor relationship and to have detailed knowledge about individual source intensities. The European Union annually reports emission

sources of regulated pollutants according to the emission sectors compiled in NFR (nomenclature for reporting) categories. Over the period of 1990 to 2019 PM emission showed a decreasing trend in Austria (Anderl et al. 2021). In 2019, the NFR sector *1.A Fuel combustion activities* has been identified as the most significant contributor to the TSP, PM_{10} and $PM_{2.5}$ emissions ins Austria, accounting for 44%, 52% and 83%, respectively (Anderl et al. 2021). Within this sector largest contributions can be attributed to the *NFR category 1.A.4b* which compiles emissions from small combustion processes, residential heating, household ovens and stoves. Other fuel related contributors to the PM burdens compiled in the NFR sector 1.A refer to: (i) transportation activities (*NFR 1.A.3*), (ii) energy industry (*NFR 1.A.1*) and (iii) the manufacturing industries and construction (*NFR 1.A.2*) (Anderl et al. 2021). The contributions of the compiled *NFR sector 1.A* are given in **Figure 2** highlighted in dark blue.

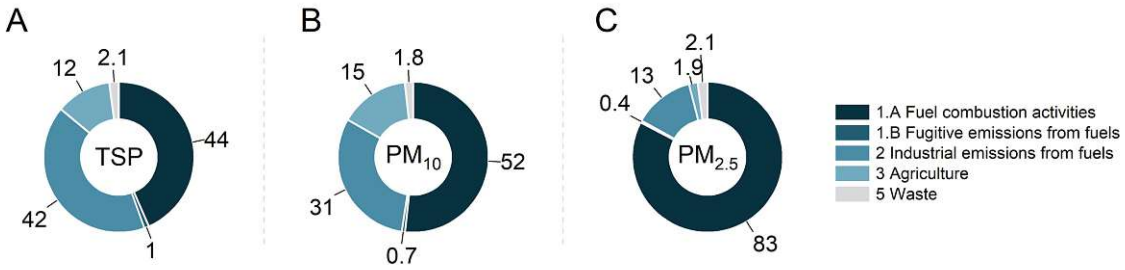

Figure 2 A-C. Share of NFR sectors (%) to particulate emissions in 2019 in Austria. (Data compiled from Anderl et al. (2021) (Anderl et al. 2021)).

Besides PM, combustion activities, such as residential heating emit a variety of toxic and carcinogenic compounds including polycyclic aromatic hydrocarbons (PAHs) (e.g. Ozgen et al. 2014, Sturmlechner et al. 2019, Zhang et al. 2021). Previous studies reported that emissions are strongly influenced by the following: (i) design of appliances, (ii) type of fuel, and (iii) the combustion conditions (e.g. Gonçalves et al. 2011, Pettersson et al. 2011, Orasche et al. 2012, Ozgen et al. 2014, Sturmlechner et al. 2019). In case of PAH emissions the sector comprising fuel combustion activities (NRF category 1.A) has been identified as the most dominant emission source in Austria, accounting for 96% of the total PAH emissions in 2019 (Anderl et al. 2021). Emissions of TSP and particle-bound PAHs representing the real-life situation in Austrian homes has been conducted within a field measurement campaign realized in the scope of the *Clean Air by biomass* project. Up to date emission factors are discussed in further detail within the resulting publication (Kirchsteiger et al. 2021), and are also compiled and presented within Chapter 4.

1.1.4. Air quality guidelines in case of PAHs

Airborne PAHs have been investigated for a couple of decades now. To protect human health, several monitoring programs were installed to monitor PAH emissions and their respective ambient concentrations. The first internationally binding document was the Convention on Long-range Transboundary Air Pollution (1979) which was later on extended resulting in the Aarhus Protocol on Persistent Organic Pollutants (POPs) in 2003. This protocol has been adapted several

times with the newest version entering into force by 2022 (UNECE 2022). The Aarhus protocol focusses on a list of 16 substances, comprising pesticides, industrial chemicals and by-products/contaminants which are regulated within the Regulation (EC) 850/2004 by the European Union (European Union 2004b). It lists also four PAH congeners (i.e. benzo(a)pyrene, benzo(b)fluoranthene, benzo(k)fluoranthene and indeno(1,2,3-cd)pyrene) and states the basis for establishing emission inventories from stationary sources. Emission inventories relying on emission factors are necessary to profoundly evaluate the influence of specific sources on air quality. Emission factors can be either derived by lab-testing of appliances aiming to represent close to real-life conditions (e.g. Gonçalves et al. 2011, Kistler 2012, Ozgen et al. 2014) or obtained from field measurements (e.g. Spitzer et al. 1998, Sturmlechner et al. 2019). Emissions and the respective emission factors further affect the implementation of mitigation strategies to evaluate the impact on ambient air. Legal documents for the monitoring of ambient air quality do not only include limit values for PM_{10} or $PM_{2.5}$ (or other air pollutants), also a limit value for the benzo(a)pyrene (BaP) concentration has been implemented by the European Union. As BaP is the most studied compound among PAH congeners, it is also listed as a marker substance in Air Quality Standards from many European countries. Thus, an annual limit value for BaP of 1 ng/m^3 in PM_{10} samples was set by the European Union (Directive 2004/107/EC (European Union 2004a)), which is assumed to Austrian law within the Immissionschutzgesetz – Luft (IG-L). However, as rising evidence about the carcinogenic and toxic properties of more PAH congeners is published, the working group on ambient air pollution of the European Union stated a position paper, enlarging the focus and suggesting the analysis of more PAH congeners (European Union 2001). This position paper lists following additional PAHs to monitor: fluoranthene, benzo(b)fluoranthene, benzo(k)fluoranthene, benzo(j)fluoranthene, benzo(a)anthracene, indeno(1,2,3-c,d)pyrene and dibenzo(a,h)anthracene. The US EPA further enlarged the palette of PAHs of interest and presented a list also known as the 16 US EPA priority PAHs. All quantification methods, which were modified or developed within this thesis focus on a broader palette of PAH congeners, including all PAHs listed by the EU and US EPA.

1.1.5. Review of PAH concentrations reported across Europe

The European air quality monitoring mainly focusses on the PAH marker compound BaP. Some European countries still struggle to attain the annual limit value for BaP (1 ng/m^3) set by the European Union. In 2018, fourteen member states reported annual BaP concentrations exceeding 1 ng/m^3, whilst highest concentrations were observed in the Eastern and Central part of Europe (EEA 2020). Apparently, elevated BaP concentrations were mainly reported at urban and suburban locations across Europe (EEA 2020). An excerpt of BaP concentrations observed across Europe as given in **Table 1**.

Table 1. Atmospheric PAH concentrations observed at different European sites. PAH levels refer to the average concentration observed while values given in brackets refer to (min-max) values observed at the respective measurement site. Values highlighted with * refer to the median concentration observed.

Reference	Country/region	City	Date	PM fraction	# PAHs (x)	$\sum_x$PAH (ng/m^3)	BaP (ng/m^3)
(Khan et al. 2018)	Italy (Veneto region)	Belluno	2012-2013 one year measurement	$PM_{2.5}$	8	19.6 ± 19.0 (0.4 – 66.2)	3.4
		Conegliano	2012-2013 one year measurement	$PM_{2.5}$	8	13.3 ± 14.9 (0.3 – 49.1)	2.2
		Vicenza	2012-2013 one year measurement	$PM_{2.5}$	8	8.6 ± 9.8 (0.3 – 41.5)	1.4
		Benezia-Mestre	2012-2013 one year measurement	$PM_{2.5}$	8	9.6 ± 11.3 (0.3 – 41.5)	1.8
		Padua	2012-2013 one year measurement	$PM_{2.5}$	8	11.1 ± 13.4 (0.4 – 70.4)	1.9
		Rovigo	2012-2013 one year measurement	$PM_{2.5}$	8	7.0 ± 7.7 (0.2 – 37.6)	1.1
(Pietrogrande et al. 2022)	Italy (Po Valley)	Bologna	Feb-Mar 2020	$PM_{2.5}$	15	5.03 ± 2.30 (2.25 – 10.14)	0.58 ± 0.11
(Zioła and Słaby 2020)	Poland (Krakow Country)	Skawina	Feb – Dec 2019	$PM_{2.5}$	16	60.14 ± 67.17 (9.00 – 237.91)	4.26 ± 4.36 (1.00 – 16.80)
(Tomaz et al. 2016)	France	Grenoble	Jan 2013 – Jan 2014	$PM_{2.5}$	21	4.96 (0.28 – 36.23)	0.42 (0.01 – 3.54)
(Oleagoitia et al. 2018)	Spain (Basque Country)	Urretxu	Oct 2011 – Oct 2012	$PM_{2.5}$	11	0.73* (0.55 - 8.56)	0.05* (Max:1.11)
		Azpeitia	Oct 2011 – Oct 2012	$PM_{2.5}$	11	0.90* (0.55 - 9.15)	0.05* (Max: 1.12)

1.2. Polycyclic aromatic hydrocarbons

1.2.1. Sources and formation routes of PAHs

PAHs are organic pollutants generated as by-products during incomplete combustion derived from petrogenic or pyrogenic processes (e.g. Bjørseth 1983, Manzetti 2013, Patel et al. 2020). Thus, PAHs are introduced into the environment by various sources including natural processes, i.e. forest fires and volcanic eruptions, or anthropogenic sources, i.e. oil- and drilling processes and traffic exhaust (petrogenic PAHs) or by combustion of organic material (pyrogenic PAHs) (Manzetti 2013). However, anthropogenic sources are more dominant than their natural counterparts, and the most significant contributions can be attributed to residential wood combustion, traffic related and industrial activities (e.g. Lima, Farrington, and Reddy 2005, Manzetti 2013, Abbas et al. 2018, Patel et al. 2020).

In general, the formation of PAHs is favored under suboptimal combustion conditions, e.g. insufficient air supply and temperature, improper ignition and poor fuel quality. During the combustion process itself, organic molecules are fragmented into smaller unstable subunits, i.e. cleavage of C-C and C-H bonds resulting in the formation of free radicals (e.g. Lima, Farrington, and Reddy 2005, Ravindra, Sokhi, and Vangrieken 2008, Abbas et al. 2018). These radicals combine under the formation of acetylene which further reacts via rapid radical mechanisms or Diels-Alder condensations to the primal aromatic ring (Ravindra, Sokhi, and Vangrieken 2008, Reizer, Viskolcz, and Fiser 2022). The high stability of six-membered ring systems and re-establishment of aromaticity drives the formation of polyaromatic ring structures by further reactions of the primal aromatic ring involving smaller molecules, i.e. reactive molecules with two or three carbons such as acetylene (Abbas et al. 2018). The formation of those polyaromatic structures is intertwined with the formation of soot particles by functioning as molecular precursors (Reizer, Viskolcz, and Fiser 2022).

To date, several hundred PAH congeners have been identified in individual source tests, showing that PAHs are always emitted as complex mixtures of various structural isomers and derivates, e.g. oxy- and nitro-PAHs (e.g. Ravindra, Sokhi, and Vangrieken 2008, Manzetti 2013, Keyte, Harrison, and Lammel 2013, Abbas et al. 2018). Specific PAHs have been identified as indicators for a certain emission source and are therefore used as tracer substances for source apportionment. However it has to be noted that most sources show similar PAH signatures resulting in intrasource variability but intersource similarity (Galarneau 2008), which is the reason why ratios between individual PAHs used for source apportionment (i.e. diagnostic ratios) are widely discussed and must be interpreted carefully (Tobiszewski and Namiesnik 2012).

1.2.2. Molecular structure, topography and physico-chemical properties of PAHs

The group of PAHs sums up compounds with two or more fused aromatic rings. PAHs solely containing carbon and hydrogen are also known as parent-PAHs (p-PAHs), while alkylated or substituted, e.g. nitro-, oxy- and hydroxy-analogue, are also present in the environment (Sparling 2016, Abbas et al. 2018, Zhang et al. 2021). In all cases, the molecular arrangements of the fused ring system can either be linear (i.e. rings are located on a straight line), angular (i.e. rings are

located on different straight lines, angle =120°) or cluster arrangements (Bjørseth 1983, Gupte et al. 2016). **Figure 3** highlights the possible molecular arrangements of PAHs.

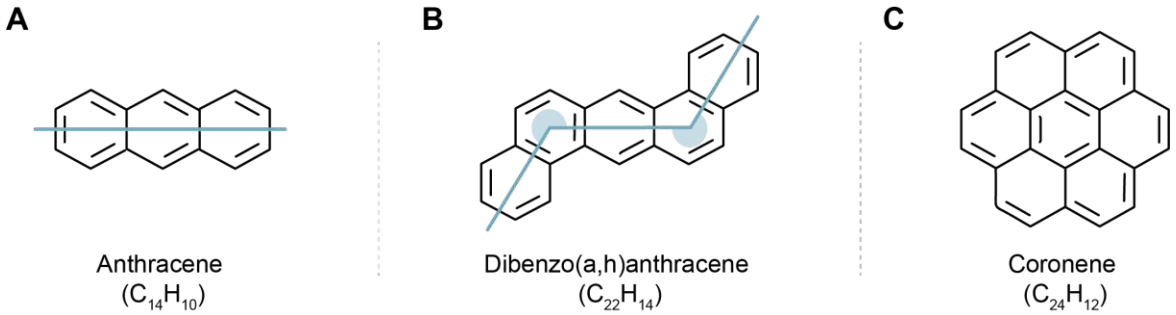

Figure 3 A-C. Molecular arrangements of **(A)** linear, **(B)** angular and **(C)** cluster PAHs. The blue line and areas highlight the arrangement of fused aromatic rings with the embedded angle.

Many physical and chemical properties of PAHs depend on their size (i.e. mean number of carbon centers) and the topology of the ring system (i.e. type of ring linkage) (Bjørseth 1983, Gupte et al. 2016, Patel et al. 2020). Based on their ring structure, PAHs are grouped in alternant PAHs (i.e. all rings are six-membered) and non-alternant PAHs (i.e. additionally including ring systems with less than six carbon atoms) (Bjørseth 1983, Patel et al. 2020, Reizer, Viskolcz, and Fiser 2022). However, the most common classification of PAHs refers to the size of their ring system (i.e. number of conjugated aromatic rings) and thus the molecular weight. Low-molecular weight PAHs (LMW PAHs) sum up compounds with two or three aromatic rings, while the class of high-molecular weight PAHs (HMW PAHs) includes PAHs with four or more aromatic rings (Patel et al. 2020). HMW PAHs are in general more stable PAHs having higher melting points. With increasing molecular weight and size, the PAHs water solubility and volatility decreases, resulting in changes of their gas-particle partitioning.

1.2.3. Gas-particle partitioning of PAHs

Another complexity when studying PAHs arises due to their different volatilities. While individual congeners are either found in the gas or the particle phase, some of them may be present in both phases, i.e. gaseous and particulate phase and consequently they get distributed between the gas, particle and droplet phase (Keyte, Harrison, and Lammel 2013). Hence, understanding the partitioning of PAHs in either of the phases is of special concern because additionally to different reaction mechanism it effects, among others, compound toxicity (e.g. dose-response relationships are linked to the physical form of the compound during exposure), deposition of gases and particles and consequently the choice and behavior of source tracers (Pankow et al. 1994). Furthermore, it determines the sampling methods needed for a proper characterization of the single compound. The phase distribution of PAHs is in general described by the compound- and temperature dependent *gas-particle partitioning coefficient* K_p *(*$m^3/\mu g$*)* (see **Eq. 1**) The phase partitioning of compound *i* is given by the gas-particle partitioning coefficient K_p defined as the compounds concentration in the gaseous (c_{ig}) and particulate phase (c_{ip}) and the mass concentration of particulate matter (c_m).

$$K_p = \frac{c_{ip}}{(c_{ig} * c_m)}$$

Eq. 1. Compound and temperature dependent gas-particle partitioning coefficient *Kp* ($m^3/\mu g$). Equation according to Keyte et al. (2013) (Keyte, Harrison, and Lammel 2013)

It has to be noted, that K_p is temperature dependent (i.e. K_p increases with T) and operationally defined and is thus occasionally biased by sampling artefacts (Pankow et al. 1994). However, the distribution of PAHs between the gas and particle phase underlies two different mechanisms, i.e. (i) adsorption on the particle surface or (ii) absorption into organic matter (Keyte, Harrison, and Lammel 2013). Considering the various kinds of interaction possible between the different phases, it is expected that a combination of adsorption and absorption processes takes place (Pankow 1994).

In case of adsorption being the dominating process, the gas-particle partitioning coefficient K_p can be expressed using **Eq. 2**. The adsorption process is influenced by the ambient temperature T, the surface concentration of sorption sites N_s, the specific surface area of PM A_m and the enthalpies of desorption from a surface (Q_1) and vaporization of the super-cooled liquid (Q_v) and indirectly influenced by p_L^0, the vapor pressure of the super-cooled liquid.

(i) K_p in case of adsorption

$$K_p = \frac{N_s * A_m * T * e^{\frac{(Q_1 - Q_v)}{RT}}}{16 * p_L^0}$$

Eq. 2. K_p in case of adsorption being the dominant process. Equation according to Keyte et al (2013) (Keyte, Harrison, and Lammel 2013)

Due to the lipophilic character of PAHs the absorption to the carbon rich fraction of PM, organic matter (OM) and black carbon (BC) or elemental carbon (EC) is more likely (Lohmann and Lammel 2004). Lohmann and Lammel (2004) postulate that absorption to the active surface sites of BC are likely to happen first, while absorption to OM becomes slowly important if the surface sites of BC are already occupied (Lohmann and Lammel 2004). If absorption processes to the surface of both, OM and BC, are assumed to be the dominant processes K_p is defined by **Eq. 3.** This process of absorption to the surface of OM described by the octanol-air partitioning coefficient K_{OA}, the mass fraction of organic matter f_{OM}, the density of octanol (ρ_{oct}), the mean molecular weights of octanol (MW_{oct}) and organic matter (MW_{OM}) and the activity coefficients of the absorbing component in octanol (γ_{oct}) and organic matter (γ_{OM}). While the counterpart of absorption to the surface of BC involves the mass fraction of black carbon (f_{BC}), the density of BC (ρ_{BC}), the for absorption available surfaces of atmospheric BC and diesel soot ($a_{atm\text{-}BC}$ and a_{soot}, respectively) and the partitioning coefficient between diesel soot and air $K_{soot\text{-}air}$.

(ii) K_p in case of absorption to OM and BC

$$K_p = 10^{12}\left(f_{OM}\frac{MW_{oct} * \gamma_{oct}}{(\rho_{oct} * MW_{OM} * \gamma_{OM})}K_{OA} + f_{BC}\frac{a_{atm-BC}}{a_{soot} * \rho_{BC}}K_{soot-air}\right)$$

Eq. 3. K_p in case of absorption being the dominant process. Equation according to Keyte et al. (2013) (Keyte, Harrison, and Lammel 2013)

Besides that, other newly emerging pollutants such as micro- and nanoplastics show similarities in terms of hydrophobicity and lipophilicity leading to a sorption of PAHs. The relationship and interaction of both co-occurring pollutant classes, i.e. PAHs and different polymers, is introduced and discussed in Chapter 5.

1.2.4. Atmospheric reactivity, removal processes and environmental fate of PAHs

It is well known that compound specific parameters highly influence their distribution and chemical reactivity within the environment. PAHs with high aromatic character are preferably found in the particulate phase and known to be chemically stable (Keyte, Harrison, and Lammel 2013). An increase in molecular size coming along with a larger condensed ring system however, leads to a higher tendency of light absorption which consequently enhances photo reactivity. PAHs found in the particulate phase are mainly involved in heterogeneous reactions, while gaseous PAHs are more susceptible for homogeneous transformation reactions (Keyte, Harrison, and Lammel 2013). Besides compound specific properties, the half-lives of PAHs depend on the prevailing atmospheric conditions (e.g. concentration of trace gases, solar radiation, humidity and temperature) and the nature of the sorbent of which PAHs are adsorbed to (Kamens et al. 1988, Matsuzawa, Nasser-Ali, and Garrigues 2001). The magnitude of influences of the sorbents on the photo reactivity of PAHs has been recently reported, by showing that the adsorption of PAHs to diesel exhaust particles had an stabilizing effect suppressing their degradation (Matsuzawa, Nasser-Ali, and Garrigues 2001).

Considering the atmospheric reactivity of PAHs, the main sink of gaseous PAHs are gas phase reactions preferentially occurring with the OH radical or the NO_3 radical (Abbas et al. 2018). PAHs associated with PM have a more complex environmental fate. As already mentioned, they mainly undergo heterogeneous reactions either leading to their removal from the atmosphere or to their substitution yielding more toxic analogues (e.g. Manzetti 2013, Keyte, Harrison, and Lammel 2013). Heterogeneous reactions are very complex multiphase reactions influenced by a rich palette of factors, e.g. the prevailing meteorological condition, the reactivity and concentration of the atmospheric oxidant, physico-chemical properties of the PAH molecule itself, and the type of sorbent (Keyte, Harrison, and Lammel 2013). The heterogenous reaction of p-PAHs with OH radicals is known to be the most dominant pathway of degradation resulting in the hydroxylated derivates (OH-PAHs) (Keyte, Harrison, and Lammel 2013). Nitro-PAHs (N-PAHs) are generated by the reaction of their parent counterparts with atmospheric traces of NO_x or HNO_3 (Keyte, Harrison, and Lammel 2013). This reaction mechanism also yields peroxy radicals, which may

have further impact on various tropospheric reactions. The reaction of p-PAHs with O_3 catalyzed by UVA radiation results in another substituted analogue group known as oxygenated PAHs (oxy-PAHs, O-PAHs) (Abbas et al. 2018).

The environmental fate of parent-PAHs is controlled by various factors including physical and chemical properties, interactions with other pollutants as well as deposition or transport processes. Once PAHs are emitted into the atmosphere, they may be transported over long distances even to remote or pristine areas and deposited via the two common pathways of dry or wet deposition. Particle-bound PAHs are mainly deposited by precipitation or dry deposition (Ravindra, Sokhi, and Vangrieken 2008). The direct fall out of particle-bound PAHs is strongly depending on the particle size but also on meteorological parameters such as wind speed and humidity. The removal process of wet deposition mainly refers to gaseous PAHs, by sorption to particles or the dissolution within cloud water or rain droplets and the subsequent deposition in form of rain or snow (e.g. Lei and Wania 2004, Lima, Farrington, and Reddy 2005, Ravindra, Sokhi, and Vangrieken 2008). The scavenging efficiency of rain or snow depends on compound specific characteristics, characteristics of the snow and the atmospheric temperature leading to a different scavenging behavior among compartments: (i) at temperatures around the freezing point, rain is the more efficient scavenger of vapors of small organics as the surface of liquid water droplets available for sorption is bigger than the respective one of snow and (ii) there is a difference between the scavenging of gaseous and particulate compounds, i.e. snow ice crystals have proven to be more efficient of scavenging of vapors of larger, non-polar and water insoluble compounds (Lei and Wania 2004). Scavenged compounds may be subsequently deposited via different pathways. In high altitudes the form of precipitation depends on the unique features of the respective ecosystem, especially temperatures markedly below 0°C result in preferred precipitation in form of snow, rime, graupel or hail (Wania et al. 1998). The gas and particle scavenging processes of organic molecules found in snow packs tend to transpire in four different forms: (1) organics bind to the ice surface, (2) organics are adsorbed to particles, (3) vapor contains organics and (4) organics dissolve in the liquid phase (Wania et al. 1998). Many organic compounds and amongst them also PAHs showed higher total scavenging ratios in snow rather than rain, i.e. PAHs tend to accumulate or enrich in snow (Lei and Wania 2004).

1.2.5. Mechanism of PAH toxicity

Besides their persistency and their ability of bioaccumulation and atmospheric transformation to even more toxic substances some PAHs show mutagenic and carcinogenic potential. This especially affects O-PAHs and N-PAHs, but also many p-PAHs. After entering the human body via inhalation, ingestion or dermal absorption PAHs may reach the human blood stream by binding to lipoproteins. There PAHs may undergo different phases of metabolism (i.e. *phase 1: activation* by introduction of a polar reactive group followed by *phase 2: detoxification* by binding to an endogenous substituent to increase water solubility) (Ewa and Danuta 2017). The general goal of these metabolic pathways is to detoxify an exogenous compound in order to secrete it. However, sometimes the detoxification process leads to the formation of much more reactive and toxic intermediates which holds true for some PAHs. In order to understand the molecular basis of PAH carcinogenicity, compound-specific features like electronic density and structural confirmation play a crucial role (Ewa and Danuta 2017). Some PAH congeners possess a so-called ‘bay’ or

'fjord' region (see **Figure 4** A), which is known to be the important reactive site taking part in the metabolic transformation and a useful predictor for possible PAH carcinogenicity. BaP is used as a common PAH marker substance and a known procarcinogen, metabolized by different pathways, i.e. radical cation pathway, o-quinone pathway or diol-epoxide pathway (Sparling 2016). One metabolic route involves the microsomal cytochrome systems P450 (CYP450) which forms chemically active intermediates by inducing oxidations in the bay or fjord region of the p-PAH involving the CYP1A1/CYP1B1 enzymes (see **Figure 4** B) (Sparling 2016). The consequently formed PAH epoxides may enter the nucleus and further bind to the DNA, and in case of BaP binding preferentially occurs to the nucleic bases guanin or adenine (Larsen and Larsen 1998, Sparling 2016, Ewa and Danuta 2017). In most cases, this pre-mutation change is recognized and repaired, but in some cases the formation of the PAH-DNA-adduct initiates a point mutation which may induce carcinogenesis.

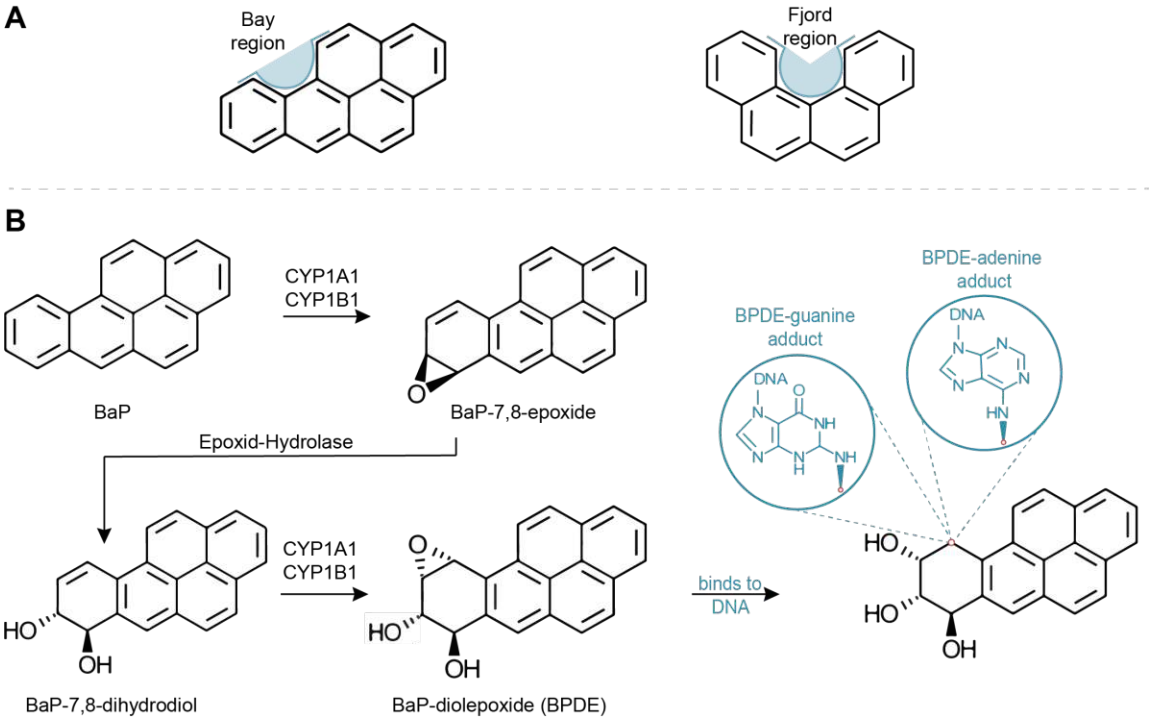

Figure 4 A-B. (A) The bay und fjord regions of PAH, i.e. BaP und Benzo[c]phenanthrene, highlighting the important areas for metabolic activation. **(B)** The PAH epoxide pathway, i.e. oxidation and hydrolysis of BaP involving the CYP450 system (i.e. CYP1A1 and CYP1B1 enzymes) to a form that facilitates the binding to DNA.

1.2.6. Toxicity assessment of the exposure to PAH mixtures

PAHs are always emitted as complex mixture of several congeners and literature reports several methods of toxicity estimations and the most common one refers to the BaP equivalent (BaP_{eq}) method, which is also used within this work. This method aims to estimate the overall toxicity of emitted PAHs and is the method of choice recommended within the Provisional Guidance for Quantitative Risk Assessment of Polycyclic Aromatic Hydrocarbons by the EPA (EPA/600/R-93/089). To assess the overall toxicity, concentrations of individual PAH congeners are multiplied with the respective toxic equivalent factors (TEFs). TEF values are factors commonly used to

describe the carcinogenic potencies of individual PAHs relatively to the toxicity of BaP. BaP is a widely studied compound and proven carcinogen, also listed as one of the most toxic PAHs among the 16 US EPA priority PAHs, yielding a TEF value of 1. All TEF values were evaluated relatively to the toxic potency of BaP. Within this thesis TEF values obtained from Larsen and Larsen were applied to assess the carcinogenic properties of the PAH mixture (Larsen and Larsen 1998). The respective TEF values used are summarized in **Table 2**. In special cases, four congeners, benzo(a)anthracene and chrysene as well as benzo(b)fluoranthene and benzo(k)fluoranthene, were quantified as sum. To avoid underestimation of toxicity regarding those four congeners concentrations were multiplied using the higher TEF.

Table 2. Toxic equivalency factors proposed by Larsen and Larsen (1998) which were used in this study. Note, that TEF values are not available for every PAH congener studied within this work.

Analyte	Abbreviation used in this work	TEF acc. to Larsen and Larsen (1998)
Fluorene	Fluo	0.0005
Phenanthrene	Phen	0.0005
Anthracene	Anthr	0.0005
Fluoranthene	Fla	0.05
Pyrene	Pyr	0.001
Benzo(a)anthracene	BaA	0.005
Chrysene	Chry	0.005
Benzo(b)fluoranthene	BbF	0.1
Benzo(k)fluoranthene	BkF	0.05
Benzo(j)fluoranthene	BjF	0.05
Benzo(ghi)fluoranthene	BghiFla	0.01
Benzo(e)pyrene	BeP	0.002
Benzo(a)pyrene	BaP	1
Indeno(1,2,3-c,d)pyrene	IcdP	0.1
Benzo(ghi)perylene	BghiP	0.02
Dibenzo(a,h)anthracene	DBahA	1.1
Coronene	Cor	0.01
Dibenzo(a,e)pyrene	DBaeP	0.2
Dibenzo(a,h)pyrene	DBahP	1
Dibenzo(a,i)pyrene	DBaiP	0.1
Dibenzo(a,l)pyrene	DBalP	1
Anthanthrene	Anthan	0.3

Chapter 2 Methodological Background

The use of modern instrumental analytics makes it possible to gain detailed knowledge of chemical composition of diverse matrices. Environmental analytics deals with various matrices, which show different characteristics and also varying pollution levels. This highlights the need of different analytical techniques, offering and combining high selectivity and sensitivity. The work presented in this thesis is based on several analytical methods and protocols, which are being introduced in the following chapter. **Section 2.1.** summarizes the basics of gas chromatography briefly discussing the basics of gas liquid chromatography and the principles of the underlying separation. **Section 2.2.** introduces the principles of mass selective detection based on electron ionization and quadrupole mass filters. Changes in matrix and varying samples volumes are analytically challenging and require the application of a highly sensitive method. Therefore, principles of proton transfer reaction – time of flight – mass spectrometry are discussed in **section 2.3**.

2.1. Basic principles of gas chromatography

To date, gas chromatography (GC) is the most important and commonly used analytical separation technique for the determination of low molecular weight compounds. The combination of GC with mass spectrometry (MS) provides quantitative information of complex mixtures in multi-component analysis. This introductory section gives only an overview of the two coupling techniques, i.e. GC-MS and GC-MS/MS, used within this thesis. **Section 2.1.1.** summarizes the basics gas chromatographic separation and the major parts of a respective setup, while **section 2.1.2.** deals with the basic principle of a chromatographic separation using a gas liquid chromatography setup.

2.1.1. Gas-liquid chromatography

Generally, the gas chromatographic separation is based on the interaction of an analyte with the stationary phase, i.e. separation column. For that, the beforehand vaporized sample containing a complex mixture of analytes is introduced into the column via an inert mobile phase, which is only necessary for transporting the analytes through the system. The interaction of an analyte with the column results in a different rate of transport of the compounds and thus separation of analytes. In general, two gas-chromatographic techniques are prominent in literature, namely (i) gas-solid chromatography (GSC) and (ii) gas-liquid chromatography (GLC). As all analyses presented in this work refer to measurements realized with GLC systems (hereinafter referred to as GC system/setup), this is the only technique discussed in more detail within this thesis.

Gas-liquid chromatography is one of the standard systems used in environmental labs. A commercially available GC system consists of the following basic, but most important components:

(i) **Injection system:** In most cases a liquid sample is introduced in a heated injector block using an automated micro syringe system (i.e. commonly known as autosampler). Based on the injector type chosen (e.g. split/splitless injector, programmable temperature vaporizer etc.) and micro syringes, sample sizes vary from a few microliter to smaller volumes of 1 µl or even smaller. Working with liquid samples poses two challenges, i.e. the liquid sample has to be abruptly vaporized to avoid analyte discrimination and analytes have to sustain vaporization, which means, no decomposition is allowed to happen. Decomposition may be prevented by prior derivatization, i.e. silylation or alkylation (Hübschmann 2015).

(ii) **Carrier gas/mobile phase:** The vaporized sample is transported into the column system by a chemically inert and dry mobile phase. Depending on the analytical problem to solve, different mobile phases may be used, e.g. H_2, He, N_2, Ar, CO_2. The mass transfer between phases the two phases (i.e. the mobile and stationary phase) depends upon the interaction time with the stationary phase and thus also on the flow of the mobile phase. Commonly used flows range between 1-25 mL/min (Hübschmann 2015).

(iii) **Stationary phase** installed in a temperature controlled **GC oven:** In order to ensure a time and cost efficient separation of analytes, separation is usually achieved by applying a temperature gradient which is controlled by the GC oven itself. The GC oven contains the respective pre- and separation column (in some cases also post-column). The pre-column is usually only a small part (up to 1 m) of deactivated fused silica (FS) column, which prevents the separation column from damage and does not contribute to analyte separation. The stationary phase, commonly known as separation column, however, is often referred to as the heart piece of a GLC system, necessary for the retention of analytes. GLC separation columns consist of an immobilized liquid stationary phase, e.g. polymers, fluorocarbons, liquid crystals and depending on the analytes of interest, coatings differ in polarity, volatility and temperature stability. In special cases, often depending on the detector or instrument coupling method used, a post-column with smaller inner diameter than the separation column is installed. This post-column however, does

not interact with the already separated analytes and consequently does not act as a second separation step. Post-column installations are often used in coupling setups to mass spectrometers acting as restriction capillaries to keep the pressure drop in a certain range.

(iv) **Detector/coupling device:** The development of GC systems permits a rich palette of detectors and coupling methods. Besides, the standard detectors, e.g. flame ionization detector or thermal conductivity detector, complex coupling systems enable even more sensitive ways of analysis. The coupling of GC with a mass selective detector is described in the following **section 2.2.**

2.1.2. Basic principles of the chromatographic separation using a GLC system

In GLC the separation of analytes is due the partitioning between the gaseous mobile phase and the liquid stationary phase (e.g. polymers, hydrocarbons, liquid crystals), which is immobilized on the surface polymer coating of the separation column. As already discussed, some setups may include pre- and post-column installations, fulfilling different tasks but not involved in the retention process. Generally, the retention of an analyte is based on the equilibrium of its distribution between the stationary and mobile phase, which is described by the partitioning coefficient K (see **Eq. 4**). The equilibrium constant K is defined by the molar concentrations of the analyte i in the stationary phase ($c_{i,s}$) and mobile phase ($c_{i,m}$) (Skoog and Leary 1992).

$$K = \frac{c_{i,s}}{c_{i,m}}$$

Eq. 4. Partitioning coefficient of the analyte I between the stationary phase s and mobile phase m.

Elution of analytes starts whenever a single portion of the sample is introduced to the head of the separation column and evolves by a constant flow of the mobile phase. As the chemically inert mobile phase is only necessary in terms of analyte transport, a complex mixture of analytes is separated by the different strength of interaction and distribution of compounds within the separation column. The time one specific compound interacts with the stationary phase is called retention time (t_R), which is temperature depended and defined by the chemical properties of the analyte and stationary phase (Skoog and Leary 1992). In a certain chromatographic setup, two compounds ideally show different migration rates and are thus separated from each other. Compounds with a higher partitioning coefficient K will be more strongly retained in the stationary phase, consequently it will take more time to pass on to the detector. This separation is explained by the columns specific selectivity factor α, which is defined by partition ratios (according to **Eq. 5**) of substances A and B, respectively. K_B refers to the partition ratio of the stronger retained analyte B, while K_A refers to the partition ratio of the faster eluted analyte A (Skoog and Leary 1992).

$$\alpha = \frac{K_B}{K_A}$$

Eq. 5. Selectivity factor α of a certain column for two analytes A and B

2.2. Basic principles of mass selective detection

Mass selective detection is based on the separation of compounds differing in their mass over charge ratio (*m/z*), and to allow that, compounds have to be ionized aforehand. To date, many different mass selective detectors and ion sources are commercially available. This section solely focuses on the combination of electron ionization with quadrupole mass spectrometers, as these are the techniques used in combination with the gas chromatographic separation in this thesis.

2.2.1. Electron ionization

Election ionization (EI) is a standard ionization techniques installed in most GC-MS systems. **Figure 5** A presents a schematic figure of an electron ionization source. Analyte molecules present in the GC effluent enter the ionization chamber and the outer shell electrons of the analyte interact with the stream of high-energy electrons thermally emitted by filaments (Skoog and Leary 1992). Commercially available instruments use an ionization energy of 70eV, where the de Broglie wavelength matches the length of a typical bond in an organic molecule (≈ 14 nm) (Hübschmann 2015). It has to be noted, that in most cases the necessary energy for ionization of organic molecules is lower than the applied one of 70eV, but kept constant for reasons of comparability of mass spectra. **Figure 5** B visualizes the increase in ion current in dependence of the ionization energy applied. First ions can be observed when ionization potential (IP; highlighted as yellow flash) is reached. After reaching the appearance potential (red eye) in the threshold region (1) the generation of molecular ions starts. The ion signal continues to increase (i.e. built up region (2)) until it reaches an energy plateau (3) which is commonly used for routine operation because of the stable formation of fragment ions. Generally, EI leads to strong ionization and further fragmentation, which is due to a maximizing effect by resonance. Initial ionization is achieved by the loss of an electron resulting in the formation of a molecular ion $ABCD^{\bullet+}$ (see **Figure 5** C). *ABCD* represents an analyte molecule, while $ABCD^{\bullet+}$ its *molecular ion*, which is a radical ion with the same molecular weight as the molecule itself (Hübschmann 2015). Fragmentation however, depends not only on the amount of excess energy, but also on the internal stabilization of the molecule itself. After interaction with the electron beam, molecules are left in highly excited states (i.e. vibrational and rotational) and subsequent relaxation usually leads to extensive fragmentation by various mechanism (**Figure 5** C). Fragment ions differ in m/z from the molecular ion and are called *daughter ions*.

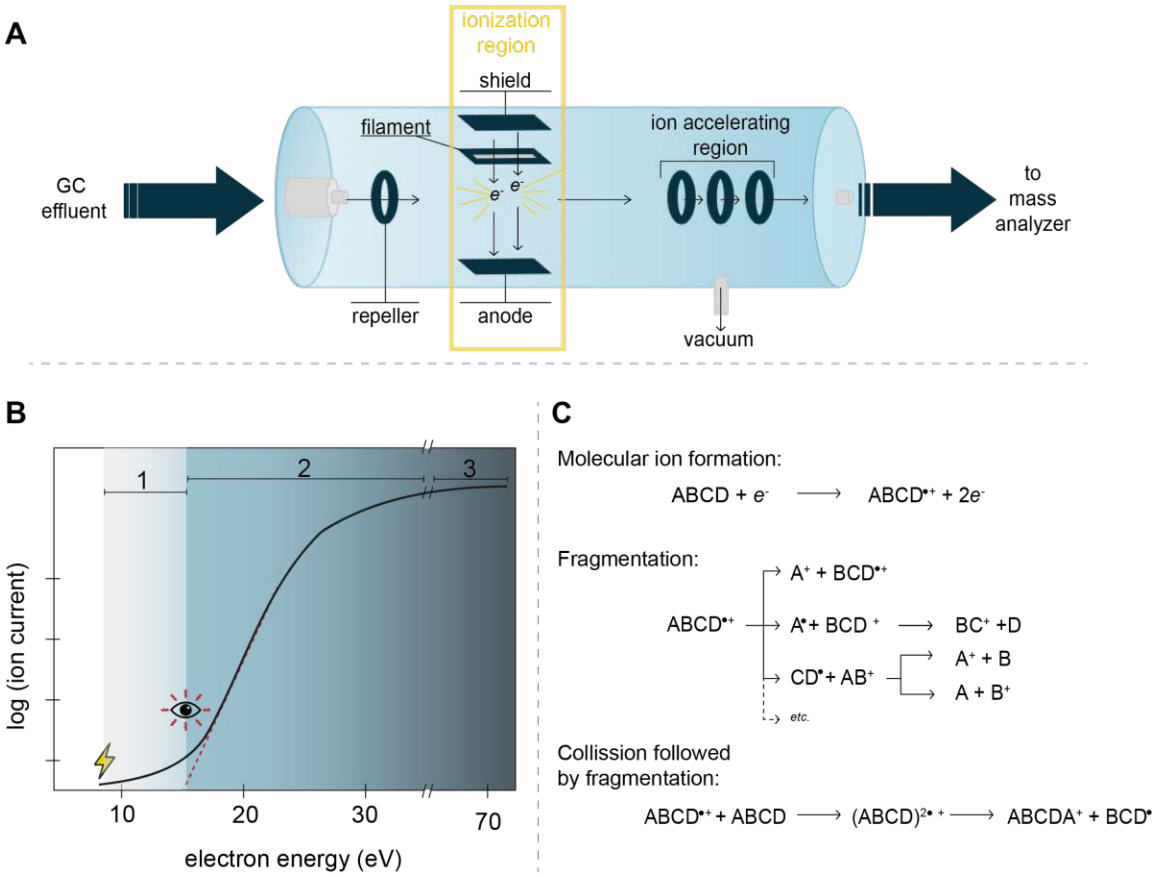

Figure 5 A-C. (A) Schematic figure of an electron ionization (EI) source. **(B)** Relationship between ion current and electron energy assuming a constant flow of substance into the source (on the basis of (Hübschmann 2015)). The yellow flash visualizes the ionization potential, the red dashed line marks the appearance potential, while highlighted regions mark different reaction conditions, i.e. (1) threshold region, (2) built-up region and (3) region of routine operations. **(C)** Exemplified list of typical reaction in an electron ionization source (according to (Skoog and Leary 1992)).

2.2.2. Quadrupole mass filter

Quadrupole mass filters are compact and price efficient instruments and the most common mass analyzer used so far. The heart piece of this mass analyzer are its four parallel hyperbolic metal rods arranged around a central axis inside a vacuum chamber, which serve as electrodes. **Figure 6** A presents a schematic figure of a linear quadrupole mass analyzer. Ion transmission is achieved by applying a direct current (DC) and high frequency alternating current (AC) to the quadrupole rods, with each pair having the opposite polarity (Skoog and Leary 1992). Due to the resulting oscillating electric field only one specific m/z ratio has a stable path of motion (i.e. does not respond to the fluctuating field) and successfully passes on to the detector. **Figure 6** B visualizes the stability regions of three different ions, i.e. $m_1<m_2<m_3$. Ions passing the quadrupole filter need to sustain stable motions in both, the x and y-axis, i.e. motion has to be in the stability region (Douglas 2009). However, it was shown, that there is more than one stability region and most quadrupole mass filters are operated in the first one, which is mainly due to the lower voltages applied. Depending on the voltages applied, different m/z ratios have different stability regions on a single axis. By simultaneously increasing the voltages of DC and AC (i.e. scanning with a quadrupole) various stability regions are passed, which allows the resolution of different masses

(Douglas 2009). All other ions not matching this specific m/z ratio do not move stable and collide with the rods and are therefore not passed on to the detector at this certain time.

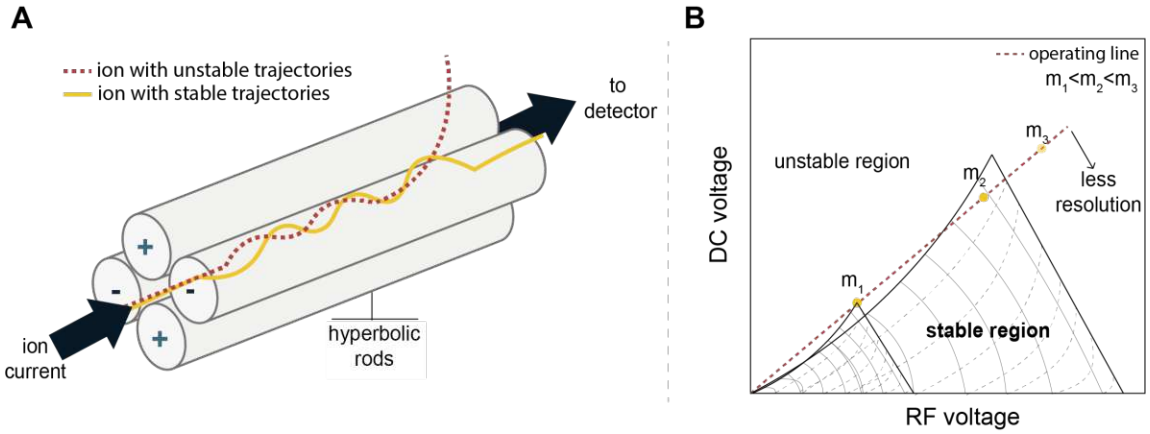

Figure 6 A-B. (A) Schematic figure showing a quadrupole mass analyzer, with two ion motions, i.e. unstable path and stable path of motion. **(B)** Stability regions with the operating line (red dashed line) and three ions, with $m_1<m_2<m_3$ (according to Douglas (2009) (Douglas 2009)).

2.4. Basic principles of Proton transfer reaction - time of flight - mass spectrometry

Proton transfer reaction - time of flight - mass spectrometry (PTR-ToF-MS) is an analytical technique developed for the detection of gaseous compounds in air (Hansel et al. 1995). Since its development in the 1990s, the field of applications expanded and PTR-ToF-MS is used in various sectors such as environmental or biological research, real-time breath analysis or indoor air quality (Blake, Monks, and Ellis 2009, IONICON Analytik 2022). This technique combines ultra-high sensitivity with high mass selectivity, which is consequently accompanied by low limits of detection (IONICON Analytik 2022). The following section introduces the basics of PTR-ToF-MS, beginning with **section 2.4.1**. which focuses on the principles of chemical ionization based on proton-transfer reaction. **Section 2.4.2**. introduces the principles of ion mobility mass spectrometry while **section 2.4.3.** covers the basis of time of flight mass analyzers.

2.4.1. The ionization process based on proton transfer reaction

Proton transfer reaction refers to the chemical ionization involving the neutral gaseous compounds and the primary ions (H_3O^+). The first experimental setup for these purposes was introduced by Hansel et al. (1995) (Hansel et al. 1995); and is to date, still the most commonly applied form of ion sources used for PTR-MS. Using hydronium ions as primary ions has a big advantage as all potential contaminant ions produced during the ionization process (e.g. O^+, OH^+ and H_2O^+) are highly reactive and thus rapidly react to form H_3O^+ ions (Blake, Monks, and Ellis 2009). The experimental setup involved in the ionization is illustrated in **Figure 7** A and is built up by three main parts: (i) an ionization chamber, (ii) a source drift (SD) region and (iii) a drift tube (DT) (Hansel et al. 1995). The primary ions are produced in the ion source by electron ionization of a

water vapor induced by a hollow cathode glow discharge source (HCGD) by different ionization reactions, which are given in **Figure 7** B. Primary ions are subsequently extracted into the rather short source drift region, which is the section where the ions produced by the HCGD further react to H_3O^+ ions. The final reactions occurring in the source drift region yielding H_3O^+ ions are given in **Figure 7** C. The total efficiency of the ion source leads to primary ions with a purity of >99.5%, which is controlled by an adequate electric field. The applied electric field further ensures, that all reactant ions are present as unsolvated hydronium ions (H_3O^+) and suppresses clustering of the H_3O^+ with water molecules (Boschetti et al. 1999).

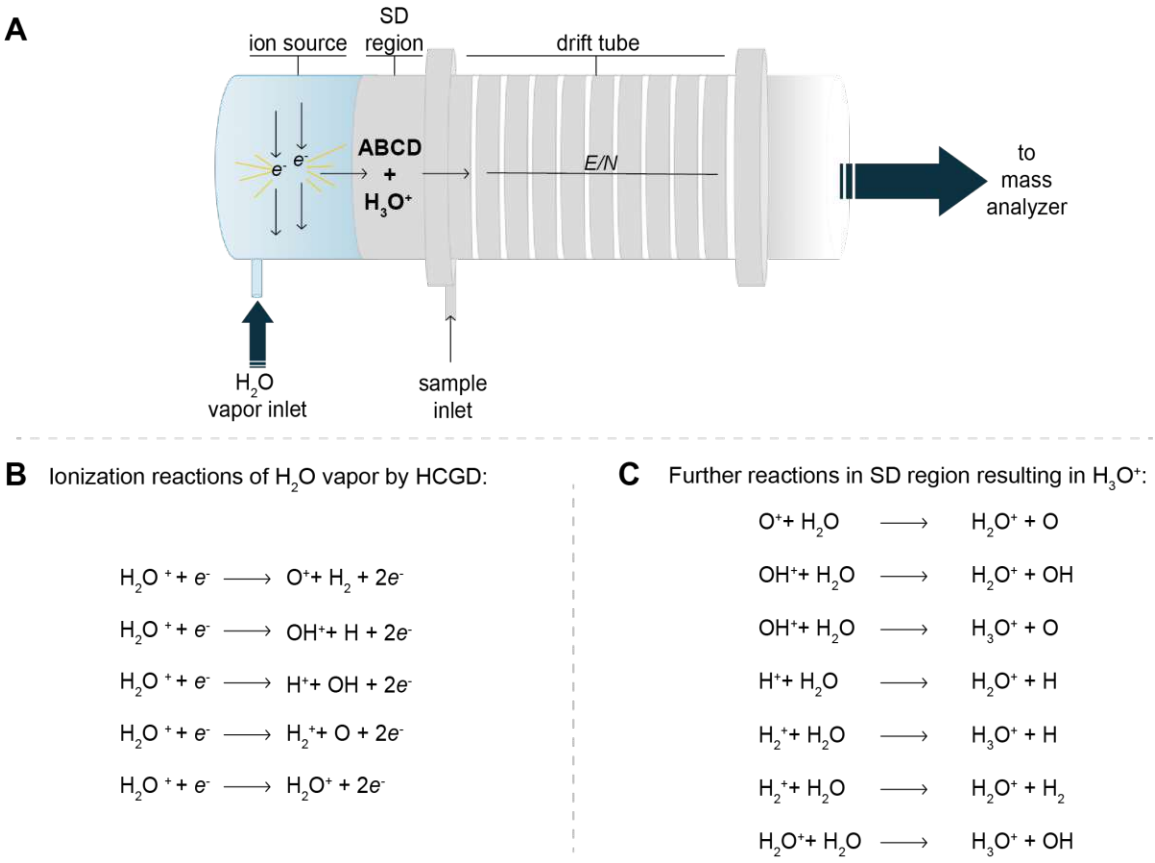

Figure 7 A-C. (A) Schematic figure of the ionization region including the HCGD ion source, source drift (SD) region and the drift tube (DT). **(B)** Sequence of ionization reactions involving electrons emitted by the HCGD and water vapor. **(C)** Sequence of the consecutive reactions happening in the SD region resulting in an almost pure stream of hydronium ions.

Finally, H_3O^+ ions are transferred into the drift region by the application of an electric field (Hansel et al. 1995). In the drift tube neutral gas molecules (*ABCD*) are introduced, where they encounter the H_3O^+ ions and finally undergo ionization following the chemical reaction listed in **Eq. 6**.

$$H_3O^+ + ABCD \rightarrow (ABCD)H^+ + H_2O$$

Eq. 6. Ionization reaction involving the primary ions (H_3O^+) and the neutral gas molecule ABCD

The proton transfer is realized under very well defined conditions and energetically favorable whenever the analytes proton affinity (PA) exceeds the one from water (PA_{H2O} = 691 kJ/mol) (Peterson et al. 1998). This is the case for almost all volatile and semi-volatile compounds and thus, also the PAHs studied in this thesis. The main components of air as well as low mass alkanes (< C_9) and small alkene molecules (< C_3) have a PA lower than water and are consequently not ionized. The pressure of the drift tube ranges between 2 and 4 mbar. The DT consist of up to 10 stainless-steel electrodes separated by Teflon insulators (Blake, Monks, and Ellis 2009). Each of the electrodes is operated at a different voltage in order to create a uniform electric field in the axial direction. Similar to the source drift region, the drift tube is typically operated at an electric field strength (E) of 60 V/cm. In the PTR community this is expressed in terms of the E/N values, where N refers to the gas number density (Blake, Monks, and Ellis 2009). The E/N value is given in Townsend (Td), referring to a practical unit of 1 Td = 10^{-17} cm^2/V. E/N ratios typically range between 100 and 140 Td. High E/N values lead to a higher number of energetic collisions and reduce the formation of cluster ions (i.e. $H_2O.H_3O^+$, $(H_2O)_2.H_3O^+$). The dimer and trimer cluster ions are preferably formed at low E/N values and due to their different reaction possibilities with the analytes they lead to more complicated and complex mass spectra. Due to this, the DT is usually operated a high E/N ratio which suppresses the formation of water clusters. This however, also increases the possibility of fragmentation of the analyte. After passing the DT, ions enter the mass spectrometer.

2.4.2. Time of flight mass analyzer

PTR sources coupled to a time of flight mass analyzer (ToF-MS) is the start of the art coupling method used in PTR instruments as it is a fast method allowing the parallel detection of several mass-to-charge (m/z) ratios over an (theoretically) unlimited mass range (Hübschmann 2015, IONICON Analytik 2022). In order to achieve that, modern PTR-ToF-MS setups include the following parts: (i) an acceleration region, (ii) a hexapole which acts as ion guide (optional), (iii) a field free region and (iv) a detector, which is usually a micro channel plate (MCP) detector (IONICON Analytik 2022). All those different ToF components are operated at low pressure (usually around 10^{-6} mbar) in order to ensure a long mean free path of the ions and to prevent them from colliding with each other or the background gas. A schematic figure of the ToF setup is given in **Figure 8**.

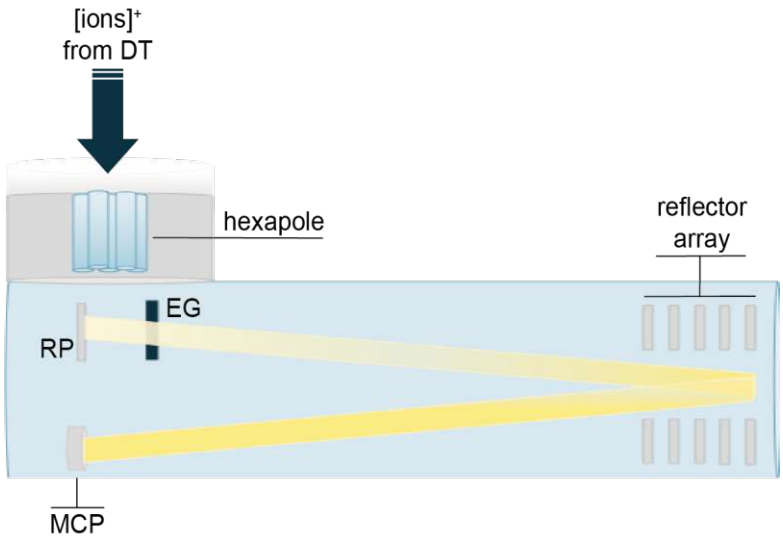

Figure 8. Schematic figure of an orthogonal acceleration time of flight (oa-ToF) analyzer including an hexapole ion guide. Abbreviations: DT = drift tube, RP = repeller plate, EG = extractor grid, MCP = microchannel plate detector. According to Notø (2021) (Notø 2021)

Separation of ions is achieved based on their different velocities. The ions exiting the DT are focused using a hexapole as ion guide, which increases sensitivity and mass resolution (IONICON Analytik 2022). The ions then enter the acceleration region, which consist of two electrodes: (i) the repeller plate (RP) and (ii) an extractor grid (EG). While filling the acceleration region with ions, the two electrodes are operated at the same potential. This changes when ions are pulsed into the field free region by the application of a high voltage pulse to the EG. The focused and accelerated ions are then transferred to the field free region where they are separated based on their velocities. The ions are accelerated using an electrical potential, and thus enter the field free region with identical kinetic energies. Thus, their velocities solely depend on the ion mass (TOFWERK 2022). The time of flight of individual ions is described by the following equation (**Eq. 7**):

$$t_{TOF} = l * \sqrt{\frac{1}{2eV} * \frac{\boldsymbol{m}}{\boldsymbol{z}}}$$

Eq. 7. Time of flight (t) for one m/z ratio under a certain acceleration pulse.

Whereas the time of flight (t_{TOF}) depends on the length of the flight path (l), the potential difference V between the RP and EG, and the elementary charge e.

The coupling of a continuous ion source, as it is the case for PTR, with a discontinuous ToF-MS is usually realized in the orthogonal way (oa-ToF-MS). Among others, state-of-the art PTR-ToF-MS instruments are realized in a V-shaped setup, as longer flight paths improve the spatial and temporal mass resolution (TOFWERK 2022). In order to achieve that, ions are reflected using a so called 'ion mirror' towards the MCP detector. This 'ion mirror' consists of a series of electrodes (reflector array) with increasing repulsive potential (Notø 2021). At the end of the flight path, the separated ions are detected using a microchannel plate (MCP) detector based on the extraction of secondary electrons and their amplification. Lastly, the generated signal is converted and further processed.

Chapter 3 Experimental Details

The following chapter aims to specify details about the individual setups and techniques used in this thesis. **Section 3.1.** presents the specifications of used GC-MS and GC-MS/MS setups, while **section 3.2.** describes the parameters used for PTR-ToF-MS measurements. **Section 3.3.** introduces the physico-chemical properties of key analytes. The specifications of chemical used for the analytical procedures are listed in **section 3.4.** Sample handling and preparation techniques used and developed within this thesis are given in **section 3.5.**

3.1. Details about the GC-MS and GC-MS/MS setups used within this work

Table 3 lists the specification and method parameters applied to the GC-MS and GC-MS/MS methods. Note, that throughout this thesis method parameters evolved as method modifications are necessary when enlarging the analyte palette.

Table 3. Specification and characteristics of used GC-MS and GC-MS/MS setups used within this work. Specifications of columns are listed as follows: length, inner diameter and film thickness. Abb.: FS=fused silica, SSL= split/splitless, AEI= advanced election ionization, deact. = deactivated, SSL= split/splitless, ID = inner diameter, FTh = film thickness.

Injector	Liner	Mobile phase/ column flow	Stationary phase setup			Coupling device	Ion source/ ionization technique	Application
			Pre-column	Separation column	Post-column			
SSL injection volume: 1 µL	Agilent, SSL liner, single taper, ID= 4 mm	He 5.0 Flow: 1 mL/min	1 m deact. FS (ID:0.25 mm)	DB-5MSi (30 m, 0.25 mm, 0.25 µm)	none	Single quadrupole MS (Agilent, HP5973)	EI (common geometry)	Ambient and emission samples (chapter 4)
SSL injection volume: 1 µL	Agilent, SSL liner, single taper, ID= 4 mm, ultra inert version	He 5.0 Flow: 1 mL/min / 1.3 mL/min	1 m deact. FS (ID:0.25 mm)	ZB-5MSplus (high temp), (30 m, 0.25 mm, 0.25 µm)	none	Single quadrupole MS (Agilent, HP5973)	EI (common geometry)	Ambient and emission samples (chapter 4/5)
SSL injection volume: 1 µL	Thermo Scientific, SSL liner, single taper, ID= 4 mm	He 5.0 Flow: 1.5 mL/min	1 m deact. FS (ID:0.25 mm)	ZB-5MSplus (high temp), (30 m, 0.25 mm, 0.25 µm)	none	Triple quadrupole MS (Thermo Scientific TSQ9000) collision gas: Ar 5.0	EI (advanced geometry by Thermo Fisher AEI)	Snow samples (first attempt, Section 6.1.)
SSL injection volume: 1 µL	Thermo Scientific, LinerGOLD, single taper, ID= 4 mm	He 5.0 Flow: 1.5 mL/min	1 m deact. FS (ID:0.25 mm)	Rxi-PAH (60 m, 0.25 mm, 0.10 µm)	0.6 m deact. FS (ID = 0.10 mm)	Triple quadrupole MS (Thermo Scientific TSQ9000) collision gas: Ar 5.0	EI (advanced geometry by Thermo Fisher AEI)	Snow samples (modified setup, Section 6.2.)

3.1.1. GC-MS and GC-MS/MS operating conditions

Throughout the method development, measurement were realized using different temperature programs and method parameters, all of them according to recent literature (see **Table 4**).

Table 4. Final GC-MS and GC-MS/MS operating conditions used within this work.

Setup details	**GC-MS (Agilent system)**	**GC-MS (Agilent system)**	**GC-MS/MS (Thermo Scientific system)**	**GC-MS/MS (Thermo Scientific system)**
Sample matrix	Emission and ambient PM (Chapter 4)	ambient PM (Chapter 5)	Surface snow samples (Section 6.1.)	Surface snow samples (Section 6.2.)
Injector	injection volume: 1 µL, mode: pulsed splitless, pulse pressure: 2.80 bar (0.20 min) T=300°C	injection volume: 1 µL, mode: pulsed splitless, pulse pressure: 2.80 bar (0.20 min) T=300°C	injection volume: 1 µL, mode: splitless with surge, surge pressure 169 kPa (for 1 min) T=300°C	injection volume: 1 µL, mode: splitless with surge, surge pressure 169 kPa (for 1 min) T=250°C
Temperature program	Start: 55°C (hold 1 min) Ramp: 25°C/min up to 320°C (hold 8 min) Final run time: 19.60 min	Start: 55°C (hold 1 min) Ramp 1: 25.0°C/min up to 240°C Ramp 2: 5°C/min up to 290°C Ramp 3: 4°C/min up to 315°C (hold 5 min) Final run time: 29.65 min	Start: 55°C (hold 1 min) Ramp: 20°C/min up to 320°C (hold 8 min) Final run time: 22.25 min	Start: 110°C (hold 3 min) Ramp 1: 30°C/min up to 195°C Ramp 2: 1.50°C/min up to 245°C Ramp 3: 1.75°C/min up to 295°C Ramp 4: 3.00°C/min up to 335°C (hold 11 min) Ramp 5: 15°C/min to 275°C Final run time: 90.50 min
Mobile phase flow	1.0 mL/min	1.3 mL/min	1.5 mL/min	1.5 mL/min
MS setup details	MS transfer line T=300°C Ion source T=300°C	MS transfer line T=300°C Ion source T=300°C	MS transfer line T=280°C Ion source T=280°	MS transfer line T=280°C Ion source T=280°

3.1.2. Qualifier and quantifier ions used in this thesis

Different ionization methods used in mass spectrometry often yield a fragmentation of analytes and so does electron ionization, which is also known to be a rather harsh ionization technique. The application of qualifier and quantifier ions is based on the usage of more than one m/z for analyses, which also allows to identify structural isomers. A list of used qualifier and quantifier ions within this thesis is given in the respective GC-MS/MS sections. The qualifier ion is used as confirmation ion of the respective analyte and described by one (or more) m/z signals characteristic for fragments of the analyte. While the quantifier ion marks one specific m/z signal, which states the basis for quantification. Peak ratios of quantifier to qualifier ions are further used for identification and ratios are described within standardized procedures (ÖNORM EN 16181:2018 and EN ISO 22892). Both legal documents were used in terms of guidance and qualifier and quantifier ions were chosen on the basis of an additionally done literature survey.

3.1.3. Qualitative analysis using an internal standard calibration

The quantitative analysis of data derived from GC-MS or GC-MS/MS measurements is based on an internal calibration method. This method evaluates the PAH concentrations based on the ratio of the area of one specific PAH to the peak area of the respective internal standard (IST). A linear regression between A_{PAH}/A_{IST} and the ratio of the PAH/IST amount (n_{PAH}/n_{IST}) states the basis for quantification. Internal standard calibration is routinely used in analytical labs because of its benefits, i.e. suppresses setup variations and injected volume variations. The standard requirements of IST are the following: (i) similar analytical behavior as the analyte of interest, (ii) not found in sample itself, (iii) measurement of IST is not affected by target analytes or matrix interferences. A recommendation of deuterated PAHs for internal calibration are given in ÖNORM EN 16181:2018. This legal document was used as means of guidance but deuterated substances were chosen aiming to cover the whole range of volatility of PAHs quantified within this work. A dilution series containing all PAHs of interest and 135TPB and recovery standard (hereinafter referred to as RST) as well as internal standard (single substance or d-PAH mix, hereinafter referred to as IST) was prepared. The dilution series consisted of up to 15 standard solutions varying in PAH concentration. All solutions were diluted using a cyclohexane dichloromethane mixture (1:1, v/v) with gas tight Hamilton glass syringes and glass pipettes. As PAHs show differences in volatility we modified the internal standard procedure within the scope of this thesis. One aim of method development conducted within this thesis was to enlarge the palette of PAHs and thus applying an IST mix covering the palette of volatilities is necessary. Analyses done with a single IST solely refer to d_{12}-chrysene as internal standard, while the IST mix contains the following substances: d_{10}-acenaphthene, d_{10}-flouranthene, d_{10}-phenanthrene, d_{12}-chrysene, d_{12}-perylene, d_{12}-benzo(ghi)perylene. Quantification of PAHs derived from particulate samples refers to the single IST procedure (**Chapter 4**), while PAHs derived from aqueous samples (**Chapter 6**) and results presented in Chapter 5 solely refer to the IST mix solution.

3.2. PTR-ToF-MS setup used within this work

3.2.1. Thermal desorption protocol and PTR-ToF-MS conditions

Thermal desorption (TD) of semi-volatiles was achieved by applying a temperature protocol, which heated up the sample vial and transferred the evaporated analytes into the PTR-ToF-MS using zero air or N_2 (5.0) as carrier gas. The operating conditions for TD and PTR-ToF-MS analyses are summarized in **Table 5**. PTR-ToF-MS measurements were realized at an acquisition rate of 1000 ms with an E/N of 120 Td and mass spectra covered a m/z range up to 400/457 Da.

Table 5. Operating conditions of the TD-PTR-ToF-MS setup. † Results presented in Chapter 5 refer to N_2 as carrier gas and were done using both the PTR 8000 and PTR 4000 setup, while PAH method development presented in Chapter 7 refers to zero air as carrier gas and measurements were done solely using a PTR 4000 setup.

Setup	**TD-PTR-ToF-MS (PTR 8000, PTR 4000 - updated version, Ionicon Analytik Austria)**
TD protocol	Start: 35°C (hold time 3 min) Linear ramp 40°C/min up to 360°C (hold time 5 min) Final run time: 17 min Carrier gas: zero air, flow= 100 mL/min or N_2 (5.0), flow= 50 mL/min †
Inlet	Heated sampling line, T = 180°C
Foreline	Pressure: 2.50 mbar
Drift tube	Pressure: 2.95 mbar Voltage: 530 V T= 120°C
E/N	120 Td

3.2.2. Data processing using PTRwid

Raw data was transferred to another computer and evaluated using PTRwid. PTRwid is a user friendly tool used for data processing developed by Holzinger (Holzinger 2015). All data presented within this work has been processed using PTRwid, using the following features: (i) creating a unified mass list, (ii) peak integration, i.e. extraction of counts per second (cps) and parts per billion by volume (ppbV) values, (iii) extended processing which includes the averaging and merging of data. Here, the main reasons of the individual processing steps are described briefly. A more detailed explanation about the mathematical background of each individual step is given in Holzinger (2015) (Holzinger 2015). The first data processing step unifies the mass list, as different samples yield results at slightly different m/z or operating conditions change over time (Holzinger 2015). Exporting of cps and ppbV data was done subsequently, by which raw data undergoes different processing steps including correction for physical limitations of the ion

detection system and peak integration for all ions chosen in the mass list (Holzinger 2015). By that, cps and ppbV data was exported for each measurement. Lastly, extended processing was done by which the response of each *m/z* in a measurement is averaged over a pre-defined time period. All data discussed within this thesis was averaged from 50°C onwards over a period of 10 minutes similar to the procedure described in earlier works (Materić et al. 2017, Materić et al. 2020). The integration step includes signals generated during the linear TD ramp and ends right before the TD is stopped and cooling starts. Conversion of the measured signal in cps to concentration (in ppbV) was calculated according to **Eq. 8**, and refers to the basic principles of proton transfer reactions, which occur in the drift tube (DT). The concentrations measured depends on the reaction rate coefficient k, the residence time t_{res} of the primary ions (i.e. H_3O^+) in the DT, the signal of the protonated analyte ion and primary ion in *cps*, and their respective mass to charge ratios, i.e. m/z_{H3O+} and $m/z_{(ABCD)H+}$.

$$ppbV = \frac{1}{kt_{res}} * \frac{[(\mathrm{ABCD})H^+]}{[H_3O^+]} * \frac{\sqrt{(m/z)_{H3O+}}}{\sqrt{(m/z)_{(ABCD)H+}}}$$

Eq. 8. Conversion of raw ion signal into concentration information given in ppbV, equation according to Materić et al. (2021) (Materić et al. 2021)

3.2.3. PTR-ToF-MS calibration procedure and calculation of ion transmission

Calibration of the PTR-ToF-MS setup was realized using a fast injection setup as described by Holzinger et al. (2019) (Holzinger et al. 2019). Calibration and thus determination of sensitivity is based upon 12 volatile compounds included in a VOC calibration gas mix (nitrogen/benzene mix, UN1956, National Physical Laboratory). All calibrations were done according to a lab SOP, which included the measurement of lab air for 1 minute followed by 10 fast injections of the calibration gas, waiting time for 30 seconds and a second set of 10 fast injections of the calibrations gas. By sticking to this calibration procedure, visual data investigation was not only easier but also faster and easy to compare among other calibrations.

Relative transmission curves were retrieved by the evaluation of the calibration measurements using the cps values measured for the volatile compounds in the calibration gas standard that do not fragment significantly. Ion transmission was calculated based on the following *m/z*: 21, 37, 42, 45, 59, 71, 73, 79, 107, 121, 133, 181, 355, 371. At the peak of the injection signal, the cps of the calibration compounds were collected and used for the transmission calculation. The transmission of the instrument was calculated according to the method described by Holzinger (2019) (Holzinger et al. 2019). This resulted in a transmission function which was used to calculate the instrument response in cps to concentration in ppbV. The transmission function was a piece-wise defined function composed of a 4th order polynomial low mass pass filter, and a 6th order polynomial high mass pass filter. Extended details about retrieving the transmission based on a combination of functions and parameters which are heavily depending on the instrument and operating procedures is presented by Holzinger et al. (2019) (section 2.2.1 in the respective publication) (Holzinger et al. 2019).

During the time period of September to December 2021 we calibrated the PTR-ToF-MS system every day and updated transmissions whenever the response of respective ions changed significantly. Updated transmission curves are visualized in **Figure 9** A, while the response of the respective ions observed during calibrations is given in **Figure 9** B. Lower masses varied in a higher degree, while higher masses were underestimated only a little. Updating and modifying transmissions did not show a more precise picture, and masses observed for PAH measurements were not significantly underestimated. Thus we agreed to work with the transmissions and exported data according to them.

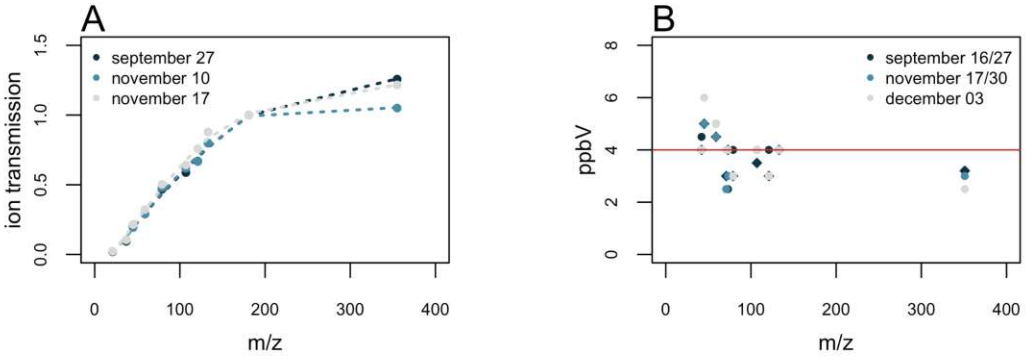

Figure 9 A-B. (A) Ion transmission curves normalized to m/z 181. **(B)** Calibration response for five different compounds. The red reference line highlights the reference concentration of the calibration gas compounds of 4 ppbV.

3.3. PAHs of interest

In the scope of this thesis the major focus is laid on p-PAHs. All quantified congeners are listed by the EU and within the US EPA priority list. For one application, i.e. PTR-ToF-MS experiments, we additionally included two N-PAHs. Modifications of the GC-MS/MS methods allowed the simultaneous quantification of p-PAHs and substituted ones, which are also listed in **Table 6**. As quantification is based on an internal standard procedure **Table 6** also comprises the properties of those compounds. The spectrum of all PAHs worked with in this thesis and their physical and chemical properties are listed in the following table.

Table 6. Structure, physical and chemical properties of PAHs. Molecular weights and the monoisotopic masses were retrieved from pubchem.com (https://pubchem.ncbi.nlm.nih.gov). * N-PAHs were only used for PTR ionization experiments, as they fragment in an extended way due to EI ionization. (†) The GC-MS setup used for PAH quantification for particulate samples did not allow a sufficient separation of the two isomers BbF and BkF, thus results refer to the sum of both abbreviated as BbkF.

Formula	Name	Abbreviations used in this work	Molecular weight (g/mol)	Monoisotopic mass (g/mol)	Phase partitioning	Toxicity class per IARC	US EPA priority PAH	EU-PAH
$C_{10}H_8$	Naphthalene	Naph	128.17	128.0626	Gas	2B	x	
$C_{12}H_8$	Acenaphthylene	Acy	152.20	152.0626	Gas	3	x	
$C_{12}H_{10}$	Acenaphthene	Ace	154.12	154.0783	Gas	3	x	
$C_{13}H_{10}$	Fluorene	Fluo	166.22	166.0783	Gas	3	x	
$C_{14}H_{10}$	Anthracene	Anthr	178.23	178.0783	Gas/Particle	3	x	
$C_{14}H_{10}$	Phenanthrene	Phen	178.23	178.0783	Gas/Particle	3	x	
$C_{16}H_{10}$	Fluoranthene	Fla	202.26	202.0783	Gas/Particle	3	x	
$C_{16}H_{10}$	Pyrene	Pyr	202.26	202.0783	Gas/Particle	3	x	
$C_{17}H_{12}$	Benzo(b)fluorene	BbFluo	216.28	216.0939	Gas/Particle	3		
$C_{18}H_{10}$	Benzo(ghi)fluoranthene	BghiFla	226.30	226.0783	Particle	3		
$C_{18}H_{12}$	Chrysene	Chry	228.29	228.0939	Particle	2B	x	x
$C_{20}H_{12}$	Benzo(a)anthracene	BaA	228.29	228.0939	Particle	2B	x	x
$C_{18}H_{12}$	Triphenylene	TriPh	228.30	228.0939	Particle	3		
$C_{20}H_{12}$	Benzo(a)fluoranthene	BaF	252.32	252.0939	Particle	3		
$C_{20}H_{12}$	Benzo(b)fluoranthene	BbF †	252.32	252.0939	Particle	2B	x	x
$C_{20}H_{12}$	Benzo(k)fluoranthene	BkF †	252.32	252.0939	Particle	2B	x	x
$C_{20}H_{12}$	Benzo(j)fluoranthene	BjF †	252.32	252.0939	Particle	2B		x
$C_{20}H_{12}$	Benzo(e)pyrene	BeP	252.32	252.0939	Particle	3		
$C_{20}H_{12}$	Benzo(a)pyrene	BaP	252.32	252.0939	Particle	1	x	x
$C_{20}H_{12}$	Perylene	Per	252.32	252.0939	Particle	3		

Formula	Name	Abbreviation used in this work	Molecular weight (g/mol)	Monoisotopic mass (g/mol)	Phase partitioning	Toxicity class per IARC	US EPA priority PAH	EU-PAH
$C_{22}H_{12}$	Anthanthrene	Anthan	276.30	276.0939	Particle	3		
$C_{22}H_{12}$	Indeno(1,2,3-c,d)pyrene	IcdP	276.33	276.0939	Particle	2B	x	x
$C_{22}H_{12}$	Benzo(ghi)perylene	BghiP	276.33	276.0939	Particle	3	x	x
$C_{22}H_{14}$	Dibenzo(a,c)anthracene	DBacA	278.35	278.1096	Particle	3		
$C_{22}H_{14}$	Dibenzo(a,h)anthracene	DBahA	278.35	278.1096	Particle	2A	x	x
$C_{24}H_{12}$	Coronene	Cor	300.35	300.0939	Particle	3		
$C_{24}H_{12}$	Dibenzo(a,e)pyrene	DBaeP	302.28	302.1096	Particle	3		x
$C_{24}H_{12}$	Dibenzo(a,h)pyrene	DBahP	302.28	302.1096	Particle	2B		x
$C_{24}H_{12}$	Dibenzo(a,i)pyrene	DBaiP	302.28	302.1096	Particle	2B		x
$C_{24}H_{12}$	Dibenzo(a,l)pyrene	DBalP	302.28	302.1096	Particle	2A		x
$C_{10}H_7NO_2$	1-Nitronaphthalene	N-Naph	173.17	173.0477	Particle	3		
$C_{16}H_9NO_2$	1-Nitropyrene	N-Pyr	247.25	247.0663	Particle	2A		
$C_{10}H_8O$	2-Naphthol	OH-Naph	144.17	144.0575	Particle			
$C_{16}H_{10}S$	Benzo(b)naphtho(1,2-	BbNaphS	234.30	234.0503	Particle	3		
$C_{12}D_{10}$	d_{10}-Acenaphthene	d_{10}-Ace	164.27	164.1410	Gas			
$C_{14}D_{10}$	d_{10}-Phenanthrene	d_{10}-Phen	188.29	188.1410	Gas/Particle			
$C_{18}D_{12}$	d_{12}-Chrysene	d_{12}-Chry	240.40	240.1692	Particle			
$C_{20}D_{12}$	d_{12}-Benzo(a)pyrene	d_{12}-BaP/dBaP	264.40	264.1692	Particle			
$C_{20}D_{12}$	d_{12}-Perylene	d_{12}-Per	264.40	264.1692	Particle			
$C_{22}D_{12}$	d_{12}-Benzo(ghi)perylene	d_{12}-BghiP	288.40	288.1692	Particle			
$C_{24}H_{18}$	1,3,5-Triphenylbenzene	135TPB	306.40	306.1409	Particle			

Table 6 continued. Structure, physical and chemical properties of PAHs. Molecular weights and the monoisotopic masses were retrieved from pubchem.com (https://pubchem.ncbi.nlm.nih.gov). * N-PAHs were only used for PTR ionization experiments, as they fragment in an extended way due to EI ionization. (†) The GC-MS setup used for PAH quantification for particulate samples did not allow a sufficient separation of the two isomers BbF and BkF, thus results refer to the sum of both abbreviated as BbkF.

3.4. Specification of chemicals used within this work

Organic solvents, reference material and other chemicals: Dichloromethane (Supelco, p.a.), cyclohexane (Supelco, p.a.), acetone (Supelco, p.a.), iso-propanol (Supelco, p.a.), acetone technical grade (PanReac AppliChem, 99.5%) sodium sulfate (Sigma aldrich, 99.0%), ERM® - CZ100 (fine dust, PM_{10}-like, JRC)

p-PAHs: Naphthalene (Neochema, 99.6%), acenaphthylene (Neochema, 95.6%), acenaphthene (Neochema, 99.0%), fluorene (Neochema, 98.0%), phenanthrene (Neochema, 98.0%), anthracene (Neochema, 99.0%), fluoranthene (Neochema, 98.0%), pyrene (98.6%), benzo(a)anthracene (Neochema, 99.1%), triphenylene (Neochema, 98.0%), chrysene (Neochema, 98.4%), benzo(b)fluoranthene (Neochema, 99.9%), benzo(j)fluoranthene (Neochema, 99.7%), benzo(k)fluoranthene (Neochema, 99.3%), benzo(a)fluoranthene (Neochema, 99.9%), benzo(ghi)fluoranthene (Neochema, 99.6%), anthanthrene (Neochema, 99.6%), benzo(b)fluorene (Neochema, 99.4%), benzo(e)pyrene (Neochema, 97.7%), benzo(a)pyrene (Neochema, 99.9%), perylene (Neochema, 99.0%), indeno(1,2,3-cd)pyrene (Neochema, 99.3%), dibenzo(a,h)anthracene (Neochema, 98.0%), dibenzo(a,c)anthracene (Neochema, 97.0%), benzo(ghi)perylene (Neochema, 95.0%), cyclopenta(c,d)pyrene (Neochema, 99.0%), dibenzo(a,e)pyrene (Neochema, 99.6%), dibenzo(a,i)pyrene (Neochema, 99.9%), dibenzo(a,h)pyrene (Neochema, 99.0%), dibenzo(a,l)pyrene (Neochema, 99.4%), coronene (Neochema, 98.4%),

d-PAHs: d_{10}-acenaphthene (Neochema, 99.9%), d_{10}-fluoranthene (Neochema, 99.2%), d_{10}-phenanthrene (Neochema, 99.2%), d_{12}-chrysene (Neochema, 99.9%), d_{12}-perylene (Neochema, 99.9%), d_{12}-benzo(ghi)perylene (Neochema, 98.7%), d_{12}-benzo(a)pyrene (Neochema, 98.5%),

x-PAHs: 1-nitro-naphthalene (Fluka, purum), 1-nitro-pyrene (Sigma, 99.0%), benzo(b)naphtho(1,2-d)thiophene (Neochema, 99.0)

Other: 1,3,5-triphenylbenzene (Neochema, 97.0%),

3.5. Sample preparations procedures used for GC-MS and GC-MS/MS analysis

Extracting PAH from different sample matrices makes the application of different analytical procedures indispensable. The following section highlights the different extraction and sample preparation steps used for particulate matter (emission and ambient PM samples) samples and snow samples, as both of them were analyses using GC coupled to either a single quadrupole or a triple quadrupole MS.

3.5.1. Extraction of PAHs from particulate samples

The quantitative determination of PAHs derived from particulate samples, i.e. TSP emission samples and ambient $PM_{2.5}$ samples, was performed according to DIN EN 15549:2008. A schematic step-by-step approach is given in **Figure 10**. For that, filter aliquots (quartz fiber filters, Pall Life Sciences®) were spiked with a certain volume of recovery standard (RST) (d_{12}- BaP) and extracted two times using a dichloromethane and cyclohexane mixture (1/1, v/v). After sonification for 30 minutes the extracts were filtered using a syringe filter (Chromafil®Xtra GF/PTFE-20/25, pore size: 1.0/0.20 µm) and transferred into a TurboVap® vial. After merging the two extracts (total volume of 12 mL) into the TurboVap® vial, a certain volume of the internal standard (IST) was added. IST solutions were adapted within the progress of this thesis, thus some analyses refer to single substance IST, i.e. d_{12}- Chrysene (results presented in Chapter 4), while we enlarged the IST palette to a mixture of several substances covering the volatilities of all quantified analytes (results presented in Chapter 5), i.e. d_{10}-acenaphthene, d_{10}-flouranthene, d_{10}-phenanthrene, d_{12}-chrysene, d_{12}-perylene, d_{12}-benzo(ghi)perylene. After that, extracts were contracted to a final volume of 0.5 mL under N_2 (5.0) using a TurboVap© evaporation chamber. Samples were analyzed using an HP6890 gas chromatograph (GC) equipped with an Agilent HP-5MS, non-polar capillary column (30 m x 0.25 mm x 0.25 µm) and coupled with an Agilent 5973 mass spectrometer (MS) with an electron ionization (EI) source and selected ion monitoring (SIM) mode (for more detailed info see **Table 3**). More details about the temperature program used and GC-MS parameters are given in **section 3.1**.

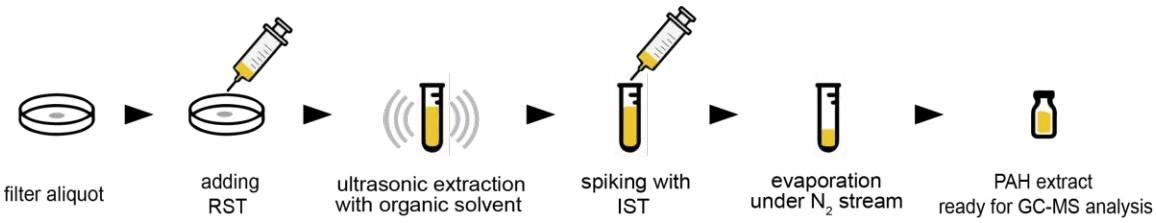

Figure 10. Schematic step-by-step approach of the sample preparation method used for the extraction of PAHs from particulate samples, i.e. TSP emission samples and ambient PM samples.

Quality assurance:

The same sample preparation procedure was used for the preparation of blanks. In case of particulate samples blanks either refer to (i) laboratory blanks, i.e. clean quartz fiber (Pall Life Sciences ®) filter aliquots or (ii) field blanks, i.e. quartz fiber filters (Pall Life Sciences ®) which were brought to the sampling location, experienced the same surroundings and environmental influencing factors but without having air volume drawn through them. Filter aliquots of particulate samples and both blank types were prepared as described above and subsequently analyzed using the same GC-MS setup under the same conditions.

3.5.2. Extraction of PAHs from surface snow samples

Differently to the PAH quantification of particulate samples, no standardized method for PAHs derived from snow samples is available. Extracting PAHs from snow samples, however, requires a more extensive sample preparation method as the one used for particulate samples. Thus, we worked on the development of a method for the parallel quantification of several PAHs and 135TPB, which is a tracer substance generated during the combustion of polyethylene material (Simoneit, Medeiros, and M. 2005). Methods presented in recent literature mainly refer to the application of solid phase extraction (SPE) (e.g. Usenko et al. 2006, Gabrieli, Vallelonga, et al. 2010, Walsh, Schrlau, and Simonich 2014) or liquid-liquid-extraction (LLE) (e.g. Lei et al. 2015, Xie et al. 2020, Kozhevnikov et al. 2021). Although, some studies refer to the extraction based on LLE, we ran into some difficulties with most of them caused by a rather large sample volume, e.g. hardly visible phase interface and high wastage of organic solvent. Regarding those obstacles, we classified the LLE extraction procedure as neither user-friendly nor green. Because of that, we focused on the development of a sample preparation procedure based on SPE. As environmental samples always contain a complex mixture of various analytes, SPE columns used within this work are based on a two-layered separation. This bifunctionality allows the separation of PAHs from other structurally similar compounds, such as humic-like substances (HULIS). HULIS comprise high molecular organic compounds, mainly consisting of aromatic molecules having aliphatic side chains with polar terminal groups (e.g. hydroxyl, carboxyl, carbonyl) leading to their high polarity and water-solubility (Salma, O'cskay, and Láng 2008). The first adsorbent layer of the ISOLUTE PAH© SPE column consist of aminopropyl groups interacting with HULIS, consequently preventing them from contaminating the extract. The second layer contains octadecyl groups which retain PAHs by adsorption. SPE hereby not only serves as a means of changing the sample matrix and preconcentration step, but also (and importantly) as purification step by removing structurally similar compounds.

Column conditioning procedure:

Within this thesis, we used ISOLUTE PAH© (Biotage, ISOLUTE PAH 1.5 g/6 mL) SPE columns, which were conditioned as follows: first, 5 mL of isopropanol (i-prop) were rinsed through the SPE column at a flow rate of 5 mL/min, equilibration was achieved by rinsing with 5 mL of MilliQ-water containing 2% i-prop (v/v) also at a flow rate of 5 mL/min.

SPE sample preparation and SPE retention process:

The sampling procedure is a step-by-step approach (see **Figure 11**) beginning with melting of the snow sample (volume >1000 mL) overnight at room temperature. Because of the semi-volatile properties of some PAH congeners, no assistance, e.g. microwave, was used for melting. Samples were weighted in prior using a common laboratory balance. After that, i-prop was added to the aqueous solution, to achieve a final mixture of 10% i-prop in snow (v/v). This was done based on recommendation of the manufacturer of the solid phase extraction (SPE) columns used for PAH extraction as it ensures better wetting. In order to evaluate analyte loss during the sampling procedure, we spiked the i-prop/sample mixture with a certain volume of recovery standard (RST,

d_{12}-BaP). Afterwards, the sample was loaded using a semi-automated SPE system, equipped with Teflon tubes and adapters at a flow rate of 20 mL/min. Analyte elution was achieved by adding two times 5 mL of a cyclohexane/dichloromethane mixture (1/1, v/v). Before applying vacuum to achieve the elution, the column was soaked with the solvent for two minutes. As extract may still contain traces of water, a Na_2SO_4 drying cartridge was installed in line. Finally, the extract was spiked with a certain volume of IST mix, concentrated to a final volume of 0.5 mL under N_2 atmosphere using a TurboVap® evaporation chamber and ready for the analysis using a GC-MS/MS setup.

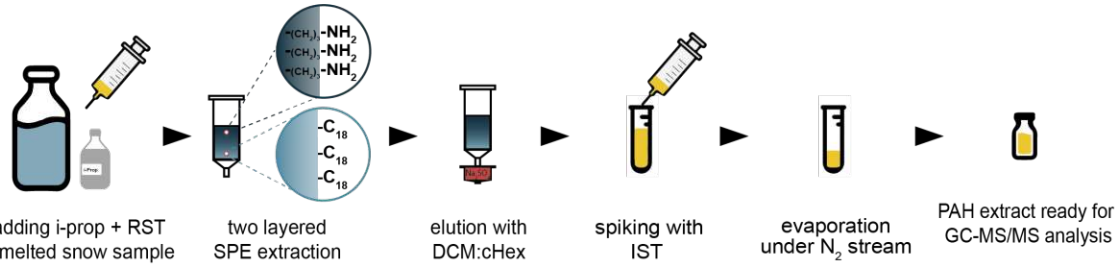

Figure 11. Schematic step-by-step approach of the sample preparation method used for the extraction of PAHs from snow samples. Note that pre-conditioning of the SPE cartridge is not shown here.

Quality assurance:

As not only PAHs may interact and further be eluted during the SPE preparation, a set of different blanks was prepared and analyzed. The different blank types refer to the following: (i) column blanks, i.e. the SPE columns was conditioned and afterwards eluted using the organic solvent mixture, (ii) sample packaging blanks, i.e. packaging material used for sampling (glass jars and commercially available plastic bags) were filled with a certain amount of Milli-Q water and frozen overnight or rinsed. All samples and blank types underwent the sample preparation procedure as described above and were subsequently measured using a GC-MS/MS setup using the same conditions. Conditions used for the GC-MS/MS analysis are given in **section 3.1**.

3.6. Sample preparations procedures used for PTR-ToF-MS analysis

The following sections highlight the sample preparation techniques used for PAH analysis and also for the preparation of cloud water samples.

3.6.1. Preparation of quartz fiber filters spiked with PAHs for PAH mass spectra and calibration purposes

In order to establish a PAH mass spectra library, we prepared quartz fiber filter aliquots (Pall Life Sciences ®, diameter of 8 or 7 mm) spiked with single substances. To avoid virgin contaminations with organic material of the filter itself, filter aliquots were prebaked overnight at 480°C and stored in a desiccator with a saturated atmosphere of water. This leads to the saturation of all active sites and prevents sorption of other compounds from the atmosphere. For spiking we prepared stock

solutions using solid single substance PAHs, which were dissolved in an organic solvent mixture (dichloromethane and cyclohexane, 1/1, v/v) yielding a concentration of roughly 0.5 mg/mL each. The following PAHs were used for analysis: acenaphthene (Ace), phenanthrene (Phen), fluorene (Fluo), benzo(a)pyrene (BaP), benzo(e)pyrene (BeP), benzo(ghi)perylene (BghiP), chrysene (Chry), pyrene (Pyr), perylene (Per), coronene (Cor), d_{12}-benzo(a)pyrene (dBaP), 1-nitronaphthalene (N-Naph) and 1-Nitropyrene (N-Pyr). Different volumes of stock solution (µL range) were then spiked onto the beforehand prepared quartz fiber filter aliquot. As sample humidity affects the fragmentation in the drift tube (Pang 2015), and in order to remove the organic solvent mixture, filters aliquots were dried at 30°C in an oven. We additionally aimed to investigate the linearity of the PTR-ToF-MS signal over several orders of magnitude. Therefore, filter aliquots spiked with a certain volume of single substance PAH solutions were prepared. Those covered a concentration range of 1.5 – 50 ng and were used for calibration purposes. The filter preparation procedure is visualized in **Figure 12**.

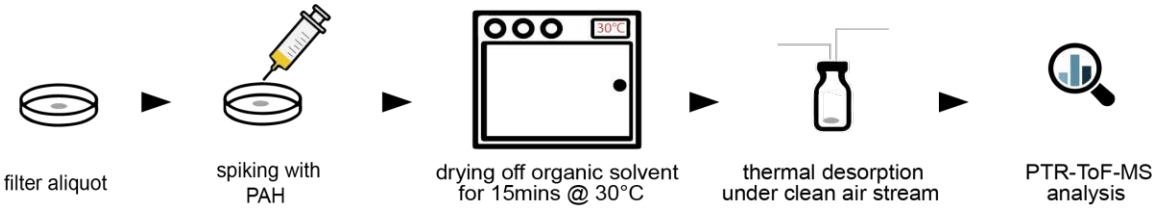

Figure 12. Schematic step-by-step approach of the preparation of filters used for PAH fingerprints and PAH calibrations. Also blank filters were prepared following the same procedure, just without PAH spiking.

Quality assurance:

As quartz fiber filters may also release (semi-) volatile compounds during one thermal desorption run, a set of different blanks was measured and prepared. Different blanks comprise: (i) only pre baked filter aliquots, (ii) pre-baked filter aliquots with 10 µL organic solvent mixture, (iii) pre-baked filter aliquots with or (iv) without solvent dried at 30°C in the oven. PAH filters and blank filters were then analyzed using a PTR-ToF-MS setup with thermal desorption in prior. Conditions used for the TD and PTR-ToF-MS analysis are given in **section 3.2**.

3.6.2. Sample preparation procedure of cloud water and snow profile samples

The sample preparation procedure used for cloud water (CWs) and snow profile (SPs) samples is visualized in **Figure 13**. Both samples, i.e. cloud water and snow profile samples were collected at Sonnblick Observatory, a glacier in Austria (3106 m asl). Samples aliquots of 0.5 mL (CWs) or 1 mL (SPs) were transferred into clean, prebaked (overnight at 250°C) vials. Afterwards, sample vials were placed in a low-pressure-evaporation (LPE) system. Maximum distance (at least 4 cm) was maintained between the single samples to avoid cross contamination. Sample preparation based on low-pressure-evaporation removes water (sample matrix) while limiting the loss of semi-volatile compounds and avoiding contamination with lab air (Materić et al. 2017). Low pressure was achieved by using a rotary vacuum pump and the sample matrix was trapped using liquid N_2. A more detailed description of the LPE setup is given in Materić et al. (2017) (Materić et al. 2017).

After all matrix was evaporated (this was achieved after evaporating for roughly 4 hours), samples were capped with prebaked Teflon caps and analyzed using TD-PTR-ToF-MS similar to previous works (Materić et al. 2020, Peacock et al. 2018, Materić et al. 2017, Materić et al. 2019). Samples were thermally desorbed and analyzed using the same conditions as used for PAH filters. Those conditions are given in **section 3.2**.

In order to assess the recovery we spiked CW samples either with a certain volume of PAH solution or a filter aliquot where PAHs were adsorbed to in prior. PAH filters for cloud water spiking were prepared according to the same procedure described in **section 3.6.1**.

Figure 13. Schematic step-by-step approach of the sample preparation method used for cloud water samples. A more detailed description of the used setup is given in Materić et al. (2017) (Materić et al. 2017).

Chapter 4 PAHs derived from particulate samples

PAHs in particulate matter were quantified in both, ambient as well as emission samples. The quantification method of PAHs was done using a GC-MS system, for the theoretical background see Chapter 2. This chapter highlights results for PAHs and states an excerpt of the respective publications, i.e. Kirchsteiger et al. (2020) and (2021) (Kirchsteiger et al. 2020, Kirchsteiger et al. 2021). The overall aims of measurements conducted in flue or in the ambient are different; hence this chapter is subdivided into the following: **Section 4.1.** deals with PAH concentrations found in emissions samples also highlighting the importance of field testing to calculate representative emission factors needed to derive mitigation measures. While **section 4.2.** discusses the PAH concentrations obtained from ambient samples, i.e. $PM_{2.5}$, which are usually found in lower concentrations and are needed to evaluate the direct impact of PM pollution to people and the environment.

Parts of this chapter are already published in Kirchsteiger et al. (2021) and Kirchsteiger et al. (2020) as is also illustrated below. Verbatim transferred parts are indicated as indented sections. Still, additional information is provided here: **Section 4.1.3.** calculation of emission factors, and **section 4.2.5.** toxic risk assessment of ambient PAH concentrations.

4.1. Emission measurements

Emission factors (EFs) are important to profoundly evaluate the influence of specific sources on air quality and state the basis for the further implementation of mitigation strategies. EFs can be either derived by lab-testing of appliances realized under well-defined conditions (Ozgen et al. 2014, Klauser, Carlon, et al. 2018, Kistler 2012, Schmidl et al. 2011, Gonçalves et al. 2011), or obtained from field measurement campaigns representing real-life conditions (Spitzer et al. 1998). Although the European Union strongly promotes the use of solid biomass for energy production,

the data set of EFs comprising the variety of appliances and burnt fuels is limited and gets even smaller when field measurements reflecting real-life emissions are discussed. Therefore, results presented in this section present up to date EFs derived from field measurements using appliances installed in people's homes.

4.1.1. Field measurement campaign and tested appliances

Field measurements were realized within the *Clean Air by biomass* project within the time period of January to February 2018 in a small municipality located in the Austrian region of Styria. All tested appliances were tested during the same heating period and devices refer to firewood room heaters (RH) produced by Austrian manufacturers. Thus, all tested appliances were of comparable design, installed in people's homes and used as additional heating source. A detailed evaluation of gaseous emissions observed within combustion experiments of the same appliances is given in Sturmlechner et al. (2019) (Sturmlechner et al. 2019).

Tested RHs cover the portfolio of Austrian log wood stoves. Device 1 and 4 present currently widespread cheap to middle-price devices in the Austrian market, while device 2 and 3 are a high-priced ones differing in high heat storage capacity (device 2 has higher heat storage capacity). The characteristics of tested room heaters are given in **Table 7.**

Table 7. Characteristics of tested room heaters (RH) including the year of construction, nominal heat output, EN standard and all possible air supply settings. Table was taken from Kirchsteiger et al. (2021) (supplementary data) (Kirchsteiger et al. 2021).

	Year of construction	Nominal heat output	EN standard	Air supply
device 1 (RH1)	2013	8 kW	EN 13240	separate primary/secondary air supply, manual adjustment of both flaps possible
device 2 (RH2)	2017	8 kW	EN 13240	combined primary/secondary air control, manual adjustment of the combined flap possible
device 3 (RH3)	~1997	8 kW	ÖNORM M 7520	three different air supply possibilities: primary, secondary and air flow through the grate, manual adjustment of three different flaps possible
device 4 (RH4)	2013	7.3 kW	EN 13240	separate primary/secondary air supply, manual adjustment of both flaps possible

Experiments were realized using fuels provided by the user itself. Tested fuel types comprise commonly used fuels in Austria (i.e. spruce, larch and beech) and the properties of representative fuel samples were tested according to the following standards: ISO 16948 (elemental analysis), ISO 18134-2 (water content) and ISO 18122 (ash content). Fuel composition was similar, i.e. C(wt%): 49 – 51%, H(wt%): 5.9 – 6.3%, N(wt%): 0.1%, accompanied with very low ash contents (a(wt%): 0.4 – 0.9%). The water content of used fuels showed higher variations ranging from 6.5 – 15%.

4.1.2. Sampling setup and combustion experiments

Experiments were realized with an in-house developed sampling probe, which was constructed during a previous research project aiming to develop, test and validate a new technique for BaP measurements (Klauser, Schwabl, et al. 2018). In order to get a realistic view on ambient emissions, sampling of total suspended particle (TSP) was divided into two fractions. Sampling of both fractions was done consecutively. A scheme of the sampling system is provided in **Figure 14.** TSP was sampled on quartz fiber filters in the hot flue gas flow (TSP_{130} sampled at ≥130°C) and after dilution in the cooled flue gas flow (TSP_{40} sampled at 40°C) promoting the recondensation of volatile species, resulting in a dilution ratio of 1:10. TSP_{40} filters include condensable compounds. TSP_{130} sampling was realized according to VDI2066 using a heated sampling line at 130°C which is significantly above typical dew point temperatures of flue gases (dew point: 40-50°C), strongly depending on the air excess rates. In TSP_{130} state BaP is still gaseous, whereas during TSP_{40} conditions BaP is condensed on particulate matter. However, by additional dilution the dew point temperature of water is lowered and water condensation is avoided. In this study we solely focus on emissions of TSP and particle-bound organic compounds.

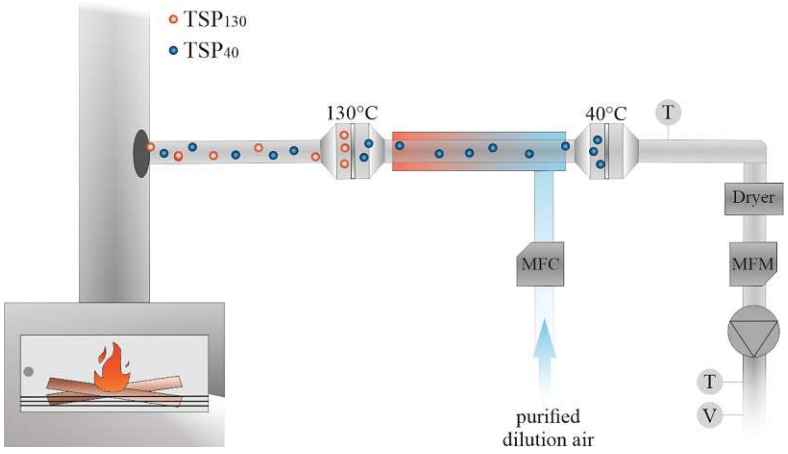

Figure 14. Scheme of TSP sampling device, modified for field-testing purposes. Abbreviations: MFC: mass flow controller, MFM: mass flow meter, T: temperature sensor, V: flow sensor. Figure was taken from Kirchsteiger et al. (2021) (Kirchsteiger et al. 2021)

The objective of the experiments was to evaluate emissions during real-life operation and their changes due to the optimization of the combustion conditions. Each test is characterized by three consecutive batches, carried out for two combustion experiments. The duration of the combustion differed among the individual batches and sampling was always started after ignition and closure of the stove door. The first batch of each experiment represents cold start conditions, i.e. the device was at ambient temperature and ignition start-up phase was included, while the consecutive two batches represent refilling batches, i.e. hot starts with a combustion chamber already heated up. Each device was tested according to two different combustion experiments: 1) three consecutive batches operated according to the users habits (UH experiments), prone to be operated under poor conditions, i.e. increased fuel load and decreased air supply, improper ignition method, poor fuel quality (sometimes also

burning of waste); 2) three consecutive batches with optimized combustion conditions (optC experiments), i.e. different placement, stacking and amount of fuel, restriction to proper fuel type or reduction of log size, ignition from above, optimized air supply. UH experiments represent the situation which happens in real life showing the diversity of the users' behavior, for these four comparable room heaters. A detailed descriptions of realized tests including fuel mass, air flow settings and ignition method is given in **Table 8**. The use of waste-paper and carton during the ignition process as well as ignition from the bottom and too little air supply were most common. The number of improvements needed to reach optC experiments was different for the single experiments due to different user behavior. In the end conditions of optC experiments followed a strict protocol, i.e. ignition from above, hot starts with completely opened air supply. Refilling was defined based on the CO_2 concentrations according to the *beReal test method* (Reichert et al. 2016). For all optC batches, measurements were continued until the CO_2 concentration reached 25% of the $CO_{2,max}$ concentration if the absolute CO_2 concentration was already under 4%. If the $CO_{2,max}$ concentration was below 12% and flames were extinguished at an absolute CO_2 concentration of 3%, recharging was done at this point. The end of UH batches were defined by the users' habit.

Table 8. Observed maloperations during cold starts of UH experiments. Room heaters are abbreviated as RH. Table was taken from Kirchsteiger et al. (2021), supplementary data (Kirchsteiger et al. 2021).

	Method of ignition	Fuel and its arrangement	Burning of waste material	Overload
device 1 (RH1)	bottom	campfire with shavings	x	-
device 2 (RH2)	bottom	at the bottom shavings, paper and other waste material, firewood in the middle covered with paper and other waste material	x	x
device 3 (RH3)	bottom to middle	cross joints without shavings	-	-
device 4 (RH4)	bottom	cross joints, without shavings, at the bottom paper and other waste material	x	x

4.1.3. Calculation of emission factors

Generally, emission factors are defined as the mass of a pollutant emitted per unit, so they can be reported in several ways – e.g. referring to the amount of fuel burnt or the energy produced. This thesis presents EF given in mg/MJ or µg/MJ, which refer to the respective energy produced using the related fuel parameters, i.e. chemical composition and thermodynamic parameters. To evaluate ambient emissions of discontinuously measured analytes (i.e. TSP, OC, EC, and PAHs), results represent the sum of the hot and cooled flue gas fraction (sum of TSP_{130} and TSP_{40}) and were calculated batch-wise. The analyte mass referred to the respective flue gas volume at standard temperature and pressure (STP: 273.15 K and 101.325 Pa) and to 13% O_2 in dry flue gas and was calculated according to **Eq. 9**. The EF ($EF_{i,STP,13\%O2,\,batch}$) of the analyte *i* is linked to the respective

mass deposited on the filter during the batch ($m_{i,filter}$), the sampled flue gas volume of batch *i* ($V_{i,STP,13\%O2}$), and the calculated necessary air volume $V_{f,dry}$, which is calculated based on the fuels' composition *f* in dry state and the net calorific value $H_{b,u}$ for each tested appliance *b*.

$$EF_{i,STP,13\%O2,batch} = \frac{\sum_{i=1}^{n} m_{i,filter}}{\sum_{i=1}^{n} V_{i,STP,13\%O2}} * \frac{V_{f,dry}}{H_{b,net}}$$

Eq. 9. Calculation of EFs for each analyte i, given in mg/MJ or µg/MJ, respectively

The time weighted means were calculated over three consecutive batches for each device and results were normalized to the time of the respective experiment. Median values refer to the median composition representing all tested room heaters for both sets of experiments, i.e. UH or optC experiment.

4.1.4. Changes of emissions of target analytes due to different combustion conditions

Besides the emission factors for the sum of 12 PAHs this section additionally presents EFs of TSP and the carbonaceous fractions including organic carbon (OC), elemental carbon (EC), the anhydrosugar Levoglucosan (Lev). EFs were calculated according to **Eq. 9**, for each tested device and batch as well as for the whole experiment (summing up three consecutive batches). More details about the analytical procedures used for the quantification of carbonaceous compounds can be found in Kirchsteiger et al. (2021) (Kirchsteiger et al. 2021). Briefly, OC and EC were determined with a thermal-optical method (OCEC Analyzer, Sunset Laboratory Inc.) using the EUSAAR 2 protocol (EN 16909:2017-06), while levoglucosan was analyzed via ion chromatography with pulsed amperometric detection (HPAE-PAD) according to the procedure presented by Iinuma et al. (2009) (Iinuma et al. 2009). As these parameters are used only as a comparison for the PAH results and no further details are given within this thesis.

A summary table of EFs is given in **Table 9** and results obtained during UH experiments are visualized in **Figure 15** A-E. No matter of experiment design and analyte, highest EFs were obtained during cold starts, while consecutive hot starts showed quite similar EFs. Variations like these are already observed earlier (Schmidl et al. 2011, Gonçalves et al. 2011, Orasche et al. 2012, Ozgen et al. 2014), especially during combustion experiments realized batch-wise, and highlight the need of extensive measurement campaigns to derive reliable overall EFs.

Table 9. Time weighted EFs of TSP, OC, EC, Lev and PAH_{12} for each device and combustion experiment. Mean values refer to the sum of hot and cold starts except for *device 2 UH. The hot start of device 2 realized under UH conditions was excluded from evaluation of carbonaceous compounds caused by implausible EC due to a contamination of the filter. Experiment is abbreviated as exp.

		TSP mg/MJ	OC mg/MJ	EC mg/MJ	Lev mg/MJ	PAH_{12} mg/MJ
UH exp.	RH 1	194 ± 76.7	95.8 ± 42.7	55.1 ± 18.7	0.73 ± 0.31	6.62 ± 3.29
	RH 2*	269 ± 54.8	35.9 ± 16.8	86.8 ± 30.2	0.53 ± 0.01	1.43 ± 0.42
	RH 3	132 ± 16.9	36.8 ± 4.94	32.5 ± 9.10	1.27 ± 0.39	0.79 ± 0.16
	RH 4	408 ± 83.4	177 ± 41.8	115 ± 22.6	3.92 ± 1.29	12.51 ± 0.94

Table 9 continued. Time weighted EFs of TSP, OC, EC, Lev and PAH_{12} for each device and combustion experiment. Mean values refer to the sum of hot and cold starts except for *device 2 UH. The hot start of device 2 realized under UH conditions was excluded from evaluation of carbonaceous compounds caused by implausible EC due to a contamination of the filter. Experiment is abbreviated as exp.

		TSP	OC	EC	Lev	PAH_{12}
		mg/MJ	mg/MJ	mg/MJ	mg/MJ	mg/MJ
optC exp.	RH 1	139 ± 42.8	42.8 ± 16.9	63.9 ± 26.4	1.29 ± 0.48	1.01 ± 0.25
	RH 2	104 ± 33.1	61.2 ± 25.7	16.7 ± 2.16	3.81 ± 1.74	0.44 ± 0.16
	RH 3	86.5 ± 8.2	54.3 ± 5.86	3.81 ± 0.61	5.78 ± 0.79	0.26 ± 0.05
	RH 4	124 ± 5.44	34.6 ± 2.02	37.3 ± 3.66	0.29 ± 0.10	0.45 ± 0.04

EFs obtained during UH experiments scatter in a wider range and were found to be higher than those observed for optC experiments. During UH combustion experiments time weighted means for EF_{TSP} including all batches (hot and cold starts) were in the range from 132 – 408 mg/MJ (see **Figure 15** A). Highest EFs appeared during cold starts and are highlighted in blue, presenting up to 6 times higher emissions than those observed during hot starts. EFs of consecutive hot starts (black flags) showed rather low variations and also lower absolute values, which can be attributed to the higher temperature of the combustion chamber itself. This holds true for other target analytes, time weighted means of EFs for OC and EC were in the range of 35.9 – 177 mg/MJ and 32.5 – 115 mg/MJ, i.e. OC emissions were slightly higher than those found for EC. Again cold starts yielded EF_{OC} values up to 9 times higher and EF_{EC} values up to 4 times higher than those observed during consecutive hot starts. One data point, i.e. hot start of device 2, was excluded from further evaluation of carbonaceous species due to an implausible result for EC, most likely due to a contamination of the filter. The anhydrosugar levoglucosan is one marker compound which is commonly used to identify the influence of biomass combustion in ambient samples (Simoneit et al. 1999, Schmidl et al. 2008). Overall, time weighted mean emissions obtained from UH experiments were in the range from 0.53 – 3.92 mg/MJ. In most cases, EFs of Lev followed the already discussed trend with higher emissions during cold starts, representing up to 7 times higher emissions than they occurred during hot starts (see **Figure 15**). Device 3 showed less pronounced variations of EF_{Lev} and highest emissions occurred during one hot start batch.

Similar to UH experiments, EFs from optC experiments showed high variations within the consecutive batches, also caused by highest emissions during the cold start. However, the optimization of combustion conditions lead to a clear decrease of particulate emissions ranging from 86.5 – 139 mg/MJ. Generally, EF_{TSP} were up to 4 times higher during cold starts, while EFs of consecutive batches did not show pronounced variations. Regarding carbonaceous compounds, EFs obtained during UH experiments (**Figure 15** A-E) were clearly higher than EFs obtained during optC experiments (**Figure 15** F-J). Considering the individual OC and EC emission, both combustion experiments (i.e. UH and optC) showed slightly higher OC emissions than those found for EC. Time weighted means of EFs for OC and EC were in the range of 34.6 – 61.2 mg/MJ and 3.81 – 63.9 mg/MJ. Again higher EFs were obtained

during cold starts, with EF_{OC} values up to 8 times higher and EF_{EC} values up to 7 times higher than those observed during consecutive hot starts. EFs of device 2 and 4 showed rather low variations within the OC and EC emissions, resulting in higher EFs also during hot starts. Time weighted mean emissions obtained during optC experiments covered a wider range, than those from UH experiments, with EFs of Lev varying between 0.29 – 5.78 mg/MJ. Highest EFs of Lev were found during cold starts, representing up to 11 times higher emissions than they occurred during hot starts. Device 3 showed less pronounced variations of EF_{Lev} and highest emissions occurred during one hot start.

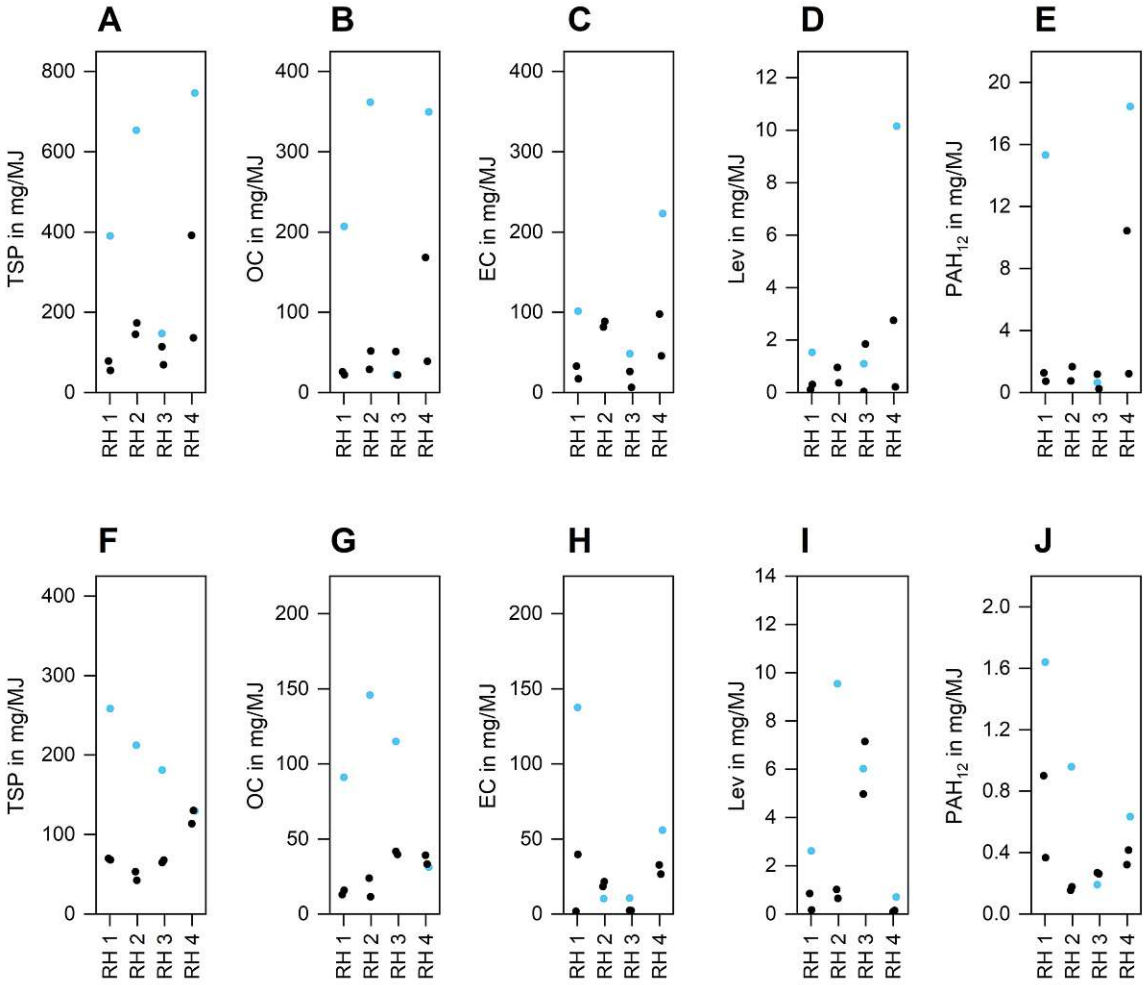

Figure 15 A-J. (A-E) Emission factors of TSP, OC, EC, PAH_{12} and Lev of three consecutive batches for four tested room heaters (RH 1-4) under UH conditions. Blue highlighted points represent emissions of cold start experiments while black highlighted points represent emissions of consecutive batches (hot starts). **(F-J)** Emission factors of TSP, OC, EC, PAH_{12} and Lev of three consecutive batches for four tested room heaters (RH 1-4) under optimized combustion conditions. Blue highlighted points represent emissions of cold start experiments while black highlighted points represent emissions of consecutive batches (hot starts). Note the different y-axis compared to the upper parts of the figure. Figure was modified for the used in this thesis, the published version can be found in Kirchsteiger et al. (2021) (Kirchsteiger et al. 2021).

4.1.5. Changes of PAH emissions due to different combustion conditions and comparison to results reported in literature

Time weighted mean EF_{PAH12} values were found to be higher during UH experiments (i.e. 0.78 – 12.5 mg/MJ), than during optC experiments (i.e. 0.25 to 1.01 mg/MJ). **Figure 15** E and J visualize the EFs for the sum of 12 PAHs for both types of experiment.

Similar to analytes already discussed, highest EFs for the sum of PAH_{12} could be observed during cold starts. EFs from cold starts were up to 15 times higher during UH experiments and up to 6 times higher during optC experiments than those observed during hot starts. However, PAHs quantified in this study represent only a small fraction of particulate emissions, with median values ranging from 1 – 3% of TSP emissions, which could be diminished to a maximum of 1% of TSP emissions due to the optimization of combustion conditions.

For individual PAHs no distinct difference of cold vs hot start conditions was observed and, thus, presented values refer to the time weighted mean composition within three consecutive batches (including hot and cold starts). As PAHs presented in this study were quantified from the particulate fraction, 2- and 3- ring congeners, which are primarily found in the gas phase, were not quantified. Highest emissions of BaP were obtained during UH experiments and yielded median emissions of 293 µg/MJ, while a clearly lower median value of 24.5 µg/MJ was observed for optC experiments. Presented median values comprise results from all four tested appliances derived within either the UH or optC experiments. Petterson et al. focused on the emissions of wood stoves realized under two operation modes (i.e. normal conditions and closed air inlets and moist fuel). BaP emissions obtained under both operation modes showed similar variations, in the range of 16 – 300 µg/MJ (Pettersson et al. 2011), overlapping with results found in this study. In contrast to that, Orasche et al. investigated PAH emissions from log wood stoves realized under optimal conditions. As expected, BaP emissions reported by Orasche et al. (12 – 17 µg/MJ for spruce and 9 – 11 µg/MJ for beech) were clearly lower than those obtained here, i.e. in field measurements, even during optC experiments (Orasche et al. 2012). These results show that maloperations substantially increase the burden of PAHs. A trend of decreasing EFs with number of condensed rings can be observed, i.e. highest EFs were found for 4-ring congeners (2607 µg/MJ for UH, 321 µg/MJ for optC experiments), followed by EFs of 5-ring congeners (1128 µg/MJ for UH, 101 µg/MJ for optC experiments) and lowest EFs were reported for 6-ring congeners (283 µg/MJ for UH, 22.6 µg/MJ for optC experiments).

4.1.6. Spearman rank analysis of PAHs emissions with other emitted compounds

In order to evaluate the correlation among individual PAH congeners and also with other quantified analytes correlation coefficients using the Spearman's rank were calculated. Correlation coefficients are listed in **Table 10** and were considered as significant with a p-value less than 0.05.

With exception of DBahA, most PAHs showed significantly high correlations among each other. Lower correlations of individual congeners with DBahA may be caused by the diminished data set for DBahA, because only device 1 and 4 emitted DBahA concentrations above the limit of detection. Especially high correlations found for Chry + BaA, BbF + BkF, BeP, BaP, Per and IcdP may indicate common formation pathways. Comparison with previous studies is rather difficult because the number of PAHs analyzed differs among studies, thus results were additionally compared to ones obtained from natural sources. Vicente et al., evaluated, among others, the amount of PAHs emitted from wildfires in Portugal (Vicente et al. 2017). They also reported high correlations for lighter PAH congeners such as Fla, but also for DBahA. Overall, PAH_{12} emissions showed a good correlation (r=0.75) with TSP emissions, while the correlations of individual congeners to TSP were rather low. Furthermore, **Table 10** also lists the correlations between individual PAHs with other analytes quantified in this study. PAH_{12} showed a higher significant correlation to EC (r=0.70) than observed for OC (r=0.59), further PAH_{12} to Lev emissions did not show a significant correlation (r=0.11).

Table 10. Spearman rank correlation matrix between individual PAHs and other quantified analytes. Correlations with coefficients ≥ 0.80 with a p-value < 0.05 were considered as significant (bold). Table was taken from Kirchsteiger et al. (2021) (Kirchsteiger et al. 2021).

	TSP	**Lev**	**OC**	**EC**	**Fla**	**Pyr**	**Chry + BaA**	**BbF + BkF**	**BeP**	**BaP**	**Per**	**IcdP**	**BghiP**	**DBahA**	**PAH_{12}**
TSP	1.00														
Lev	0.44	1.00													
OC	0.79	0.53	1.00												
EC	0.71	0.07	0.48	1.00											
Fla	0.83	0.23	0.68	0.71	1.00										
Pyr	0.79	0.23	0.66	0.66	0.98	1.00									
Chry + BaA	0.65	0.03	0.48	0.67	0.90	0.93	1.00								
BbF + BkF	0.58	-0.07	0.41	0.66	0.86	0.87	0.96	1.00							
BeP	0.58	-0.07	0.39	0.62	0.87	0.89	0.97	0.98	1.00						
BaP	0.55	-0.09	0.40	0.64	0.85	0.88	0.96	0.98	0.99	1.00					
Per	0.67	0.00	0.50	0.60	0.85	0.88	0.96	0.97	0.99	0.99	1.00				
IcdP	0.73	0.06	0.59	0.67	0.88	0.90	0.96	0.95	0.96	0.96	0.95	1.00			
BghiP	0.73	0.05	0.56	0.68	0.89	0.91	0.93	0.90	0.92	0.91	0.95	0.99	1.00		
DBahA	0.60	0.63	0.62	0.54	0.77	0.77	0.81	0.79	0.81	0.80	0.79	0.91	0.88	1.00	
PAH_{12}	0.75	0.11	0.59	0.70	0.97	0.98	0.97	0.94	0.96	0.94	0.95	0.96	0.95	0.81	1.00

4.1.7. PAH emission profiles

Consistent PAH profiles could be observed for almost all batches within either the UH or the optC experiment. **Figure 16** presents the share of individual PAHs to PAH_{12} emissions and the respective relative standard deviations for all four tested devices under both combustion experiments ((A) UH experiments and (B) optC experiments). During both combustion experiments, highest shares were found for Fla and Pyr, while lowest shares were obtained for Per. The comparison of the emission profiles of both combustion experiments visualizes a shift towards low molecular weight PAHs (LMW PAHs) due to optimized conditions. During UH experiments (**Figure 16** A) the share of 4 ring congeners accounted for 65%, while it increased to 73% during optC experiments. Even though, previous studies investigated a different number of PAHs, similarities of dominating LMW PAHs in emissions of residential wood combustion could be observed (Samae et al. 2021, Pettersson et al. 2011, Orasche et al. 2012). Among 5-ring congeners, BbF + BkF showed the highest share of PAH_i/PAH_{12} emissions (12% for UH experiments and 11% for optC experiments), followed by the share of BaP/PAH_{12} accounting for a maximum of 10% of total PAH_{12} emission during UH and 9% during optC experiments. In this respect no marked change occurred. Although the number of optimizations differed among devices, it lead to a pronounced reduction of PAH_{12} emissions to 11% during optC experiments compared to UH experiments, while emissions of the highly toxic BaP could be decreased to 8%. Thus, the optimization of combustion conditions lead to a shift of PAH emission patterns, pictured in **Figure 16** C. Relative emissions of LMW PAHs to total PAH content increased while the share of high molecular weight PAHs (HMW PAHs), i.e. 5- and 6-ring congeners showed ambivalent behavior. Although the total emission of PAH_{12} decreased, the share of 5-ring congeners was not affected at all, showing neglectable changes (see **Figure 16** C). A similar situation can be observed for 6-ring congeners. During UH experiments similar contributions of IcdP and BghiP could be observed within the respective devices, while the shares varied within optC experiments. It has to be noted, that only device 1 and 4 showed quantifiable concentrations of DBahA.

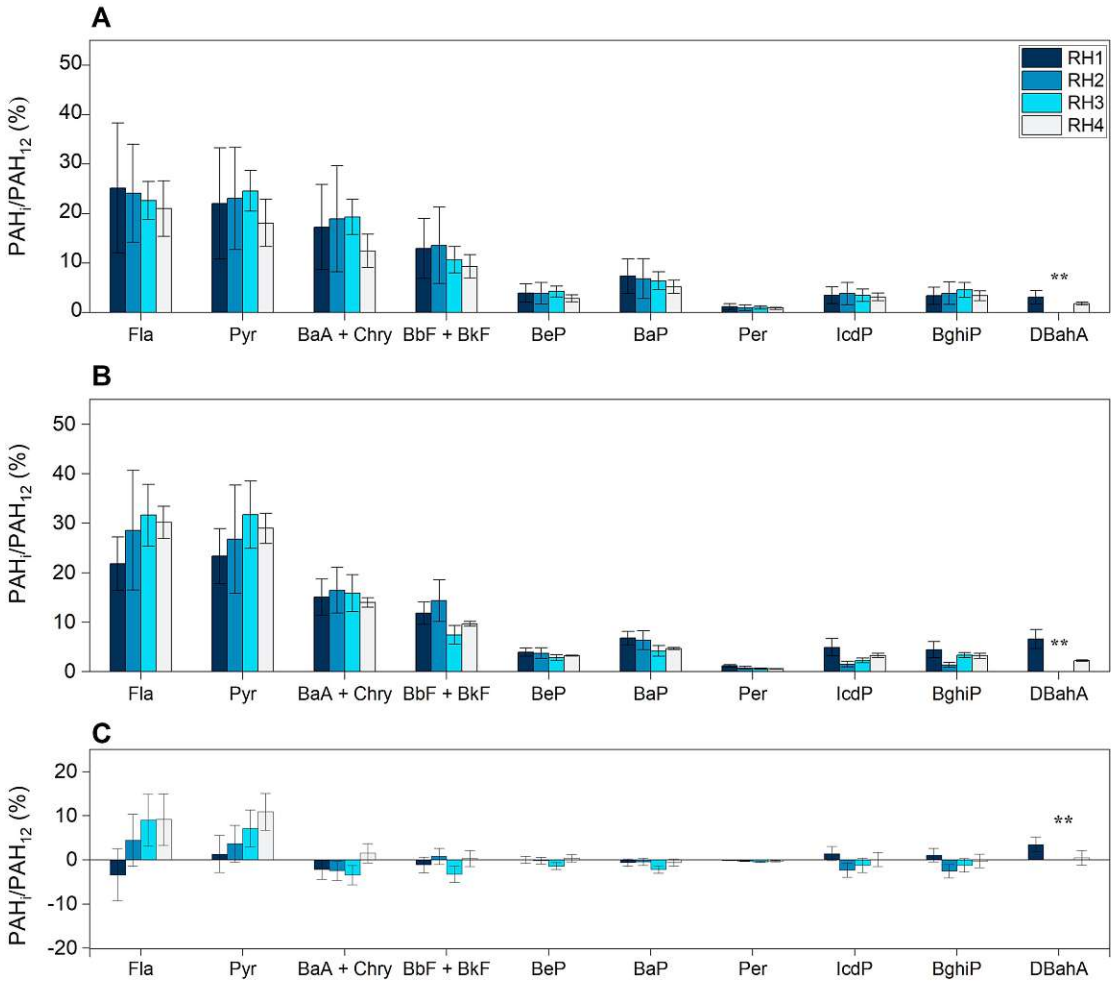

Figure 16 A-C. Emission patterns of individual PAHs of **(A)** UH experiments and **(B)** optC experiments. Error bars represent the relative standard deviation within the consecutive batches. No quantifiable DBahA concentrations (highlighted with *) could be obtained for device 2 and 3. **(C)** Change of PAH_i to PAH_{12} partitioning due to optimization of combustion conditions. In this case error bars display the standard deviations of changes. Results are sorted in an ascending order of carbon atoms. Figure was modified for the use in this thesis and the published version can be found in Kirchsteiger et al. (2021) (Kirchsteiger et al. 2021)

4.1.8. Toxic risk assessment and diagnostic ratios of emission samples

The overall toxicity was evaluated on the basis of BaP_{eq} emissions. BaP_{eq} showed considerable differences for both experiments, i.e. UH and optC. BaP_{eq} values of UH experiments, did not only show higher absolute values yielding 0.02 – 2.37 mg/MJ, they were also characterized by higher variations. OptC experiments revealed a shift to higher emissions of LMW PAHs, resulting in lower BaPeq values accompanied with less pronounced variations, ranging from 0.01 – 0.30 mg/MJ. These results clearly highlight, that the optimization of combustion conditions not only results in a distinct decrease of PAH_{12} emission, but also to a shift to PAHs with lower toxicity. Quite similar shares of BaP to BaPeq were observed during UH experiments and optC experiments, accounting for 54% and 55%, respectively. Although, the sample

size of DBahA was smaller, the contributions of DBahA to the BaPeq emissions showed similar results, yielding 23% and 24% for UH and optC experiments.

Diagnostic ratios of specific PAHs are widely used to identify the influence of possible emission sources such as biomass or fossil fuel combustion, i.e. traffic related emissions (Galarneau 2008, Tobiszewski and Namiesnik 2012). Besides that, diagnostic ratios also show intrasource variabilities and intersource similarities (Galarneau 2008). However, most emission sources do not show unique PAH signatures and ambient air contains a complex mixture of PAHs, which probably undergo a variety of atmospheric processes. Still the evaluation of PAH diagnostic ratios of specific emission sources may help to characterize the relevant sources. Generally, congener ratios observed in this study scatter in a wider range than previously reported ones. Fla/(Fla+Pyr) ratios were in the range of 0.47 - 0.54 for UH experiments and 0.47 – 0.52 for optC experiments. Ratios of IcdP/(IcdP+BghiP) showed an even more pronounced variation ranging from 0.39 – 0.59 for UH experiments and 0.44 – 0.60 for optC experiments. Both congener ratios are used to distinguish between source types and are in good agreement with those reported by Orasche et al. and Klauser et al. who investigated emissions of beech and spruce combustion (Orasche et al. 2012, Klauser, Schmidl, et al. 2018). The ratios observed for IcdP/(IcdP+BghiP) during the experiments done by Klauser et al. were slightly higher than those observed in this study (Klauser, Schmidl, et al. 2018). As BaP and BeP show a different behavior in photodegradation, the congener ratio BaP/(BaP+BeP) evaluates if particles did already undergo atmospheric degradations. Literature data suggests, that atmospheric degradations leads to BaP/(BaP+BeP) ratios below 0.5 while freshly emitted particles show congener ratios around 0.5 (Tobiszewski and Namiesnik 2012). UH experiments showed median values for BaP/(BaP+BeP) of 0.64 while slightly lower median congener ratios of 0.61 were found for optC experiments. As the present study solely evaluates freshly emitted particles, we recommend that also BaP/(BaP+BeP) ratios above 0.5 have to be considered as so. For comparison **Table 11** also lists congener ratios of the combustion of fuels with similar elemental composition but different combustion type. Congener ratios obtained in this study are in the range of recently reported ones for biomass combustions, however, the pronounced variability of each ratio emphasizes that single ratios are not representative for sources emitted under different circumstances. Comparing these ratios with those listed by Galarneau show a rather blurring transition for Fla/(Fla+Pyr) ratios of various sources. In the case of IcdP/(IcdP+BghiP) no overlapping of ratios can be observed, however, the IcdP/(IcdP+BghiP) ratio reported for wood combustion marks the lower range compared to additionally listed ones. This might be attributed to the fact, that all other studies investigated the PAH congener ratios of biomass commonly used in Europe, while Galarneau focused on fuels typically used in the US. This leads to the conclusion, that the evaluation of diagnostic ratios and emissions profiles for commonly used combustion systems in the area of interest is crucial to reveal the impact of different sources.

Table 11. PAH diagnostic ratios presented for this study including results published previously. [a] for better comparison only fuels with similar elemental composition were considered. [b] range includes hot and cold start conditions. [c] mean values and standard deviations calculated from EFs reported in US EPA (US EPA 1998). The table was taken from Kirchsteiger et al. (2021) (Kirchsteiger et al. 2021)

			Fla/(Fla+Pyr)	IcdP/(IcdP+BghiP)	BaP/(BaP+BeP)
(Kirchsteiger et al. 2021)	room heater	UH experiments	0.47 – 0.54	0.39 – 0.59	0.53 – 0.66
		optC experiments	0.47 – 0.52	0.44 – 0.60	0.48 – 0.65
(Orasche et al. 2012)	log wood stove under optimal conditions	spruce[b]	0.50 – 0.52	0.52 – 0.54	0.62 – 0.65
		beech[b]	0.49 – 0.50	0.53 – 0.57	0.61 – 0.64
(Klauser, Schmidl, et al. 2018)	firewood room heater	beech firewood, only experiments without catalyst	0.44 - 0.52	0.72 - 0.79	0.50 - 0.60
(Gonçalves et al. 2011) [a]	woodstove	golden wattle[b]	0.38 - 0.46	0.53 - 0.59	-
		eucalypt[b]	0.44 - 0.46	0.53 - 0.58	-
(Galarneau 2008) [c]	wood combustion		0.51 ± 0.16	0.42 ± 0.18	-
	diesel vehicles		0.40 ± 0.05	0.19 ± 0.13	-
	gasoline vehicles		0.52 ± 0.13	0.32 ± 0.11	-
	coal combustion		0.57 ± 0.21	0.48 ± 0.29	-

4.1.9. Conclusion

This chapter evaluates real-life emissions in Austria, investigating appliances installed in people's homes, fed with the fuel provided by the end user.

Measurements were conducted within a field measurements campaign realized in the scope of the *Clean Air by biomass* project. To evaluate the impact of the users' habit two types of combustion experiments were performed, one representing the diversity of possible maloperations (UH experiments) and one realized under optimized conditions following a strict optimization protocol (optC experiments). As special focus was laid on PAHs, sampling was realized using a dilution system adapted for the use in the field. Generally, optimization lead to a clear decrease of most compounds (i.e. TSP, OC, EC, PAH), however, emissions of the anhydrosugar levoglucosan were not affected at all. Total PAH emissions could be clearly reduced and PAH patterns of both combustion experiments showed a trend of decreasing EFs with increasing number of condensed rings. Moreover, optimization lead to a shift towards low molecular weight PAHs and thus, less toxic ones, clearly reflected by

lower toxicity equivalents. Relative emissions of LMW PAHs to the PAH_{12} content mostly increased while the share of HMW PAHs showed ambivalent behavior, i.e. the share of 5-ring congeners only showed neglectable changes, while 6-ring congeners showed decreasing shares. The overall toxicity of PAH emissions was evaluated on the basis of BaP equivalents, clearly highlighting that it can be reduced due to optimized combustion conditions. Correlation analysis using the Spearman's rank method showed significantly high correlations among the individual PAH congeners, and rather low ones with other target substances.

These results show that user training is of similar importance as changes in technology, because maloperations may counteract technological improvements. The high variations found for biomass combustion show, that EFs are only representative when a diversity of maloperations and appliances is considered. However, it is quite difficult to draw a firm conclusion about their effects on source apportionment, possible reduction measures or emission inventories. This would require an even more extensive evaluation of EFs obtained from field measurements, which is accompanied by much higher costs and effort as ones obtained from lab-testing.

4.2. PAHs in ambient samples

PM is a complex mixture and ambient concentration at one specific location is a combination of the local impact and the initial pollution load (Lenschow et al. 2001, Puxbaum et al. 2004). As consequence, air quality can either be dominated by emissions occurring locally or by regional as well as long range transport of air masses (Almbauer et al. 2000). In January and February 2017 high pollution of PM occurred in mid-Europe (EEA 2019) also affecting air quality in Austria. Comprehensive analysis of PAHs allowed to evaluate the differentiation between local effects and regional transport, in respect to concentrations and congener patterns.

Part of this section is already published in Kirchsteiger et al. (2020) as is also illustrated below. Verbatim transferred parts are indicated as indented sections. Still, additional information is presented in **section 4.2.5.** dealing with the toxic risk assessment based on the BaP_{eq} method.

4.2.1. Sampling sites and particulate matter sampling

Filter samples were collected within the air quality network in Styria at the sampling station Graz Don Bosco (DB). Thus, maintenance of the stations was performed by the provincial government of Styria (Department 15). The sampling station is in an urban environment nearby a road crossing and thus influenced by the urban surroundings. At Graz Don Bosco sampling of PM_{10} and $PM_{2.5}$ was performed with Digitel high volume samplers (HVS), which was programmed to sample in 24-hour intervals. Filters were changed automatically and subsequently PM mass was determined gravimetrically according to EN 1234:2014. $PM_{2.5}$ was collected on quartz fiber filters (Pall Life Sciences) and available for chemical analyses.

The sampling station DB (LON 15.41643°, LAT 47.05702°, 358 m asl) represents an urban environment. At the background station Bockberg (BB) (LON 15.49583°, LAT 46.87139°, 449 m asl) PM_{10} mass was determined with a beta attenuation mass monitor MetOne BAM 1020 (EN 16450:2017). Due to its location further South and the higher elevation BB is not directly influenced by anthropogenic emissions and thus represents a regional background station. Time period under investigation was 02.01. - 31.03.2017. 24h samples were grouped to sample pools covering 2 to 10 days. The definition of the pools was based on the PM_{10} mass concentrations determined at DB and the ratio of PM_{10} concentrations determined at DB and BB.

4.2.2. $PM_{2.5}$ and PM_{10} concentrations

Figure 17 A shows the daily PM concentrations at the urban sampling station DB and BB for the period under investigation. The PM_{10} concentrations observed between 02.01. - 31.03.2017 ranged from 9.9 µg/m^3 to 140 µg/m^3. On 01.01.2017 (following fireworks on New Year's Eve) a maximum concentration of 157 µg/m^3 of PM_{10} mass was measured, but due to the influence of fireworks this day is excluded from further evaluations in this study. During the sampling period 34 days with a PM_{10} concentration exceeding 50 µg/m^3 and thus violating the EU short time PM_{10} limit value were observed, with 21 days of exceedances already occurring in January 2017. Considering the whole year of 2017, 54 days violating the EU short time PM_{10} limit value occurred, showing a marked change to the general decreasing trend of annually occurring days of exceedances (Amt der Steiermärkischen Landesregierung 2018). $PM_{2.5}$ concentrations at the urban sampling station DB followed the trend of PM_{10}, with concentrations between 5.6 and 120 µg/m^3, giving an average $PM_{2.5}$ to PM_{10} ratio of 0.7. As expected lower PM_{10} concentrations, ranging between 5.1 and 123 µg/m^3, were observed at the background site BB. Still, days with especially high PM_{10} concentrations, as occurring especially during the second half of January, reveal rather similar PM concentrations at DB and BB pointing towards the influence of a pollution period observed across a wider area.

The differences in PM concentrations at DB and BB are evaluated via DB/BB PM_{10} ratios (see **Figure 17** A, light blue shading). During the whole sampling period DB/BB PM_{10} ratios ranged between 1.0 and 4.3, and between 1.0 and 3.9 when only days with PM_{10} concentrations above 50 µg/m³ are considered. As chemical analysis could not be performed for the whole data set selected filters were pooled to represent characteristic time periods. This pooling was classified on the basis of PM_{10} concentrations. Time periods selected for chemical analysis are marked in grey in **Figure 17** B. In total 14 sampling pools were analyzed covering 64 (of 89) days of the sampling period. Highest PM concentrations occurred during January and are represented by six sampling pools covering 19 days of January. Time periods of February and March are represented by five and three sampling pools covering 25 and 20 days, respectively.

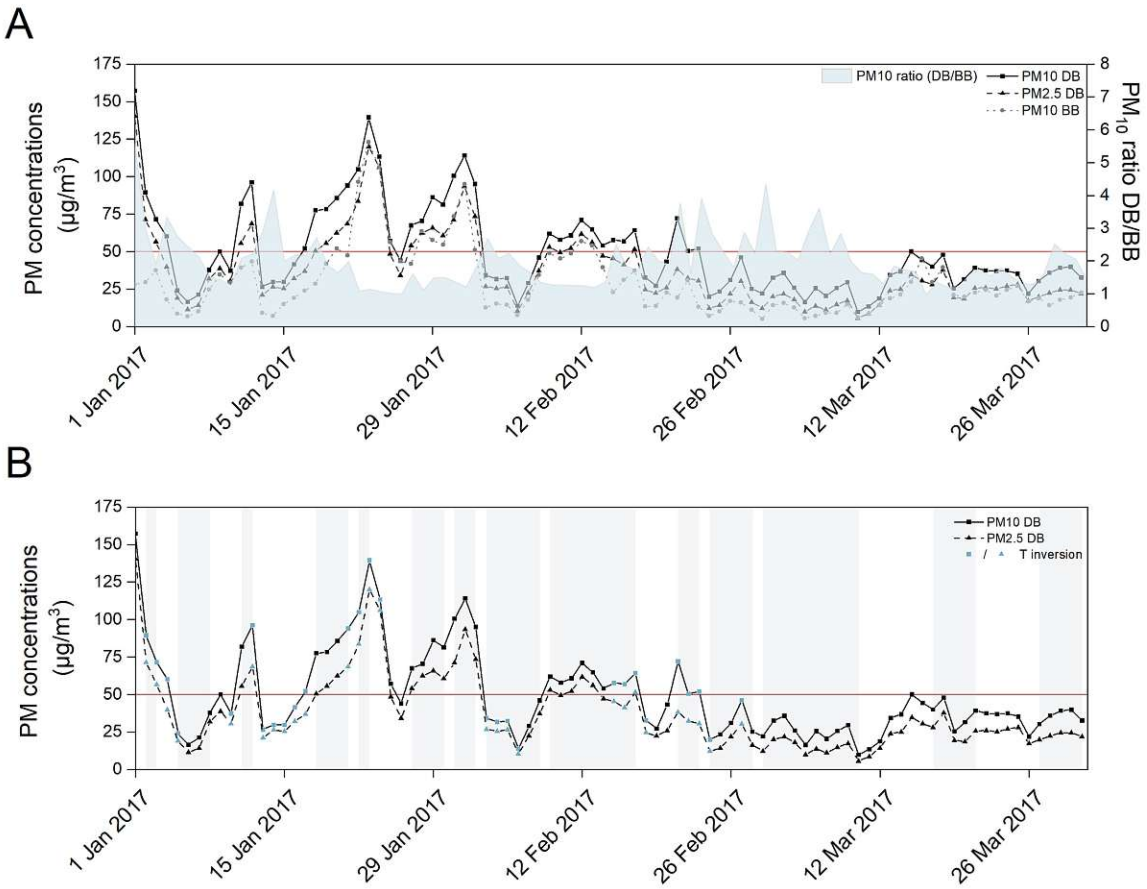

Figure 17 A-B. (A) Daily PM_{10} and $PM_{2.5}$ concentrations of the urban sampling site DB, daily PM_{10} concentration of the reference site BB, PM_{10} ratio between the sampling site and reference site (DB/BB). **(B)** Daily PM_{10} and $PM_{2.5}$ concentrations of the urban sampling site DB. Grey areas mark selected time periods and the red line marks the 50 µg/m³ limit value set by the European Commission. Blue highlighted flags mark days flawed by temperature inversion (according to WLKC733). The figure was modified for the use in this thesis and the published version can be found in Kirchsteiger et al. (2020) (Kirchsteiger et al. 2020).

Highest PM concentrations are represented by the filter pools of the time periods of 02.01. - 03.01.2017, 11.01. - 12.01.2017, 22.01. - 23.01.2017, 31.01. - 02.02.2017, 09.02. - 17.02.2017 and 21.02. - 23.02.2017. Based on their DB/BB PM_{10} ratios, which indicate differences or conformity between the PM concentrations determined within the city and the background site, we postulate a subdivision of these six periods into two scenarios: 1) DB/BB PM_{10} ratio larger than 2 representing a pollution period determined mainly at the urban station i.e. a local character and a marked urban impact; 2) DB/BB PM_{10} ratios smaller or equal to 1.5 representing comparable PM concentrations on both sampling sites pointing towards larger scale pollution episodes. In the following we will refer to these scenarios as 'scenario 1' and 'scenario 2', respectively. **Table 12** summarizes detailed information about the six time periods of interest i.e. average temperature, average DB PM_{10} and DB $PM_{2.5}$ concentrations and DB/BB PM_{10} ratios. PM ratios smaller than 1.5 or larger than 2.0 were found in March as well, but were not evaluated in detail because of PM_{10} concentrations below the daily limit value.

Table 12. Average temperature, average PM_{10} and $PM_{2.5}$ concentration and PM_{10} urban/background ratio of time periods representing scenario 1 and 2. Abbreviations: L = local, R = regional. The table was taken from Kirchsteiger et al. (2020) (Kirchsteiger et al. 2020).

Date	average Temperature (°C)	DB PM_{10} conc ($\mu g/m^3$)	DB $PM_{2.5}$ conc ($\mu g/m^3$)	DB/BB PM_{10} ratio	Class
02.01. - 03.01.2017	-2.7	80.5	64.0	2.5	L
11.01. - 12.01.2017	-7.8	89.1	62.2	2.2	L
22.01. - 23.01.2017	-5.2	122	102	1.1	R
31.01. - 02.02.2017	-4.8	103	79.5	1.5	R
09.02. - 17.02.2017	+0.6	61.1	50.9	1.5	R
21.02. - 23.02.2017	+5.9	58.2	33.7	3.1	L

Concentrations of both, PM_{10} and $PM_{2.5}$, were higher when temperatures were below 0°C, despite of the classification to one of the scenarios, but concentrations determined for scenario 2 reach higher up. Regarding the two cases above 0°C, again scenario 2 shows higher PM concentrations, especially for $PM_{2.5}$. The $PM_{2.5}/PM_{10}$ ratio was found to be lower during time periods of scenario 1 (average $PM_{2.5}/PM_{10}$ ratio 0.68) indicating a higher influence of urban sources i.e. primary emissions, than for scenario 2 (average $PM_{2.5}/PM_{10}$ ratio 0.82), indicating a higher contribution of secondary aerosols.

4.2.3. Prevailing meteorological conditions during the sampling period

The city of Graz is situated southeast of the Alps and located in a valley of the river Mur, forming a basin which is surrounded by mountains. High PM burdens coincide normally with one or multiple of the following meteorological phenomena: stagnant weather conditions, calm winds and limited ventilation, cold ambient temperatures leading to a shallow boundary layer, temperature inversions inhibiting vertical mixing. The meteorological conditions on regional basis were characterized using the WLKC733 weather classification (Philipp et al. 2010), which provides information on dominant wind direction, cyclonicity at 925 hPa and 500 hPa and dominance of wet or dry conditions. For local conditions we consider measurements of ambient air temperature and wind direction and wind speed. Of these covariates, temperature is most important as it is relatively variable over the study period. Wind speeds are generally modest in Graz during winter times. Over the study period daily mean wind speed was found for most days to be below 1.5 m/s (and daily maxima below 3 m/s). To contrast urban and rural background conditions we focus on PM burdens and ambient meteorological conditions at the urban site DB and background site BB. As the city of Graz is prone to temperature inversions, due to its valley location, we diagnose the presence of a local temperature inversion by determining the air temperature gradient from measurements at the sites DB and Kalkleiten (at ~ 12 km distance located on a hill encompassing the basin).

From a meteorological perspective stagnant conditions have been dominating during January and February 2017. Furthermore, extended periods with cold temperatures

(< 0°C) occurred, particularly during January, favoring PM accumulation within the shallow boundary layer. The regional uniform evolution of ambient air temperatures indicates a relatively homogeneous boundary layer as its depth is determined by ambient temperatures. Meteorological data for the city of Graz indicates the presence of a temperature inversion (blue highlighted symbols in **Figure 17** B). Contrasting PM data for DB with those of other Styrian and Austrian sites indicates however, that this local inversion is not the dominant driver of PM pollution. In fact widespread increases in PM abundance have been reported on larger scale due to enhanced European pollution backgrounds (EEA 2019). In contrast the PM pools sampled during 11.01. – 12.01.2017 and 21.02. – 23.02.2017 carry the signature of an enhanced contribution of local urban emissions to the Graz PM burden. For both periods a temperature inversion is diagnosed. Contrasting PM burdens for DB with data from the sites BB and Hartberg indicates that this temperature inversion has been a localized phenomenon trapping urban emissions within the boundary layer. For the data pool sampled during 09.02. – 17.02.2017 stagnant conditions have been diagnosed. The regionally homogeneous cold temperatures indicate a shallow boundary layer and combined consideration of urban, rural and background monitoring sites indicates a regionally enhanced PM background.

4.2.4. $PM_{2.5}$ associated PAH profiles

Ten PAHs including fluoranthene, benzo(a)anthracene, chrysene, benzo(b,k)fluoranthene, benzo(e)pyrene, benzo(a)pyrene, perylene, indeno(1,2,3-cd)pyrene, benzo(ghi)perylene and dibenzo(ah)anthracene were quantified for all time periods. The sum of all 10 quantified PAHs is in the following abbreviated as ΣPAH_{total}. **Table 13** presents average PAH concentrations as well as the standard deviations, medians and ranges for each congener associated to $PM_{2.5}$ samples at Graz DB. Concentrations of BaP, the primary representative of PAHs and a known carcinogen (class 1 by IARC (IARC 2010)), ranged between 0.51 to 8.4 ng/m^3 (median: 2.2 ng/m^3). The highest concentrations of BaP was measured during 02.01. – 03.01.2017, a time period still showing influences of local activities at NYE, where ΣPAH_{total} concentrations reached 102 ng/m^3. ΣPAH_{total} concentrations varied from 4.6 to 56 ng/m^3 (17 ng/m^3) within the period under investigation. PAH levels reported in this study are comparable to recent results reported in other European cities (Manoli et al. 2016, Khan et al. 2018). With proceeding time, a decreasing trend of ΣPAH_{total} concentrations was observed and highest concentrations could be observed for BbkF followed by BaA and BaP.

Table 13. $PM_{2.5}$ associated PAHs at the urban sampling station Graz DB, 02.01. – 31.03.2017. Overview of 14 sample pools, except for DBahA* where only 7 sample pools showed quantifiable concentrations. (†) The GC-MS setup used did not allow a sufficient separation of the two isomers BbF and BkF, thus results presented in this section refer to the sum of both, abbreviated as BbkF. The table was taken from Kirchsteiger et al. (2020) (Kirchsteiger et al. 2020).

Abbr.	PAH	Mean (ng/m^3)	Standard deviation (ng/m^3)	Median (ng/m^3)	Range (ng/m^3)
Fla	Fluoranthene	0.56	0.95	0.38	0.12 - 2.9
BaA	Benzo(a)anthracene	2.4	2.9	1.7	0.45 - 8.4
Chry	Chrysene	2.1	2.2	1.9	0.57 - 6.7
BbkF (†)	Benzo(b,k)fluoranthene	2.7	2.7	2.6	0.81 - 8.6
BeP	Benzo(e)pyrene	1.9	2.0	1.8	0.53 - 6.6
BaP	Benzo(a)pyrene	2.2	2.4	2.0	0.51 - 8.4
Per	Perylene	0.26	0.3	0.20	0.08 - 1.0
IcdP	Indeno(1,2,3-cd)pyrene	2.0	2.1	2.0	0.20 - 7.1
BghiP	Benzo(ghi)perylene	2.6	2.4	2.5	0.69 - 8.6
DBahA	Dibenzo(a,h)anthracene	0.31*	0.6	1.1*	0.28 - 2.0*

The ratio of ΣPAH_{total} to $PM_{2.5}$ ranged between 0.19 and 0.88 ng/µg and the corresponding ratios of $BaP/PM_{2.5}$ varied between 0.02 and 0.13 ng/µg over the whole sampling period. With increasing time not only PAH patterns changed also the $\Sigma PAH_{total}/PM_{2.5}$ ratios decreased (**Figure 18**). Generally increasing temperatures related to a change in meteorological conditions result in lower PAH emissions, due to reduced residential heating activities and higher degradation of PAHs. This is already visible during the end of the period under investigation which agrees with previously reported differences between summer and winter (Khan et al. 2018, Manoli et al. 2016). However, a clear difference in $\Sigma PAH_{total}/PM_{2.5}$ ratio was observed when a filter pool belonging to scenario 1 was analyzed. During that time period (21.02. - 23.02.2017) PAH concentrations within the city are much higher than at the background site leading to an increase in $\Sigma PAH_{total}/PM_{2.5}$ ratio. Generally lower $\Sigma PAH_{total}/PM_{2.5}$ ratios were found during time periods of scenario 2 (0.36 ng/µg) i.e. a larger scale pollution period. Time periods of scenario 1 showed a more pronounced urban influence and thus higher $\Sigma PAH_{total}/PM_{2.5}$ ratios (0.60 ng/µg). Highest $PAH/PM_{2.5}$ ratios were found for BaP, BghiP and BbkF during time periods of scenario 1 with average ratios of 0.08 ($BaP/PM_{2.5}$), 0.09 ($BghiP/PM_{2.5}$) and 0.09 ng/µg ($BbkF/PM_{2.5}$). Time periods of scenario 2 showed lower ratios of 0.05 ng/µg for both $BaP/PM_{2.5}$ and $BghiP/PM_{2.5}$ ratios and 0.06 ng/µg for $BbkF/PM_{2.5}$.

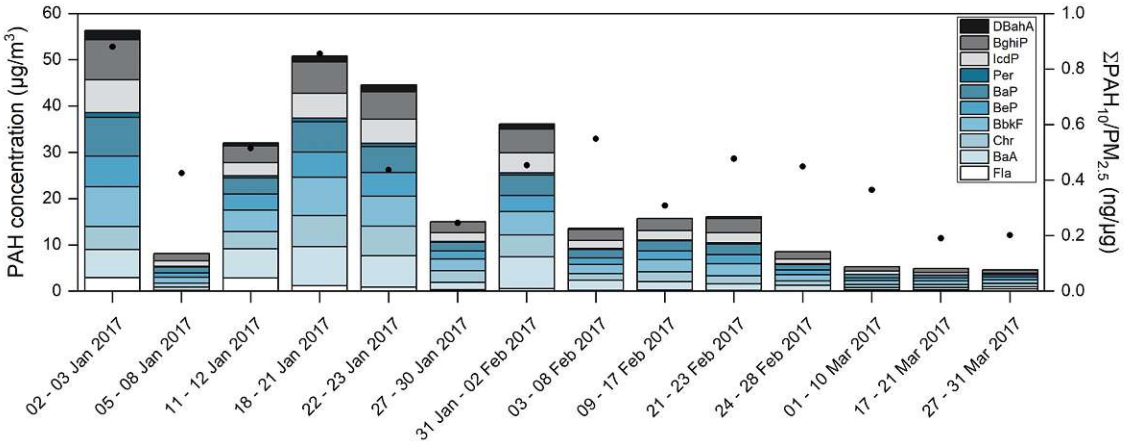

Figure 18. PAH profiles according to their classification of molecular weights. MMW PAHs shown in light colors (white to blue) and HMW PAHs are highlighted in darker colors (dark blue to grey/black) black dots mark the $\Sigma PAH_{10}/PM_{2.5}$ ratios. The figure was modified for the use in this thesis and the published version can be found in Kirchsteiger et al. (2020) (Kirchsteiger et al. 2020).

4.2.5. Toxic risk assessment of ambient PAH concentrations

The toxicity of PAHs differs among molecular weight. According to the IARC many of the heaviest are categorized as already known (class 1), probable (class 2A) or possible (group 2B) human carcinogens (IARC 2010). Thus, quantified PAHs were grouped in middle molecular weight PAHs (MMW) containing 4-ring congeners and high molecular weight PAHs (HMW) containing 5- and 6-ring congeners. PAHs consisting of 2- and 3 condensed rings are not included in the evaluation presented here, as those congeners are preferably found in the gaseous phase. Due to their different phase partitioning selective sampling of volatile PAHs is usually done using polyurethane foam (PUF) additionally to high volume samplers which allows the selective sampling of higher molecular weight PAHs (Kim and Kim 2015). During all time periods HMW PAHs were identified as the major components with PAH concentrations ranging from 2.9 to 42 ng/m^3 corresponding to 60 – 79% of the ΣPAH_{total} concentrations. The overall toxicity of atmospheric PAH concentrations was evaluated on the basis of the BaP_{eq} method described in **section 1.2.5.** BaP_{eq} results presents additional information to which has already been published in Kirchsteiger et al. (2020) (Kirchsteiger et al. 2020). Briefly, individual congener concentrations were multiplied with the respective toxic equivalency factors (TEFs) presented by Larsen and Larsen (Larsen and Larsen 1998). Consequently, BaP_{eq} followed the same seasonal trend observed for PAH concentrations, i.e. highest BaP_{eq} (12.6 ng/m^3 during the time period of 02.01. – 03.01.2017) were observed during the beginning of the sampling period and they decreased with increasing time. Lowest BaP_{eq} were observed during the time period in late February, i.e. 24.02. – 28.02.2017 yielding 1.48 ng/m^3. Comparing the toxicity of time periods assigned to the two beforehand scenarios, i.e. more influenced by local emissions or higher regional character did not show considerable differences in their average toxicity. Time periods assigned to scenario 1, i.e. urban impact, showed slightly higher BaPeq yielding 7.03 ng/m^3, while time periods assigned to scenario 2, i.e. regional character yielded BaPeq of 6.02 ng/m^3. However, the BaP_{eq} concentration observed for time periods assigned to the 'local' class reach higher up and BaP_{eq} concentrations vary between 3.31 – 12.6 ng/m^3. BaPeq concentrations observed for the 'regional' class scatter in a narrower range between 2.69 – 8.59 ng/m^3. For time periods assigned to the 'local' class MMW

PAHs contributed on average 2.1% to the overall BaP_{eq} concentration, while even lower contributions (1.3%) were observed within time periods assigned to the 'regional' class. Within both time periods, the main contributor to the overall toxicity are BaP and DBahA, both congeners were found in slightly higher concentrations in samples assigned to the class with higher urban impact. MMW PAHs contributed only a little to the overall toxicity.

4.2.6. Conclusion

Ambient PAH concentrations showed decreasing trend with time, which is in line with a seasonal trend. This was expected as with proceeding time activities related to residential heating decrease. Highest PAH concentrations were observed on the days right after NYE (02.01. – 03.01.2017) with peak ΣPAH_{total} concentrations reaching 102 ng/m^3. Considering the whole sampling period, highest contributions of individual PAH congeners could be ascribed to BbkF, BaA and BaP. Relative contributions of those congeners presented a quite diverse picture. $BbkF/PAH_{total}$ contributions slightly increased with proceeding time with contributions varying between 14 – 18%. BaA/PAH_{total} and BaP/PAH_{total} contributions did not show a seasonal trend with contributions varying between 8.5 – 20% and 11 – 17%, respectively.

Based on a comparison of the urban (DB) and the background (BB) site, i.e. DB/BB PM_{10} ratios, two scenarios were identified: 1) time periods with DB/BB PM_{10} ratios > 2, which may be linked to a higher urban impact; 2) time periods with DB/BB PM_{10} ratios ≤ 1.5, which may be related to pollution periods observed across a wider area. Pronounced differences in the chemical characterization of the respective samples and in source apportionment show the feasibility of this simple 'dual-site' approach.

Time periods with DB/BB PM_{10} ratios > 2: Several $PM_{2.5}$ associated components (saccharides, EC, PAHs) were found to be higher during time periods indicating higher local influence than those observed for time periods with more regional character. Meteorological data analysis confirmed the occurrence of local inversions during those time periods favoring the accumulation of locally produced air pollutants. Details about the extended chemical analysis, meteorological analysis and source apportionment are given in Kirchsteiger et al. (2020) (Kirchsteiger et al. 2020). Focusing on ambient PAH concentrations presented the following: Time periods assigned to the scenario of higher local influences also showed higher $PAH_{10}/PM_{2.5}$ ratios. Besides that, during these time periods higher ratios of PAHs related to traffic emissions and combustion (BbkF, BaP and BghiP) were found. The additionally presented toxicity assessment based on the BaPeq concentrations strengthened the sample classification method. However, both time periods did not show considerable differences in toxicity. The BaP_{eq} concentrations observed within time periods assigned to the class markedly influenced by urban sources showed slightly higher BaP_{eq} concentrations yielding on average 7.03 ng/m^3 than those observed during the time period influenced by regional transport of air masses (6.02 ng/m^3). BaP_{eq} concentrations observed within the 'local' class reached higher up to maximum BaP_{eq} concentrations of 12.6 ng/m^3, while BaP_{eq} concentrations observed within the 'regional' class scatter in a narrower range.

Chapter 5 PAHs and their interaction with different polymer types

This chapter deals with the interplay of polymer types with PAHs. **Section 5.1.** highlights the emerging situation of microplastics in the environment, while the following **section 5.2.** reviews the ability of PAH sorption onto microplastics. For the first time, atmospheric concentrations of ultrafine microplastics and nanoplastics are presented in **section 5.3**. Additionally, this section highlights ambient PAH levels and discusses the correlations among the key analytes. Finally, **section 5.4.** deals with the resulting environmental implications of these findings.

Measurements were realized within a research stay at Utrecht University funded by the *Christiana Hörbiger* award in 2019. Support by supervisors and colleagues at Utrecht University namely Rupert Holzinger and Dušan Materić is gratefully acknowledged. Quantification of PAHs was done at TU Wien using the modified method in accordance to EN DIN 15549:2008. Modifications refer to the application of an internal standard mix (six deuterated substances) and are described in **chapter 3**.

Part of this chapter has been recently submitted to the Journal of Hazardous Material. Still, additional information is provided here: **Section 5.1** and **5.2** and in the **subchapters 5.3.3**. and **5.3.4.** The same set of samples has been analyzed and discussed within **section 4.2**. The following section focusses on measurements on a different time scale, i.e. on a daily basis and also on different key analytes and an enlarged palette of PAHs.

5.1. The emerging role of plastic debris in the environment

In recent times the research focus on microplastics (MPs, 5 mm to 1 µm) and nanoplastics (NPs, < 1 µm) has rapidly risen. Nowadays, plastic compounds define the way to live as they combine a lot of favorable properties such as high versatility, durability and resistance, being low in weight but highly adaptable. In order to satisfy the society's needs, plastic production has drastically risen over the past years, and in 2020 367 million tons of plastics were produced worldwide (Plastics Europe 2021). Of these 307 million tons worldwide, 55 million tons were produced in Europe, this accounts for 15% of the total plastic production worldwide (Plastics Europe 2021). Plastic compounds usually have a life time up to 50 years, and then undergo post lifetime processing such as being disposed in landfills, used for energy production or being recycled. Although recycling of plastic compounds is favored, only 32.5% of 29.1 million tons collected plastic waste has been recycled in 2018 (Plastics Europe 2020). There is a discrepancy in the plastics mass balance, which is not caused by the rather long time of the plastic compounds. The remaining mismanaged macro plastic waste (> 5 mm) is often exposed to different environments leading to a degradation of plastic compounds yielding micro- and nano- sized fraction (MPs and NPs).

To date, MPs have been reported in nearly all environmental compartments. Most of them referring to the aquatic systems, e.g. oceans (e.g. Rios et al. 2010, Hirai et al. 2011, Avio, Gorbi, and Regoli 2017), riverine systems (e.g. Mai et al. 2020), lakes and surface waters (e.g. Materić, Peacock, et al. 2022), soil and sediments (e.g. Corradini et al. 2019). Although, the research focus is shifting to other compartments as well, knowledge about MPs as air pollutants is scarce, as discussed in the review by Sridharan et al. (2021) (Sridharan et al. 2021). The main source of airborne MPs are, among others, abrasion products of synthetic textiles, furniture, tires or dust. MPs were identified in ambient aerosols and atmospheric deposition in (sub-)urban environments (e.g. Dris et al. 2016, Cai et al. 2017, Klein and Fischer 2019, Wright et al. 2020). Generally plastic components are produced on land, mostly in industrial areas, from there they mainly enter the environment, from where they accumulate and are transported over wider areas. The identification of MPs in remote areas and the possibility of atmospheric transport have been previously reported (e.g. Allen et al. 2019, Materić et al. 2021, Bergmann et al. 2022, Materić, Kjaer, et al. 2022).

Besides finding MPs and NPs in different environmental matrices, the influence of those compounds on the fate and risk of other co-existing compounds such as PAHs enhances concern. To date it is well known, that MPs have the ability to adsorb organic pollutant like PAHs (Wang et al. 2020, Torres et al. 2021), which pose an even high environmental and toxicological threat.

5.2. The sorption ability of PAHs to polymers

MPs and PAHs are totally different compound classes. However, they have some things in common: both gained much interest due to their persistency, ubiquitous occurrence and negative health outcomes. Furthermore, they show similarities in terms of having hydrophobic and lipophilic properties making sorption processes likely. For most contaminants the sorption to MPs increases with their hydrophobicity (Wang et al. 2020). PAH concentrations adsorbed to MPs have been found to exceed the PAH concentrations found in the respective aquatic phase by several orders of magnitude (Rochman et al. 2013). Mai et al. (2020), for example, extracted different

persistent organic pollutants (POPs) from the collected MP samples, indicating that MPs may act as possible vectors of PAHs, but also other organic pollutants, i.e. polychlorinated biphenyls (PCBs) and polybrominated diphenyl ethers (PBDEs) (Mai et al. 2020). Similar findings were presented by extracting the 16 US EPA priority PAHs from floating marine plastic debris (Rios et al. 2010). High PAH and PCB concentrations have been reported, which also matches the ones commonly found in marine sediments (Rios et al. 2010). A difference of the sorption ability of organic compounds has been reported among polymer types (e.g. Guo et al. 2012, Wang and Wang 2018, Zhang et al. 2020). The important parameters of polymer types influencing the sorption/desorption mechanism of organic pollutants are: specific surface area, particle size, crystallinity, degree of cross-linking and spatial arrangement of the polymer itself (Wang et al. 2020). The interaction will also be modified by environmental transformation mechanism, e.g. photooxidation and abrasion of MPs, which leads to a loss of mechanical integrity and stability as well as changes in chemical behavior (Fotopoulou and Karapanagioti 2015). Regarding air pollution Gasperi et al (2018) already mentioned the possibility of adverse health effects due to PAHs associated with MPs (Gasperi et al. 2018). A first indication of the co-occurrence of MPs and PAHs in ambient air was given by Akhbarizadeh et al. (2021) (Akhbarizadeh et al. 2021). However, literature describing similar relationships or correlations indicating possible carrier activities for atmospheric samples is scarce and their combined impact on ecosystems is still not fully understood.

5.2.1. Sorption kinetics of PAHs to polymers

Generally, the interaction of MPs with a possible sorbate can be described by six different sorption mechanism, i.e. (i) electrostatic interaction, (ii) pore filling, (iii) Van der Waals forces, (iv) hydrogen bonding, (v) π-π interaction and (vi) hydrophobic interactions (Torres et al. 2021). Whether the sorption is described by one dominant mechanism or as a combination of many, it is strongly depending on the physico chemical properties of the sorbent and sorbate itself (Fred-Ahmadu et al. 2020, Torres et al. 2021). Physical and chemical properties affect the sorption ability and mechanism of organic pollutants in many different ways. As already mentioned, the major influencing factors of the MP are among others, the crystallinity and thus the arrangement of the molecular chains or functional groups (Guo et al. 2012, Zhang et al. 2020). However, as the MP enters the environment it is additionally influenced by the characteristics of the environmental compartment such as the prevailing pH value, salinity or ionic strength but also by the chemical behavior of the pollutant which sorbs to the MP (Fred-Ahmadu et al. 2020).

As most MPs and PAHs found in the environment have hydrophobic properties, the main driving force of their interaction are hydrophobic interactions, i.e. interaction between two non-polar substances, or π-π interactions, i.e. stabilization between aromatic compounds, causing PAHs to adsorb on the surface of MPs. Besides that, some studies also investigated the interaction of PAHs and MPs on the basis of pore filling as the more dominant mechanism (Bakir, Rowland, and Thompson 2012). When it comes to mixtures of pollutants, the situation gets even more complex, as sorption is not caused by one major mechanism anymore. Thus, most published works focus on the sorption of single substances or bi-solute systems to different MP compounds. For that, three different sorption models, i.e. linear, Freundlich and Langmuir are most commonly used. The linear model is based on a linear relationship and describes hydrophobic interactions and van der

Waals processes best, while the Freundlich and Langmuir models are more complex. The Freundlich isotherm model is based on an exponential fit and describes both linear and nonlinear sorption of a multilayer system on a heterogeneous surface. The Langmuir isotherm model is defined by five different linearized Langmuir isotherm models, all of them describing a monolayer sorption process to homogeneous surfaces.

Zhang et al. investigated the sorption of five PAHs to three different polymer types, i.e. polyurethane (PT), polyurea (PU) and urea-formaldehyde (UF), which are commonly used in pesticide encapsulation (Zhang et al. 2020). All sorption profiles showed an initial rapid portion of PAH sorption to the individual polymers followed by gradually reaching an equilibrium (Zhang et al. 2020). Among the investigated polymer types, PU showed the highest sorption coefficient, followed by PT and UF. The authors further postulate, that the main cause of different sorption capacities among polymer types can be attributed to differences in their textures (Zhang et al. 2020). Bakir et al. (2012), investigated competitive sorption effects of a bi-solute systems including phenanthrene and DDT to plasticized polyvinyl chloride (PVC) and ultra high molecular weight PE. They did not only report a competitive sorption behavior of those compounds, moreover they postulate that pore-filling processes take place during the sorption process (Bakir, Rowland, and Thompson 2012). Sorption coefficients of PAHs to different polymer types are listed in **Table 14**.

Most sorption experiments are done under well-defined lab-conditions (e.g. Lee, Shim, and Kwon 2014, Seidensticker et al. 2017, Wang and Wang 2018), while only a limited number of works refers to sorption experiments of organic pollutant to MPs realized within field-measurements (Rochman et al. 2013). Rochman et al. (2013), for example, investigated the affinity of marine plastic pollution to organic contaminants realized within a long-term field measurement experiment. Higher PAH sorption abilities have been reported for PE and PP, while lower ones were found for PET or PVC (Rochman et al. 2013). Besides that, the PAH content reaches an adsorption equilibrium after a certain time which is of special importance in terms of accumulation and bioavailability (Rochman et al. 2013). Similar findings have been presented within lab-testing (Zhang et al. 2020). As parameters used for lab experiments often differ to the ones occurring in the environment (e.g. seasonality, oxidative conditions, pH, salinity, presence of co-occuring substances, microorganism), attention has to be given when extrapolating adsorption/desorption results to various environmentally important compartments (Wang et al. 2020).

Sorption and desorption kinetics are important mechanism controlling the bioavailability, bioaccumulation and toxicity of MPs and their sorbed pollutants (Wang et al. 2020). The variety of parameters influencing the adsorption of PAHs to MPs also applies to desorption processes. Desorption of pollutants is mainly influenced by particle size, polymer type, residence time and partitioning coefficients (Seidensticker et al. 2017), and pollutant specific properties such as the molecular structures (e.g. functional groups, special structure and hydrophobicity) (Wang et al. 2020).

Table 14. Review of already published sorption coefficients of different PAHs to a variety of polymer types. All sorption coefficients were measured within sorption experiments under well-defined conditions (i.e. lab experiments). K_{OC} refers to the sorption coefficient normalized to the OC content and was calculated as the following: $K_{OC} = K_d/f_{OC}$, whereas f_{OC} represents the organic carbon content. Abbreviations: PU = polyuria, PT = polyurethane, UF = urea-formaldehyde resin, PE = polyethylene, PS = polystyrene, PVC = polyvinylchloride.

Reference	PAH congener	Polymer type	Sorption coefficient normalized to OC content K_{oc} (L/kg)	Sorption coefficient K_d (L/kg)	Sorption model
(Zhang et al. 2020)	Naph	PT	$1.41*10^4$	$1.01*10^4 \pm 1.88*10^2$	linear
	Naph	PU	$2.81*10^4$	$1.71*10^4 \pm 5.74*10^2$	linear
	Naph	UF	$1.4*10^4$	$8.11*10^3 \pm 1.34*10^2$	linear
(Guo et al. 2012)	Naph	PE	$5.14*10^2 – 9.35*10^2$		Freundlich model
(Zhang et al. 2020)	Phen	PT	$1.32*10^5$	$9.49*10^4 \pm 1.33*10^3$	linear
	Phen	PU	$4.80*10^5$	$2.94*10^5 \pm 1.53*10^4$	linear
	Phen	UF	$1.42*10^5$	$7.96*10^4 \pm 2.02*10^3$	linear
(Guo et al. 2012)	Phen	PE	$9.93*10^3 – 14.8*10^3$		Freundlich model
(Zhang et al. 2020)	Pyr	PT	$1.75*10^5$	$1.26*10^5 \pm 3.08*10^3$	linear
	Pyr	PU	$1.19*10^6$	$7.30*10^5 \pm 2.05*10^4$	linear
	Pyr	UF	$1.94*10^5$	$1.09*10^5 \pm 1.00*10^3$	linear
(Wang and Wang 2018)	Pyr	PE		$11.7*10^3$	Freundlich model
	Pyr	PS		$5.8*10^3$	Freundlich model
	Pyr	PVC		$5.9*10^3$	Freundlich model

5.3. The relationship between PAHs and single polymer types at an urban sampling site in Austria

Results presented in this section refer to sample from the urban sampling station Graz Don Bosco. Filters have also been used within a different research focus, whereas an excerpt of the obtained results has been presented in **chapter 3** and also within a peer reviewed publication (Kirchsteiger et al. 2020). Differently to the results presented in **chapter 3**, results presented in this section refer to 24 h samples and no grouping of filters to sample pools was performed. All results presented in this section were measured independently and ultrafine microplastics and nanoplastics (<2.5 µm

aerodynamic diameter, UFMNP) was quantified using the TD-PTR-ToF-MS method, while particle-bound PAHs were quantified using the modified GC-MS method.

A manuscript related to the results presented in **chapter 5** has been recently been submitted to the *Journal of Hazardous Materials*.

5.3.1. Sampling site, PM concentration and sample classification

$PM_{2.5}$ sampling was done at an urban sampling station in Graz Don Bosco (hereinafter referred as GDB) and Bockberg (hereinafter referred to as BB). The time period of interest covers the time from 02.01.2017 to 31.03.2017. Details about the sampling methods and the sample pretreatment can be found in **section 4.2.1**. A detailed evaluation of the $PM_{2.5}$ and PM_{10} concentration is given in **section 4.2.3**. And a more detailed description on PM data, chemical analysis and macro-tracer based source apportionment of grouped samples is presented in Kirchsteiger et al. (2020) (Kirchsteiger et al. 2020). Samples discussed here and in **section 4.2.** refer to the same sampling locations and time period, but differently to results presented earlier, here we focus on a daily evaluation.

As explained in **section 4.2.3**, we identified time periods influenced by different source contributions, i.e. long range transport or local sources using a rather simple approach based on differences in PM_{10} concentration determined at GDB and BB. Different to the two scenarios presented in **section 4.2.3.**, now samples were classified in 'local', 'unassigned' and 'regional'. By doing so, the sub-groups 'local' and 'regional' consist of 10 samples, while 9 samples are regarded as unassigned (mass ratio between 1.5 and 2). A summary listing the sample size, median PM_{10} and $PM_{2.5}$ concentrations as well as the observed PM_{10} ratios between GDB and BB are given in **Table 15**.

Table 15. Sample size and median PM_{10} and $PM_{2.5}$ concentrations as well as PM_{10} GDB/BB ratios for the three assigned subclasses. Results refer to the median value and minimum and maximum observed values are given in brackets. Note that the sample size changes in terms of PAH quantification, as 6 samples were not available for analysis.

	local	**unassigned**	**regional**
sample size (n)	10	9	10
median PM_{10} concentration ($\mu g/m^3$)	24.6 (16.6 – 96.3)	67.5 (31.0 – 95.1)	83.9 (25.4 - 140)
median $PM_{2.5}$ concentration ($\mu g/m^3$)	17.6 (11.4 – 68.6)	54.2 (18.5 – 73.6)	64.1 (19.5 - 120)
PM_{10} ratio (GDB:BB)	2.37 (2.09 – 2.87)	1.73 (1.53 – 1.99)	1.21 (1.09 - 1.50)

5.3.2. Atmospheric concentrations of particle-bound PAHs

Particle-bound PAH concentrations showed a decreasing trend following a general seasonal pattern and peak concentrations were found on days during January (see **Figure 19** A). In general, total PAH concentrations, hereinafter referred as $\sum_{23}$PAHs, were in the range of 5.25 – 25.4 ng/m^3, with average concentrations of 13.6 ng/m^3. However, PAH concentrations showed a distinct drop during the first days of sampling in January. Lowest PAH contributions were found on the

06.01.2017 ($\sum_{23}$PAH = 5.25 ng/m^3), which was a day accompanied by minimum $PM_{2.5}$ concentrations (11.4 µg/m^3). Highest $\sum_{23}$PAH concentrations were found on 21.01.2017 (25.4 ng/m^3), which was not the day accompanied by lowest temperature (-5.1°C). A seasonal trend of total PAH concentrations is very well known and in accordance with European findings (e.g. Manoli et al. 2016, Khan et al. 2018, Pietrogrande et al. 2022) and mainly caused by higher tendency for residential heating due to cold temperatures, but also highlights the importance of the prevailing meteorological conditions favoring temperature inversion. Among European cities, mean PAH concentrations show a rather diverse picture, e.g. ∑PAH concentrations of 72.8 ±16.6 ng/m^3 were observed during winter time (i.e. December 2018 – February 2019) in Milan (Hakimzadeh et al. 2020), or urban ∑PAH concentrations of up to 112 ng/m^3 were observed during November at an urban area in Poland (Trusz, Ghazal, and Piekarska 2020). On the contrary clearly lower mean $\sum_{13}$PAH concentrations 11 ± 5.3 ng/m^3 were observed during the cold period (i.e. Feb – March 2012) at an urban traffic site in Thessaloniki (Manoli et al. 2016) or in Italy were $\sum_{8}$PAH concentrations yielding 20.9 ± 14.4 ng/m^3 were observed during winter time (2012-2013) (Khan et al. 2018).

Investigating PAH contributions on the single congener level reveals that highest average PAH contributions were attributed to BbjkF (2.58 ng/m^3), while lowest average contributions were found for Per (0.18 ng/m^3). BaP concentrations were in the range of 0.18 – 2.14 ng/m^3, with peak concentrations observed on 21.01.2017, while lowest BaP concentrations were observed on the 06.01.2017. Comparisons of the overall PAH concentration with other studies is often very difficult as most studies refer to a different number of PAHs and sometimes also to a different congener combination. However, almost all studies quantify BaP, which is a known carcinogen (IARC 2010) and thus listed as priority compound by the US EPA. Average BaP concentrations (1.14 ng/m^3) observed in this study are higher than those reported in recent literature, which may be attributed to the fact that this work mainly focusses on days violating the European short-time limit value. Pietrogrande et al. (2022) reported BaP concentrations of 0.55 ± 0.11 ng/m^3 during winter time (Pietrogrande et al. 2022), while similar findings were reported at an urban traffic site in Thessaloniki with average winter-time BaP concentrations of 0.86 ± 0.43 ng/m^3 (Manoli et al. 2016).

The PAH variability in relation to the $PM_{2.5}$ mass throughout the study period was evaluated using the mass ratio of $\sum_{23}$PAH/$PM_{2.5}$ (see **Figure 19** B). The contributions of PAHs to the overall $PM_{2.5}$ mass were in the sub-‰ range, varying between 0.13 – 0.68 ng/µg. Still, the first days of January (05.01. – 08.01.2017) showed some differences, as $\sum_{23}$PAH/$PM_{2.5}$ ratios increased reaching its maximum of 0.68 ng/µg on the 07.01.2017, followed by a rapid drop to 0.39 ng/µg on the next day (08.01.2017). A similar situation was again observed in late February with $\sum_{23}$PAH/$PM_{2.5}$ ratios of 0.66 ng/µg (24.02.2017) again followed by a drop the next day (0.49 ng/µg). A seasonal trend of the PAH/PM can be attributed to meteorological conditions favoring pollutant accumulation during winter time, e.g. stagnant weather conditions, limited ventilation and cold ambient temperatures (Masiol et al. 2013, Khan et al. 2018). This holds true for the situation observed on the 24.02.2017, where a local temperature inversion was identified (Kirchsteiger et al. 2020). High $\sum_{23}$PAH/$PM_{2.5}$ ratios observed on the 07.01.217, however, could not be linked to local temperature inversion (Kirchsteiger et al. 2020).

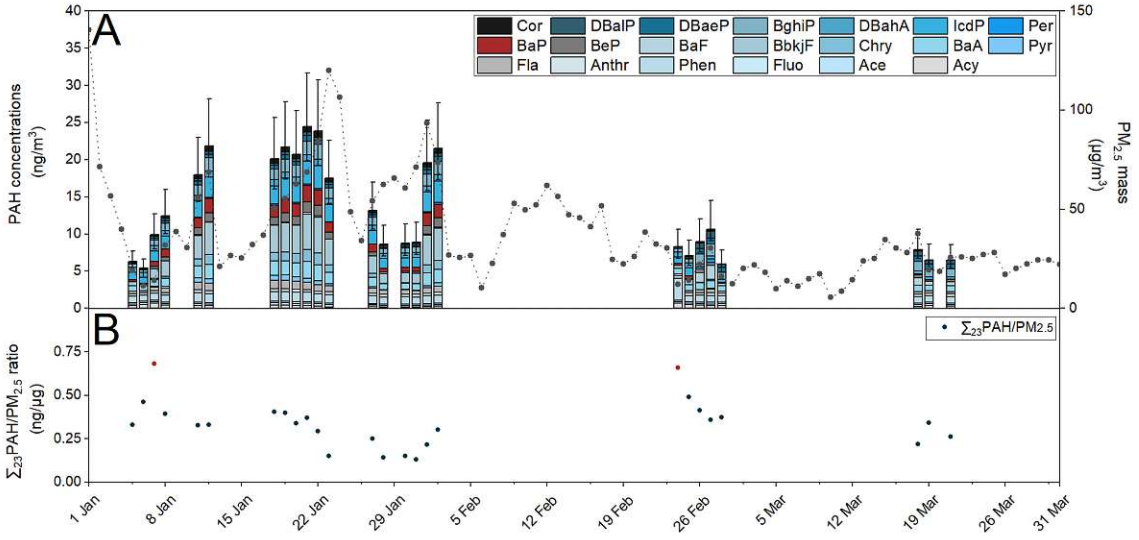

Figure 19 A-B. (A) $PM_{2.5}$ mass (µg/m³) and particle-bound PAH concentrations (ng/m³). Each congener is highlighted in a different color. Error bars represent the measurement uncertainty of ± 30%. **(B)** PAH variability visualized as the $\sum_{23}PAH/PM_{2.5}$ ratio throughout the sampling period of 02.01. – 31.03.2017. Red dots highlight the highest observed $\sum_{23}PAH/PM_{2.5}$ ratios.

5.3.3. Toxic risk assessment of particle-bound PAH concentrations

Overall toxicity of daily samples was evaluated by calculating the respective BaP equivalent (BaP_{eq}) concentrations (for further details **see section 1.2.5.**). For that, toxic equivalency factors presented by Larsen and Larsen were applied (Larsen and Larsen 1998). Differently to results presented in **section 4.3.5.**, here we present a toxicity assessment for daily $PM_{2.5}$ samples and differences among the beforehand assigned classes, i.e. local, unassigned and regional.

BaP_{eq} concentrations followed the same seasonal trend observed for PAH concentrations, i.e. higher BaP_{eq} concentrations were observed during sample days of January and they increased with proceeding time ranging from 0.99 – 4.69 ng/m³. Highest BaP_{eq} concentrations were observed on the 21.01.2017 and lowest one on the 28.02.2017. Comparing the BaP_{eq} concentrations for samples among the beforehand assigned classes presents some differences. Samples of the 'unassigned' class showed highest average BaPeq concentrations of 3.07 ng/m³, followed by the 'regional' class (BaP_{eq}=2.47 ng/m³), whilst lowest average BaP_{eq} concentrations were observed within the 'local' class (2.13 ng/m³). Higher BaP_{eq} concentrations observed for the 'regional' class than among 'local' samples may be attributed to additional input of pollutants due to regional transport of air masses, while the local input stagnates. Among classes, BaP_{eq} concentrations scatter in a similar range, i.e. 1.09 – 4.69 ng/m³ (unassigned), 1.09 – 4.56 ng/m³ (regional) and 0.99 – 4.22 ng/m³ (local).

5.3.4. Atmospheric concentrations of ultrafine micro- and nanoplastics

During the time period of interest, ultrafine microplastics and nanoplastics <2.5 µm aerodynamic diameter (UFMNP) averaged at 238 ng/m³ (ranging from 16.7 to 557 ng/m³) (n=29). The average

mass contribution of UFMNP to $PM_{2.5}$ is 0.67%, with maximum contributions of 1.9%, while the average contributions of OM and EC came up to 38 and 5.7%, respectively (visualized in **Figure 20** A). The remaining $PM_{2.5}$ mass, which is not explicitly mentioned here, was mainly inorganic ions and mineral dust. A detailed chemical evaluation and source apportionment of samples representing this time period is presented elsewhere (Kirchsteiger et al. 2020). Throughout this section we discuss the fraction of organic matter (OM), which is derived by the applying a conversion factor to the OC concentration. The applied conversion factor (1.5) corroborates with conversion factors solely focussing on the polymer types. Based on the molecular structures of the three key polymers conversion factors are: 1.60 (OC solely consist of PET) and 1.17 (OC solely consists of PP or PE). Focussing on a mix of organic compounds we applied a conversion factor of 1.5 (i.e. OM = 1.5*OC). This conversion factor is based on studies conducted in Europe and the US and has already been applied in Kirchsteiger et al. (2020) (Kirchsteiger et al. 2020). The contribution of UFMNP to OM reaches an average value of 1.7% and a maximum value of 4.5%, (see **Figure 20** B). **Figure 20** C depicts the average polymer type contributions considering all analysed samples. A timeline of measured UFMNP sub grouped in the individual polymer types is given in **Figure 20** D. A list of atmospheric concentrations of all key components discussed is given in **Figure 20**. In contrast to $PM_{2.5}$ mass UFMNP concentrations did not show a declining trend from January to March (see **Figure 20** D). Peak UFMNP concentration occurred during the time period of 18.01. – 23.01. 2017, but also in February and March. High UFMNP concentrations observed during the first time period, i.e. 18.01. – 22.01.2017 were accompanied by rather high $PM_{2.5}$ concentrations (50.7 – 83.9 µg/m^3), while this was not the case for the samples from late February and March ($PM_{2.5}$: 22.1 – 37.6 µg/m^3). Interestingly UFMNP concentrations determined from 23.01. – 02.02.2017 were rather low, although $PM_{2.5}$ reach even higher values than in the preceding period of 18.01.-22.02.2017. Lowest UFMNP concentrations could be observed on the 06.01.2017 with 16.7 ng/m^3, when overall $PM_{2.5}$ was also a minimum (11.4 µg/m^3).

Different detected polymer types refer to polyethylene terephthalate (PET), polypropylene (PP) and polyethylene (PE), which are among the most demanded polymer types in Europe and mainly used for packaging, building and construction purposes (Plastics Europe 2021). The occurrence of these three types of polymers agrees with data reported previously from cities in France and China (Dris et al. 2016, Cai et al. 2017) or for background environments (Allen et al. 2022), which all report important contributions of PET, PP and PE in deposited nano to microplastics. We did not find other emerging polymer types such as polystyrene or polyvinyl carbonate in our samples. However, relative contributions of different polymer types observed in atmospheric deposition samples varies within a yearly timeline (Allen et al. 2022).

PET was found to be the most prominent polymer in the urban $PM_{2.5}$ samples. It was found in the majority of samples (n=25), contributing on average 50% to the overall UFMNP mass (see **Figure 20** C). The atmospheric concentrations of PET ranged from 10.6 to 256 ng/m^3. In 2020, PET demand in Europe was more than 4 million tonnes which accounts for 8.4% of all polymer types used (Plastics Europe 2021).

The number of matches for PP and PE in the urban $PM_{2.5}$ samples was lower, although PP and PE are the top two demanded polymer types in Europe, with demands of more than 14 and 9 million tonnes, respectively (Plastics Europe 2021). Considering these two polymer types, PP was found in a larger number of samples (n=16) than PE (n=12) with relative contributions accounting for

27 (PP) and 23% (PE) of the overall UFMNP mass. The atmospheric concentrations of PP were in the range of 8.49 to 326 ng/m^3, while slightly lower ones were observed for PE, ranging from 8.16 to 290 ng/m^3 (n=12).

Polymer patterns seem to change with proceeding time indicating that also source impacts or transport and transformation processes within the atmosphere change. Changes are particularly evident at the end of January, when only PET was identified, although $PM_{2.5}$ concentrations were rather high. Starting on 20.01.2017 and lasting end of January a winter episode of high pollution occurred across Europe, accompanied with long-range transport of PM (EEA 2019). Samples derived later, i.e. during February and March show a more diverse contribution of polymer types and PP and PE becoming more abundant than PET. We cannot give a reason for these differences in polymer patterns currently, but there is evidence that this effect was visible at a larger scale. Materić et al (2021) analysed nanoplastics deposited onto the snow cover at a remote site in the Austrian Alps (Sonnblick Observatory) (Materić et al. 2021). The observation time covered 26.02. -20.03.2017 and thus the second half of the measurements presented here. Only PET was determined until 25.02.2017, while later samples showed PP concentrations being more dominant (Materić et al. 2021). This PET dominated period, of which we unfortunately do not have any measurements, directly follows our PET period. Still another high pollution episode is reported from 09.02.-17.02.2017 (EEA 2019).

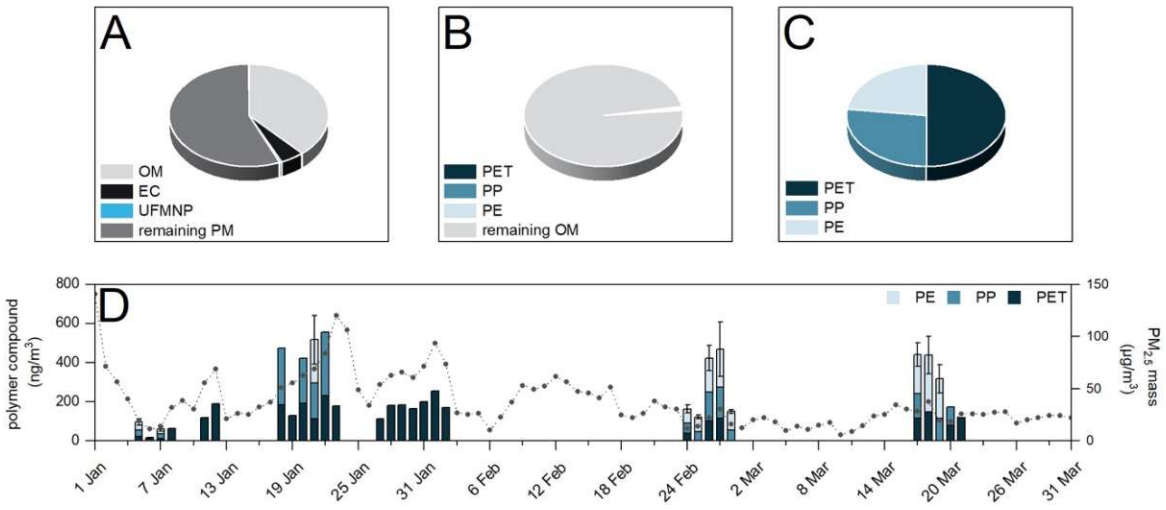

Figure 20 A-D. (A) Average $PM_{2.5}$ composition with focus on the carbonaceous fraction, **(B)** average contributions of the individual polymer types with special focus on the fraction of organic matter (OM) and **(C)** average polymer type contribution to the overall UFMNP mass for all samples. **(D)** Atmospheric UFMNP and $PM_{2.5}$ concentrations observed throughout the sampling period. Error bars at UFMNP concentration represent the measurement uncertainty of ± 30%.

5.3.5. Differences of key analytes between the assigned classes

Figure 21 A presents the atmospheric $PM_{2.5}$ concentrations grouped according to the three different classes, i.e. local, unassigned and regional. Visual investigation of the boxplot already points out that $PM_{2.5}$ concentrations of the regional class were higher (median: 64.1 µg/m^3) than the ones observed for samples of the local (median: 17.6 µg/m^3) and unassigned class (median:

54.2 µg/m^3). Statistical evaluation of the $PM_{2.5}$ concentration based on one-way ANOVA strengthened this indication and identified a significant difference among those classes (F-value = 4.949, p-value = 0.0151). Statistical evaluation was also done for the individual polymer types, UFMNP and PAH and BaP concentrations observed among classes.

Figure 21 B presents the boxplot of atmospheric PET concentrations for the local, unassigned and regional data sets, yielding median concentrations of 31.5 ng/m^3, 113 ng/m^3 and 180 ng/m^3, respectively. We could observe a significant difference of atmospheric PET concentrations between the assigned classes (F-value = 4.565, p-value = 0.0204) and median concentrations followed the trend of the overall picture of $PM_{2.5}$. In case of the other two quantified polymer types, median concentrations were quite different. PP was identified as the second most abundant polymer type (see **Figure 21** C) and was mostly found in samples assigned to the local class, yielding median concentrations of 40.5 ng/m^3 (local). Still, several samples of the other classes missed PP. Therefore, investigation of the whole data set (mostly consisting of zero values) covering a concentration rang from not detectable (n.d.) to 230 ng/m^3 and n.d. to 326 ng/m^3 for both, the unassigned and regional class. Nevertheless, samples matching for PP showed maximum concentrations, like 230 ng/m^3 (unassigned class) and 326 ng/m^3 (regional class). The same situation can be observed for PE. Again, PE was mainly found in local samples (n=7) resulting in median concentrations of 33.3 ng/m^3 (maximum: 195 ng/m^3). Some samples assigned to the unassigned and the regional class, again showed concentrations below the limit of detection and among samples in which we could find PE, maximum values were determined, yielding concentrations of 221 ng/m^3 (unassigned class) and 290 ng/m^3 (regional class). For both, PP and PE, we could not detect a statistical difference among classes using one-way ANOVA. Also, for UFMNP no significant difference between the assigned classes could be observed. Median concentrations were 136 ng/m^3 (local), 170 ng/m^3 (unassigned) and 228 ng/m^3 (regional) and thus follow the same trend as $PM_{2.5}$ concentrations.

Differences in $\sum_{23}$PAH and BaP concentrations among the beforehand assigned classes are depicted in **Figure 21** F-G. By tendency, samples assigned to the unassigned class showed higher median PAH concentrations (median $\sum_{23}$PAH concentration of 17.5 ng/m^3) than those found in samples assigned to the local or regional assigned samples accounting median $\sum_{23}$PAH concentrations of 8.80 and 9.16 ng/m^3. The same holds true for BaP, the most studied PAH congener and a known carcinogen. Highest median BaP concentrations were found among samples assigned to the unassigned class (1.36 ng/m^3), followed by samples assigned to the regional class (0.53 ng/m^3), whilst lowest median BaP concentrations were observed within samples assigned to the local class (0.33 ng/m^3). Within all three classes, some samples did not show quantifiable amounts of BaP, all of them occurred at the end of the sampling period (26.02. – 21.03.2017). No statistical difference among classes based on one-way ANOVA could be identified for both, the $\sum_{23}$PAH and BaP concentrations.

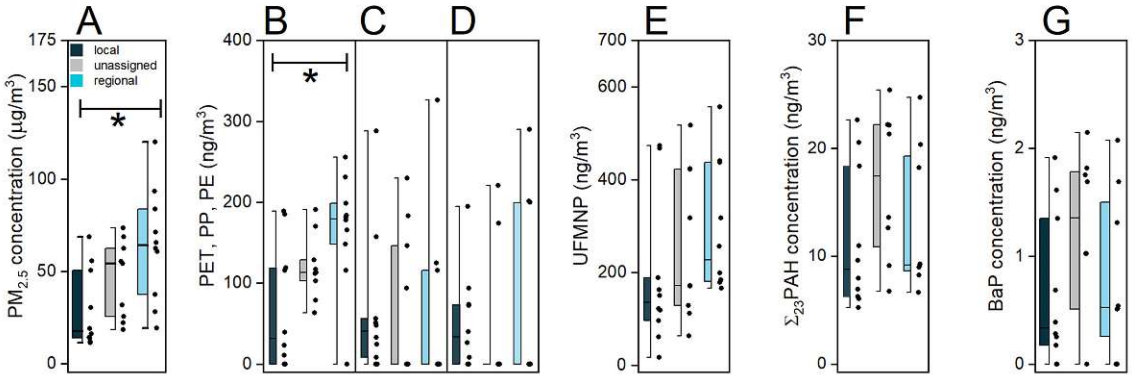

Figure 21 A-G. Comparison between three different classes, i.e. local, unassigned and regional, based on the atmospheric **(A)** $PM_{2.5}$ concentrations and of quantified **(B-D)** polymer types, **(E)** UFMNP and micro constituents of PM, i.e. **(F)** $\sum_{23}$PAHs and **(G)** BaP as PAH marker substance. Observations of one class are always displayed as boxplot accompanied by the data points itself (black dots). Statistical data analysis was done using one-way ANOVA (for PET and UFMP) or two-sample t-test (for PP and PE, only for local and unassigned classes). Differences were considered as significant when p-value < 0.05, and are highlighted with "*".

5.3.6. Correlations of polymer types with $PM_{2.5}$ mass, OM and EC

Spearman rank coefficients (ρ) were used to investigate the relationship between the polymer types and $PM_{2.5}$ mass as well as PM macro constituents. As the single polymers could not be quantified in every sample, samples yielding zero values were excluded from correlation analysis.

Figure 22 A-F presents the correlations with $PM_{2.5}$, OM and EC showing Spearman rank coefficients $\rho > 0.8$ and p-values < 0.05 which were considered as significantly high monotonic ones.

PP shows significantly high monotonic correlations with $\rho > 0.8$ with all macro constituents. For PP the data set refers to a sample size of 15 samples including all classes, though the data set of the regional and unassigned classes is markedly reduced, as several samples showed readings below the detection limit. Highest significant correlations were observed between PP and OM (ρ=0.97). PE concentrations (n=12) show significantly high monotonic correlations with $PM_{2.5}$ mass (ρ=0.89) and OM (ρ=0.88). EC is also significantly correlated, but yielded a Spearman rank coefficient slightly below 0.8 (ρ=0.76). Again, the data set for regional and unassigned samples is markedly reduced. In case of PET, the most abundant polymer, the most comprehensive data set could be evaluated. PET showed significant monotonic correlations with all target compounds, i.e. OM (ρ=0.78) and EC (ρ=0.53) but only the correlation with the $PM_{2.5}$ mass (ρ=0.81) exceeded $\rho > 0.8$, thus being highly correlated. For all polymers it is possible to summarize all data points with one trend line. As soon as the polymer is detectable, the correlations with $PM_{2.5}$, OM or EC are consistent for all samples.

UFMNP showed weak correlations with all target compounds, i.e. $PM_{2.5}$ (ρ=0.45), OM (ρ=0.46). With exception of EC (ρ=0.51), no significant monotonic relationship was found. The data set seems to be separated into two, which is mainly caused by the fact, that we could not quantify each single polymer in all of the samples, i.e. higher UFMP concentrations represent samples matching the fingerprints of more than one polymer, while lower concentrations are the samples

missing PP and/or PE. These findings highlight the importance of analysing and interpreting individual polymer types.

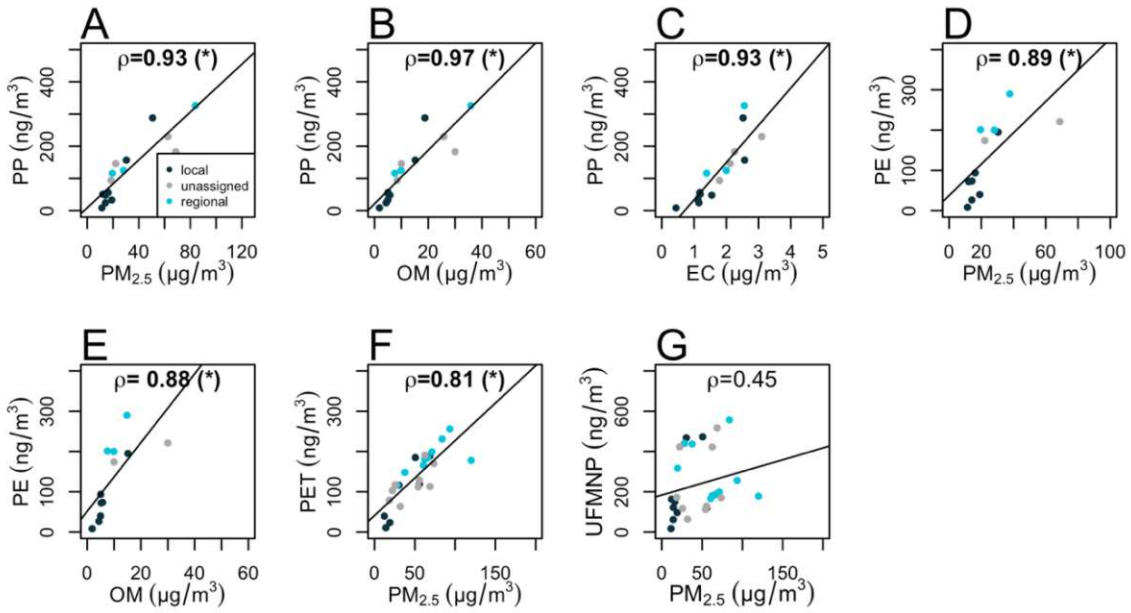

Figure 22 A-G. Intercomparison of quantified compounds, i.e. PP, PE and PET and UFMNP with $PM_{2.5}$, OM and EC classified in local (dark blue points), unassigned (grey points) and regional (light blue points) episodes. (*) Highlighted Spearman's rank coefficients mark correlations with a p-value <0.05 were considered as significantly monotonic.

5.3.7. Correlations of polymer types with individual PAH congeners

Significantly high monotonic correlations between polymers and PAH congeners are given in **Figure 23** A-I, highlighting correlations with $\rho > 0.8$ and p-values < 0.05.

Among all polymer types, PP concentrations showed the highest number of significant and high correlations with single PAH congeners. These are found for PP and the highly toxic and carcinogenic high molecular weight (HMW) congeners BaA (ρ=0.82), BeP (ρ=0.84), BghiP (ρ=0.90) and DBaiP (ρ=0.90). Also, PP significantly correlated with two low molecular weight (LMW) PAHs, i.e. Acy (ρ=0.82) and Anthr (ρ=0.94). Again the assignment to sample classes does not effect the correlation between polymer and PAH congener, as long as the polymer is detected. Besides a significant correlation of PE with the LMW congener Anthr (ρ=0.89), PE also highly correlated with three HMW PAHs, i.e. BghiP (ρ=0.84), and two of the dibenzopyrene isomers, i.e. DBaeP (ρ=0.83) and DBaiP (ρ=0.81). Interestingly, we did not find a significant correlation among PE and 135TPB, which has been recently used as a tracer substance of the combustion of PE in atmospheric samples (e.g. Simoneit, Medeiros, and M. 2005, Islam et al. 2020, Furman et al. 2021). 135TPB is structurally very different to PAHs as it does not consist of fused benzene rings and thus does not belong to the group of PAHs. We included it in our analyses to get a first impression whether a possible correlation between polymers and PAH congeners could be due to joint emissions during plastic combustion. As no correlation between 135TPB and PE was obtained, a co-emission during combustion seems to be unlikely for our samples. Although PET

was the most abundant polymer type, no significant monotonic correlation among PET and any of the PAH congeners could be observed. These findings agree with previously reported results for aquatic systems, where it was mentioned that PE and PP show higher sorption abilities than other polymers (Rochman et al. 2013, Fotopoulou and Karapanagioti 2015). Differences in sorption behavior of the individual polymer types may be attributed to their differences in molecular structure. Rubbery polymers such as PE and PP tend to sorb higher amounts of pollutants (Rochman et al. 2013), due to their flexible and expanded structure which is concomitant with a higher accessibility and permeability for partitioning of hydrophobic substances (Wang et al. 2020). Conversely, glassy polymer types such as PET show lower sorption capacity (Rochman et al. 2013), due to their dense and highly cross-linked structure (Wang et al. 2020).

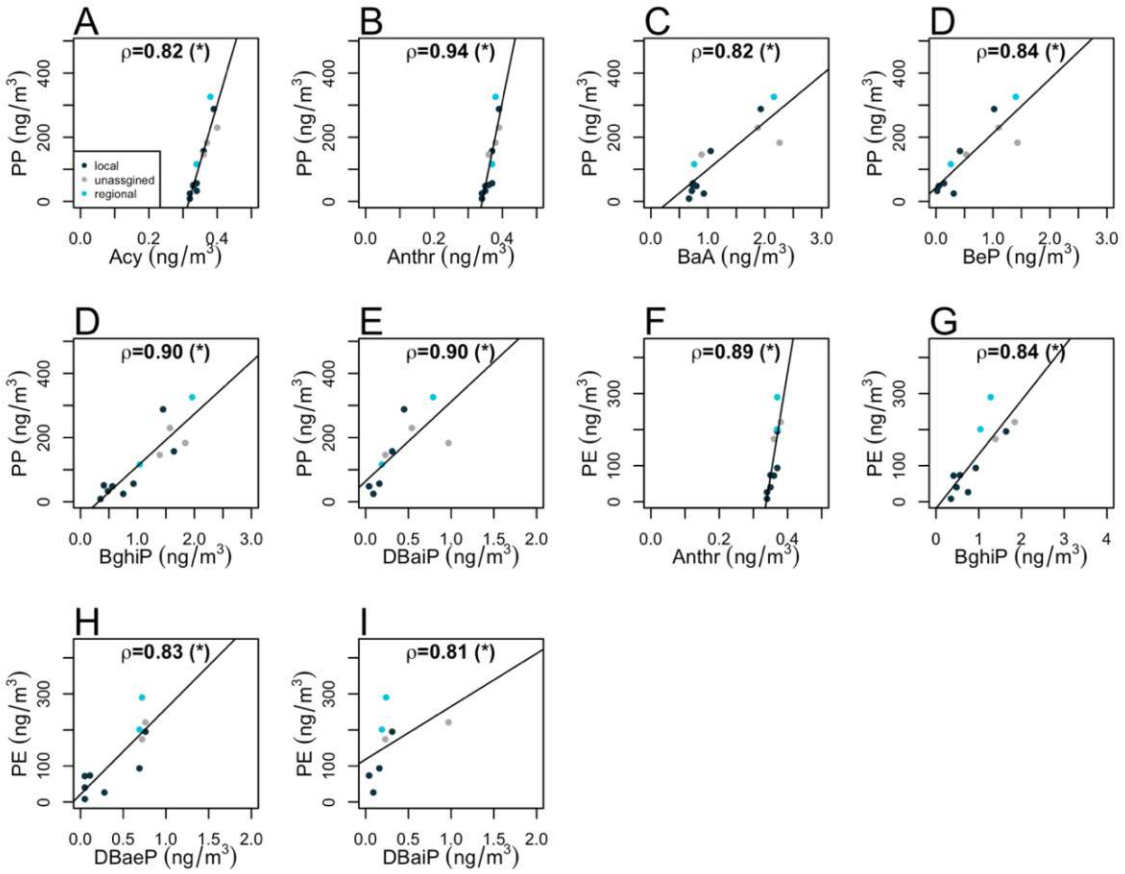

Figure 23 A-I. Intercomparison of quantified PP and PE concentrations with those of individual PAH congeners. Note, that this figure only highlights significantly high monotonic correlations with Spearman rank coefficients >0.8 and p-values < 0.05. Sampling days for each assigned class are highlighted in different colors, i.e. local (dark blue points), unassigned (grey points) and regional (light blue points).

Grouping PAH congeners according to their molecular weight, i.e. LMW versus HMW PAHs, indicates that correlations are more likely for LMW than for HMW PAHs. We quantified five different LMW PAHs and two of them showed significantly high monotonic relationships with PP and PE, while for HMW PAHs only five out of 18 congeners significantly correlated with the respective polymer types. The correlations given in **Figure 23** for LMW PAHs are more pronounced than the respective relations between PAHs and OM or EC, again pointing to special interactions between UFMNP and organic and toxic pollutants. For HMW PAHs this behavior is

less pronounced. Correlations between BaA, BeP, BghiP and DBaiP with EC is similar or even more pronounced compared to the conditions reported in **Figure 23**. Possibly, LMW PAHs utilize polymers as carrier in the environment, while HMW PAHs, which are preferably found in the particle-phase do not rely on such a vehicle.

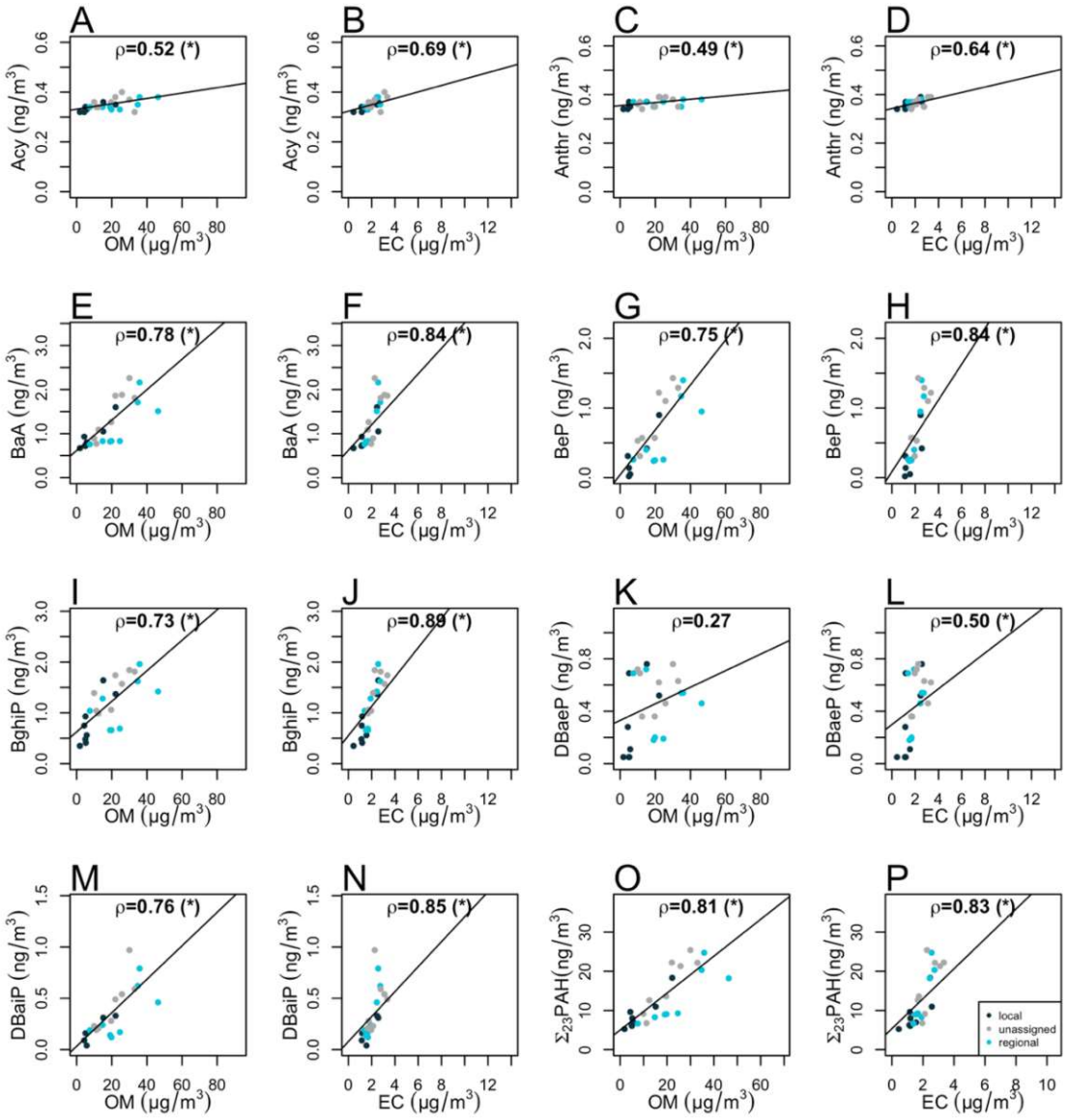

Figure 24 A-P. Intercomparison of PAH congener and the overall $\sum_{23}$PAH concentrations with the concentrations of organic matter (OM) and elemental carbon (EC). Sampling days for each assigned class are highlighted in different colors, i.e. local (dark blue points), unassigned (grey points) and regional (light blue points). (*) Highlighted Spearman's rank coefficients mark correlations with a p-value <0.05 were considered as significantly high monotonic.

5.4. Environmental implications, conclusion and outlook

The main source of airborne plastic compounds are, among others, abrasion products of synthetic textiles, furniture, tires or dust. Once macro plastics enter the environment, they undergo a variety of transformation mechanism, e.g. photooxidation and abrasion which leads to a loss of mechanical integrity and stability as well as changes in chemical behavior (Fotopoulou and Karapanagioti 2015). To date, MPs have been reported in nearly all environmental compartments. The detection of ultrafine microplastics and nanoplastics (UFMNP) in urban particulate matter samples widens the palette of environmental compartments in which plastic particles have been reported. Our results present, for the first time, atmospheric concentrations on the level of single polymer types. By analysing 29 daily $PM_{2.5}$ samples within the time period of 02.01. – 31.03.2017, we were able to quantify atmospheric concentrations of three emerging polymers, i.e. polyethylene terephthalate (PET), polypropylene (PP) and polyethylene (PE). Among those, PET has been identified as the most prominent polymer type accounting for 50% of the overall UFMNP mass, while polypropylene (PP) and polyethylene (PE) accounted for 27% and 23%, respectively. On average, UFMNP compose 0.67% of the overall $PM_{2.5}$ mass. On the single polymer level, highest concentrations amount for 256 ng/m^3 (PET), 326 ng/m^3 (PP) and 290 ng/m^3 (PE). These findings clearly highlighting the emerging role of polymer compounds in atmospheric samples.

Although MPs and PAHs are totally different compound classes, they show similarities in very environmentally important key variables, i.e. persistency, ubiquitous occurrence and negative health outcomes. As several studies already reported the ability of PAH sorption to MPs, there is a growing need in investigating this relationship and present a first step towards the understanding of their combined impact on ecosystems. Therefore, we additionally quantified the atmospheric concentrations of 23 individual PAH congeners. Overall PAH concentrations were on average 13.6 ng/m^3. We identified significantly high monotonic correlations of PP and PE with single PAH congeners including highly toxic and carcinogenic ones (i.e. Acy, Anthr, BaA, BeP, BghiP, DBaeP and DBaiP). Although PET was the most abundant polymer type, no significantly high correlation was found among PAH congeners. These findings agree with results obtained from sorption experiments in aqueous systems, where higher abilities for PAH adsorption were found for PP and PE, than for other polymer types. It appears that correlations are more likely among LMW PAHs and polymer types than observed for HMW PAHs, indicating possible carrier activities of UFMNP for LMW PAHs. The present work is the first one discussing relationships of polymer compounds and PAHs found in urban particulate matter samples and highlights the importance of further studies to improve the understanding of polymers as PAH vehicles for atmospheric transport and the potential health outcomes.

Chapter 6 PAHs derived from surface snow samples

Shifting the focus from atmospheric PAH concentrations to the quantification of PAHs in the liquid phase is challenging and requires the modification or even development of novel quantification methods. Methodological basics of the analytical method used are presented in **Chapter 2**. **Section 6.1.** presents the development of a GC-MS/MS method used for first analysis of surface snow samples and gives insights in the obstacles observed during method development and the consequential changes such as setup and method modifications. **Section 6.2.** highlights the required changes and lessons learnt during the first attempt of PAH quantification from snow samples, while **section 6.3.** presents the actually realized changes and modifications, for both the sampling procedure and GC-MS/MS method in detail. Further this section presents the application of the modified method to surface snow samples from different locations in Austria. **Section 6.4.** discusses the results obtained from both sets of experiments with literature, while **section 6.5**. concludes this chapter and presents environmental implications and the toxic risk assessment of observed results.

A manuscript for publication of data presented within chapter 6 is in preparation.

6.1. Development of a sampling and quantification method for PAHs from surface snow samples – the first attempt

6.1.1. Details about the GC-MS/MS setup, temperature program and quantification method

PAH quantification derived from surface snow samples was realized using a GC-MS/MS setup by Thermo Fisher (more details about the used setup are given in **Table 3** in **section 3.1.**). Briefly, the column used for quantification was a commercially available ZB5MSplus column

(30 m x 0.25 mm x 0.25 µm) with 1 m of deactivated fused silica column used as a pre column. The inlet temperature was set at 300°C, operated in splitless with surge mode (169 kPa surge pressure) and a surge duration of 1 min.

In order to investigate a suitable temperature program we tested several ones given in literature (e.g. Cvetkovic et al. 2016, Jeffery et al. 2018). With the given instrumental setup we achieved the most sufficient resolution of individual PAHs with the following temperature program: Start temperature at 55° (hold time for 1 min), linear temperature gradient from 55°C to 320°C with a ramp of 20°C/min, hold time at 320°C for 8 min. As mobile phase we used He (5.0) with a flow rate of 1.5 mL/min. With the given temperature program it was possible to determine the concentration of 17 parent PAHs, 4 deuterated congeners and 135TPB in one chromatographic run (see **Figure 25**). Data acquisition was realized in timed method, using separate time windows for congener groups. Especially the separation of PAH isomers is analytically challenging. We did not achieve a sufficient separation of the benzofluoranthene isomers (i.e. BbF and BkF, highlighted in yellow) with the given setup. Thus, presented results refer to the sum of those isomers.

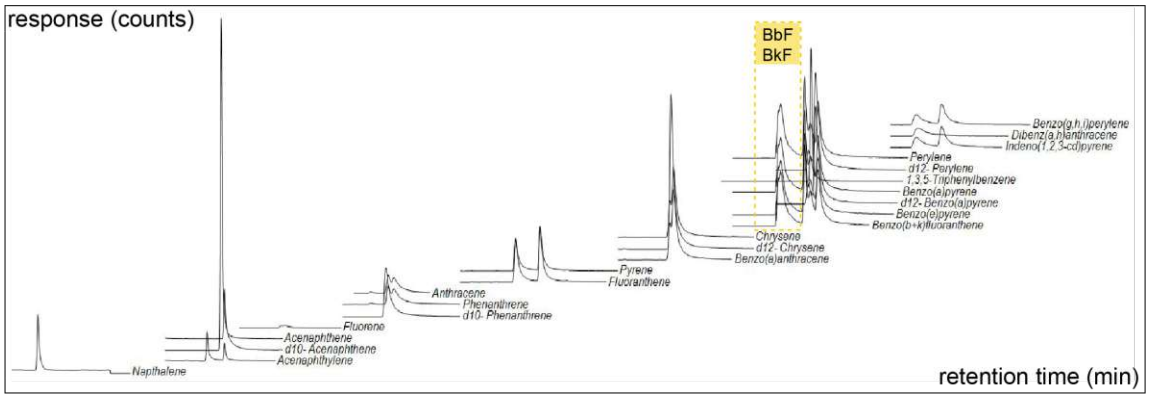

Figure 25. GC-MS/MS chromatogram of a calibration standard (4 µg/L) in multi-reaction monitoring (MRM) mode and timed acquisition. The yellow highlighted area marks the two benzofluoranthenes isomers (BbF and BkF). Note that axis miss ticks, the highest response observed during the depicted run was $6*10^6$ counts and the total run time was 22.25 min.

Table 16 lists all quantified PAH congeners, the chromatographic and mass selective parameters, i.e. precursor and product ion masses derived under given collision energies for the PAHs of interest. As quantification was realized using an internal standard calibration, **Table 16** additionally presents the grouping of individual PAH congeners based on the respective IST group (group 1: all PAHs within this group refer to the internal standard one, etc.). Calibration standards cover a concentration range from 0.1 to 49 µg/L.

Table 16. List of PAHs of interest for surface snow analysis including the retention time, precursor and product ion mass generated under the given collision energies.

	Analyte	Abbr.	Retention time (min)	Precursor ion mass	Product ion mass	Collision energy	IST group
p-PAHs	Naphthalene	Naph	5.80	128.1	77.1	30	1
				128.1	102.0	20	
	Acenaphthylene	Acy	7.70	152.1	102.0	30	1
				152.1	126.1	20	
				152.1	151.0	25	
	Acenaphthene	Ace	7.90	153.1	126.1	40	1
				153.1	151.1	40	
				154.0	152.0	35	
	Fluorene	Fluo	8.52	165.1	163.1	30	1
				166.1	164.1	30	
				166.1	165.1	40	
	Phenanthrene	Phen	9.70	178.1	152.1	25	2
				178.1	176.1	20	
	Anthracene	Anthr	9.80	178.1	152.1	25	2
				178.1	176.1	20	
	Fluoranthene	Fla	11.15	202.1	176.1	35	2
				202.1	200.1	30	
				202.1	201.1	20	
	Pyrene	Pyr	11.40	202.1	176.1	35	3
				202.1	200.1	30	
				202.1	201.1	20	
	Benzo(a)anthracene	BaA	12.90	228.1	114.1	60	3
				228.1	226.1	30	
	Chrysene	Chry	12.90	228.1	224.1	60	3
				228.1	226.1	30	
	Benzo(b)fluoranthene	BbF	14.10	252.1	248.1	60	3
				252.1	250.1	30	
	Benzo(k)fluoranthene	BkF	14.15	252.1	248.1	60	3
				252.1	250.1	30	
	Benzo(e)pyrene	BeP	14.40	252.1	248.1	60	4
				252.1	250.1	30	
	Benzo(a)pyrene	BaP	14.45	252.1	248.1	60	4
				252.1	250.1	30	
	Perylene	Per	14.55	252.1	248.1	60	4
				252.1	250.1	30	
	Indeno(1,2,3-cd)pyrene	IcdP	15.80	276.1	272.1	60	4
				276.1	274.1	40	

Table 16 continued. List of PAHs of interest for surface snow analysis including the retention time, precursor and product ion mass generated under the given collision energies.

	Analyte	Abbr.	Retention time (min)	Precursor ion mass	Product ion mass	Collision energy	IST group
p-PAHs	Dibenz(a,h)anthracene	DBahA	15.80	278.1	274.1	60	4
				278.1	276.1	30	
	Benzo(ghi)perylene	BghiP	16.15	276.1	272.1	60	4
				276.1	274.1	40	
RST	d_{12}- Benzo(a)pyrene	d_{12}-BaP	14.40	264.2	260.1	30	4
				264.2	264.2	40	
IST	d_{10}- Acenaphthene	d_{10}-Ace	7.86	164.1	160.0	30	1
				164.1	162.0	20	
				164.1	164.1	30	
	d_{10}- Phenanthrene	d_{10}- Phen	9.67	188.1	158.0	30	2
				188.1	160.0	30	
				188.1	188.1	30	
	d_{12}- Chrysene	d_{12}-Chry	12.90	240.2	236.1	30	3
				240.2	240.2	30	
	d_{12}- Perylene	d_{12}-Per	14.50	264.2	230.0	30	4
				264.2	260.0	30	
non-PAHs	1,3,5-Triphenylbezene	135TPB	14.00	306.0	289.0	40	4
				306.0	306.0	60	
				306.0	306.0	8	

6.1.2. Evaluation of blank samples

In order to evaluate possible contamination from the sampling process itself, we quantified the PAH content of the sampling equipment. Freshly fallen snow is only available in a rather short time window and as we aimed to investigate a big data set of samples including different sampling locations we had to partly outsource sampling and develop a rather simple but efficient sampling procedure. Thus, surface snow sampling was partly realized by different people using commercially available plastic bags (for household use), but also done using glass jars. It has to be noted, that the number of samples done for plastic bags was larger (n=19), while only three measurements were available for blanks obtained from glass jars. **Figure 26** A depicts the level of contamination obtained for 'plastic bag blanks' and **Figure 26** B for 'glass jar blanks'. PAH amounts derived from both blank groups show a decreasing trend with increasing molecular weight. Considering the 'plastic bag blanks', some high molecular weight PAHs could not even be quantified in the majority of blanks. **Figure 26** clearly highlights that especially the extraction of PAHs with lower molecular weight will experience flaws, when samples were collected with plastic bags. This could be attributed to matrix effects or sample contamination by possible leaching of PAHs from the plastic bag itself. When it comes to the PAH concentrations derived from glass jar blanks, results present a different picture. PAHs quantified from blanks taken in

glass jars show drastically lower contamination (up to 10 times lower). As experiments presented in this subchapter are described by three data points, it is recommended to realize more experiments using glass jars as sampling device in order to make statistically meaningful assumptions.

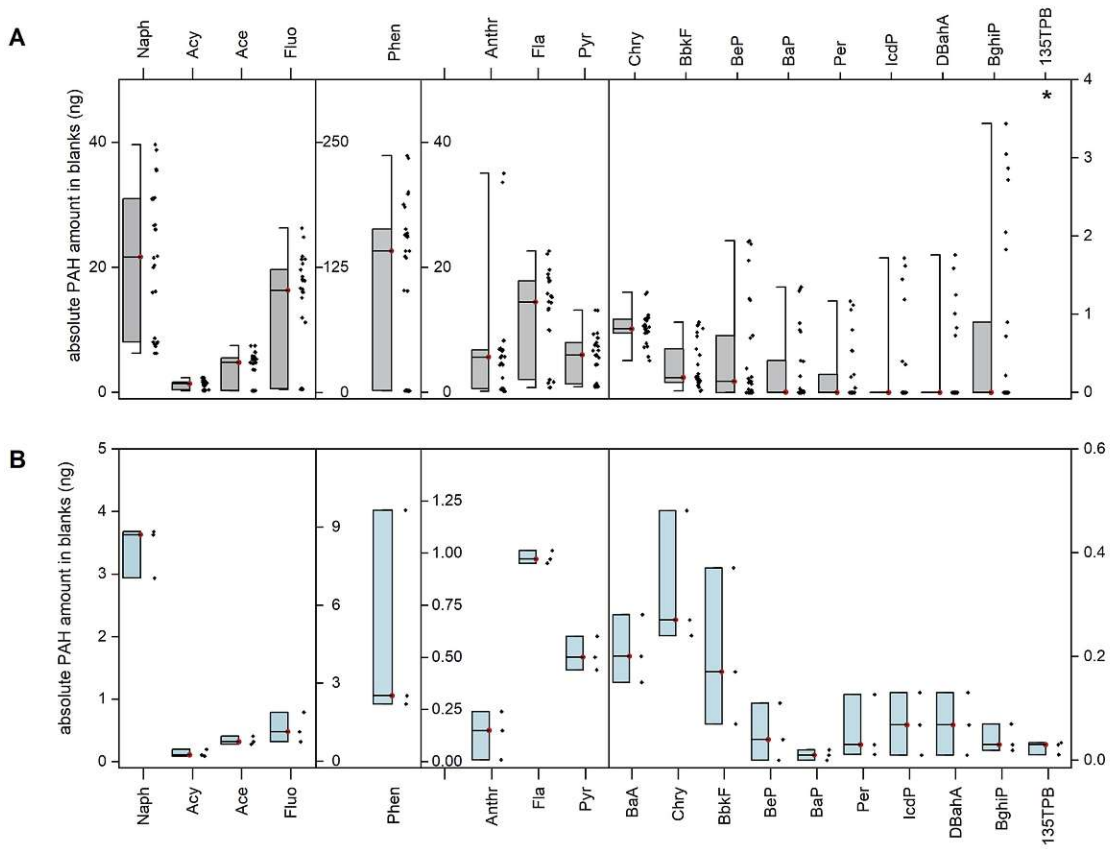

Figure 26 A-B. Absolute PAH amounts found in blank samples, i.e. **(A)** plastic bags and **(B)** glass jars. Note that the dataset of plastic bags was higher (n=19) than those quantified for glass jars (n=3). Whiskers of boxplots mark the minimum and maximum concentrations observed. The boxplot itself marks the respective percentiles, i.e. 25th, median (red dot) and 75th percentile. Plastic bags showed no quantifiable amount of 135TPB, this is highlighted with *.

The highest signal found in blanks could be attributed to Phen derived from plastic bags. Also Phen contributions found in glass jars showed higher response as concentrations observed for other PAH congeners. It is believed that the pronounced Phen response may be attributed to contaminations during sample preparation procedure or to leaching from the plastic reservoirs as chemicals were added to the it. Comparing the mass spectra derived from the calibration standard measurement with reference mass spectra derived from the NIST databank (NIST MS Search 2.3) confirmed each other, i.e. library search suggested Phen as best hit for the unknown mass spectrum of Phen (see **Figure 27** A). The same picture is given when comparing the mass spectrum derived from the measurement of a 'plastic bag blank' (i.e. plastic bag filled with ultrapure water, spiked with d_{12}-BaP, underwent SPE procedure) with the reference spectrum (see **Figure 27** B). All mass spectra derived from measurements (depicted in red) are missing responses in the low mass range, as the mass range recorded within those measurements was limited to 100-350 Da. This mass

range covers the mass ranges of analytes but excludes signals for fragments with low masses at all. Because of that, m/z lower than 100 are not depicted in the mass spectra which describes the differences among them. To tackle a possible contamination of the GC-MS/MS system we additionally compared mass spectra derived from measurements of the organic solvent with the library spectra derived from the NIST databank. The comparison of the mass spectra observed during the matrix measurement point out that the Phen signals are not caused by contamination of the GC-MS/MS setup itself (see **Figure 27** C). Small signals appearing throughout the whole mass range can be attributed to depletion of the column material. The most pronounced signal noticeable in **Figure 27** C refers to m/z 207, which is a commonly used indicator for the identification of column bleeding as this signal is caused as a result of the formation of hexamethylcyclotrisiloxane. The separation column was newly installed and used for the first time conducing these measurements. The stationary phase of the installed separation column consist of a phenyl-arylene-dimethylpolysiloxan phase with a temperature stability up to 350°C (agile temperature mode). Although it is labelled as low bleed column we could see some response of column bleed in the mass spectrum, which we attribute to the high sensitivity of our system. Gabrieli et al. (2010) applied a similar blank and sample preparation procedure as presented in this work, also yielding high responses for Phen (highest ones were reported for BaA) (Gabrieli, Vallelonga, et al. 2010). Authors attributed the Phen input in blank samples (508 ± 155 pg/kg) to the SPE cartridges (C18, Supelco Discovery) rather than to an additional input caused by the ultrapure water or contamination during sampling (Gabrieli, Vallelonga, et al. 2010). The Phen input observed within our experiments, no matter of sampling reservoir, is clearly higher than reported by Gabrieli et al. (2010). However, only a small amount of Phen (and even smaller amounts of other PAHs) could be attributed to the used SPE cartridges (ISOLUTE PAH, Biotage), as the extraction yielded maximum Phen amounts of 2.65 ng (average = 2.22 ng, n=8). Based on these results we are not yet able to draw a firm conclusion about the additional Phen input, but expect more than one sources of contamination. However, PAH contributions caused by the sample preparation procedure are expected to not vary with the applied blank/sample volume to the glass jar or plastic bag. Thus for future experiments, it is recommended to enlarge the sample volumes, so that PAH peak areas easily exceed those method parameters during data processing.

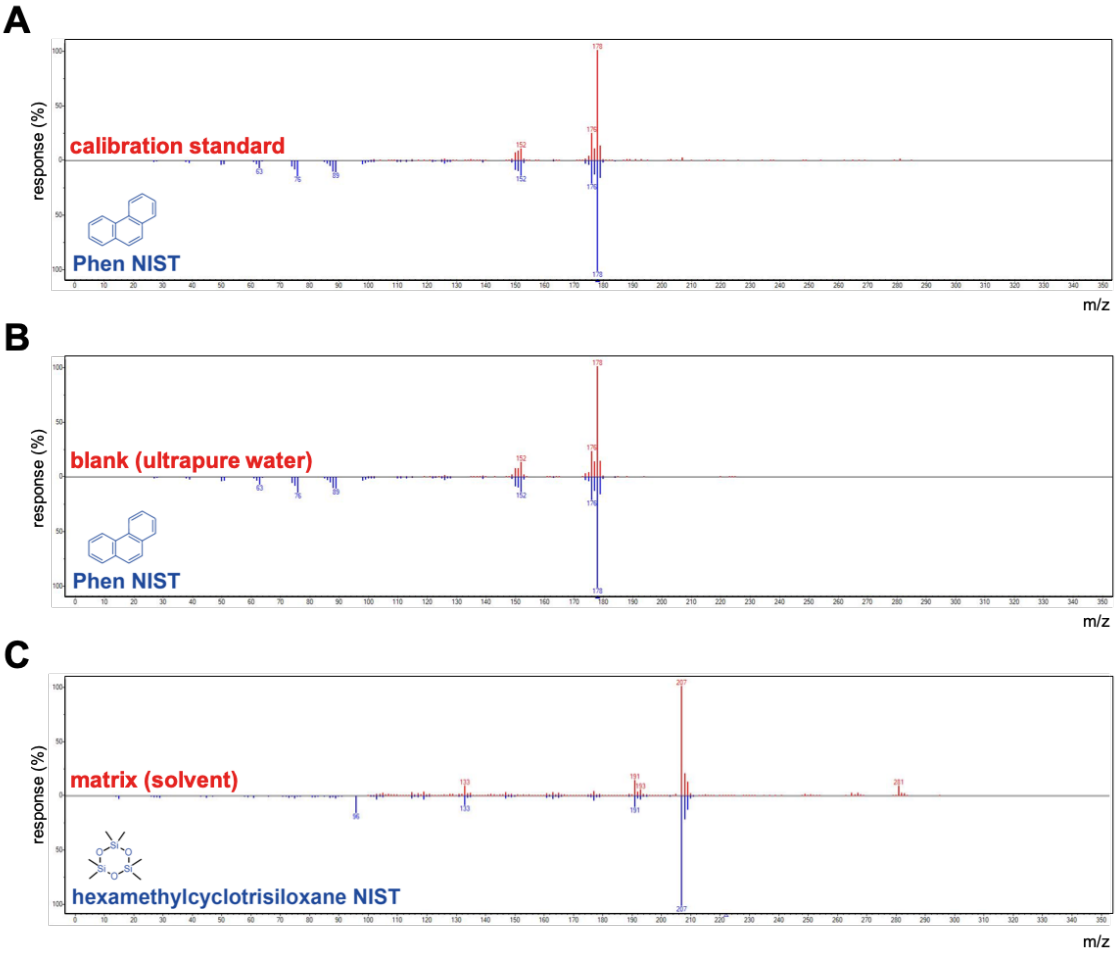

Figure 27 A-C. Comparison of mass spectra derived from measurements to reference spectra from the NIST databank. **(A)** Mass spectrum retrieved for the Phen peak of one calibration standard compared to a reference mass spectrum. **(B)** Mass spectrum retrieved from a blank measurement (only ultrapure water added to plastic bag) compared to the reference mass spectrum of Phen. **(C)** Mass spectrum of a matrix measurement (cHex) and the best hit found by the NIST library, which indicates column bleeding. All reference mass spectra were extracted from the NIST databank (NIST MS Search 2.3) via Chromeleon 7.2.10 ES.

6.1.3. Calculation of the method's limit of detection

Quality assurance was checked by realizing different blank measurements. Blanks were prepared using the same commercially available plastic bags (hereinafter referred to as plastic bag blanks) or also glass jars (hereinafter referred to as glass jar blanks) which were used for surface snow sampling. For that, plastic bags or glass jars were filled with about 1000 mL of ultrapure water (Milli-Q) and stored at -18°C until blanks they were frozen. Afterwards they underwent the same sample preparation procedure are mentioned in **section 3.5.2**. The calculation of the method's limit of detection (LODs) and quantification (LOQs) was realized according to DIN EN 3245:2008 by multiplying the standard deviations of blank samples with the respective student t factor ($t_{95\%,n}$ for LOD and $t_{99\%,n}$ for LOQ). **Table 17** sums up the calculated LODs and LOQs for all PAHs quantified from 'plastic bag' and 'glass jar blanks'. In terms of comparison, LODs and LOQs are given in ng/L, which was realized by conversion with the applied volume of Milli-Q water (on average 384 mL). As some compounds could not be quantified in more than three blank

measurements (i.e. IcdP, DBahA, 135TPB), we could not calculate the respective method parameters.

Table 17. Calculated LODs and LOQs based on blank data, i.e. plastic bags or glass jars used for sampling. LODs and LOQs were calculated using the respective student t factor.

	plastic bags		glass jars	
Analyte	**LOD (t, 95%)**	**LOQ (t, 99%)**	**LOD (t, 95%)**	**LOQ (t, 99%)**
	ng/L	**ng/L**	**ng/L**	**ng/L**
Naph	39.5	54.8	9.24	27.7
Acy	2.06	2.85	1.12	3.37
Ace	5.77	8.00	1.46	4.38
Fluo	21.3	29.5	4.55	13.6
Phen	205	285	76.1	228
Anthr	50.4	69.9	1.85	5.56
Fla	19.1	26.6	1.50	4.49
Pyr	13.5	18.7	1.09	3.26
BaA	0.50	0.69	0.98	2.95
Chry	0.98	1.35	1.86	5.59
BbkF	0.78	1.08	2.35	7.04
BeP	1.36	1.88	0.62	1.87
BaP	1.06	1.61	0.08	0.25
Per	0.58	1.74	0.99	2.96
IcdP	n.a.	n.a.	0.93	2.79
DBahA	n.a.	n.a.	0.93	2.79
BghiP	2.25	6.75	0.40	1.21
135TPB	n.a.	n.a.	0.20	0.61

6.1.4. The minimal required sample volume sufficient for PAH analysis

PAH contributions strongly depend on source contributions and thus differ between sampling locations. Consequently, the required sample volume is also affected by the chosen sampling location and its influences. PAH extraction from surface snow samples derived from the most pristine area possible, i.e. Dome C in Antarctica, demands a sample volume of 10 L to sufficiently extract and enrich PAHs using liquid-liquid extraction (Xie et al. 2020), while clearly lower samples volumes are sufficient using solid phase extraction (Gabrieli, Vallelonga, et al. 2010, Walsh, Schrlau, and Simonich 2014). The PAH content derived from snowpacks of the Tyrolean Alps ($\sum_{24}$PAHs= 0.5 – 8.4 ng/L), for example, was realized by a solid phase extraction using a sample volume of 30 L (Arellano et al. 2014). On the contrary, lower volumes of up to 2 L have proven to be sufficient for PAH quantification from different snow layers from five European Mountains using membrane extraction disks ($\sum_{22}$PAHs= 16 – 81 ng/L among three sampling sites) (Carrera et al. 2001). Comparing the range of PAH concentrations found by Arellano et al. (2014) ($\sum_{24}$PAHs= 0.5 – 8.4 ng/L) and Carrera et al. (2001) ($\sum_{22}$PAHs= 16 – 81 ng/L among three sampling sites) clearly highlights the importance of adapting the sample volume to its influencing parameters such as source contributions and sampling location, as higher volumes allow the quantification of PAH congeners found in the sub-ppb to ppt level. However, the required sample

volume does not solely depend on external parameters, but also changes, if the given setup is modified or if the sampling procedure itself changes. In our case, clearly higher sample volumes are required if sampling is going to be pursued with plastic bags as those especially complicate the quantification of LMW PAHs. Considering this for a single PAH congener such as Phen, which has been reported to be a dominant PAH congener found in snow samples (e.g. Franz and Eisenreich 1998, Carrera et al. 2001, Arellano et al. 2014), would even complicate the quantification of Phen derived from snow samples at an urban sampling station as median Phen concentrations of 394 ng/L were reported by Izvekova et al. (2020) (Izvekova et al. 2020). Glass jars show lower PAH contamination which would also allow the use of lower sample volumes. As we aimed for a user-friendly sampling method using sampling material commonly used in households, we decided to use both, plastic bags and glass jars for sampling while keeping in mind, that we might run into problems due to contamination.

6.1.5. Surface snow sampling

Surface snow samples were taken at different locations across Austria including different surroundings. Detailed information about the surrounding and type of area are listed in **Table 18**. Locations vary in surroundings and thus source influences including a background station at Sonnblick Observatory and locations influenced by human activity, i.e. next to the street or a skiing area. As we aimed to develop a user-friendly sampling procedure, sampling was realized by several people. Freshly fallen snow is only available in a rather short time window and surface snow sampling was realized in parallel to the method development. Because of that we did not restrict the sampling procedure to only one type of sampling reservoir, keeping in mind that LMW PAH quantification may be flawed or not even possible due to high blank contamination. Several people who have been instructed to the sampling procedure realized sampling under the following conditions: about 500 g of surface snow was sampled with a clean shovel or nitrile/latex gloves or by simply overturning the commercially available plastic bag, which was also used for storage. All samples were stored in the plastic bags at -18°C until sample preparation was realized.

Table 18. Detailed information of different sampling stations used for surface snow sampling, i.e. information about the surrounding, date of surface snow sampling and the average sampling volume used for analysis.

Sample abbr.	Region	Info	Date of sampling	Average sample	sample size n
SBO	Sonnblick, Salzburg	background, roof of observatory, 3106 m asl	16.03.2021	309	6
HW	Hochwechsel, Styria	rural background, 1700 m asl	27.12.2020	344	4
MAS	Masenberg, Styria	rural background, 1261 m asl	24.12.2020	421	4
HR	Hochrindl, Carinthia	rural background	17.03.2021	484	7
VF	Vorau, Styria	rural, field	23.12.2020	465	2
WOL	Wolkersdorf, lower Austria	rural, next to street	15.01.2021	465	3
KPT	Klippitztörl, Carinthia	rural, skiing resort nearby, 1460 m asl	24.02.2021	589	6

6.1.6. PAH content of surface snow samples

Individual and total PAH concentrations scatter in a wide range and **Table 19** lists the average PAH concentrations for all samples showing quantifiable amounts of at least 4 congeners. Total PAH concentrations (hereinafter referred to as $\sum_{17}$PAHs, as we would have been able to quantify 17 individual congeners) observed at the different locations varied between 8.60 and 40.5 ng/L. We could observe concentrations of more than four PAH congeners in samples of 43% of the sampling locations, i.e. three sampling locations showed quantifiable PAH amounts of four or more congeners. Even though we could observe clear PAH signals in the chromatograms of all sampling locations, peak areas did not exceed the blank correction and LOD filtration resulting in not quantifiable amounts. This was the case for samples taken at SBO, HW, HR and WOL, which are consequently excluded from further evaluations.

Table 19 presents the PAH concentrations observed for sampling locations with quantifiable amounts of more than four congeners, i.e. MAS, VF and KPT. Highest overall PAH concentrations were found at Masenberg (MAS) yielding $\sum_{17}$PAH concentrations of 40.5 ng/L. MAS presents a rural background station (1261 m asl) and the most pristine one showing contributions for more than four congeners, even though we extracted on average 421 mL of melted surface snow. PAH contributions observed at the rural location Vorau (VF) were lower than those observed at the respective background station MAS, yielding $\sum_{17}$PAH concentrations of 11.5 ng/L. This may be attributed to the fact, that amounts of only four PAH congeners exceeded the blank correction, while MAS showed contributions of 9 different congeners. Another difference is, VF samples did not show quantifiable amounts of LMW PAHs, while those comprise 42% of the total PAH load at MAS. MAS was also the only sampling location where BaP concentrations exceeded blank correction, yielding average concentrations of 2.10 ng/L. BaP concentrations found at MAS are lower than those observed at an urban sampling station in Russia reporting mean BaP concentrations of 6 ng/L (Izvekova et al. 2020), which can be attributed to the lack of direct urban influences at MAS. The third sampling site showing quantifiable amounts of seven PAH congeners was Klippitztörl (KPT). Samples taken at KPT represent a rural area nearby a skiing resort, expecting rather pronounced PAH concentrations. However, the overall PAH concentrations observed at KPT were slightly lower to ones observed at MAS, i.e. $\sum_{17}$PAH concentration = 34.1 ng/L. Although results of MAS and KPT were in a similar range, they differ in PAH patterns. At KPT, LMW PAHs contribute 78% to the overall PAH concentration, while lower contributions were observed at MAS. These findings not only indicate a decreasing trend of PAH contributions with increasing molecular weight. As KPT is situated at about 1460 m asl findings also state that LMW PAH contributions increase with altitude, which corroborates with previous findings. More details about LMW contributions and their dependence on altitude is discussed in **section 6.4**.

Table 19. Concentrations of individual PAH congeners, overall PAH ($\sum_{17}$PAH) and 135TPB concentrations and the recovery rate of d_{12}BaP observed in surface snow samples from three different sampling locations. Note, that this table only lists locations which showed quantifiable amounts of four or more PAH congeners. More details about the sampling locations are given in **Table 18**. Presented concentrations refer to the average PAH concentrations in ng/L for each sampling location after data processing, i.e. blank correction (plastic bag or glass jar) and LOD correction.

Analyte	MAS	VF	KPT
	ng/L	ng/L	ng/L
Naph	14.0	n.d.	19.7
Acy	2.86	n.d.	4.85
Ace	n.d.	n.d.	2.12
Fluo	n.d.	n.d.	n.d.
Phen	n.d.	n.d.	n.d.
Anthr	n.d.	n.d.	n.d.
Fla	n.d.	n.d.	n.d.
Pyr	n.d.	n.d.	3.30
BaA	2.27	1.95	0.36
Chry	3.76	2.32	2.35
BbkF	6.45	4.90	1.33
BeP	1.75	n.d.	n.d.
BaP	2.10	n.d.	n.d.
Per	n.d.	n.d.	n.d.
IcdP	5.09	2.34	n.d.
DBahA	n.d.	n.d.	n.d.
BghiP	2.21	n.d.	n.d.
$\sum_{17}$PAH	**40.5**	**11.5**	**34.1**
135TPB	n.d.	n.d.	n.d.
d_{12}BaP recovery %	**59**	**39**	**76**

6.1.7. Recovery rate of d_{12}-BaP in surface snow samples

Even tough PAHs in snow are of increasing concern, still no certified reference material is available for this kind of matrix. Investigating the recovery for d_{12}-BaP in particulate samples is suggested by a standardized method for routine PAH analysis (DIN EN 15549:2008). Accordingly, we realized recovery tests by spiking d_{12}-BaP (6 ng absolute, dissolved in DCM:cHex, 1/1, v/v) to the surface snow sample prior to the sample preparation procedure, i.e. when the snow was still in the original sampling reservoir (plastic bags or glass jars). As d_{12}-BaP spiking present the first step of sample preparation, recovery rates consider all losses during the entire procedure (i.e. from sample preparation to quantification), which may be extrapolated to the other PAHs. The recovery rate was also calculated according to DIN EN 15549:2008 and evaluated as adequate when it was in the range of 80 to 120%. Comparing the obtained recovery rates as depicted in **Figure 28** indicate that most of them could be found within the given range. However, still a considerable number of samples exceeded the range accompanied by slightly lower recovery rates than desired. An underestimation of the recovery can be mainly attributed to (i) analyte losses during the sample preparation procedure, e.g. spilling of sample as we did not have an automated SPE system yet or (ii) a phase separation of the added RST (dissolved in organic solvent) from the aqueous matrix enhancing adsorption processes to the sampling reservoir (plastic bags or glass jars). While overestimations are mainly attributed to due to

pipetting errors. As a consequence we modified the amount of RST for the second set of experiments to avoid possible errors.

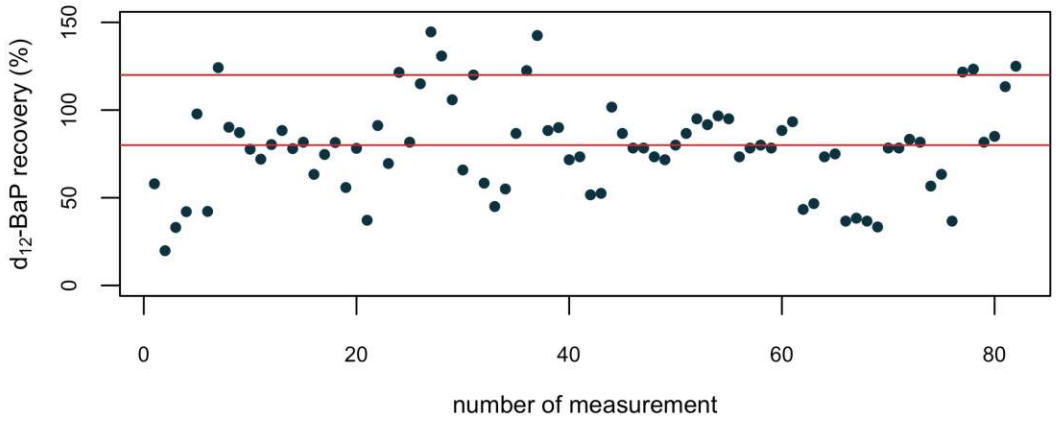

Figure 28. Recovery rate of d_{12}-BaP observed in surface snow samples. Red lines highlight the boundaries of 80 and 120%.

Gabrieli et al. (2010) also investigated the recoveries of spiked snow samples using a SPE sample preparation procedure (Gabrieli, Vallelonga, et al. 2010). The authors evaluated the recovery for 12 different PAH congeners, all of them are included in our analyte list too but we did not use them for recovery purposes. Recoveries reported by Gabrieli et al. (2010) scatter among congeners ranging from 71 (Anthr) – 91% (BghiP) (Gabrieli, Vallelonga, et al. 2010). Additionally, authors reported that they were able to increase the recovery by a threefold SPE elution step, i.e. DCM, cHEx and DCM in this order (Gabrieli, Vallelonga, et al. 2010).

The efficiency of the PAH elution from the SPE column was also evaluated within the scope of the present work. This was done on the basis of the quantified amount of d_{12}-BaP. Each elution step was repeated a second time using the same mixture of DCM:cHex (1/1, v/v), resulting in two fractions per sample. Fraction 1 contains all PAHs eluted during the first elution step, while fraction 2 contains the remaining PAHs. With this dual elution we investigated whether one elution step is sufficient enough to elute the majority of PAHs or if a second one is needed. The average recovery of d_{12}-BaP found in the second fraction accounted for 4.7%. Since this amount is below 5% we assumed that the majority of PAHs is eluted during the first step and in terms of time and cost efficiency we decided that no second elution step is needed. Consequently all results presented in the following refer to fraction 1, i.e. after the one and only elution step.

6.2. Conclusion and suggestions/modifications for the second attempt

The previous section presents first experiments for the extraction and quantification of PAHs from surface snow samples derived from different sampling locations across the eastern and southern part of Austria. Measurements were realized using an in-house developed GC-MS/MS method and applying a user-friendly and efficient sampling procedure. However, during method

development some obstacles came up and were to overcome, which results in the following modifications and improvements:

(i) Different blank analysis pointed out, that the use of plastic bags for sampling is not recommended as they showed pronounced PAH contaminations in the low molecular weight PAH range (i.e. Naph, Fluo, Phen, Fla). The additional Phen input may be attributed to leaching or diffusion enhancement as i-prop and the RST (dissolved in DCM:cHex) were added in the plastic bag itself. The PAH concentrations of blanks realized in glass jars, showed lower responses and thus sampling should be realized solely using glass jars. If possible glass jars should be washed with acetone and prebaked at high temperatures (> 250°C) in order to remove all the organic residue in prior. Besides that the use of brown or dark glass is more favored as it suppresses possible PAH loss due to UV degradation.

(ii) As most PAH concentrations were below the LOD we suggest to increase the sampling volume. During the first set of experiments we aimed to develop a user-friendly and efficient sampling procedure using household materials. As freshly fallen snow is only available within a rather short time window, sampling was partly outsourced to beforehand instructed people who sampled roughly 500 mL of surface snow. It was proven, that this was not sufficient enough to quantify a rich palette of PAHs and thus sample volume should be increase to at least 1000 mL or even more.

(iii) The increase of the sampling volume also demands modifications of the SPE procedure, as the extraction of larger volumes is more time consuming and additionally complicates handling enhancing analyte losses due to spilling of the melted snow sample. Therefore, we recommend to (semi-)automate the SPE sampling procedure using durable and organic solvent stable parts.

6.3. Improvements of the sampling preparation procedure and analytical GC-MS/MS method modifications

6.3.1. Development of an automated SPE setup

To avoid the loss of sample during sample preparation we automated the SPE setup by using a vacuum pump, Teflon tubes and connectors. Besides the automatization of the SPE procedure, we further aimed to limit analyte loss caused by drying of the organic extract. Instead of drying the organic extract using Na_2SO_4 and a subsequent filtration process (main source of analyte loss), we used Na_2SO_4 drying cartridges in line with the SPE columns. Note, that the Na_2SO_4 drying cartridge was only installed and used during the elution process and not during sample extraction. A schematic figure of the setup used for the extraction step is illustrated in **Figure 29** A. To achieve a full automatization of the setup, it was necessary to evaluate the drop rate in dependence of the applied vacuum. Therefore, drop rates were evaluated at different pressures for different solvents or solvent mixtures. All tested solvents are used within the sample preparation process. The relationship of drop rates depending on the applied vacuum is given in **Figure 29** B. For sample preparation two different pressure settings were used, i.e. (i) >1000 mL surface snow were

extracted using the pressure setting at -0.5 bar which results in a drop rate of 20 mL/min, (ii) PAH elution from the SPE column was achieved using a DCM:cHex mix (1:1, v/v) at the pressure setting at -0.1 bar which yields a drop rate of about 1 mL/min.

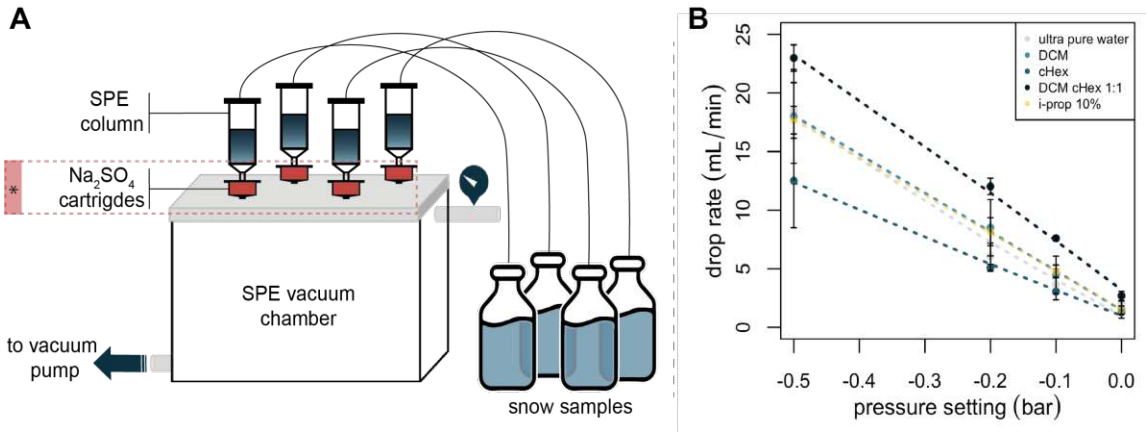

Figure 29 A-B. (A) Schematic visualization of the automated SPE setup using Teflon tubes and connectors. **(B)** Drop rate in dependence of the pressure setting at the vacuum chamber for different solvents used, i.e. ultrapure water, dichloromethane, cyclohexane, dichloromethane: cyclohexane 1:1 mix, iso-propanol (10%). (*) Note, that Na_2SO_4 drying cartridges were only installed and used during the elution step with cHex:DCM.

6.3.2. Instrumental changes in GC-MS/MS setup

As we did not achieve a satisfying resolution for some isomers, e.g. benzofluoranthenes, we changed the GC-MS/MS setup as follows:

(i) Changes of liner from the commonly used one, to an ultra-inert liner (i.e. Thermo Gold- UI, 4 x 6.5 x 78.5 mm)
(ii) Installation of a specialized PAH column: Rxi-PAH (60 m x 0.25 µm x 0.10 µm)
(iii) Installation of a post column (deactivated FS, 0.5 m) in order to achieve a better vacuum in the MS/MS

The parameters and specifications given in **section 3.1.** refer to the final and optimized GC-MS/MS setup.

6.3.3. Modifications of the GC temperature program and MS/MS parameters

To achieve a satisfying separation of in total 37 PAHs the temperature program was modified as following: start temperature of 110°C (hold time for 3 mins), linear ramp of 30°C/min up to 195°C, second ramp of 1.50°C/min up to 245°C, third ramp of 1.75°C/min up to 295°C, fourth ramp of 3.00°C/min up to a maximum temperature of 335°C (hold time for 10 mins) and lastly a cooling step with a decreasing ramp of 15°C/min to 275°C. The total run time was 96 minutes. More details about the final settings are given in **Table 3** and **4**.

Due to the changes of the GC-MS/MS setup and the modification of the temperature curve, we were able to expand the PAH palette to a number of 29 parent PAHs, 6 dPAHs and 2 substituted ones and 135TPB. Separating complex PAH mixtures using GC with EI ionization is difficult as most PAHs yield similar fragmentation patterns and having similarities in vapor pressures and boiling points (Manzano, Hoh, and Simonich 2012), and enlarging the PAH palette is accompanied by several analytical challenges and often requires several chromatographic runs. In terms of cost and time efficiency, methods quantifying several PAH congeners in a single chromatographic run are favored and additional ones are published consistently (e.g. Anderson et al. 2015, Mueller et al. 2019). Therefore, GC column suppliers design special polymer modification to sufficiently separate isobaric PAHs (e.g. Agilent, Restek). Within the present work we applied the Rxi-PAH column designed by Restek which combines several advantages: (i) due to its higher phenyl-content compared to other columns, the Rxi-PAH column also allows the resolution of isobaric PAHs while suppressing interferences of Chry and TriPh for example, and (ii) the special arylene modification and surface bonding of this stationary phase allow the measurement of nonvolatile HMW PAHs like dibenzopyrene isomers (Restek Corporation 2021). Again, data acquisition was realized in timed mode using several time windows. A chromatogram presenting the simultaneous quantification of all PAH congeners and 135TPB and the sufficient separation of the benzofluoranthenes (yellow highlighted) and dibenzoyprene isomers (highlighted in light blue) in a single chromatographic run is given in **Figure 30**.

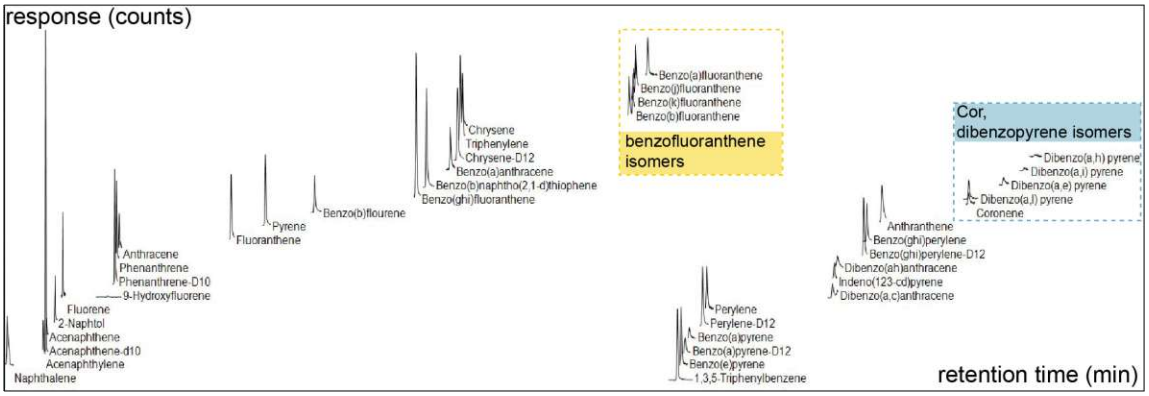

Figure 30. GC-MS/MS chromatogram of a calibration standard (25 ng/L) in multi-reaction monitoring (MRM) mode and timed acquisition. The sufficiently separated dibenzofluoranthene isomers are highlighted in yellow while the separated dibenzopyrene isomers and Cor are highlighted in blue. Note, that axis miss ticks. The highest response observed during this run was $1.1*10^6$ counts and the total run time was 90.50 min.

Table 20 lists the MS/MS transitions of the enlarged PAH palette used within the modified method. Quantification was realizes using an internal standard mix covering the range of volatility of the respective PAHs. The recovery was evaluated on the basis of d_{12}-BaP according to DIN EN 15549:2008. Calibration standards cover a concentration range from 0.7 to 70 ng/L and assigned internal standard classes as well as RST and IST compounds are listed in **Table 20**.

Table 20. List of extended PAH palette for surface snow analysis including the retention time, precursor and product ion mass generated under the given collision energies.

Analyte	Abbr.	Retention time (min)	Precursor ion mass	Product ion mass	Collision Energy	IST group
Acenaphthylene	Acy	10.67	152.1	126.1	20	1
			152.1	102.0	30	
Acenaphthene	Ace	10.96	153.1	126.1	45	1
			153.1	151.1	40	
Fluorene	Fluo	12.25	165.1	163.1	30	1
			166.1	164.1	30	
Phenanthrene	Phen	16.70	178.1	152.1	25	2
			178.1	176.1	20	
Anthracene	Anthr	16.92	178.1	152.1	30	2
			178.1	176.1	35	
Fluoranthene	Fla	25.98	202.1	176.1	35	2
			202.1	200.1	30	
Pyrene	Pyr	28.65	202.1	176.1	35	3
			202.1	200.1	30	
			202.1	201.0	30	
Benzo(b)fluorene	BbFluo	32.55	216.0	213.0	40	2
			216.0	215.0	35	
			216.0	216.0	8	
Benzo(ghi)fluoranthene	BghiFla	41.00	226.0	226.0	8	3
			226.0	224.0	30	
Benzo(a)anthracene	BaA	43.65	228.1	224.1	60	3
			228.1	226.1	30	
Triphenylene	TriPh	44.30	228.1	226.1	30	3
			228.1	202.1	35	
Chrysene	Chry	44.61	228.1	224.1	60	3
			228.1	226.1	30	
Benzo(a)fluoranthene	BaF	59.01	252.1	248.1	60	3
			252.1	250.1	30	
Benzo(b)fluoranthene	BbF	57.52	252.1	248.1	60	3
			252.1	250.1	30	
Benzo(k)fluoranthene	BkF	57.81	252.1	248.1	60	3
			252.1	250.1	30	
Benzo(j)fluoranthene	BjF	58.03	252.1	248.1	60	3
			252.1	250.1	30	

Table 20 continued. List of extended PAH palette for surface snow analysis including the retention time, precursor and product ion mass generated under the given collision energies.

	Analyte	Abbr.	Retention time (min)	Precursor ion mass	Product ion mass	Collision Energy	IST group
	Benzo(e)pyrene	BeP	60.87	252.1	248.1	60	4
				252.1	250.1	30	
	Benzo(a)pyrene	BaP	61.45	252.1	248.1	60	4
				252.1	248.1	60	
	Perylene	Per	62.70	252.1	248.1	60	4
				252.1	250.1	30	
	Indeno(123-cd)pyrene	IcdP	74.15	276.1	272.1	60	4
				276.1	274.1	40	
	Dibenzo(ah)anthracene	DBahA	73.70	278.1	274.1	60	4
				278.1	276.1	30	
	Dibenzo(a,c)anthracene	DBacA	74.00	278.0	276.0	45	4
				278.0	277.0	40	
	Benzo(ghi)perylene	BghiP	76.75	276.1	272.1	60	5
				276.1	274.1	40	
	Anthanthrene	Anthan	77.85	276.0	138.0	30	5
				276.0	274.0	40	
				276.0	276.0	8	
	Coronene	Cor	84.95	300.0	150.0	45	5
				300.0	299.0	40	
				300.0	300.0	20	
	Dibenzo(a,i)pyrene	DBaiP	85.00	302.2	300.1	40	5
				302.2	298.2	60	
	Dibenzo(a,e)pyrene	DBaeP	87.65	302.2	300.1	40	5
				302.2	298.2	60	
	Dibenzo(a,l)pyrene	DBalP	89.25	302.2	300.1	40	5
				302.2	298.2	60	
	Dibenzo(a,h)pyrene	DBahP	90.13	302.2	300.1	40	5
				302.2	298.2	60	
xPAHs	Benzo(b)naphtho(2,1-d)thiophene	BbNaphS	41.55	234.0	232.0	35	2
				234.0	234.0	8	
	2-Naphthol	OH-Naph	11.55	144.0	144.0	8	1
				144.0	116.0	8	
				144.0	115.0	30	
RST	d_{12}-benzo(a)pyrene	d_{12}-BaP	62.35	264.2	256.1	60	4
				264.2	260.1	30	

Table 20 continued. List of extended PAH palette for surface snow analysis including the retention time, precursor and product ion mass generated under the given collision energies.

	Analyte	Abbr.	Retention time (min)	Precursor ion mass	Product ion mass	Collision Energy	IST group
IST	d_{10}-acenaphthene	d_{10}-Ace	12.25	164.1	162.0	20	1
				164.1	160.0	30	
				164.0	164.0	30	
	d_{10}-phenanthrene	d_{10}-Phen	16.55	188.1	158.0	30	2
				188.1	160.0	30	
				188.1	188.1	30	
	d_{12}-chrysene	d_{12}-Chry	44.18	240.2	232.1	60	3
				240.2	236.1	30	
	d_{12}-perylene	d_{12}-Per	63.75	264.2	260.0	30	4
				264.2	230.0	30	
	d_{12}-benzo(ghi)perylene	d_{12}-BghiP	74.50	288.1	284.1	30	5
				288.1	288.1	30	
	1,3,5-Triphenylbezene	135TPB	61.75	306.0	289.0	40	3

6.3.4. Evaluation of blank contaminations

Contamination with PAHs from the sampling equipment and sampling glass jars from the sample handling and preparation severely impact the quality of results as we have seen during the first set of experiments. The main change in sampling refers to the switch to solely use glass jars for surface snow sampling. Blank measurements refer to 1000 mL Milli-Q water which was added to the glass jar. Due to the use of glass jars instead of plastic bags, we observed significantly lower blank values (see **Figure 31**) and many analytes could not even be detected within blank measurements, i.e. BbFla, BkFla, BjFla, BaFla, BeP, BaP, Per, DBacA, DBahA, IcdP, BghiP, DBaeP, DBalP, DBaiP, DBahP, Cor, BbNaphS and 135TPB. For most quantifiable PAHs, concentrations derived from the different sampling jars (n=14) did not show pronounced variations. Lowest average concentrations were obtained for Chry (0.04 ng), while highest ones were observed for Phen (4.16 ng), followed by Fluo (1.57 ng) and Fla (1.01 ng). Comparing PAHs by their molecular weight, i.e. LMW and HMW, LMW PAHs showed the highest response of congeners found in blank samples. We found Acy, Ace, Fluo, Phen, Anthr and Fla in almost all blanks, while only Pyr, BbFla, BghiFla, BaA, Chry and Anthran showed significant concentrations among HMW PAHs. These findings are similar to previously published ones by Gabrieli et al. (2010), who used a similar SPE sample preparation (C18, Supelco) and blank preparation (ultrapure water) procedure (Gabrieli, Vallelonga, et al. 2010). Although we were able to report lower levels of PAH contamination by changing to glass jars as sampling reservoirs, our results observed for LMW PAHs are still higher than the ones observed by Gabrieli et al. (2010), who reported maximum PAH contaminations for Phen yielding 508 ± 155 pg/kg (Gabrieli, Vallelonga, et al. 2010). Among substituted PAHs, i.e. OH-Naph or BbNaphS, highest concentrations were observed for OH-Naph (0.39 ng), while BbNaphS could not be quantified in any of the blanks.

The same holds true for the only non-PAH compound quantified within this set of experiments, i.e. 135TPB, which did not show any contributions in blank samples. These results indicate, that semi-volatile LMW PAHs found in the gaseous phase possible adsorb to the surface of the glass jars or may be leaked from the plastic cap of those, while HMW PAHs, which are preferably found in the particulate phase do not show this behavior. Furthermore, results nicely highlight the importance of properly investigating the individual steps of sample preparation to avoid contamination and highlights obstacles which may rise during method development. For future experiments, all (surface) snow sampling should be realized using glass jars. Prebaking those glass jars and closing them immediately after cooling down may also lower contributions of LMW PAHs. However, those tests were not realized within this work but should be seen as impulse for future steps.

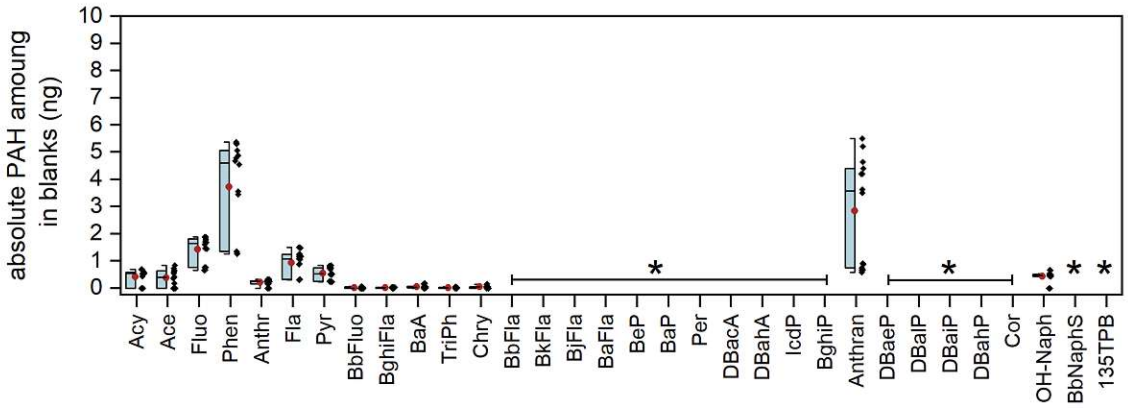

Figure 31. PAH concentrations found in blank samples derived from glass jars. Whiskers of boxplots mark the minimum and maximum concentrations observed. The boxplot itself marks the respective percentiles, i.e. 25th, median (red dot) and 75th percentile. Glass jars showed no quantifiable amount of BbFla, BkFla, BjFLa, BaFla, BeP, BaP, Per, DBacA, DBahA, IcdP, BghiP, DBaeP, DBalP, DBaiP, DBahP, Cor, BbNaphS and 135TPB, this is highlighted with *.

6.3.5. Calculation of the method's limit of detection

The calculation of the method's limit of detection (LOD) and quantification (LOQ) was realized according to DIN EN 3245:2008 by multiplying the standard deviations of blank samples with the respective student t factor ($t_{95\%,n}$ for LOD and $t_{99\%,n}$ for LOQ). Blanks samples refer to an aliquot of 1000 mL Milli-Q water, with which the respective glass jars used for sampling were rinsed after being cleaned several times. **Table 21** sums up the calculated LODs and LOQs for all PAHs which were found in quantifiable amounts in at least three samples. Thus, **Table 21** only shows an excerpt of quantified PAHs within this set of experiments. Responses observed within surface snow sample measurements and measurements of spiked blanks samples clearly exceeded the presented limits. Note, that all results presented in the upcoming sections underwent LOD filtration on the ng level.

Table 21. Calculated LODs and LOQs based on blank data obtained from glass jars used for sampling. LOD and LOQs were calculated using the respective student t factor. Note, that only LOD and LOQ limits were calculated for PAHs showing detectable amounts in more than three samples. Thus, this table presents and excerpt of PAHs analyzed within this set of experiments.

Analyte	LOD (t,95%) (ng/L)	LOQ (t, 99%) (ng/L)
Acy	0.60	0.83
Ace	0.64	0.89
Fluo	1.05	1.46
Phen	3.63	5.03
Anthr	0.22	0.30
Fla	0.94	1.31
Pyr	0.49	0.68
BbFluo	0.06	0.08
BghiFla	0.03	0.04
BaA	0.11	0.16
TriPh	0.04	0.05
Chry	0.11	0.16
Anthran	4.19	5.82
OH-Naph	0.42	0.59

Comparing the LODs and LOQs obtained within the second set of experiment with the respective ones derived from glass jars within the first attempt are similar. For most PAHs LODs and LOQs vary in comparable ranges. Within the first set of experiments, highest responses were observed for Phen (LOD: 76.1 ng/L, see **Table 17**). This phenomenon can also be observed within the second set of experiments, however in a significantly lower extent (LOD: 3.63 ng/L). High Phen contributions tend to be caused by impurities of the cleaning equipment used or by leaching from the materials used for sampling. It would need a more detailed analysis of every single sampling and sample preparation step to draw a firm conclusion about the additional Phen input. Generally, lower average responses of PAHs observed within the second set of experiments may also be attributed to the higher data set. While glass jar blanks were described by only three data points within the first set of experiments, sampling realized for the second attempt was solely done in glass jars and thus the data set describing blanks comprises 14 data points.

6.3.6. Surface snow sampling

Again, surface snow samples were taken at different locations across Austria. Detailed information about the surrounding and type of area are listed in **Table 22**. Locations vary in surroundings including a background station at Sonnblick Observatory and locations influenced by human activity (rural and urban). Again, sampling was realized by several people, who have been instructed to the sampling procedure and the sampling procedure was the following: in prior to sampling, cleaning of the glass jar was recommended with hot water. Sampling was realized with a clean shovel or nitrile/latex gloves or by simply overturning the glass jar. All samples were stored at -18°C until sample preparation was realized. In order to calculate the method's limit of

detection (LOD), blanks using the same glass jars (after cleaning them with acetone) were prepared. For that, glass jars were filled with 1000 mL of ultrapure water and afterwards they underwent the same sample preparation procedure are mentioned in **section 3.5.2**.

Table 22. Detailed information of different sampling stations used for surface snow sampling, i.e. information about the surrounding, date of surface snow sampling and the average sampling volume used for analysis.

Sample abbreviation	Region	Info	Date of sampling	Average sample volume (mL)	sample size n
SBO_OBS	Sonnblick Observatory, Salzburg	background, roof of observatory, 3106 m a.s.l	20. 04.2022	1275	5
SBO_VT	Hüttwinkl, Salzburg	rural, parking lot at SBO valley station	20. 04.2022	1434	3
VO	Vorau, Styria	Rural, small village	26.12.2021	372	2
VIE_M	Vienna, Meidling	Urban	09.12.2021	1071	3

6.3.7. PAH concentrations of surface snow samples

Individual and total PAH concentrations scatter in a wide range (see **Table 23**), which can be traced back to the very different sampling locations, all of them presenting a different strength of source contributions. Presented results were corrected with the respective blank concentrations and underwent LOD filtration on the level of ng values. The PAH palette could be successfully enlarged compared to the first set of experiments and total PAH concentrations present the sum of 31 different PAH congeners (hereinafter referred to as $\sum_{31}$PAHs) and 135TPB. $\sum_{31}$PAH concentrations observed at the different locations varied between 49.5 and 969 ng/L. Highest average $\sum_{31}$PAH concentrations were observed at the sampling location in Vorau (VO) and are even higher as PAH concentrations found in VIE samples (Meidling) where average $\sum_{31}$PAH concentrations yielded 434 ng/L. These differences in total PAH contributions may be attributed to the fact, that 'VIE' samples present the situation of freshly fallen snow, while samples taken in Vorau, i.e. 'VO' samples present already altered snow (some days). Both sampling sites present traffic influenced sites. 'VIE' sampling was realized in a park in the city, while 'VO' sampling was realized right next to the street in a village. Clearly lower $\sum_{31}$PAH concentrations were observed at the more remote sampling locations presented within this set of experiments. Two sample sets were taken at remote locations in Salzburg: (1) at the valley station in a parking lot in Hüttwinkltal (SBO_VT), (2) at the roof of Sonnblick Observatory (SBO_OBS). Interestingly, higher $\sum_{31}$PAH concentrations were found for the most remote sampling location SBO_OBS ($\sum_{31}$PAH = 85.7 ng/L), which is also known to be a European background monitoring station. Lower ones were observed at the nearby valley station ($\sum_{31}$PAH = 49.3 ng/L), which is at times influenced by traffic. Contributions of individual PAH congeners show a declining trend with molecular weight and thus volatility. We could not detect contributions of the highest molecular weight PAH studied within this set of experiments in any of our samples, i.e. Anthran. Besides, that PAH patterns change with sampling locations. While the overall PAH concentrations obtained from the remote locations, i.e. SBO_OBS and SBO_VT are clearly dominated by Phen and Fla,

this changes when investigating samples influenced by human activity. 'VIE' and 'VO' samples show a more diverse PAH pattern and also dominating PAHs change. The overall PAH concentrations derived from 'VIE' samples were dominated by HMW PAH congeners such as Fla and BbFla clearly indicating a higher urban influence. While this changes when investigating the diverse PAH pattern derived from 'VO' samples. Here, the overall PAH concentrations were dominated by major contributions of LMW PAHs such as Fluo and Phen indicating a shift in source impacts. A similar trend can be observed for BaP, the most studied PAH congener and known carcinogen. Lowest BaP concentrations were observed at SBO_OBS yielding 2.79 ng/L and could not even be detected at the valley station at SBO. Higher BaP concentrations were found at the locations influenced by human activity, i.e. VIE and VO yielding similar concentrations of 15.9 and 16.1 ng/L, respectively. Similar results were obtained for the only non-PAH compound measured, i.e. 135TPB, which could only be detected at the urban sampling locations resulting in 1.28 (VIE) and 0.66 ng/L (VO).

Table 23. Concentrations of individual PAH congeners, $\sum_{31}$PAHs and 135TPB observed in surface snow samples from different sampling locations. More details about the sampling locations are given in **Table 22**. Presented concentrations refer to the average PAH concentrations in ng/L for each sampling location after data processing, i.e. blank correction and LOD filtration realized on the ng level.

	SBO_OBS (ng/L)	SBO_VT (ng/L)	VIE (ng/L)	VO (ng/L)
Acy	0.89	0.82	1.34	10.1
Ace	1.24	1.00	1.11	45.4
Fluo	2.83	1.98	2.16	206
Phen	14.8	8.49	26.8	352
Anthr	1.47	0.48	1.26	7.72
Fla	15.3	10.9	63.2	73.9
Pyr	8.38	4.91	40.4	66.5
BbFluo	0.84	0.40	4.48	2.00
BghiFla	1.81	1.29	14.7	12.4
BaA	4.06	1.43	16.9	11.2
TriPh	1.18	1.05	9.22	5.76
Chry	4.32	2.54	29.1	19.7
BbFla	4.67	3.26	42.9	20.41
BkFla	1.84	1.18	19.5	n.d.
BjFla	1.98	1.36	27.5	8.34
BaFla	1.67	n.d.	4.23	10.6
BeP	4.08	2.00	27.9	17.8
BaP	2.79	n.d.	15.9	16.1
Per	n.d.	n.d.	2.24	n.d.
DBacA	0.98	n.d.	1.93	0.13
DBahA	3.07	2.26	14.4	2.48
IcdP	3.11	2.73	37.4	27.3
BghiP	1.61	n.d.	20.5	20.1
Anthran	n.d.	n.d.	n.d.	n.d.

Table 23 continued. Concentrations of individual PAH congeners, $\sum_{31}$PAHs and 135TPB observed in surface snow samples from different sampling locations. More details about the sampling locations are given in **Table 22**. Presented concentrations refer to the average PAH concentrations in ng/L for each sampling location after data processing, i.e. blank correction and LOD filtration realized on the ng level.

	SBO_OBS (ng/L)	SBO_VT (ng/L)	VIE (ng/L)	VO (ng/L)
DBaeP	0.97	n.d.	1.93	2.43
DBalP	1.22	n.d.	2.68	4.66
DBaiP	0.36	n.d.	0.31	5.68
DBahP	0.18	n.d.	n.d.	13.8
Cor	n.d.	n.d.	2.37	5.95
OH-Naph	n.d.	1.14	0.64	n.d.
BbNaphS	0.10	0.12	0.51	0.05
$\sum_{31}$PAHs	**85.7**	**49.3**	**434**	**969**
135TPB	n.d.	n.d.	1.28	0.66
d_{12}BaP recovery (%)	70%	64%	79%	86%

6.3.8. Toxic risk assessment of PAHs found in surface snow samples

The overall toxicity was evaluated on the basis of BaP equivalents (BaP_{eq}), which were calculated by applying the total equivalency factors (TEF) presented by Larsen and Larsen (Larsen and Larsen 1998). The spatial distribution of BaP_{eq} concentrations among the locations under consideration presents clear differences showing that absolute PAH concentrations do not reflect the total risk. Snow samples from urban influenced locations yielded highest BaP_{eq} concentrations, i.e. 49.3 ng/L (VIE) and 48.3 ng/L (VO), while clearly lower ones were found for the remote sites (SBO_OBS: BaP_{eq} conc. = 9.66 ng/L and SBO_VT: BaP_{eq} conc. = 3.81 ng/L). Lower BaP_{eq} concentrations are mainly driven by the higher contributions of LMW PAHs, which are less toxic ones and thus show lower TEF values. Urban influenced samples did not only show higher contributions of HMW PAHs leading to higher BaP_{eq} concentrations, also higher overall PAH concentrations could be observed. Note, that the TEFs presented by Larsen and Larsen cover a limited palette of PAH congeners (n=21). As we were able to quantify 31 different PAH congeners, the toxicity considering all PAH congeners possibly exceeds the BaP_{eq} concentrations, posing an even higher environmental risk.

6.3.9. Recovery rate of d_{12}-BaP

Again, snow samples were spiked using d_{12}-BaP as recovery compound. This time the spiked amount refers to 5 ng absolute d_{12}-BaP, which was added to the snow sample prior to the sample preparation procedure. This allows to investigate the loss of d_{12}-BaP during the whole SPE procedure and evaporation process, which may be extrapolated to the other PAHs as well. Again, the recovery rate was calculated according to DIN EN 15540:2008 and evaluated as adequate when it was in the range of 80 to 120%. Within this set of experiments, a considerable number of samples exceeded the range by showing slightly lower recovery rates than desired (see **Figure 32**). The average recovery rate for d_{12}-BaP found within 29 samples was 74%. In general,

underestimations are mainly attributed to analyte losses during the sample preparation procedure, e.g. d_{12}-BaP adsorbs to the surface of the glass jar or to the Teflon tubes or connectors use for the automatization of the SPE setup. Underestimations of the recovery between measurement 13 and 21 can be attributed to abrupt and unpredictable changes in the GC-MS/MS setup. Contrary to that, overestimations are mainly attributed to due to pipetting errors and those happened only twice throughout this set of experiments.

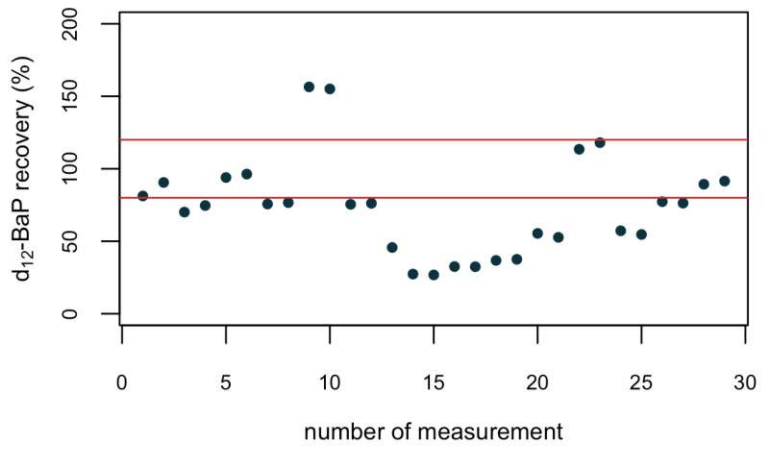

Figure 32. Recovery rate of d_{12}-BaP observed in surface snow samples. Red lines highlight the boundaries of 80 and 120%.

As d_{12}-BaP was spiked to the frozen snow sample in prior to the sample preparation procedure, presented recovery rates refer to the recovery over the entire analytical method. Recoveries obtained for the optimized experiments (as presented in this section) range between 27 and 157% and corroborate with previously published ones. The average recovery rate was 74%, which is higher than recovery rates published by Walsh et al. (2014) (Walsh, Schrlau, and Simonich 2014). Authors investigated the average analytical recovery rate also using a semi-automated SPE setup (with Teflon connectors) for PAH extraction from snow. Walsh et al. (2014) observed average analytical recovery rates of 47 ±5% for several PAH congeners (Walsh, Schrlau, and Simonich 2014), while higher ones were observed by Usenko et al. (2006) using a similar setup as presented here (average recovery of PAHs ranges between 41.1 to 118.3%) (Usenko et al. 2006). The main difference between spiking experiments presented in this work with previously published ones refers to the total amount of key analytes spiked to the samples. Walsh et al. (2014) realized spiking experiments by adding 150 ng of PAHs (Walsh, Schrlau, and Simonich 2014), while Usenko et al. (2006) added even higher amounts of 300 ng of key analytes (Usenko et al. 2006). Thus, for future experiments it is recommended to increase the amount of recovery substance by at least one order of magnitude, i.e. adding > 50 ng of key analytes.

6.4. Comparison of results obtained within this work with literature

The average PAH concentrations found in this study vary in a wide range, clearly reflecting the influences of different sources, such as emissions from residential heating or traffic related emissions. Lowest overall PAH concentrations were reported at background and remote (rural) sampling locations (SBO, MAS), while peak concentrations were observed at locations highly

influenced by urban activity, i.e. in the city, next to a street/highway. As most studies refer to a different number of PAH congeners, comparison is rather difficult. Besides that, most previous works have been focused on PAH concentrations from snow packs from high altitudes to describe the atmospheric transport of PAHs (e.g. Carrera et al. 2001, Gabrieli, Decet, et al. 2010, Arellano et al. 2014). **Table 24** lists the overall PAH and BaP concentrations observed within this work and additionally presents previously published results as means of comparison. Generally, the overall PAH concentrations observed at the highest sampling location studied within this work were similar to those found across Europe. 'SBO_OBS' samples studied within the second set of experiment yielded $\sum_{31}$PAH concentrations of 85.7 ng/L, while lower ones were observed at the respective valley station 'SBO_VT' yielding $\sum_{31}$PAH concentrations of 49.3 ng/L. These results are similar to results previously presented for snowpacks from different altitudes in the Tatra mountains (Slovakia), where an increase of PAH with altitude was observed (Arellano et al. 2014). PAH concentrations observed at locations showing higher urban influence (i.e. VIE and VO, 434 and 969 ng/L, respectively) are higher than those observed at an urban location in the Eastern Italian Alps (155 ng/kg at urban sites) (Gabrieli, Decet, et al. 2010). Higher average PAH concentrations were observed in snow samples derived from a Russian city (Ivanovo), where $\sum_{12}$PAH concentrations yielded 940 ng/L, which are similar to our findings. It has to be noted, that results present for VIE and VO in this work refer to an overall PAH concentration of 31 PAH congeners.

However, all findings presented within this work and also from previously published ones show a clear trend of high LMW PAH contributions observed in snow. This especially holds true for surface snow samples derived from higher altitudes, i.e. SBO, HW, MAS, where a clear predominance of semi-volatile PAHs could be observed (no matter which set of experiment is considered). Similar PAH patterns mainly dominated by Phen and Fla has been reported previously (Carrera et al. 2001, Gabrieli, Decet, et al. 2010, Na et al. 2011, Arellano et al. 2014, Izvekova et al. 2020). Our results indicate, that gas scavenging by snow as an important removal process from LMW PAHs in the atmosphere. This may be attributed to the fact, that LMW PAHs are usually found in the gaseous phase and are thus not removed as efficiently from the atmosphere as HMW PAHs, which are usually associated with aerosols (Franz and Eisenreich 1998). Due to the cold prevailing temperatures at high altitudes, LMW PAHs may condense/adsorb to atmospheric particles which enhances concentrations of LMW PAHs in the particulate phase (Carrera et al. 2001). This however changes, during melting processes. Melting leads to the redistribution of key analytes in all phases (i.e. frozen, melted, gaseous) and thus melted snow does not reflect the atmospheric phase distribution (Wania et al. 1998).

PAH patterns change when investigating samples from urban to rural sampling locations, i.e. contributions of HMW PAHs such as Pyr, BaA and BbFla get more pronounced (VIE and VO). The higher proportion of HMW PAHs is in line with higher overall PAH concentrations and points to a higher amount of particles in the snow. Similar trends have been observed by Carrera et al. (2001) where a higher amount of particles in the snow samples is accompanied by higher contributions of HMW PAHs (Carrera et al. 2001). Therefore, it would be useful to implement a filtration step prior to the SPE sampling procedure to evaluate the proportion of particles and also particle-bound PAHs in the snow sample itself. Carrera et al. (2001) divided the snow sample into two fractions, i.e. particles were separated via filtration and subsequently extracted, while the dissolved PAH fraction was extracted using SPE, and also analyzed them separately (Carrera et

al. 2001). However, this additional step would not provide information about the phase distribution of quantified PAHs, as LMW PAHs may also be adsorbed to particles.

Table 24. Average PAH concentrations measured in the scope of this work (first and second set of experiments) and comparison to literature. Values are given in ng/L . Abbreviations: asl=above sea level, n.d. = not detected, n.m. = not explicitly mentioned. † Results presented by (Gabrieli, Decet, et al. 2010) are given in ng/kg.

Ref.	Location	Location info	Sample info	PAH info	overall PAH concentration (ng/L)	BaP (ng/L)	dominant PAH congeners
This study, Section 6.1.	MAS	rural, background	surface snow	$\sum_{17}$PAHs	40.5	2.10	Naph
	VF	rural, field	surface snow	$\sum_{17}$PAHs	11.5	n.d.	Fluo, Pyr
	KPT	rural, skiing resort	surface snow	$\sum_{17}$PAHs	34.1	n.d.	Fluo
This study, Section 6.3.	SBO_OBS	background	surface snow	$\sum_{31}$PAHs	85.7	2.79	Phen, Fla
	SBO_VT	rural	surface snow	$\sum_{31}$PAHs	49.3	n.d.	Phen, Fla
	VIE	urban	surface snow	$\sum_{31}$PAHs	434	15.9	Fla, BbFla
	VO	rural, next to street	surface snow	$\sum_{31}$PAHs	968	16.1	Fluo, Phen
(Franz and Eisenreich 1998)	Minneapolis /St. Paul		surface snow	$\sum_{17}$PAHs	477	37	Acy, Phen, Fla
(Carrera et al. 2001)	Alps	Gossenkölle (Austria)	snowpack	$\sum_{22}$PAHs	17	n.m.	Phen, Fla, Pyr
		Jöri (Switzerland)	snowpack	$\sum_{22}$PAHs	16	n.m.	Phen
		Starolesnianske (Slovakia)	snowpack	$\sum_{22}$PAHs	81	n.m.	Fla, Pyr, Phen
(Izvekova et al. 2020)	Ivanovo (city)	urban, NE of moscow	surface snow, full depth of snow cover	$\sum_{12}$PAHs	940	3	Fla, Phen, Pyr
(Gabrieli, Decet, et al. 2010)†	Valbelluna area, Eastern Italian Alps	urban	snowpack	$\sum_{15}$PAHs	155†	2	Naph, Fla, Phen
		rural and remote alpine sites	snowpack	$\sum_{15}$PAHs	49†	0.7	

Table 24 continued. Average PAH concentrations measured in the scope of this work (first and second set of experiments) and comparison to literature. Values are given in ng/L . Abbreviations: asl=above sea level, n.d. = not detected, n.m. = not explicitly mentioned. † Results presented by (Gabrieli, Decet, et al. 2010) are given in ng/kg.

Ref.	Location	Location info	Sample info	PAH info	overall PAH concentration (ng/L)	BaP (ng/L)	dominant PAH congeners
(Arellano et al. 2014)	Tatra Mountains (Slovakia)	below Skalnate Pleso station (1683 m asl)	snowpack	$\sum_{20}$PAHs	90	n.m.	Fla, Pyr, Phen
		Lomnica Pass (2150m asl)	snowpack	$\sum_{20}$PAHs	130	n.m.	
		Lomnica Peak (2634m asl)	snowpack	$\sum_{20}$PAHs	305	n.m.	
(Na et al. 2011)	Fildes Peninsula	Background, SW of Antarctica	snow samples	$\sum_{16}$PAHs	117.7	n.m.	Naph, Fluo, Phen

6.5. Conclusion, environmental implications and toxic risk assessment

By modifying the GC-MS/MS method we were able to successfully separate 37 different PAH congeners including substituted, unsubstituted and deuterated congeners and 135TPB, a tracer substance found during plastic burning events (Simoneit, Medeiros, and M. 2005). Surface snow samples showed quantifiable contributions of up to 31 different PAHs congeners and individual samples also contributions of 135TPB. The average PAH concentrations varied in a wide range depending on source influences. Lowest contributions were found at remote locations and highest ones at urban sampling locations. Urban influenced samples also showed highest overall PAH concentrations. Within both sets of experiments, PAH patterns were mainly dominated by LMW PAH congeners. As already discussed, these findings agree with previously published ones and indicate the gas scavenging ability of snow.

Furthermore, the spatial distribution of BaP_{eq} concentrations among the locations under consideration presents clear differences in toxicity showing that absolute PAH concentrations do not reflect the total risk. Both urban influenced sites yielded BaPeq concentrations in a similar range, i.e. 49.3 ng/L (VIE) and 48.3 ng/L (VO), while lower ones were found for the remote sites (SBO_OBS: BaP_{eq} conc. = 9.66 ng/L and SBO_VT: BaP_{eq} conc. = 3.81 ng/L). Lower BaP_{eq} concentrations are mainly driven by the higher contributions of LMW PAHs, which are less toxic ones and thus show lower TEF values. Urban influenced samples did not only show higher contributions of HMW PAHs leading to higher BaP_{eq} concentrations, also higher overall PAH concentrations could be observed. Considering the fact, that we quantified a larger PAH palette, than the one discussed by Larsen and Larsen may indicate that the overall toxicity may be not reflected entirely.

Chapter 7 Development of a PAH quantification method using a TD-PTR-ToF-MS setup and its application to cloud water and snow samples

This chapter focusses on the method development for the PAH quantification using a TD-PTR-ToF-MS setup and the later application to cloud water and snow samples. **Section 7.1.** discusses the results obtained during the method development, i.e. blank measurements, the methods' limit of detection, single PAH mass spectra and PAH calibration curves. **Section 7.2.** deals with the application of the developed method to cloud water and snow samples.

Measurements were realized within a research stay at Utrecht University funded by the *LIONS sponsorship 2021* (LIONS club Wien St. Stephan). Support by supervisors and colleagues at Utrecht University namely Rupert Holzinger, Dušan Materić and Hanne Ø. Notø is gratefully acknowledged.

7.1. Method development

7.1.1. Single mass spectra of PAH reference filters

Thermal desorption of PAHs and the following analysis using PTR-ToF-MS resulted in rich but quite distinct mass spectra containing signals for more than 300 ions. **Figure 33** A-K visualizes the individual mass spectra for the associated PAHs. PAH mass spectra indicate a very clear response for the protonated molecular ions. We did not identify any fragmentation due to thermal degradation of the PAHs as mass spectra show very weak signals in the lower mass range (below 100 Da). This corresponds with the main advantage of using PTR as ionization technique, as it

does not induce significant fragmentation (Boschetti et al. 1999). Comparing the intensities of PAH signals presents a diverse picture. Low molecular weight PAHs (LMW PAHs) which are also the more volatile ones (i.e. Ace, Fluo and Phen, see **Figure 33** A, B and D), were not accompanied by the highest intensities observed among key analytes. Phen presents the compound having the lowest proton affinity (PA) of 820.1 kJ/mol, while Fluo showed a slightly higher PA with 831.5 kJ/mol (see **Table 25**). The definition of PA refers to the negative change of enthalpy during the gas phase reaction of a proton with a neutral molecule (Kumar et al. 2020). For tested PAHs, PA increases with molecular weight. Thus we attribute rather low response of tested key analytes to difficulties in thermal desorption and not to problems in PTR. Note, that PA is related to structural properties of each molecule and thus influenced by fundamental factors describing molecular interactions, e.g. electron density, polarization, charge transfer or electron delocalization (Morokuma 1977). High responses could be observed for high molecular weight PAHs (HMW PAHs), i.e. Pyr, Chry, dBaP and BeP, but also for analyzed nitro-PAHs, i.e. N-Naph and N-Pyr. When it comes to even higher molecular weight PAHs the response is decreasing, which may be attributed to decreasing vapor pressure leading to a more difficult thermal desorption. The highest response was observed for Chry, which consists of four membered benzene rings with a vapor pressure of $8.0 * 10^{-5}$ Pa (at 25°C) (Yagishita et al. 2015), while already lower signals were observed for BaP, which is the best studied PAH consisting of five membered benzene rings having an even lower vapor pressure of $7.3 * 10^{-7}$ Pa (at 25°C) (Yagishita et al. 2015). These findings may indicate that compounds in the higher mass range were not thermally desorbed from the quartz fiber filter. A similar phenomenon has been reported earlier, where the desorption efficiency of different compounds was investigated using quartz fiber filters or aluminum foil as support for key analytes, also including two PAH congeners (Dorst 2014). The author reported that quartz fiber filters complicate the desorption due to analyte adsorption to the filter material. We used this information as a kind of boundary, keeping in mind that we do not thermally desorb 100% of the analyte from the quartz fiber filter. Hence, we were demonstrably able to thermally desorb 11 different PAHs including two N-PAHs and one deuterated analog with this thermal desorption protocol.

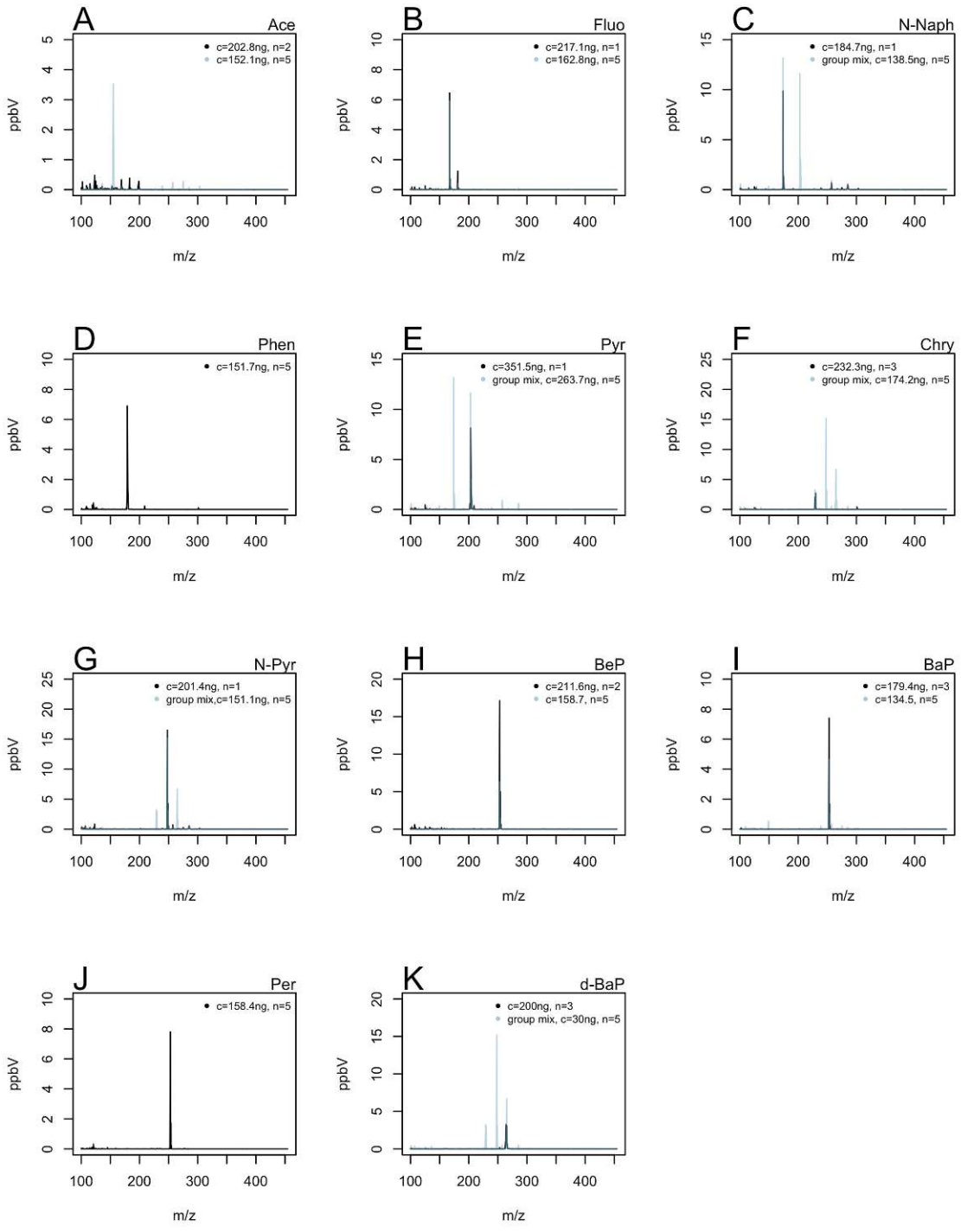

Figure 33 A-K. Full mass spectra of PAH (mass range: 100.080 – 454.494 Da). Note, that some compounds are visualized for two different concentration steps (highlighted by different colors).

7.1.2. Information retrieved from raw data thermograms

Figure 34 visualizes the thermograms of all key analytes during the individual TD runs. Each figure visualizes the signals of protonated molecular ions and the responses of neighboring ions. The presented thermograms refer to the raw ion signals of key analytes at a concentration of about

150 ng (the exact concentrations are given in **Table 25**). Besides the protonated signals observed during PAH measurements, **Figure 34** also presents the responses for the respective ions monitored during blank measurements. By comparing the overall behavior of protonated PAH signals with those observed during the respective blank measurements, we noticed that the blanks do not show distinct responses. These first runs suggested, that signals retrieved from blank measurements are negligible and will not influence individual PAH measurements. Thus**, Figure 34** refers to the raw data signals. Ace is a low molecular weight PAH and also the most volatile one, while BghiP is a proxy for high molecular weight PAHs and the least volatile one studied within this chapter. It can be clearly seen that LMW PAHs are easily desorbed during the TD run or even before the temperature increases. Ace is fully desorbed after approximately 200 seconds, which indicates that the desorption is mostly finished before the temperature even increases (T starts to increase after 180 seconds). This will clearly effect the quality of data leading to lower recoveries, which is described in more detail latter in this section. The desorption of HMW PAHs requires higher temperatures, which is consistent with their lower volatilities. HMW PAHs like BaP and its isomers, i.e. BeP and Per, are fully desorbed after approximately 1000 seconds, which refers to the maximum temperature of 360°C, which is also the highest temperature reached within one TD run. We did not reach a complete desorption for BghiP during one single TD run (see **Figure 34** L) as the raw signal did not reach the baseline again. In both cases, i.e. desorption is mostly finished before TD run even starts or temperature is insufficient to thermally desorb the compound, a significant fraction of the analyte is lost which is reflected in clearly lower recoveries and discussed in more detail later on. However, we want to point out that also BghiP could have been quantified by using an extended TD program. We did not modify the TD program within this work and used this information as a kind of boundary, meaning that, we are able to quantify PAHs up to the mass of BghiP. Besides differences of desorption behavior, peak shapes were also quite different among the individual PAH congeners. Although, thermograms represent measurements realized for the same concentration steps, peak shapes change with increasing molecular weight. The rapid desorption of LMW PAHs such as Ace and Fluo was accompanied by sharp peak shapes, while the peak shape observed during the desorption of HMW PAHs like BaP and its isomers results in broad, tailing peaks. This may also be also attributed to the higher volatility of those compounds.

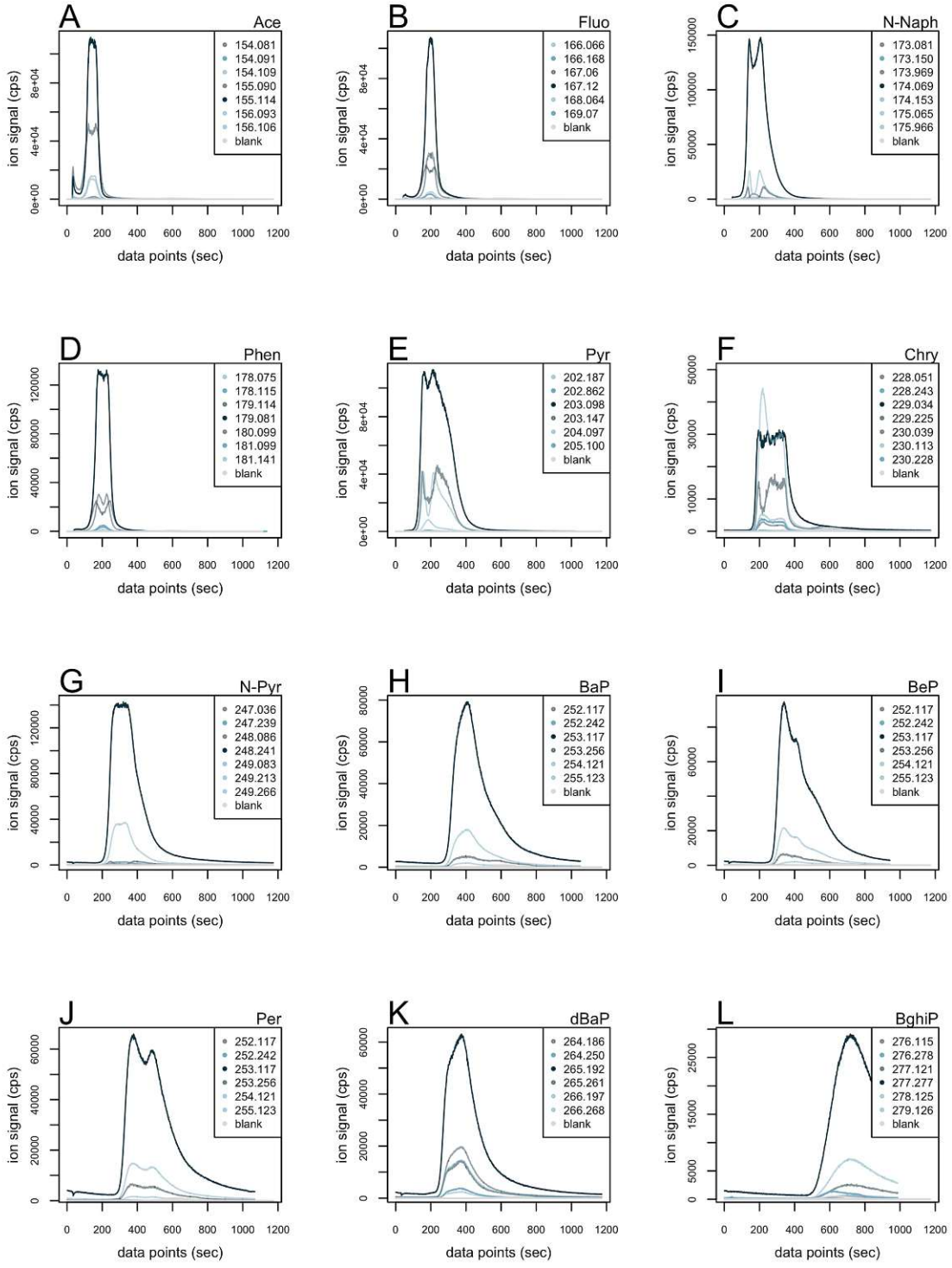

Figure 34 A-L. Thermograms of the most prominent ions in comparison to their neighboring ions and blank responses for all analytes. Thermograms represent the response of roughly 150 ng PAH compound adsorbed on a quartz fiber filter. Note, that thermograms visualize the raw data of each TD run and do not refer to already processed data.

7.1.3. Assignment of masses based on the evaluation of thermograms

The thermograms presented in **Figure 34** visualize the response for a couple of ions including the molecular ion, the protonated signal and signals of isotopes as well as blank signals of the respective masses. We could not identify any fragmentation induced by either PTR or thermal stress, nor could we detect cluster formation. Based on the information gained from the thermograms we assigned different masses to each compound, which were later also used for quantification purposes. By comparing the evolution of the different masses during the TD run, we assigned ions to each compound. Similar evolution of ions but differences in masses were attributed to an artefact in data processing and not because of differences in their molecular structure. This assumption is only valid because thermograms depict measurements of high purity single compounds, which should not be influenced by the co-desorption of isobaric interferences. **Table 25** sums up basic information about the key analytes and also the assigned masses used for qualitative and quantitative purposes. Among the tested PAHs, BghiP is the highest one in molecular weight and we successfully identified associated prominent ion signals, although with limited recovery (24%).

Table 25. Basic information regarding the key analytes. The assigned masses refer to the ion signals identified as the most prominent ones during processing of the thermograms. The listed ions signals were summed up and used for quantification purposes. Ions in brackets refer to the isotopes and were not used for quantification purposes. † The used TD program was not sufficient to fully desorb BghiP from the filter aliquot, which was also reflected by a rather low recovery rate. ‡ Proton affinities were retrieved from the NIST chemistry webbook (https://webbook.nist.gov/chemistry/pa-ser/).

Abbr	Formula	Molecular weight (g/mol)	Monoisotopic mass (Da)	PA‡ (kJ/mol)	Assigned masses (Da)	Range of calibration	Average recovery rate
Ace	$C_{12}H_{10}$	154.2	154.0783	851.7	155.090, 155.114 (156.093,156.106)	2.03 – 50.7 ng	46%
Fluo	$C_{16}H_{10}$	166.2	166.0783	831.5	167.060, 167.120, 167.136 (168.064, 169.070)	2.17 – 54.3 ng	42%
N-Naph	$C_{10}H_7NO_2$	173.2	173.0477	-	174.069 (175.065)	1.78 – 46.2 ng	127%
Phen	$C_{14}H_{10}$	178.0	178.0783	820.1	179.081, 179.114 (180.099, 181.099	2.02 – 50.6 ng	61%
Pyr	$C_{16}H_{10}$	202.3	202.0783	869.2	203.098, 203.147 (204.097, 205.100)	3.52 – 87.9 ng	81%
Chry	$C_{18}H_{12}$	228.3	228.0939	843.5	229.034, 229.225 (230.039, 230.228)	2.32 – 58.1 ng	50%
N-Pyr	$C_{16}H_9NO_2$	247.3	247.0663	-	248.086 (249.083)	1.94 – 50.4 ng	133%
BaP	$C_{20}H_{12}$	252.3	252.0939	887.0	253.117, 253.256 (254.121)	1.79 – 44.8 ng	41%
BeP	$C_{20}H_{12}$	252.3	252.0939	861.9	253.117, 253.256 (254.121)	2.12 – 52.9 ng	18%
Per	$C_{20}H_{12}$	252.3	252.0939	888.6	253.117, 253.256 (254.121)	1.58 – 39.6 ng	63%
d-BaP	$C_{20}D_{12}$	264.4	264.1692	-	264.186, 264.250, 265.192, 265.261	3.85 – 100 ng	35%
BghiP	$C_{22}H_{12}$	276.3	276.0939	876.0	277.121, 277.277 (278.125, 279.126) †	2.21 - 55.2 ng	24%

7.1.4. The method's limit of detection

We utilized the background signal observed during the analysis of system blanks (SB) (i.e. thermal desorption of clean, prebaked glass vials). All measurements were realized using the PTR setup and parameters described in more detail in **section 3.2**. **Figure 35** A visualizes the full mass spectrum of the median response for 55 SB measurements. Highest responses could be observed for masses lower than 100 Da, while neglectable responses could be detected across the mass range of 100.044 – 454.494 Da. Impurities in the system resulted in small peaks in the lower mass range (up to 100 Da). Those impurities did not influence the measurements as all ions used for quantification purposes were higher than the threshold of 100 Da and all measurements were corrected with the respective blanks and LODs. **Figure 35** B depicts the median mass spectrum observed for the mass range beginning from 100.044 Da.

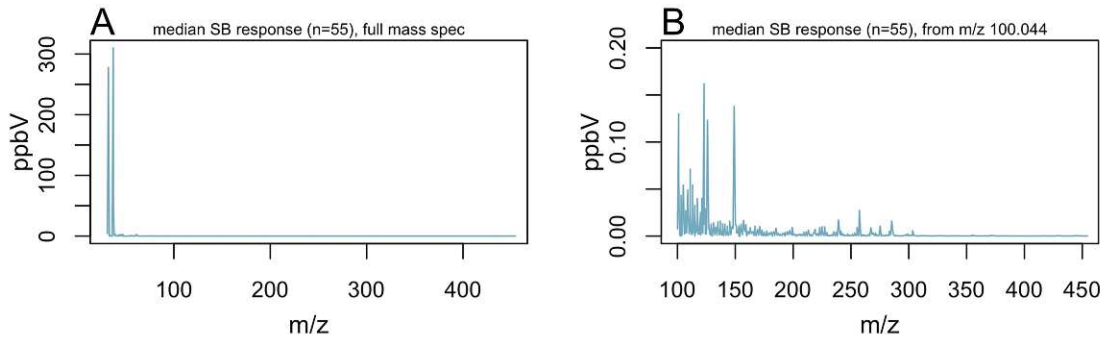

Figure 35 A-B. (A) Full mass spectrum visualizing the median response of 55 SB measurements. **(B)** Mass spectrum visualizing the median response of 55 SB measurements. The m/z range is limited to masses above 100 Da. Note the different y axes.

As already mentioned, the mass range beginning from 100 Da is the most important one as PAHs did not show severe fragmentation which would be preferably detected below 150 Da. High responses at the m/z of the protonated molecular ions of the respective PAHs were visible above 150 Da. **Table 26** lists the response of SBs observed at the masses assigned to the PAH signal. Negligible readings at masses assigned to the PAH signal (as listed in the following table) indicate that the TD-PTR-ToF-MS system was not severely contaminated at all and those minor contaminations did not influence the PAH measurements as responses observed during method development exceeded the responses of SB measurements by several orders of magnitude. Besides that, we could not observe a time related drift of the SB readings during those 55 measurements.

Table 26. Readings of system blanks (SBs, n=55) for the masses assigned to the PAH signals.

analyte	ppbV
Ace	0.028
Fluo	0.033
N-Naph	0.002
Phen	0.007
Pyr	0.003
Chry	0.009
N-Pyr	0.000
BeP, BaP, Per	0.013
dBaP	0.004
BghiP	0.002

The method's limit of detection (LOD) was calculated on the basis of all system blank (SB) measurements (n=55). For LOD calculation ppbV values were multiplied with the students t-factor at a confidence interval of 95% according to LOD = 2.01*σ_{SB}. And results (ppbV) were converted to their analogues given in ng according to the following formula (**Eq. 10**):

$$m_{PAH} = \frac{[ppbv_{\frac{m}{z}}]}{V_M} * MW_{MH+} * F_{zero\ air} * t_{int}$$

Eq. 10. Calculation of PAH recovery from PTR measurements

The ppbV signal of each m/z is converted to the mass of PAH in ng by dividing it through the molar volume V_M (= 22.4 L/mol) and by multiplication with the molecular mass of the respective protonated ion (MW_{MH+}), the flow of zero air (= 100 mL/min) and the time of integration used for data processing (t_{int}= 10 min). Integration was done when the temperature of the TD reached 50°C and from that for 10 minutes onwards. In case of Ace, a decent amount of desorbed material was not included in the exported data as it already heavily desorbed before reaching 50°C.

Table 27 lists all LODs observed for each PAH congener (i.e. for beforehand assigned masses). Ion signals observed for blanks and PAH measurements done during method development clearly exceeded the LODs and all results presented in the following sections were corrected with the respective blank and subsequently underwent LOD filtration. For all samples, checking for LOD was realized on the ppbV level.

Table 27. Detection limits given in ppbV and ng based on the measurements of system blanks (n=55) for the most abundant ions identified within the investigation of raw data thermograms. Results given in ppbV have been converted to ng considering the molar volume (22.4 L/mol) the flow into the PTR-ToF-MS system (100 mL/min) and the integration time (10 mins) and the molecular mass of the protonated ion.

LOD (n=55, t95%)	ppbV	ng
Ace	0.040	0.28
Fluo	0.198	1.48
N-Naph	0.002	0.01
Phen	0.008	0.07
Pyr	0.003	0.02
Chry	0.017	0.18
N-Pyr	0.001	0.01
BeP	0.040	0.45
BaP	0.040	0.45
Per	0.040	0.45
dBaP	0.005	0.06

Comparing the LODs retrieved from TD-PTR-ToF-MS measurements with the ones obtained during GC-MS/MS measurements (**section 6.3.3.),** both on the ng level, presented a quite diverse picture. As TD-PTR-ToF-MS measurement is known to be a highly sensitive analytical tool, we expected clearly lower LODs. This was corroborating with most of our findings as we observed lower LOD values for the majority of key analytes, i.e. Ace, Phen and Pyr. In the case of Fluo and Chry LODs were in a similar range (compare **Table 21** and **27**). Note, that key analytes differ within both experiment, i.e. N-PAHs were only analyzed within **chapter 7,** while BaP, BeP and Per did not show responses during GC-MS/MS blank measurements and thus we were not able to give information about LODs of all analytes presented in **Table 27**.

7.1.5. Interpretation of filter blank measurements

In order to evaluate if the quartz fiber filters or the organic solvent mixture (i.e. cHex and DCM, v/v, 1/1) also emit high amounts of semi-volatiles which may influence the PAH measurements, we performed the measurements of different kinds of blanks. For this, we prepared the blank filters as described in **section 3.6.1**. Boxplots for all blank groups and assigned masses are given in **Figure 36**. By comparing the presented boxplots, we cannot notice significant differences among blank groups of the given ion signals. However, ion signals of blanks realized on quartz fiber aliquots referring to a diameter of 8 mm scatter in a wider range, than observed for 7 mm diameter blanks. This may be attributed to the different sample size of blanks. The smallest number of blank measurements was conducted for the group "BS10_7", which presents the results for quartz fiber filter aliquots spiked with 10 µL organic solvent mixture. For every PAH congener, results obtained for this blank group show narrow responses. In order to conclude differences among blank groups in a verified way, we did further statistical analysis of blank measurements. The responses of blank filters exceeded the respective ones of system blanks and presented results

already underwent LOD correction. Note, that blank signals observed for the masses assigned to dBaP did not exceed the respective LOD. All presented results, i.e. PAH mass spectra measurements, calibration measurements and recovery tests with PAH spiked onto a filter aliquot were corrected with the respective blank measurements.

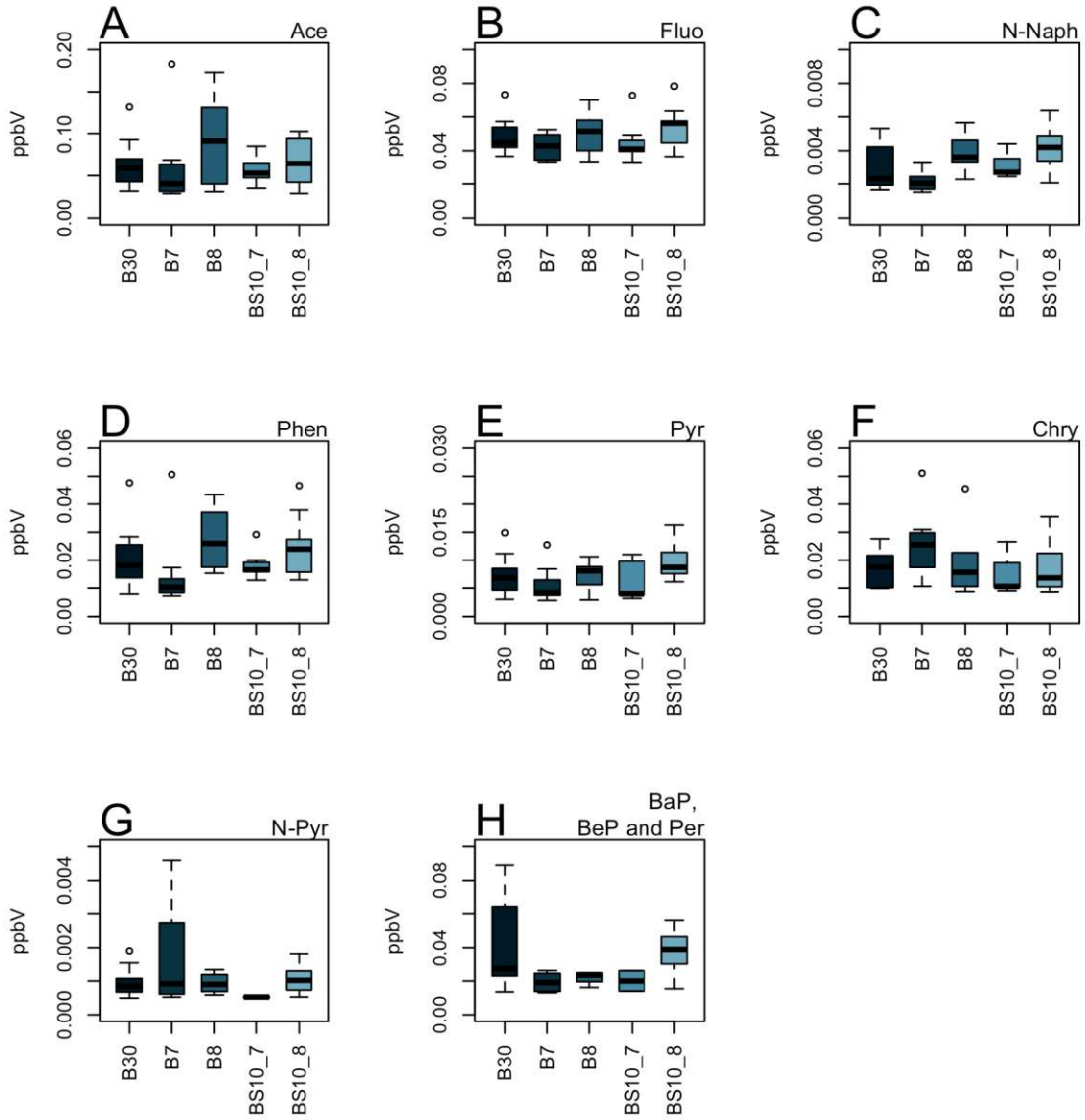

Figure 36 A-H. Boxplots visualizing the differences among blank measurements. Whiskers mark the interquartile range. More details about the different blank names is given in **Table 28**. Evaluation is based on the sum of assigned ion signals identified from the visual investigation of raw data thermograms. Each boxplot refers to the sum of the signals of assigned masses, which are given in **Table 25**.

A more detailed statistical analysis was realized to check whether there are significant differences among the blank groups or if they may be aggregated and further processed as one. Firstly, we checked our data for normality using the Shapiro Wilk test. It has to be noted, that some masses did not show a normal distribution, which we link to a limited sample size. We assume that our data follows the central limit theorem and thus we evaluated our data on a more detailed statistical

level. Meaning that ion signals from blank measurements were grouped according to their filter size and differences among the groups were evaluated using one-way ANOVA (8 mm filter aliquots) or two- sample t-test (7 mm filter aliquots). As assigned masses were the most prominent ones found when evaluating the PAH measurements, statistical data evaluation also refers to the most abundant ions identified from the raw data thermograms.

Table 28. Details about blank measurements and evaluation type. Blank filters were prepared according to the same procedure as for PAH filter measurements.

Abbr.	Blank preparation procedure	Sample size (n)	Evaluation type	Blank group
B8	8 mm punch	11	One-way ANOVA	X
B30	8 mm punch, dried at 30°C in the oven for 15 min, no organic solvent spike	17	One-way ANOVA	X
BS10_8	8 mm punch, spiked with 10 µL DCM:cHex, dried at 30°C in the oven for 15 min	19	One-way ANOVA	X
B7	7 mm punch	14	Two-sample t-test	Y
BS10_7	7 mm punch, spiked with 10 µL DCM:cHex, dried at 30°C in the oven for 15 min	7	Two-sample t-test	Y

One-way ANOVA and t-test were realized using a significance level of α=0.01. Among the blank group summing up all blanks with a diameter of the filter aliquot of 8 mm (hereinafter referred as the blank group X), significant differences were found for only two masses assigned to Phen and dBaP. As the signals referring to the blank group X for selected masses did not report significant differences for the majority of ion signals, all measurements assigned to the blank group X were grouped and further handled as one. In case of the blank group referring to a filter aliquot diameter of 7 mm (hereinafter referred to as blank group Y) results presented a different picture. The two blanks did not show a significant difference (α=0.01) for signals assigned to LMW PAHs. Significant differences among the blank group Y were found for Pyr, Chry, N-Pyr, BaP and its isomers and dBaP. Based on these results measurements done for filter aliquots with a diameter of 7 mm were corrected with the respective blanks, i.e. blank group Y was not unified and all blank corrections were done on the basis of the B7 signals.

7.1.6. Recovery rates of PAHs

Recovery rates were calculated in order to determine which fraction of the PAHs spiked onto filters for calibrations measurements is recovered by the TD-PTR-ToF-MS. For this, the detected amounts of each PAH congener was calculated according to the equation presented in **section 7.1.4.** (see **Eq. 10**). Subsequently recoveries were calculated by simply comparing the detected mass of PAH to the initially loaded PAH mass. **Table 29** lists the recovery rates calculated for each calibration measurements (i.e. average of all measurements used for calibration purposes). LMW PAHs, such as Ace and Fluo, which are also highly volatiles ones, show average recoveries of 46% and 42%, respectively. It appears that especially LMW PAHs like Ace and Fluo are hardly recovered by TD-PTR-ToF-MS. As already introduced in **section 7.1.2.**, is very likely that those highly volatile substances are lost due to evaporation processes occurring during the sample

preparation or before the thermal desorption protocol starts and are thus not even transported into the PTR-ToF-MS setup. If compounds already desorb before the TD even start, a decent amount of the respective compound is not gathered and thus excluded during data processing, as during that mass spectra are averaged and merged from a temperature of 50°C onwards for 10 minutes. This means, that Ace and Fluo signals are not fully represented by this technique. Recoveries of HMW PAHs were in the same or even higher range, yielding average recoveries of up to 63% (Per). Considering all p-PAH congeners, maximum recoveries are 124% (Pyr) which is still in an adequate range according to the DIN EN 15549:2008 (standard for BaP measurements derived from particulate matter). Highest recoveries are found for both nitrated PAH congeners, with the maximum recovery observed for N-Pyr (median: 133%, range: 91 – 202%). As drift tube parameter were kept constant, these higher recovery rates may be attributed to differences in the reaction rate constant of N-PAHs. During data processing a fixed reaction rate constant is applied and obtained results suggest, that the chosen one is not optimal to describe the proton transfer reaction rates of N-PAHs leading to overestimations. Rather low recovery rates might be attributed to the use of quartz fiber filters for sample preparation or an insufficient thermal desorption process. It has already been reported that quartz fiber filters promote the adsorption and binding of different compounds, which on the one hand binds highly volatile compounds until they are thermally desorbed, but on the other hands makes it more difficult to thermally desorb molecules with lower volatility (Dorst 2014). This effect cannot be observed in a pronounced extent when comparing the recovery rates of PAH congeners. Also, recovery rates observed for the HMW PAH congener BghiP are rather low yielding an average recovery rate of 20%. This is caused by an insufficient thermal desorption of BghiP, as described in more detail in **section 7.1.2**.

Table 29. Recovery rates obtained for calibration measurements. The median, minimum and maximum recovery rates are based on all measurement points realized during calibration.

Analyte	Recovery (%)		
	Median	Min	Max
Ace	46%	28%	94%
Fluo	42%	25%	76%
Phen	61%	39%	110%
Pyr	81%	41%	124%
N-Naph	127%	41%	178%
Chry	50%	4.6%	40%
dBaP	35%	20%	59%
N-Pyr	133%	91%	202%
BeP	56%	0.8%	103%
BaP	41%	12%	67%
Per	63%	27%	145%
BghiP	20%	4.2%	37%

7.1.7. PAH calibrations

PAH calibrations were performed by spiking quartz fiber filters with single substance covering a concentration range of about 1.5 ng to 100 ng. Detailed information about the calibrated concentration ranges of each congener is given in **Table 25**. Calibration was realized by summing up the signals identified within the investigation of the thermograms and assigned masses are also given in **Table 25**. **Figure 37** A-K visualizes the calibration plots of the assigned protonated ion signals of individual PAH congeners. Each point in the calibration plot represents the average signal observed within five individual measurements.

A highly linear relationship (R>0.94) can be observed for all quantified PAH congeners. Calibrations of LMW PAHs show highest deviations among concentration steps, while linearity improves when it comes to higher molecular weight PAHs. Pearson correlation coefficients varied between 0.9488 (Pyr) and 0.9989 (BeP). In the majority of cases, PAH calibrations did not show a very sensitive behavior and evaluation of the retrieved recoveries is discussed in **section 7.1.6**. Best results could be achieved for N-PAHs (k>0.708). N-PAHs were overestimated yielding recovery rates of 127% (N-Naph) and 133% (N-Pyr). These overestimations of N-PAHs may be attributed to the application of a sub-optimal reaction rate constant during data processing. A more detailed discussion is given in **section 7.1.6**. The lowest sensitivity was observed for dBaP, which is the deuterated analogue of BaP (average recovery rate of 35%) and in routine analysis is used as a recovery standard for BaP (according to EN 15549:2008). Low sensitivity of the calibration curve and the resulting low recovery rate of LMW PAHs may be attributed to losses during or even before the desorption, i.e. not all desorbed analyte was transported into the PTR-ToF-MS system, or already lost before the measurement was even started or not fully desorbed from the quartz fiber filter. The three HMW PAH isomers BeP, BaP and Per showed quite similar calibration parameters (see **Figure 37** H-J). Among these, the calibration curve for Per showed the highest sensitivity with an average recovery rate of 63%, followed by BeP with an average recovery rate of 56%. The recovery for BaP, the most studied PAH and known carcinogen, was 41%. These differences in sensitivity could not be attributed to fragmentation in the drift tube, nor thermal degradation during the TD process as isotopic ratios did not change within the individual calibration steps. Furthermore, we were able to exclude the occurrence of deprotonation reactions ($MH^+ + H_2O \rightarrow H_3O^+ + M$) as reason for low responses, as proton affinities of all PAHs were higher than the one of water, drift tube parameters were kept constant and signals retrieved for the deprotonated ion signals are negligible (see **Figure 34**). As individual isomers (i.e. BeP, BaP and Per) did not show unique features in the mass spectra, we were not able to selectively distinguish them. Note that, these unique features are especially important, when developing a fingerprinting algorithm, which is consequently not feasible with our dataset.

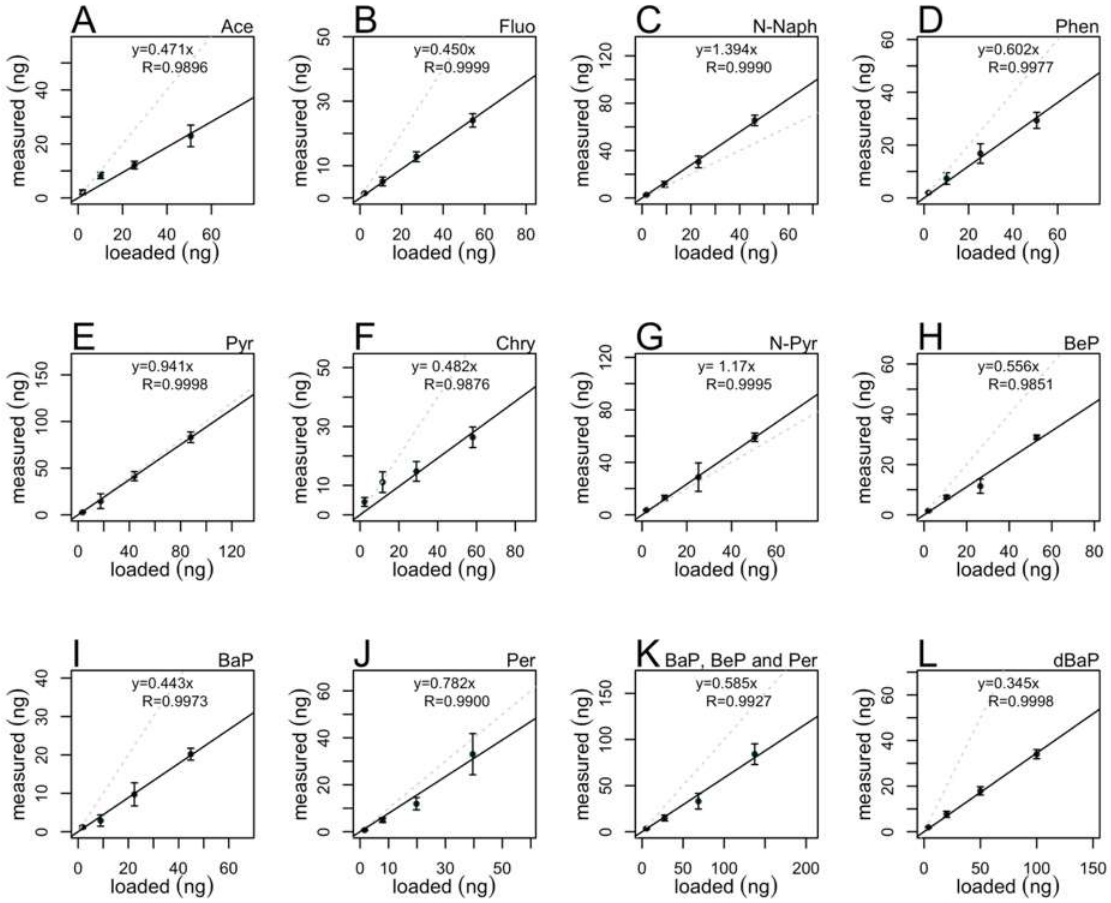

Figure 37 A-L. Calibration curves visualizing the sensitivity and linearity of the protonated ion signals for each individual congener. Each concentration step is represented by five replicas. Error bars represent the standard deviation among the individual measurements. The grey dashed line highlights a recovery of 100%.

7.2. Application to aqueous samples

7.2.1. Snow profile and cloud water sampling

Cloud water and surface snow profile samples were collected at Sonnblick Observatory, a glacier in Austria (3106 m asl), which is considered as international background station since there is no direct influence of local pollution. Snow profile samples were collected at the roof of Sonnblick Observatory and sampling was realized with vertical resolution of roughly 15 cm by simply overturning the pre-baked (overnight, 250°C) glass jars and filling them with snow. Samples were labelled according to their profile depth, i.e. SP1 presents the situation at the surface of the snow pit, while SP10 presents the situation for the deepest snow level (roughly 1 m). Note, that depth has to be regarded as an approximate value, in our case the uncertainty of sampling is ± 3 cm. All snow profile samples were taken on the 17.03.2021 around lunch time.

CWs was collected with an active cloud water sampler described by Kruisz et al. (1993) (Kruisz, Berner, and Brandner 1993). Droplets within a size range of 7 – 200 µm were collected on a Teflon impaction surface (sampling rate of 80 m^3/h) with a single impaction stage (Kruisz, Berner, and Brandner 1993), which was also applied in previous works (Hitzenberger et al. 2001, Limbeck and Puxbaum 2000). The CWs was then transferred to a pre-baked glass jars and both samples, i.e. SPs and CWs were kept frozen until analysis. While all SPs were sampled on the same day within a time frame covering 20 minutes, i.e. 17.03.2021, CWs describe different sampling points to different dates and times with a different sampling duration. All details about the analyzed CWs are given in **Table 30**.

Table 30. Details about analyzed cloud water samples (CWs). Sampling was realized on the international background site Mt. Sonnblick (3106 m asl).

CW sample ID	sampling date	sampling time	duration of sampling (h)
1608	16.03.2021	16:55	1.19
1802	18.03.2021	04:33	1.38
1805	18.03.2021	09:01	1.55
1809	18.03.2021	16:01	1.31
1813	19.03.2021	01:25	2.55

For analysis, sample aliquots of 0.5 mL cloud water samples (CWs) or 1.0 mL of snow profile samples (SPs) were transferred into clean, prebaked (overnight at 250°C) glass vials. Afterwards, sample vials were placed in a low-pressure-evaporation (LPE) system with maximum distance to avoid cross contamination as described in **section 3.6.2**. Briefly, sample preparation based on low-pressure-evaporation removes water (sample matrix) while limiting the loss of semi-volatile compounds and avoiding contamination with lab air and the method has been developed by Materić et al. (2017) (Materić et al. 2017). Afterwards, samples were thermally desorbed and analyzed using the same conditions as used for PAH filter measurements.

7.2.2. Recovery of PAHs in spiked snow profile samples

To check if specific compounds are lost during the sample preparation procedure using the LPE system, we spiked some snow profile samples (SPs) and blanks (i.e. 1 mL HPLC water) with a certain amount of PAH mix, i.e. N-Naph and dBaP. To determine which amount of PAH spiked to samples is recovered by the TD-PTR-ToF-MS, the initial recovered amount of PAH was calculated as follows: firstly, ppbV results were converted into ng (measured) according to the procedure mentioned in **section 3.2**. Secondly, the amount of PAH in ng (measured) was converted to ng (loaded) using the calibration curves obtained for PAHs, which considers the recovery rate observed for the individual PAHs. **Figure 38** visualizes the recovered amounts for N-Naph and dBaP for two different spike experiments, i.e. blue bars visualize the recovered amount for samples where PAHs were directly spiked to the aqueous sample (hereinafter referred to as directly spiked samples), while grey bars represent the recovered amount of the respective PAH, which was aforehand spiked onto an aliquot of quartz fiber filter and subsequently added to the aqueous sample (hereinafter referred to as samples with spiked filter aliquots). Based on the recovery rates

retrieved from prior PAH experiments, we expected an overestimation of N-PAHs. However, it appears that N-Naph is hardly recovered by the TD-PTR-ToF-MS, which may be attributed to evaporation processes before or during the sample preparation step using the LPE setup. Losses attributed to the LPE procedure apply only for samples as PAH experiments used for calibration purposes were prepared according to a different procedure (see **section 3.6.**). N-Naph is a volatile PAH congener, which was obviously lost due to the strong vacuum applied during the LPE sample preparation procedure. On average, N-Naph recoveries ranged between 1.8% and 4.5% for directly spiked samples and between 3.1 and 12% for samples with a spiked filter aliquot. Recovered amounts of dBaP were found to be higher and in most cases overestimated by the TD-PTR-ToF-MS setup. As we did not observe overestimations of dBaP during the single PAH and blank measurements and as fully deuterated molecules like dBaP are hardly found in the environment, we attribute this overestimations observed at the masses assigned to dBaP to isobaric interferences derived from the co-desorption of compounds from the sample itself. Average recoveries of dBaP ranged between 83 and 127% for directly spiked samples and between 80 and 151% for samples with spiked filter aliquots. Lower recoveries of dBaP were observed in aqueous blanks (spiked HPLC water, not depicted in **Figure 36**) with similar average recoveries of 91 and 90% in directly spiked and spiked filter aliquot blanks. Lower recoveries found in aqueous blanks strengthen the assumption of isobaric interferences caused by the samples. In almost all cases, recovered amounts of PAHs were higher for spikes done on quartz fiber filters than for directly spiked samples. This indicates that PAHs adsorb to the quartz fiber filter which suppresses losses before or during sample preparation but also complicates the desorption from the filter as it has been described in the previous sections. This effect has already been described by Dorst (2014), reporting differences among quartz fiber filters and aluminum foil as temporary adsorbent (Dorst 2014).

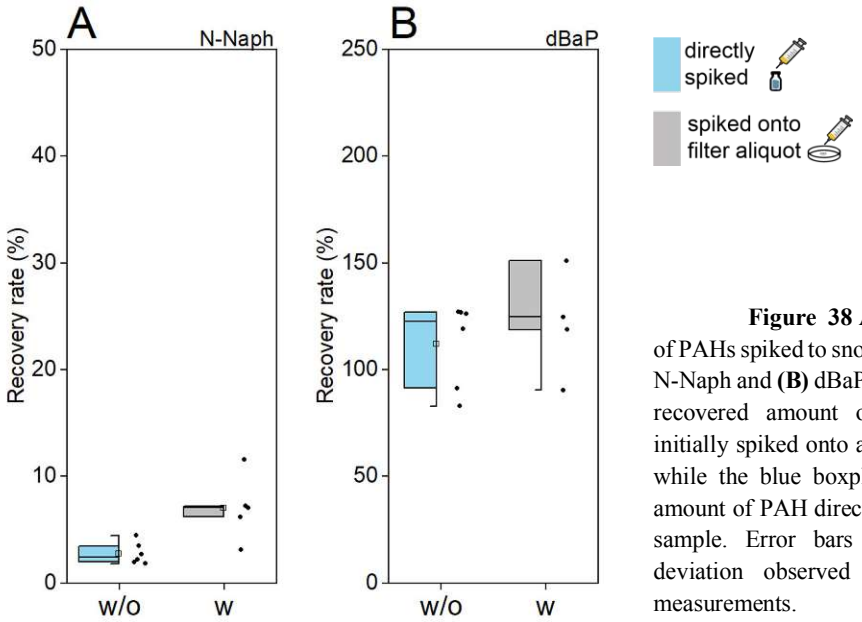

Figure 38 A-B. Recovered amount of PAHs spiked to snow profile samples for **(A)** N-Naph and **(B)** dBaP. Grey boxplots mark the recovered amount of the respective PAH initially spiked onto a quart fiber filter aliquot while the blue boxplots mark the recovered amount of PAH directly spiked to the aqueous sample. Error bars represent the standard deviation observed among the individual measurements.

7.2.3. PAH concentrations of snow profile and cloud water samples

Previously presented PAH concentrations from surface snow samples suggested to use a sample volume of at least 10 mL of cloud and snow profile samples. Especially cloud water is very limited in the sample volume, which is why we analyzed clearly lower aliquots of snow profile (1 mL) and cloud water (0.5 mL) with the highly sensitive TD-PTR-ToF-MS method. The use of these low volumes further allows to aim for higher time resolution of sampling. All samples yielded clear responses on the ppbV level for the respective masses. This means we were successfully able to conduct TD-PTR-ToF-MS analysis of cloud water and snow profile samples using volumes <1 mL. Unfortunately, we could not convert the ppbV response into their concentration analogues, i.e. ng/L, most likely due to isobaric interferences with other substances found in both sample matrices concentrations showed up way too high. Converting the ppbV readings to liquid concentrations highest values of masses assigned to PAHs were observed in the middle layer of the snow profile, which may indicate accumulation and enrichment in deeper snow layers. Besides that, we found higher responses for masses attribute theoretically to PAHs in cloud water samples taken during the night or early morning hours. As expected, information about the PAH concentrations given in ng/L based on TD-PTR-ToF-MS analysis using very low sample volumes remains unexplored. For future experiments, we aim to modify the sample preparation procedure (i.e. lower vacuum needed and higher sample volumes) to sufficiently quantify PAHs in both sample matrices.

7.3. Conclusion and outlook

Results show, that TD-PTR-ToF-MS is suitable to monitor and quantify PAHs thermally desorbed from quartz fiber filters over several orders of magnitude. Presented results nicely highlight the importance of a profound method development and design of experiments as we had to face several obstacles during this process. Applying the developed method to samples from the aqueous phase (i.e. snow and cloud water) show that a method developed for one application cannot be simply transferred to different matrices. In our case, sample support refers to quartz fiber filters used for PAH calibration measurements. We noticed, that quartz fiber filters only emit a neglectable amount of semi-volatile compounds at masses below 100 Da, which do not influence the PAH measurements at all. All ion signals retrieved during PAH measurements clearly exceeded the respective blank values and passed LOD filtration. PAH calibrations were performed by spiking quartz fiber filters with single substance PAHs covering a concentration range of about 1.5 ng to 100 ng. A high linear relationship ($R>0.94$) can be observed for all quantified PAH congeners, with Pearson correlation coefficients between 0.9488 (Pyr) and 0.9989 (BeP). However, mainly LMW PAHs did not show a very sensitive behavior, which may be attributed to losses during the desorption or even before that, i.e. not all desorbed analyte was transported into the PTR system or already lost before the measurement was even started or not fully desorbed from the quartz fiber filter. As the mass spectra of BeP, BaP and Per, three isomers, did not show unique features, we were not able to selectively distinguish between them. Note, that differences in mass spectra and especially unique features are necessary for the use of fingerprinting algorithm, which is not given with our dataset. This further complicates the application of the

developed method to other matrices as PAHs are always found in complex mixtures of congeners and environmental samples contain much more analytes, enhancing the probability of isobaric interferences. As changes in sample preparation or matrix may affect the thermal desorption behavior of the hydrophobic PAHs, we also tested the recovery rates of N-Naph and dBaP spiked to snow profile samples. In order to do so, two sets of experiments were realized, i.e. (i) one using a piece of quartz fiber filter as sample support before adding it to the sample and (ii) the other one by simply spiking PAH solution to the aqueous sample. By tendency, measurements of spiked samples yielded higher recovery rates, as if PAHs were spiked onto a quartz fiber filter aliquot before adding it to the sample. This indicates that PAHs adsorb to the quartz fiber filter suppresses losses before or during sample preparation but also complicates the desorption from the filter. Even though we observed overestimations of N-PAHs during method development, it appears that N-Naph was hardly recovered during recovery experiments from surface snow samples. This can be attributed to losses of the volatile PAH during the LPE sample preparation procedure, which was not the case for dBaP.

The application of this new method to very low volumes of snow profile and cloud water turned out to underlie higher biases than expected. Due to isobaric interferences we were not able to give information about the PAH contributions on a rather tentative level. PAHs are found in the sub-ppb to ppt range in snow and cloud water and thus place additional input to isobaric compounds. Evaluating the results on the ppbV level allows to give first insights in possible PAH contributions observed in both sample matrices. These findings absolutely encourage further research by analyzing larger sample aliquots (10 mL), which is, in case of cloud water samples, however accompanied by loss of time resolution.

Chapter 8 Summary and Outlook

The development of novel methods for the quantification of different PAH congeners is highly relevant as PAHs are always emitted as complex mixtures of various congeners and found in all environmental compartments. PAH contributions show a gradient trend in different matrices, with higher ones found near the emission source and lower ones observed in ambient samples, snow and cloud water. This thesis demonstrates the emerging need of analytical tools for the simultaneous quantification of a rich palette of PAHs optimized for various environmentally important matrices. The aim of this thesis was to quantify PAH contributions from different compartments, spanning the scope from the emission source to ambient concentrations, and enlarges the focus to compartments used for atmospheric transport and accumulation, i.e. snow and cloud water. The joint effort of partners from *BEST – Bioenergy and Sustainable Technologies GmbH*, *Land Steiermark*, *University of Natural Resources and Life Sciences (BOKU Wien)* and *Utrecht University* lead to the following achievements of this thesis:

Real-life PAH emissions were evaluated on the basis of total suspended particle samples retrieved within a field measurement campaign showing the variety of maloperations at the users' end and highlighting advantages of optimized combustion conditions. By optimizing the combustion conditions following a strict optimization protocol, the emissions of 12 PAH congeners could be decreased to a maximum of 1%. Besides that, optimization led to a shift of PAHs patterns resulting in the emission of higher contributions of LMW PAHs and thus less toxic ones reflected by clearly lower toxicity equivalents. Obtained results markedly enlarged knowledge about real-life emission factors by demonstrating that user training is of similar importance as changes in technology, because maloperations may counteract technological improvements.

Changes in emissions and related technologies also influence the ambient load of pollutants. To assess the impact of PAH emission on the ambient level, PAH quantification was realized from

ambient particulate matter samples ($PM_{2.5}$) derived from the urban sampling station Graz Don Bosco. This sampling location is a very well-known hot spot for high PM burdens and during the beginning of 2017 (Jan – March), the European Union short time limit value for the PM_{10} concentration was exceeded several times. Ambient PAH concentrations showed a decreasing trend during these three months with dominant contributions of HMW PAHs, i.e. BbkF and BaP. Dividing the time periods based on their differences in PM_{10} ratios observed at the urban site and the respective background site introduced a rather simple approach to differ between source contributions, i.e. urban influence and regional transport. Urban influenced time periods did not only show higher PAH contributions, but also higher contributions of individual PAH congeners related to traffic emission and combustion (i.e. BbkF, BaP and BghiP).

Elevated atmospheric PAH concentrations are found near the emission source, while lower contributions found in more pristine areas indicate the ability of long range transport of PAHs. PAHs are hydrophobic compounds and their sorption ability to different polymer types has already been extensively reported for the aqueous phase. Within this thesis we present a novel approach to identify possible atmospheric carrier activities of three different polymer types to 23 individual PAH congeners using a multi method approach. For the first time, we report atmospheric concentrations of ultrafine microplastics and nanoplastics (UFMNP) from urban particulate matter on the single polymer level (i.e. PET, PP and PE). Among quantified polymer types PET was observed during the entire time period (i.e. 02.01. – 31.03.2017), while PP and PE are quite variable and obviously linked to the origin and fate of air masses. A possible carrier function of PP and PE for selected micropollutants was deduced from the significant monotonic correlations between these polymers and selected PAHs. Presented results are the first ones discussing the relationship of PET, PP and PE and PAHs found in urban particulate matter samples. This work enlarges the recent focus of PAHs and polymer types observed in the aqueous phase to the atmospheric compartment and highlights the need for future research to improve the understanding of polymers as PAH vehicles for atmospheric transport and the potential health outcomes.

To investigate in which extent PAHs are deposited in various regions, we enlarged the common focus of PAH contributions to snow and cloud water samples. Shifting the focus to different environmental compartments is entailed with a couple of analytical challenges. In general, lower PAH contributions are expected in snow and cloud water samples, they, however, significantly differ in their availability and sample volume.

For PAH quantification in snow samples, we developed a novel method allowing the simultaneous quantification of up to 37 PAHs in a single chromatographic run. As the PAH concentrations in snow tend to be lower than observed in atmospheric samples, the SPE sample preparation procedure served as purification and preconcentration step using dedicated, bifunctional SPE columns. PAH concentrations found in surface snow samples across Austria vary among magnitudes and the spatial distribution of individual PAH congeners at different sampling locations is clearly reflected by their differences in toxicity. The total PAH burden observed at remote locations was dominated by LMW PAHs, which are less toxic, while samples influenced

by human activity show richer PAH patterns, which is in line with a higher overall PAH load and clearly reflects a variety of sources at urban influenced sites.

When it comes to cloud water samples, the combination of low sample volume and analyte concentration refuses the use of typically used analytical methods for PAH quantification. To accomplish this challenge, the use of a method pairing high selectivity and sensitivity is crucial. First measurements of single PAH congeners adsorbed to quartz fiber filters using a proton transfer reaction – time of flight - mass spectrometer (PTR-ToF-MS) setup yielded promising results. We successfully report the application of PTR-ToF-MS to monitor and quantify PAHs thermally desorbed from quartz fiber filters. Calibration measurements for 10 different congeners showed high linear relationships ($R>0.94$) over several orders of magnitude. Recovery tests utilized by spiking surface snow samples indicated that a prior spiking of PAHs to filter aliquots led to an adsorption of PAHs suppressing analyte losses throughout the entire sample preparation or measurement procedure. Unfortunately, the application of the developed PAH method to cloud water samples underlaid higher biases as expected as environmental samples contain much more analytes which enhances the probability of isobaric interferences. Nevertheless, results present a first step of quantifying PAHs in cloud water samples and absolutely encourage further research towards that.

With those achievements, this thesis underlines the importance of quantifying various PAHs in either of the matrices and also highlights the common fate of PAHs and other emerging pollutants. The results present analytical tools to highlight and investigate the occurrence and some of the impacts of PAHs in several environmental matrices and suggest several next steps and modifications:

(1) As quantification of BaP has to be routinely done in terms of reporting to national institutions, it is straightforward to simultaneously quantify more PAH congeners than desired. At least the quantification of all PAHs listed within the US EPA priority list can be realized by slightly modifying the temperature program under the use of the commonly used GC-MS setup for PAH quantification, i.e. 30 m of a nonpolar phenyl arylene polymer column (5% crosslinked with phenyl methylpolysiloxane). This additional step was already compiled within this work and has proven to be easily applicable to particulate samples from different origin. Still, the quantification of PAHs with molecular weights higher than 300 remains a challenge in routine analysis.

(2) The developed GC-MS/MS method for snow analysis has proven potential for analyzing surface snow samples or snowpack samples derived from remote or pristine areas. However, our results recommend to adapt the sample volume in regard of the sampling location and its influences. For samples from locations near highly influenced areas minimal sample volumes of 500 mL may be applicable for analysis, while this has to be increased for analysis of samples from remote regions (> 1000 mL). Future snow sampling should be solely realized using glass reservoirs, as those have shown to be accompanied by lower impurities.

(3) As particles in the snow sample interrupt and slow down the SPE sample preparation procedure, it would be sufficient to filtrate samples in prior to that. When doing so, it has to be kept in mind that the filtration step leads to a separation of the sample which also affects particle-bound compounds. In case of PAHs, this separation does not reflect the different phase partitioning of PAHs, as LMW PAHs may be adsorbed to particles using them for accumulation and transportation purposes.

(4) TD-PTR-ToF-MS has proven to be a sufficient method to quantify PAHs adsorbed to quartz fiber filter aliquots. The application to very low volumes of cloud water samples, however, was more complex as isobaric interferences prevented the conversion into concentrations given in ng/L. For future experiments, it is recommended to use higher amounts of samples (up to 10 mL) and maybe also implement a prior cleaning step (e.g. selective SPE) to suppress interferences with structurally similar compounds (e.g. HULIS).

(5) Isobaric interferences complicated the application of the developed multi method approach to cloud water and snow samples. Thus, modifications in data processing such as narrowing the integration windows to time frames during which the single PAHs evolved within the TD run are recommended. Even though this step leads to an enormous extension of the data set, it would significantly reduce the possibility of isobaric interferences, as only short and dedicated time periods are the center of interest.

In a nutshell, this thesis not only highlights the presence of PAHs in various environmentally important matrices, it further presents the importance of developing analytical methods to selectively quantify a variety of PAH congeners. Results show that PAHs are found in vastly different concentration ranges, depending on the matrix and the strength of source influences. The findings presented in this work encourage further research, especially to investigate the PAH contributions in cloud water samples and other vehicles used for atmospheric transport. It further highlights the interaction of PAHs with other emerging contaminants such as ultrafine micro- and nanoplastics.

Bibliography

Abbas, Imane, Ghidaa Badran, Anthony Verdin, Frédéric Ledoux, Mohamed Roumié, Dominique Courcot, and Guillaume Garçon. 2018. "Polycyclic aromatic hydrocarbon derivatives in airborne particulate matter: sources, analysis and toxicity." *Environmental Chemistry Letters* 16 (2):439-475. doi: 10.1007/s10311-017-0697-0.

Ailish, M. Graham, J. Pringle Kirsty, R. Arnold Stephen, J. Pope Richard, Vieno Massimo, W. Butt Edward, Conibear Luke, L. Stirling Ellen, and B. Mcquaid James. 2020. "Impact of weather types on UK ambient particulate matter concentrations." *Atmospheric Environment: X* 5.

Akhbarizadeh, R., S. Dobaradaran, M. Amouei Torkmahalleh, R. Saeedi, R. Aibaghi, and F. Faraji Ghasemi. 2021. "Suspended fine particulate matter (PM2.5), microplastics (MPs), and polycyclic aromatic hydrocarbons (PAHs) in air: Their possible relationships and health implications." *Environ Res* 192:110339. doi: 10.1016/j.envres.2020.110339.

Allen, Steve, Deonie Allen, Vernon R. Phoenix, Gaël Le Roux, Pilar Durántez Jiménez, Anaëlle Simonneau, Stéphane Binet, and Didier Galop. 2019. "Atmospheric transport and deposition of microplastics in a remote mountain catchment." *Nature Geoscience* 12 (5):339-344. doi: 10.1038/s41561-019-0335-5.

Allen, Steve, Dušan Materić, Deonie Allen, Anna MacDonald, Rupert Holzinger, Gael Le Roux, and Vernon R. Phoenix. 2022. "An early comparison of nano to microplastic mass in a remote catchment's atmospheric deposition." *Journal of Hazardous Materials Advances* 7. doi: 10.1016/j.hazadv.2022.100104.

Almbauer, R. A., D. Oettl, M. Bacher, and P. J. Sturm. 2000. "Simulation of the air quality during a field study for the city of Graz." *Atmospheric Environment* 34 (27):4581-4594. doi: 10.1016/S1352-2310(00)00264-8.

Amt der Steiermärkischen Landesregierung, Abteillung 15 (Ed.). 2018. Luftgütemessungen in der Steiermark - Jahresbericht 2017.

Anderl, M, C Brendle, M Gangl, S Haider, T Köther, C Lampert, N Mandl, K Pazdernik, D Perl, M Pinterits, S Poupa, M Purzner, W Schieder, G Schmidt, B Schodl, M Titz, M Wieser, R Wankmüller, and A Zechmeister. 2021. Austria's Informative Inventory Report (IIR) 2021. edited by Umweltbundesamt GmbH. Wien: Umweltbundesamt GmbH.

Anderson, K. A., M. J. Szelewski, G. Wilson, B. D. Quimby, and P. D. Hoffman. 2015. "Modified ion source triple quadrupole mass spectrometer gas chromatograph for polycyclic aromatic hydrocarbon analyses." *J Chromatogr A* 1419:89-98. doi: 10.1016/j.chroma.2015.09.054.

Arellano, L., J. O. Grimalt, P. Fernandez, J. F. Lopez, U. Nickus, and H. Thies. 2014. "Persistent organic pollutant accumulation in seasonal snow along an altitudinal gradient in the Tyrolean Alps." *Environ Sci Pollut Res Int* 21 (22):12638-50. doi: 10.1007/s11356-014-3196-x.

Avio, C. G., S. Gorbi, and F. Regoli. 2017. "Plastics and microplastics in the oceans: From emerging pollutants to emerged threat." *Mar Environ Res* 128:2-11. doi: 10.1016/j.marenvres.2016.05.012.

Bakir, A., S. J. Rowland, and R. C. Thompson. 2012. "Competitive sorption of persistent organic pollutants onto microplastics in the marine environment." *Mar Pollut Bull* 64 (12):2782-9. doi: 10.1016/j.marpolbul.2012.09.010.

Barmpadimos, I., C. Hueglin, J. Keller, S. Henne, and A. S. H. Prévôt. 2011. "Influence of meteorology on PM 10 trends and variability in Switzerland from 1991 to 2008." *Atmospheric Chemistry and Physics* 11 (4):1813-1835. doi: 10.5194/acp-11-1813-2011.

Bergmann, Melanie, France Collard, Joan Fabres, Geir W. Gabrielsen, Jennifer F. Provencher, Chelsea M. Rochman, Erik van Sebille, and Mine B. Tekman. 2022. "Plastic pollution in the Arctic." *Nature Reviews Earth & Environment*. doi: 10.1038/s43017-022-00279-8.

Bjørseth, Alf. 1983. *Handbook of Polycyclic Aromatic Hydrocarbons*. Edited by Alf Bjørseth. New York: Dekker.

Blake, R. S., P. S. Monks, and A. M. Ellis. 2009. "Proton-Transfer Reaction Mass Spectrometry." *Chem Rev* 109:861 - 896. doi: 10.1021/cr800364q.

Bolling, Anette Kocbach, Joakim Pagels, Karl Espen Yttri, Lars Barregard, Gerd Sallsten, Per E. Schwarze, Christoffer Boman, Anette Kocbach Bølling, Lars Barregård, and Gerd Sällsten. 2009. "Health effects of residential wood smoke particles: the importance of combustion conditions and physicochemical particle properties." *Particle And Fibre Toxicology* 6 (1). doi: 10.1186/1743-8977-6-29.

Boschetti, A, F Biasioli, M van Opbergen, C Warneke, A Jordan, R Holzinger, P Prazeller, T Karl, A Hansel, W Lindinger, and S Iannnotta. 1999. "PTR-MS real time monitoring of the emission of volatile organic compounds during postharvest aging of berryfruit." *Posharvest Biology and Technology* 17 (3):143 - 151. doi: 10.1016/S0925-5214(99)00052-6.

Briz-Redon, A., C. Belenguer-Sapina, and A. Serrano-Aroca. 2021. "Changes in air pollution during COVID-19 lockdown in Spain: A multi-city study." *J Environ Sci (China)* 101:16-26. doi: 10.1016/j.jes.2020.07.029.

Cai, L., J. Wang, J. Peng, Z. Tan, Z. Zhan, X. Tan, and Q. Chen. 2017. "Characteristic of microplastics in the atmospheric fallout from Dongguan city, China: preliminary research and first evidence." *Environ Sci Pollut Res Int* 24 (32):24928-24935. doi: 10.1007/s11356-017-0116-x.

Carrera, G, P. Fernandez, R. M. Vilanova, and J. O. Grimalt. 2001. "Persistent organic pollutants in snow from European high mountain areas." *Atmos. Environ.* 35:245-2554. doi: 10.1016/S1352-2310(00)00201-6.

Caseiro, Alexandre, Heidi Bauer, Christoph Schmidl, Casimiro A. Pio, and Hans Puxbaum. 2009. "Wood burning impact on PM 10 in three Austrian regions." *Atmospheric Environment* 43 (13):2186-2195. doi: 10.1016/j.atmosenv.2009.01.012.

Cincinelli, Alessandra, Cristiana Guerranti, Tania Martellini, and Roberto Scodellini. 2019. "Residential wood combustion and its impact on urban air quality in Europe." *Current Opinion in Environmental Science & Health* 8:10-14. doi: 10.1016/j.coesh.2018.12.007.

Corradini, F., P. Meza, R. Eguiluz, F. Casado, E. Huerta-Lwanga, and V. Geissen. 2019. "Evidence of microplastic accumulation in agricultural soils from sewage sludge disposal." *Sci Total Environ* 671:411-420. doi: 10.1016/j.scitotenv.2019.03.368.

Cvetkovic, Jelena S., Violeta D. Mitic, Vesna P. Stankov Jovanovic, Marija V. Dimitrijevic, Goran M. Petrovic, Snezana D. Nikolic-Mandic, and Gordana S. Stojanovic. 2016. "Optimization of the QuEChERS extraction procedure for the determination of polycyclic aromatic hydrocarbons in soil by gas chromatography-mass spectrometry." *Analytical Methods* 8 (7):1711-1720. doi: 10.1039/c5ay03248b.

De Hartog, Jeroen J., Gerard Hoek, Aadu Mirme, Thomas Tuch, Gerard P. A. Kos, Harry M. Ten Brink, Bert Brunekreef, Josef Cyrys, Joachim Heinrich, Mike Pitz, Timo Lanki, Marko Vallius, Juha Pekkanen, and Wolfgang G. Kreyling. 2005. "Relationship between different size classes of particulate matter and meteorology in three European cities." *Journal of Environmental Monitoring* 7 (4):302-310. doi: 10.1039/b415153d.

Dorst, Theo. 2014. "Detection efficiency of different compound classes by TD-PTR-MS." MSc Master thesis, Amtospheric Physics and Chemistry Group, Institute for Marine and Atmospheric research Utrecht, Utrecht University.

Douglas, D. J. 2009. "Linear quadrupoles in mass spectrometry." *Mass Spectrom Rev* 28 (6):937-60. doi: 10.1002/mas.20249.

Dris, R., J. Gasperi, M. Saad, C. Mirande, and B. Tassin. 2016. "Synthetic fibers in atmospheric fallout: A source of microplastics in the environment?" *Mar Pollut Bull* 104 (1-2):290-3. doi: 10.1016/j.marpolbul.2016.01.006.

EC. 2008. "Directive 2008/50/EC of the European Parliament and of the Council of 21 May 2008 on ambient air quality and cleaner air for Europe." *L 152/1*.

EEA. 2019. "Air quality in Europe - 2019 report." doi: 10.2800/777411.

EEA. 2020. Air quality in Europe — 2020 report.

EPA, U.S. 2019. Integrated Science Assessment (ISA) for Particulate Matter Washington: U.S. Environmental Protection Agency.

European Union. 2004a. Directive 2004/107/EC of the Eurpean Parliament and of the Council relating to Arsenic, Cadmium, Mercury, Nicke and Polycyclic Aromatic Hydrocarbons in ambient air. In *L23/3*: Official Journal of the European Union.

European Union. 2004b. Regulation (EC) 850/2004 of the European Parliament and of the Council. In *L158 (2004) 7*: Official Journal of the European Union

.

European Union, Working Group on Polycyclic Aromatic Hydrocarbons. 2001. Ambient Air Pollution by Polycyclic Aromatic Hydrocarbons (PAH) - Position Paper.

Ewa, B., and M. S. Danuta. 2017. "Polycyclic aromatic hydrocarbons and PAH-related DNA adducts." *J Appl Genet* 58 (3):321-330. doi: 10.1007/s13353-016-0380-3.

Fotopoulou, K. N., and H. K. Karapanagioti. 2015. "Surface properties of beached plastics." *Environ Sci Pollut Res Int* 22 (14):11022-32. doi: 10.1007/s11356-015-4332-y.

Franz, T. P. , and S. J. Eisenreich. 1998. "Snow scavenging of polychlorinated biphenyls and polycyclic aromatic hydrocarbons in Minnesota." *Environmental Science & Technology* 32 (12):1771-1778. doi: 10.1021/es970601z.

Fred-Ahmadu, O. H., G. Bhagwat, I. Oluyoye, N. U. Benson, O. O. Ayejuyo, and T. Palanisami. 2020. "Interaction of chemical contaminants with microplastics: Principles and perspectives." *Sci Total Environ* 706:135978. doi: 10.1016/j.scitotenv.2019.135978.

Furman, Przemysław, Katarzyna Styszko, Alicja Skiba, Damian Zięba, Mirosław Zimnoch, Magdalena Kistler, Anne Kasper-Giebl, and Stefania Gilardoni. 2021. "Seasonal Variability of PM10 Chemical Composition Including 1,3,5-triphenylbenzene, Marker of Plastic Combustion and Toxicity in Wadowice, South Poland." *Aerosol and Air Quality Research* 21 (3). doi: 10.4209/aaqr.2020.05.0223.

Gabrieli, J, P. Vallelonga, G Cozzi, P Gabrielli, A Gambaro, M Sigl, F Decet, M Schwikowski, H Gäggeler, C Boutron, P Cescon, and C Barbante. 2010. "Post 17th-Century Changes of European PAH Emissions Recorded in High-Altitude Alpine Snow and Ice." *Environ Sci Technol* 44 (9):3260-3266. doi: 10.1021/es903365s.

Gabrieli, J., F. Decet, A. Luchetta, M. Valt, P. Pastore, and C. Barbante. 2010. "Occurrence of PAH in the seasonal snowpack of the Eastern Italian Alps." *Environ Pollut* 158 (10):3130-7. doi: 10.1016/j.envpol.2010.06.042.

Galarneau, E. . 2008. "Source specificity and atmospheric processing of airborne PAHs: Implications for source apportionment." *Atmos. Environ.* 42 (35):8139-8149. doi: 10.1016/j.atmosenv.20.

Gasperi, Johnny, Stephanie L. Wright, Rachid Dris, France Collard, Corinne Mandin, Mohamed Guerrouache, Valérie Langlois, Frank J. Kelly, and Bruno Tassin. 2018. "Microplastics in air: Are we breathing it in?" *Current Opinion in Environmental Science & Health* 1:1-5. doi: 10.1016/j.coesh.2017.10.002.

Glojek, Kristina, Griša Močnik, Honey Dawn C. Alas, Andrea Cuesta-Mosquera, Luka Drinovec, Asta Gregorič, Matej Ogrin, Kay Weinhold, Irena Ježek, Thomas Müller, Martin Rigler, Maja Remškar, Dominik van Pinxteren, Hartmut Herrmann, Martina Ristorini, Maik Merkel, Miha Markelj, and Alfred Wiedensohler. 2022. "The impact of temperature inversions on black carbon and particle mass concentrations in a mountainous area." *Atmospheric Chemistry and Physics* 22 (8):5577-5601. doi: 10.5194/acp-22-5577-2022.

Gonçalves, Cátia, Célia Alves, Ana Patrícia Fernandes, Cristina Monteiro, Luís Tarelho, Margarita Evtyugina, and Casimiro Pio. 2011. "Organic compounds in PM2.5 emitted from fireplace and woodstove combustion of typical Portuguese wood species." *Atmospheric Environment* 45 (27):4533-4545. doi: 10.1016/j.atmosenv.2011.05.071.

Guarnieri, Michael, and John R. Balmes. 2014. "Outdoor air pollution and asthma." *The Lancet* 383 (9928):1581-1592. doi: 10.1016/s0140-6736(14)60617-6.

Guo, X., X. Wang, X. Zhou, X. Kong, S. Tao, and B. Xing. 2012. "Sorption of four hydrophobic organic compounds by three chemically distinct polymers: role of chemical and physical composition." *Environ Sci Technol* 46 (13):7252-9. doi: 10.1021/es301386z.

Gupte, Akshaya, Archana Tripathi, Helina Patel, Darshan Rudakiya, and Shilpa Gupte. 2016. "Bioremediation of Polycyclic Aromatic Hydrocarbon (PAHs): A Perspective." *The Open Biotechnology Journal* 10 (1):363-378. doi: 10.2174/1874070701610010363.

Hakimzadeh, Maryam, Ehsan Soleimanian, Amirhosein Mousavi, Alessandro Borgini, Cinzia De Marco, Ario A. Ruprecht, and Constantinos Sioutas. 2020. "The impact of biomass burning on the oxidative potential of PM2.5 in the metropolitan area of Milan." *Atmospheric Environment* 224. doi: 10.1016/j.atmosenv.2020.117328.

Hansel, A, A Jordan, R Holzinger, P Prazeller, W Vogel, and W Lindinger. 1995. "Proton transfer reaction mass spectrometry: on-line trace gas analysis at the ppb level." *International Journal of Mass Spectrometry and Ion Processes* 149:609-619.

Hirai, H., H. Takada, Y. Ogata, R. Yamashita, K. Mizukawa, M. Saha, C. Kwan, C. Moore, H. Gray, D. Laursen, E. R. Zettler, J. W. Farrington, C. M. Reddy, E. E. Peacock, and M. W. Ward. 2011. "Organic micropollutants in marine plastics debris from the open ocean and remote and urban beaches." *Mar Pollut Bull* 62 (8):1683-92. doi: 10.1016/j.marpolbul.2011.06.004.

Hitzenberger, R., Axel Berner, Heinrich Giebl, K Drobesch, A Kasper-Giebl, M Loeflund, H Urban, and H Puxbaum. 2001. "Black carbon (BC) in alpine aerosols and cloud water - concentrations and scavenging efficiencies." *Atmos. Environ.* 35 (30):5135-5141. doi: 10.1016/S1352-2310(01)00312-0.

Holzinger, R. 2015. "PTRwid: A new widget tool for processing PTR-TOF-MS data." *Atmospheric Measurement Techniques* 8 (9):3903-3922. doi: 10.5194/amt-8-3903-2015.

Holzinger, Rupert, W. Joe F. Acton, William J. Bloss, Martin Breitenlechner, Leigh R. Crilley, Sébastien Dusanter, Marc Gonin, Valerie Gros, Frank N. Keutsch, Astrid Kiendler-Scharr, Louisa J. Kramer, Jordan E. Krechmer, Baptiste Languille, Nadine Locoge, Felipe Lopez-Hilfiker, Dušan Materić, Sergi Moreno, Eiko Nemitz, Lauriane L. J. Quéléver, Roland Sarda Esteve, Stéphane Sauvage, Simon Schallhart, Roberto Sommariva, Ralf Tillmann, Sergej Wedel, David R. Worton, Kangming Xu, and Alexander Zaytsev. 2019. "Validity and limitations of simple reaction kinetics to calculate concentrations of organic compounds from ion counts in PTR-MS." *Atmospheric Measurement Techniques* 12 (11):6193-6208. doi: 10.5194/amt-12-6193-2019.

Hübschmann, Hans-Joachim. 2015. *Handbook of GC-MS*. Germany: Wiley-VCH Verlag GmbH & Co. KGaA.

IARC. 2010. "Some Non-heterocyclic Polycyclic Aromatic Hydrocarbons and Some Related Exposures " In *IARC Monographs on the Evaluation of Carcinogenic Risk to Humans*.

Iinuma, Yoshiteru, Guenter Engling, Hans Puxbaum, and Hartmut Herrmann. 2009. "A highly resolved anion-exchange chromatographic method for determination of saccharidic tracers for biomass combustion and primary bio-particles in atmospheric aerosol." *Atmospheric Environment* 43 (6):1367-1371. doi: 10.1016/j.atmosenv.2008.11.020.

IONICON Analytik, Ges.m.b.H. 2022. "PTR-MS." IONICON Analytik Ges.m.b.H., accessed 20.05.2022. https://www.ionicon.com/technologies/details/ptr-ms.

Islam, Md Robiul, Thilina Jayarathne, Isobel J. Simpson, Benjamin Werden, John Maben, Ashley Gilbert, Puppala S. Praveen, Sagar Adhikari, Arnico K. Panday, Maheswar Rupakheti, Donald R. Blake, Robert J. Yokelson, Peter F. DeCarlo, William C. Keene, and Elizabeth A. Stone. 2020. "Ambient air quality in the Kathmandu Valley, Nepal, during the pre-monsoon: concentrations and sources of particulate matter and trace gases." *Atmospheric Chemistry and Physics* 20 (5):2927-2951. doi: 10.5194/acp-20-2927-2020.

Izvekova, T. V., N. A. Kobeleva, A. A. Gushchin, V. I. Grinevich, and V. V. Rybkin. 2020. "Distribution of Policyclic aromatic hydrocarbons in a snow cover in the territory of Ivanovo city, Russia." *Chemosphere* 242:125150. doi: 10.1016/j.chemosphere.2019.125150.

Jeffery, J., M. Carradus, K. Songin, M. Pettit, K. Pettit, and C. Wright. 2018. "Optimized method for determination of 16 FDA polycyclic aromatic hydrocarbons (PAHs) in mainstream cigarette smoke by gas chromatography-mass spectrometry." *Chem Cent J* 12 (1):27. doi: 10.1186/s13065-018-0397-2.

Kamens, R. M., Z. Guo, J. N. Fulcher, and D. A. Bell. 1988. "Influence of Humidty, Sunlight, and Temperature on the Daytime Decau of Polyaromaty Hydrocarbons on Atmospheric Soot Particles." *Environ Sci Technol* 22:103-108. doi: 0013-936X/88/0922-0103$01.50/0.

Keyte, Ian J., Roy M. Harrison, and Gerhard Lammel. 2013. "Chemical reactivity and long-range transport potential of polycyclic aromatic hydrocarbons--a review." *Chem Soc Rev* 42 (ISSN: 0306-0012). doi: 10.1039/c3cs60147a.

Khan, Md, Mauro Masiol, Caterina Bruno, Alberto Pasqualetto, Gian Formenton, Claudio Agostinelli, and Bruno Pavoni. 2018. "Potential sources and meteorological factors affecting PM 2.5 -bound polycyclic aromatic hydrocarbon levels in six main cities of northeastern Italy: an assessment of the related carcinogenic and mutagenic risks." *Environmental Science and Pollution Research* 25 (32):31987-32000. doi: 10.1007/s11356-018-2841-1.

Kim, Y. H., and K. H. Kim. 2015. "A simple methodological validation of the gas/particle fractionation of polycyclic aromatic hydrocarbons in ambient air." *Sci Rep* 5:11679. doi: 10.1038/srep11679.

Kirchsteiger, B, F Kubik, M Kistler, Rita Sturmlechner, Harald Stressler, M. Schwabl, and A Kasper-Giebl. 2021. Real-life emissions from residential wood combustion in Austria: From TSP emissions to PAH emission profiles, diagnostic ratios and toxic risk assessment. IN PREPARATION

Kirchsteiger, Bernadette, Magdalena Kistler, Thomas Steinkogler, Christopher Herzig, Andreas Limbeck, Christian Schmidt, Harald Rieder, and Anne Kasper-Giebl. 2020. "Combination of Different Approaches to Infer Local or Regional Contributions to PM2.5 Burdens in Graz, Austria." *Applied Sciences* 10 (12). doi: 10.3390/app10124222.

Kistler, Magdalena. 2012. "Particulate matter and odor emission factors from small scale biomass combustion units." Wien, Techn. Univ., Diss., 2012.

Klauser, Franziska, Elisa Carlon, Magdalena Kistler, Christoph Schmidl, Manuel Schwabl, Rita Sturmlechner, Walter Haslinger, and Anne Kasper-Giebl. 2018. "Emission characterization of modern wood stoves under real-life oriented operating conditions." *Atmospheric Environment* 192:257-266. doi: 10.1016/j.atmosenv.2018.08.024.

Klauser, Franziska, Christoph Schmidl, Gabriel Reichert, Elisa Carlon, Magdalena Kistler, Manuel Schwabl, Walter Haslinger, and Anne Kasper-Giebl. 2018. "Effect of Oxidizing Honeycomb Catalysts Integrated in a Firewood Room Heater on Gaseous and Particulate Emissions, Including Polycyclic Aromatic Hydrocarbons (PAHs)." *Energy & Fuels* 32 (11):11876-11886. doi: 10.1021/acs.energyfuels.8b02336.

Klauser, Franziska, Manuel Schwabl, Magdalena Kistler, Irene Sedlmayer, Norbert Kienzl, Alexander Weissinger, Christoph Schmidl, Walter Haslinger, and Anne Kasper-Giebl. 2018. "Development of a compact technique to measure benzo(a)pyrene emissions from residential wood combustion, and subsequent testing in six modern wood boilers." *Biomass and Bioenergy* 111:288-300. doi: 10.1016/j.biombioe.2017.05.004.

Klein, M., and E. K. Fischer. 2019. "Microplastic abundance in atmospheric deposition within the Metropolitan area of Hamburg, Germany." *Sci Total Environ* 685:96-103. doi: 10.1016/j.scitotenv.2019.05.405.

Kozhevnikov, A. Y., D. I. Falev, S. A. Sypalov, I. S. Kozhevnikova, and D. S. Kosyakov. 2021. "Polycyclic aromatic hydrocarbons in the snow cover of the northern city agglomeration." *Sci Rep* 11 (1):19074. doi: 10.1038/s41598-021-98386-x.

Kruisz, C. , A. Berner, and B. Brandner. 1993. "A Cloud Water Sampler for High Wind Speeds." *Proceedings of EUROTRAC Symposium '92, SPB Academic Publishing, The Hague*:53 - 69.

Kumar, R., G. Li, V. A. Gallardo, A. Li, J. Milton, J. J. Nash, and H. I. Kenttamaa. 2020. "Measurement of the Proton Affinities of a Series of Mono- and Biradicals of Pyridine." *J Am Chem Soc* 142 (19):8679-8687. doi: 10.1021/jacs.0c00202.

Larsen, John C., and Poul B. Larsen. 1998. "Chemical carcinogens." *Air Pollution and Health (Hester RE, Harrison RM eds). Cambridge, UH: The Royal Society of Chemistry*:33-56.

Lee, H., W. J. Shim, and J. H. Kwon. 2014. "Sorption capacity of plastic debris for hydrophobic organic chemicals." *Sci Total Environ* 470-471:1545-52. doi: 10.1016/j.scitotenv.2013.08.023.

Lei, Xiaoning, Weiwei Li, Jianjiang Lu, Yanbin Tong, and Shanman Li. 2015. "Distribution of polycyclic aromatic hydrocarbons in snow of Mount Nanshan, Xinjiang." *Water and Environment Journal* 29 (2):252-258. doi: 10.1111/wej.12099.

Lei, Ying D., and Frank Wania. 2004. "Is rain or snow a more efficient scavenger of organic chemicals?" *Atmospheric Environment* 38 (22):3557-3571. doi: 10.1016/j.atmosenv.2004.03.039.

Lenschow, P., H. J. Abraham, K. Kutzner, M. Lutz, J. D. Preuß, and W. Reichenbächer. 2001. "Some ideas about the sources of PM10." *Atmospheric Environment* 35:S23-S33. doi: 10.1016/S1352-2310(01)00122-4.

Lima, Ana Lúcia C., John W. Farrington, and Christopher M. Reddy. 2005. "Combustion-Derived Polycyclic Aromatic Hydrocarbons in the Environment—A Review." *Environmental Forensics* 6 (2):109-131. doi: 10.1080/15275920590952739.

Limbeck, Andreas, and Hans Puxbaum. 2000. "Dependence of in-cloud scavenging of polar organic aerosol compounds on the water solubility." *Journal of Geophysical Research: Atmospheres* 105 (D15):19857-19867. doi: 10.1029/2000jd900123.

Lohmann, R., and G. Lammel. 2004. "Adsorptive and Absorptive Contributions to the Gas-Particle Partitioning of Polycyclic Aromatic Hydrocarbons: State of Knowledge and

Recommended Parametrization for Modeling." *Environ Sci Technol* 38 (14). doi: 10.1021/es035337q.

Mai, L., H. He, L. J. Bao, L. Y. Liu, and E. Y. Zeng. 2020. "Plastics Are an Insignificant Carrier of Riverine Organic Pollutants to the Coastal Oceans." *Environ Sci Technol* 54 (24):15852-15860. doi: 10.1021/acs.est.0c05446.

Manisalidis, I., E. Stavropoulou, A. Stavropoulos, and E. Bezirtzoglou. 2020. "Environmental and Health Impacts of Air Pollution: A Review." *Front Public Health* 8:14. doi: 10.3389/fpubh.2020.00014.

Manoli, Evangelia, Athanasios Kouras, Olga Karagkiozidou, Georgios Argyropoulos, Dimitra Voutsa, and Constantini Samara. 2016. "Polycyclic aromatic hydrocarbons (PAHs) at traffic and urban background sites of northern Greece: source apportionment of ambient PAH levels and PAH-induced lung cancer risk." *Environmental Science and Pollution Research* 23 (4):3556-3568. doi: 10.1007/s11356-015-5573-5.

Manzano, C., E. Hoh, and S. L. Simonich. 2012. "Improved separation of complex polycyclic aromatic hydrocarbon mixtures using novel column combinations in GC x GC/ToF-MS." *Environ Sci Technol* 46 (14):7677-84. doi: 10.1021/es301790h.

Manzetti, Sergio. 2013. "Polycyclic Aromatic Hydrocarbons in the Environment: Environmental Fate and Transformation." *Polycyclic Aromatic Compounds* 33 (4):311-330. doi: 10.1080/10406638.2013.781042.

Masiol, Mauro, Gianni Formenton, Alberto Pasqualetto, and Bruno Pavoni. 2013. "Seasonal trends and spatial variations of PM10- bounded polycyclic aromatic hydrocarbons in Veneto Region, Northeast Italy." *Atmospheric Environment* 79 (C):811-821. doi: 10.1016/j.atmosenv.2013.07.025.

Materić, D., A. Kasper-Giebl, D. Kau, M. Anten, M. Greilinger, E. Ludewig, E. van Sebille, T. Röckmann, and R. Holzinger. 2020. "Micro- and Nanoplastics in Alpine Snow: A New Method for Chemical Identification and (Semi)Quantification in the Nanogram Range." *Environ Sci Technol* 54 (4):2353-2359. doi: 10.1021/acs.est.9b07540.

Materić, D., H. A. Kjaer, P. Vallelonga, J. L. Tison, T. Röckmann, and R. Holzinger. 2022. "Nanoplastics measurements in Northern and Southern polar ice." *Environ Res* 208:112741. doi: 10.1016/j.envres.2022.112741.

Materić, D., E. Ludewig, D. Brunner, T. Röckmann, and R. Holzinger. 2021. "Nanoplastics transport to the remote, high-altitude Alps." *Environ Pollut* 288:117697. doi: 10.1016/j.envpol.2021.117697.

Materić, D., M. Peacock, M. Kent, S. Cook, V. Gauci, T. Röckmann, and R. Holzinger. 2017. "Characterisation of the semi-volatile component of Dissolved Organic Matter by Thermal Desorption - Proton Transfer Reaction - Mass Spectrometry." *Sci Rep* 7 (1):15936. doi: 10.1038/s41598-017-16256-x.

Materić, Dušan, Elke Ludewig, Kangming Xu, Thomas Röckmann, and Rupert Holzinger. 2019. "Brief communication: Analysis of organic matter in surface snow by PTR-MS – implications for dry deposition dynamics in the Alps." *The Cryosphere* 13 (1):297-307. doi: 10.5194/tc-13-297-2019.

Materić, Dušan, Mike Peacock, Joshua Dean, Martyn N. Futter, Trofim Maximov, Filip Moldan, Thomas Roeckmann, and Rupert Holzinger. 2022. "Presence of nanoplastics in rural and remote surface waters." *Environmental Research Letters*. doi: 10.1088/1748-9326/ac68f7.

Matsuzawa, S. , L. Nasser-Ali, and P. Garrigues. 2001. "Photolytic Behaviour of Polycyclic Aromatic Hydrocarbons in Diesel Particulate Matter Deposited on the Ground." *Environ Sci Technol* 35:3139-3143. doi: 10.1021/es001606q.

Morokuma, Keiji. 1977. "Why Do Molecules Interact? The Origin of Electron Donor-Acceptor Complexes, Hydrogen Bonding and Proton Affinity." *Accounts of Chemical Research* 10:294-300.

Mueller, A., N. Ulrich, J. Hollmann, C. E. Zapata Sanchez, U. E. Rolle-Kampczyk, and M. von Bergen. 2019. "Characterization of a multianalyte GC-MS/MS procedure for detecting and quantifying polycyclic aromatic hydrocarbons (PAHs) and PAH derivatives from air particulate matter for an improved risk assessment." *Environ Pollut* 255 (Pt 2):112967. doi: 10.1016/j.envpol.2019.112967.

Na, Guangshui, Chunyang Liu, Zhen Wang, Linke Ge, Xindong Ma, and Ziwei Yao. 2011. "Distribution and characteristic of PAHs in snow of Fildes Peninsula." *Journal of Environmental Sciences* 23 (9):1445-1451. doi: 10.1016/s1001-0742(10)60605-5.

Notø, Hanne Ødegaard. 2021. "Investigating Volatile Organic Compound Emissions from Boreal Lake Water Exposed to Ultraviolet Light and Ozone." Master's degree in Chemistry, Department of Chemistry, Faculty of Mathematics and Natural Sciences, University of Oslo.

Oleagoitia, Miren Begoña Zubero, Aitana Lertxundi Manterola, Jesús Ibarluzea Maurolagoitia, María Dolores Martínez López de Dicastillo, Jon Álvarez, Mikel Ayerdi Barandiaran, Amaia Irizar Loibide, and Loreto Santa-Marina. 2018. "Polycyclic aromatic hydrocarbons (PAHs) in air associated with particles PM2.5 in the Basque Country (Spain)." *Air Quality, Atmosphere & Health* 12 (1):107-114. doi: 10.1007/s11869-018-0635-8.

Orasche, Jürgen, Torben Seidel, Hans Hartmann, Jürgen Schnelle-Kreis, Judith C. Chow, Hans Ruppert, and Ralf Zimmermann. 2012. "Comparison of Emissions from Wood Combustion. Part 1: Emission Factors and Characteristics from Different Small-Scale Residential Heating Appliances Considering Particulate Matter and Polycyclic Aromatic Hydrocarbon (PAH)-Related Toxicological Potential of Particle-Bound Organic Species." *Energy & Fuels* 26 (11):6695-6704. doi: 10.1021/ef301295k.

Ozgen, Senem, Stefano Caserini, Silvia Galante, Michele Giugliano, Elisabetta Angelino, Alessandro Marongiu, Francesca Hugony, Gabriele Migliavacca, and Carmen Morreale. 2014. "Emission factors from small scale appliances burning wood and pellets." *Atmospheric Environment* 94:144-153. doi: 10.1016/j.atmosenv.2014.05.032.

Pandolfi, M., A. Tobias, A. Alastuey, J. Sunyer, J. Schwartz, J. Lorente, J. Pey, and X. Querol. 2014. "Effect of atmospheric mixing layer depth variations on urban air quality and daily mortality during Saharan dust outbreaks." *Sci Total Environ* 494-495:283-9. doi: 10.1016/j.scitotenv.2014.07.004.

Pang, X. 2015. "Biogenic volatile organic compound analyses by PTR-TOF-MS: Calibration, humidity effect and reduced electric field dependency." *J Environ Sci (China)* 32:196-206. doi: 10.1016/j.jes.2015.01.013.

Pankow, J. 1994. "An Absorption Model of Gas/Particle Partitioning of Organic Compounds in the Atmosphere." *Atmos. Environ.* 28 (2):185-188.

Pankow, J. F., L. M. Isabelle, D. A. Buchholz, W. Luo, and D. B Reeves. 1994. "Gas/Particle Partinioning of Polycyclic Aromatic Hydrocarbons and Alkanes to Environmental Tobacco Smoke." *Environ Sci Technol* 28:363-363.

Patel, A. B., S. Shaikh, K. R. Jain, C. Desai, and D. Madamwar. 2020. "Polycyclic Aromatic Hydrocarbons: Sources, Toxicity, and Remediation Approaches." *Front Microbiol* 11:562813. doi: 10.3389/fmicb.2020.562813.

Peacock, Mike, Dušan Materić, Dolly N. Kothawala, Rupert Holzinger, and Martyn N. Futter. 2018. "Understanding Dissolved Organic Matter Reactivity and Composition in Lakes and Streams Using Proton-Transfer-Reaction Mass Spectrometry (PTR-MS)." *Environmental Science & Technology Letters* 5 (12):739-744. doi: 10.1021/acs.estlett.8b00529.

Peterson, K A, S S Xantheas, D A Dixon, and T H Jr Dunning. 1998. "Predicting the Proton Affinities of H2O and NH3." *J Phys Chem A* 102 (14):2449-2454. doi: https://doi.org/10.1021/jp971510r.

Pettersson, Esbjörn, Christoffer Boman, Roger Westerholm, Dan Boström, and Anders Nordin. 2011. "Stove Performance and Emission Characteristics in Residential Wood Log and Pellet Combustion, Part 2: Wood Stove." *Energy & Fuels* 25 (1):315-323. doi: 10.1021/ef1007787.

Philipp, Andreas, Judit Bartholy, Christoph Beck, Michel Erpicum, Pere Esteban, Xavier Fettweis, Radan Huth, Paul James, Sylvie Jourdain, Frank Kreienkamp, Thomas Krennert, Spyros Lykoudis, Silas C. Michalides, Krystyna Pianko-Kluczynska, Piia Post, Domingo Rasilla Álvarez, Reinhard Schiemann, Arne Spekat, and Filippos S. Tymvios. 2010. "Cost733cat – A database of weather and circulation type classifications." *Physics and Chemistry of the Earth* 35 (9-12):360-373. doi: 10.1016/j.pce.2009.12.010.

Pietrogrande, M. C., D. Bacco, G. Demaria, M. Russo, F. Scotto, and A. Trentini. 2022. "Polycyclic aromatic hydrocarbons and their oxygenated derivatives in urban aerosol: levels, chemical profiles, and contribution to PM2.5 oxidative potential." *Environ Sci Pollut Res Int*. doi: 10.1007/s11356-021-16858-z.

Plastics Europe. 2020. "Plastics - the Facts 2020

An analysis of European plastics production, demand and waste data." PlasticsEurope, accessed May 15. https://plasticseurope.org/knowledge-hub/plastics-the-facts-2020/.

Plastics Europe. 2021. Plastics - the Facts 2021, An analysis of European plastics production, demand and waste data. edited by Plastics Europe. Belgium: Plastics Europe.

Puxbaum, H., B. Gomiscek, M. Kalina, H. Bauer, A. Salam, S. Stopper, O. Preining, and H. Hauck. 2004. "A dual site study of PM 2.5 and PM 10 aerosol chemistry in the larger region of Vienna, Austria." *Atmospheric Environment* 38 (24):3949-3958. doi: 10.1016/j.atmosenv.2003.12.043.

Ravindra, K., R. Sokhi, and R. Vangrieken. 2008. "Atmospheric polycyclic aromatic hydrocarbons: Source attribution, emission factors and regulation." *Atmospheric Environment* 42 (13):2895-2921. doi: 10.1016/j.atmosenv.2007.12.010.

Reichert, Gabriel, Rita Sturmlechner, Harald Stressler, Manuel Schwabl, Christoph Schmidl, Heike Oehler, Robert Mack, and Hans Hartmann. 2016. Deliverable D3.3 Final Report: Definition of Suitable Measurement Methods and Advanced Type Testing Procedure for Real Life Conditions.

Reizer, E., B. Viskolcz, and B. Fiser. 2022. "Formation and growth mechanisms of polycyclic aromatic hydrocarbons: A mini-review." *Chemosphere* 291 (Pt 1):132793. doi: 10.1016/j.chemosphere.2021.132793.

Restek Corporation. 2021. "New Rxi(R)-PAH GC Column ".

Rios, L. M., P. R. Jones, C. Moore, and U. V. Narayan. 2010. "Quantitation of persistent organic pollutants adsorbed on plastic debris from the Northern Pacific Gyre's "eastern garbage patch"." *J Environ Monit* 12 (12):2226-36. doi: 10.1039/c0em00239a.

Rochman, C. M., E. Hoh, B. T. Hentschel, and S. Kaye. 2013. "Long-term field measurement of sorption of organic contaminants to five types of plastic pellets: implications for plastic marine debris." *Environ Sci Technol* 47 (3):1646-54. doi: 10.1021/es303700s.

Ropkins, K., and J. E. Tate. 2021. "Early observations on the impact of the COVID-19 lockdown on air quality trends across the UK." *Sci Total Environ* 754:142374. doi: 10.1016/j.scitotenv.2020.142374.

Salma, Imre, R. O'cskay, and G. G. Láng. 2008. "Properties of atmospheric humic-like substances - water system." *Atmspheric Chemistry and Physics* 8:2243-2254. doi: 10.5194/acp-8-2243-2008, 2008.

Salvi, S., and St Holgate. 1999. Mechanisms of particulate matter toxicity. In *Clin. Exp. Allergy*.

Samae, H., S. Tekasakul, P. Tekasakul, and M. Furuuchi. 2021. "Emission factors of ultrafine particulate matter (PM<0.1 mum) and particle-bound polycyclic aromatic hydrocarbons from biomass combustion for source apportionment." *Chemosphere* 262:127846. doi: 10.1016/j.chemosphere.2020.127846.

Schmidl, Christoph, Markus Luisser, Emmanuel Padouvas, Leopold Lasselsberger, Magdalena Rzaca, Carlos Ramirez-Santa Cruz, Markus Handler, Ge Peng, Heidi Bauer, and Hans Puxbaum. 2011. "Particulate and gaseous emissions from manually and automatically fired small scale combustion systems." *Atmospheric Environment* 45 (39):7443-7454. doi: 10.1016/j.atmosenv.2011.05.006.

Schmidl, Christoph, Iain L. Marr, Alexandre Caseiro, Petra Kotianová, Axel Berner, Heidi Bauer, Anne Kasper-Giebl, and Hans Puxbaum. 2008. "Chemical characterisation of fine particle emissions from wood stove combustion of common woods growing in mid-European Alpine regions." *Atmospheric Environment* 42 (1):126-141. doi: 10.1016/j.atmosenv.2007.09.028.

Seidensticker, S., C. Zarfl, O. A. Cirpka, G. Fellenberg, and P. Grathwohl. 2017. "Shift in Mass Transfer of Wastewater Contaminants from Microplastics in the Presence of Dissolved Substances." *Environ Sci Technol* 51 (21):12254-12263. doi: 10.1021/acs.est.7b02664.

Simoneit, B. R. T., P. M. Medeiros, and Didyk B. M. 2005. "Combustion Products of Plastics as Indicators for Refuse Burning in the Atmosphere." *Environ Sci Technol* 39:6961-6970. doi: 10.1021/es050767x.

Simoneit, B. R. T., J. J. Schauer, C. G. Nolte, D. R. Oros, V. O. Elias, M. P. Fraser, W. F. Rogge, and G. R. Cass. 1999. "Levoglucosan, a tracer for cellulose in biomass burning and atmospheric particles." *Atmospheric Environment* 33 (2):173-182. doi: 10.1016/S1352-2310(98)00145-9.

Skoog, D. A., and J. J. Leary. 1992. *Principles of Instrumental Analysis*. 4th Edition ed: Saunders Collee Publishing.

Spangl, Wolfgang, and Christian Nagl. 2019. Jahresbericht der Luftgütemessungen.

Spangl, Wolfgang, and Christian Nagl. 2021. Jahresbericht der Luftgütemessungen in Österreich 2020. Vienna: Umweltbundesamt GmbH.

Sparling, D. W. . 2016. *Ecotoxicology Essentials*. London: Elsevier.

Spitzer, J., P. Enzinger, G. Fankhauser, W. Fritz, F. Golja, and R. Stiglbrunner. 1998. Emissionsfaktoren für feste Brennstoffe. Graz: Joanneum Research Report.

Sridharan, S., M. Kumar, L. Singh, N. S. Bolan, and M. Saha. 2021. "Microplastics as an emerging source of particulate air pollution: A critical review." *J Hazard Mater* 418:126245. doi: 10.1016/j.jhazmat.2021.126245.

Staehle, C., M. Mayer, B. Kirchsteiger, V. Klaus, J. Kult-Herdin, C. Schmidt, S. Schreier, J. Karlicky, H. Trimmel, A. Kasper-Giebl, B. Scherllin-Pirscher, and H. E. Rieder. 2022. "Quantifying changes in ambient NOx, O3 and PM10 concentrations in Austria during the COVID-19 related lockdown in spring 2020." *Air Quality, Atmosphere & Health*. doi: 10.1007/s11869-022-01232-w.

Sturmlechner, Rita, Christoph Schmidl, Elisa Carlon, Gabriel Reichert, Harald Stressler, Franziska Klauser, Joachim Kelz, Manuel Schwabl, Bernadette Kirchsteiger, Anne Kasper-Giebl, Ernst Höftberger, and Walter Haslinger. 2019. "Real life emission factor assessment for biomass heating appliances at a field measurement camgaign in Styria, Austria." Air Pollution Conference 2019.

Tobiszewski, M., and J. Namiesnik. 2012. "PAH diagnostic ratios for the identification of pollution emission sources." *Environ Pollut* 162:110-9. doi: 10.1016/j.envpol.2011.10.025.

TOFWERK. 2022. "Advantages of Time-of-Flight Mass Spectrometry Over Quadruopole MS." accessed 23.05.2022. https://www.tofwerk.com/advantages-time-of-flight-mass-spectrometry-over-quadrupole-ms/.

Tomaz, S., P. Shahpoury, J. L. Jaffrezo, G. Lammel, E. Perraudin, E. Villenave, and A. Albinet. 2016. "One-year study of polycyclic aromatic compounds at an urban site in Grenoble (France): Seasonal variations, gas/particle partitioning and cancer risk estimation." *Sci Total Environ* 565:1071-1083. doi: 10.1016/j.scitotenv.2016.05.137.

Tomlin, Alison S. 2021. "Air Quality and Climate Impacts of Biomass Use as an Energy Source: A Review." *Energy & Fuels* 35 (18):14213-14240. doi: 10.1021/acs.energyfuels.1c01523.

Torres, F. G., D. C. Dioses-Salinas, C. I. Pizarro-Ortega, and G. E. De-la-Torre. 2021. "Sorption of chemical contaminants on degradable and non-degradable microplastics: Recent progress and research trends." *Sci Total Environ* 757:143875. doi: 10.1016/j.scitotenv.2020.143875.

Toscano, Domenico, and Fabio Murena. 2020. "The Effect on Air Quality of Lockdown Directives to Prevent the Spread of SARS-CoV-2 Pandemic in Campania Region—Italy: Indications for a Sustainable Development." *Sustainability* 12 (14). doi: 10.3390/su12145558.

Trusz, A., H. Ghazal, and K. Piekarska. 2020. "Seasonal variability of chemical composition and mutagenic effect of organic PM2.5 pollutants collected in the urban area of Wroclaw (Poland)." *Sci Total Environ* 733:138911. doi: 10.1016/j.scitotenv.2020.138911.

UNECE, United Nations Economic Commission for Europe. 2022. The 1998 Aarhus Protocol on Persistent Organic Pollutants (POPs), as amended on 18 December 2009.

United Nations General Assembly, Human Rights Council. 2019. Issue of human rights obligations relating to the enjoyment of a safe, clean, healthy and sustainable environmentl.

US EPA. 1998. Locating and estimating air emissions from sources of polycyclic organic matter. Washington, DC: US EPA.

Usenko, S, K. J. Hageman, D. W. Schmedding, G. Wilson, and S. L. Simonich. 2006. "Trace Analysis of Semivolatile Organic Compounds in Large Volume Samples of Snow, Lake Water, and Groundwater." *Environ Sci Technol* 39 (16):6006-6015. doi: 10.1021/es0506511.

Vicente, A., A. Calvo, A. P. Fernandes, T. Nunes, C. Monteiro, C. Pio, and C. Alves. 2017. "Hydrocarbons in particulate samples from wildfire events in central Portugal in summer 2010." *J Environ Sci (China)* 53:122-131. doi: 10.1016/j.jes.2016.02.022.

Walsh, Christopher D., Jill Schrlau, and Staci M. Simonich. 2014. "Development and Use of a Method for the Determination of Polycyclic Aromatic Hydrocarbon and Organochlorine Pesticide Concentrations in Freshly Fallen Snow." *Polycyclic Aromatic Compounds* 35 (1):57-73. doi: 10.1080/10406638.2014.910239.

Wang, T., L. Wang, Q. Chen, N. Kalogerakis, R. Ji, and Y. Ma. 2020. "Interactions between microplastics and organic pollutants: Effects on toxicity, bioaccumulation, degradation, and transport." *Sci Total Environ* 748:142427. doi: 10.1016/j.scitotenv.2020.142427.

Wang, W., and J. Wang. 2018. "Comparative evaluation of sorption kinetics and isotherms of pyrene onto microplastics." *Chemosphere* 193:567-573. doi: 10.1016/j.chemosphere.2017.11.078.

Wania, Frank, J. T. Hoff, C. Q. Jia, and D. Mackay. 1998. "The effects of snow and ice on the environmental behaviour of hydrophobic organic chemicals." *Environ Pollut* 102 (1):25-41. doi: 10.1017/S0269-7491(98)00073-6.

WHO. 2013. Health effects of particulate matter - Policy implications for countries in eastern Europe, Caucasus and central Asia.

WHO. 2020. World Health Statistics 2020 - Monitoring health for the SDGs.

WHO. 2021. WHO global air quality guidlines. Particulate matter (PM2.5 and PM10), ozone, nitrogen dioxide, sulfur dioxide and carbon monoxide. Geneva.

WHO. 2022. "Sustainable Development Goals (SDGs)." World Health Organization, accessed 21.04.2022. https://www.who.int/sdg/en/.

Wright, S. L., J. Ulke, A. Font, K. L. A. Chan, and F. J. Kelly. 2020. "Atmospheric microplastic deposition in an urban environment and an evaluation of transport." *Environ Int* 136:105411. doi: 10.1016/j.envint.2019.105411.

Xie, Z., Z. Wang, O. Magand, A. Thollot, R. Ebinghaus, W. Mi, and A. Dommergue. 2020. "Occurrence of legacy and emerging organic contaminants in snow at Dome C in the Antarctic." *Sci Total Environ* 741:140200. doi: 10.1016/j.scitotenv.2020.140200.

Xie, Z., P. Zhang, Z. Wu, S. Zhang, L. Wei, L. Mi, A. Kuester, J. Gandrass, R. Ebinghaus, R. Yang, Z. Wang, and W. Mi. 2022. "Legacy and emerging organic contaminants in the polar regions." *Sci Total Environ* 835:155376. doi: 10.1016/j.scitotenv.2022.155376.

Yagishita, Mayuko, Shiho Kageyama, Shigeru Ohshima, Michi Matsumoto, Yasunobu Aoki, Sumio Goto, and Daisuke Nakajima. 2015. "Atmospheric concentration and carcinogenic risk of polycyclic aromatic hydrocarbons including benzo[c]fluorene, cyclopenta[c,d]pyrene, and benzo[j]fluoranthene in Japan." *Atmospheric Environment* 115:263-268. doi: 10.1016/j.atmosenv.2015.05.050.

Zhang, P., P. Huang, H. Sun, J. Ma, and B. Li. 2020. "The structure of agricultural microplastics (PT, PU and UF) and their sorption capacities for PAHs and PHE derivates under various salinity and oxidation treatments." *Environ Pollut* 257:113525. doi: 10.1016/j.envpol.2019.113525.

Zhang, Y., Z. Shen, J. Sun, L. Zhang, B. Zhang, H. Zou, T. Zhang, S. S. Hang Ho, X. Chang, H. Xu, T. Wang, and J. Cao. 2021. "Parent, alkylated, oxygenated and nitrated polycyclic aromatic hydrocarbons in PM2.5 emitted from residential biomass burning and coal combustion: A novel database of 14 heating scenarios." *Environ Pollut* 268 (Pt A):115881. doi: 10.1016/j.envpol.2020.115881.

Zioła, Natalia, and Krzysztof Słaby. 2020. "The Content of Selected Heavy Metals and Polycyclic Aromatic Hydrocarbons (PAHs) in PM10 in Urban-Industrial Area." *Sustainability* 12 (13). doi: 10.3390/su12135284.

Appendix A Abstracts of published works

A.1. First authored works

A.1.1. Kirchsteiger et al. (2020)

Combination of Different Approaches to Infer Local or Regional Contributions to $PM_{2.5}$ Burdens in Graz, Austria

Bernadette Kirchsteiger [1,*], Magdalena Kistler [1,†], Thomas Steinkogler [1], Christopher Herzig [1], Andreas Limbeck [1], Christian Schmidt [2], Harald Rieder [3] and Anne Kasper-Giebl [1]

[1] TU Wien, Institute of Chemical Technologies and Analytics, Getreidemarkt 9, A-1060 Vienna, Austria; eacmagda@gmail.com (M.K.); thomas.steinkogler@tuwien.ac.at (T.S.); christopher.herzig@tuwien.ac.at (C.H.); andreas.limbeck@tuwien.ac.at (A.L.); anneliese.kasper-giebl@tuwien.ac.at (A.K.-G.)

[2] Wegener Center for Climate and Global Change, University of Graz, Brandhofgasse 5, A-8010 Graz, Austria; christian.schmidt@uni-graz.at (C.S.)

[3] Institute of Meteorology and Climatology, University of Natural Resources and Life Sciences (BOKU), Gregor-Mendel-Strasse 33, A-1180 Vienna, Austria; harald.rieder@boku.ac.at (H.R.)

* Correspondence: bernadette.kirchsteiger@tuwien.ac.at (B.K.)

† Current affiliation: Office of the Federal Government of Lower Austria, Landhausplatz 1, A-3109 St. Pölten, Austria.

Abstract: In early 2017 high particulate matter (PM) levels were observed across mid-Europe, including Austria. Here we characterize PM pollution in the city of Graz during January to March 2017, a period with substantial exceedances (34 days) of the European Union (EU) PM_{10} short time limit value. This study evaluates whether the observed exceedances can be attributed to the accumulation of pollutants emitted by local sources or to a larger scale pollution episode including transport. The analyses are based on the ratios of PM_{10} concentrations determined at an urban and background site, and the analyses of chemical composition of $PM_{2.5}$ samples (i.e., water soluble ions, organic and elemental carbon, anhydro-sugars, humic-like substances, aluminum, and polycyclic aromatic hydrocarbons). Source apportionment was realized using a macro-tracer model. Overall, the combination of different approaches (PM_{10} ratios, chemical composition, and macro-tracer derived source apportionment) enabled a conclusive identification of time periods characterized by the accumulation of emissions from local sources or regional pollution episodes.

doi: 10.3390/app10124222

A.1.2. Kirchsteiger et al. (2021)

Real-life emissions from residential wood combustion in Austria: From TSP emissions to PAH emission profiles, diagnostic ratios and toxic risk assessment

Bernadette Kirchsteiger[1*], Florian Kubik[1], Rita Sturmlechner[2], Harald Stressler[2], Manuel Schwabl[2], Magdalena Kistler[1] and Anne Kasper-Giebl[1]

[1]TU Wien, Institute of Chemical Technologies and Analytics, Getreidemarkt 9, A-1060 Vienna, Austria

[2]BEST GmbH, Inffeldgasse 21b, A-8010 Graz, Austria

*corresponding author

Abstract: Residential wood combustion is, besides particulate emissions, also linked to emissions of organic compounds, comprising various toxic substances such as polycyclic aromatic hydrocarbons (PAHs). Although, literature data has shown that highest emissions occur during maloperations caused by the user itself, most studies focus on lab-testing not reflecting the situation in the field. This study evaluates the real-life situation in Austria, investigating emissions of total suspended particles (TSP) and particle-bound substances of four manually operated room heaters commonly installed in people's homes. Measurements were conducted within a field measurement campaign realized in the scope of the *Clean Air by biomass* project. To evaluate the impact of the users' habit two types of combustion experiments were performed, one representing the diversity of possible maloperations and one realized under optimized conditions following a strict optimization protocol. As special focus was laid on PAHs, sampling was realized using a dilution system adapted for the use in the field. Generally, optimization lead to a clear decrease of most compounds (i.e. TSP, OC, EC, PAH), however, emissions of the anhydrosugar levoglucosan were not affected at all. Total PAH emissions could be clearly reduced, moreover, optimization lead to a shift towards low molecular weight PAHs and thus, less toxic ones, clearly reflected by lower toxicity equivalents. Correlation analysis using the Spearman's rank method showed significantly high correlations among the individual PAH congeners, and rather low ones with other target substances.

doi: 10.1016/j.apr.2021.101127

A.1.3. Kirchsteiger and Materić et al. (2022)†

Fine micro- and nanoplastics particles ($PM_{2.5}$) in urban air and their relation to the organic pollutants and PAHs

†submitted to the Journal of Hazardous Material

Bernadette Kirchsteiger[1†], Dušan Materić[2†*], Felix Happenhofer[1], Rupert Holzinger[2], Anne Kasper-Giebl[1]

[1]Institute of Chemical Technologies and Analytics, TU Wien, Getreidemarkt 9, A-1060 Vienna, Austria

[2]Institute of Marine and Atmospheric Research Utrecht, Utrecht University, Princetonplein 5, 3584CC, Utrecht, the Netherlands

[†]Contributed equally

Abstract: Measurements of ultrafine microplastics and nanoplastics (UFMNP) on the single polymer level in ambient particulate matter ($PM_{2.5}$) were performed for an urban sampling site in Graz, Austria. During the sampling period of 02.01. – 31.03.2017 the average UFMNP concentration was 238 ng/m^3, reaching up to 557 ng/m^3. This accounts for an average contribution of 0.67% to $PM_{2.5}$ mass and 1.7% of organic matter. The individual polymer types were polyethylene terephthalate (PET), polypropylene (PP) and polyethylene (PE), which sum up the most demanded polymer types in Europe. PET was found to be the most prominent polymer in the urban samples contributing to 50% of the overall UFMNP mass, followed by PP (27%) and PE (23%). Still, relative contributions vary with time. PET was observed during the entire time period, while PP and PE are quite variable and obviously linked to the origin and fate of air masses. A possible carrier function of PP and PE for selected micropollutants can be deduced from the significant monotonic correlations between these polymers and selected polycyclic aromatic hydrocarbons, predominantly low molecular weight congeners.

A.1.4. Kirchsteiger et al. (2022)†

† A manuscript presenting results discussed in **Chapter 6** is in preparation

A.2. Co-authored works

A.2.1. Sturmlechner et al. (2019)

REAL LIFE EMISSION FACTOR ASSESSMENT FOR BIOMASS HEATING APPLIANCES AT A FIELD MEASUREMENT CAMPAIGN IN STYRIA, AUSTRIA

RITA STURMLECHNER*, CHRISTOPH SCHMIDL*, ELISA CARLON*, GABRIEL REICHERT*, HARALD STRESSLER*, FRANZISKA KLAUSER*, JOACHIM KELZ*, MANUEL SCHWABL*, BERNADETTE KIRCHSTEIGER†, ANNE KASPER-GIEBL†, ERNST HÖFTBERGER*, WALTER HASLINGER*

*BIOENERGY 2020+ GmbH, Fixed Bed Conversion Systems, Austria †Institute of Chemical Technologies and Analytics, Vienna University of Technology, Austria

Abstract: Biomass combustion is a major contributor to ambient air pollution. Thus, knowing the real life emissions of biomass heating systems is crucial. Within the project *Clean Air by biomass* a field measurement campaign was conducted. 15 biomass heating appliances were tested in households at the end user according to their usual operation. Emission factors for gaseous and particulate emissions as well as for the genotoxic and carcinogenic substance benzo(a)pyrene were evaluated and compared to current proposed European and Austrian emission factors used for emission inventories. Moreover, the shares of particles and benzo(a)pyrene in hot and cooled flue gas were determined. Results showed a high variability of emissions in the field. Highest values and ranges occurred for room heaters (TSP_{total}: 226 mg/MJ). Biomass boilers showed clearly lower emission factors (TSP_{total}: 184 mg/MJ) in the field than room heaters and also than the proposed European and Austrian emission factors, in many cases. Emission factors for tiled stoves showed a similar trend (TSP_{total}: 67 mg/MJ). The share of condensable particles in the flue gas was remarkable. Especially benzo(a)pyrene was found mostly in the condensable fraction of the particles.

A.2.2. Stähle et al. (2021)

Quantifying changes in ambient NO_x, O_3 and PM_{10} concentrations in Austria during the COVID-19 related lockdown in spring 2020

C. Staehle[1], M Mayer[1], B. Kirchsteiger[2], V. Klaus[1], J. Kult-Herdin[1], C. Schmidt[1], S. Schreier[1], J. Karlicky[1,3], H. Trimmel[1], A. Kasper-Giebl[2], B. Scherllin-Pirscher[4] and H. Rieder[1]

[1] Institute of Meteorology and Climatology, Department of Water, Atmosphere and Environment, University of Natural Resources and Life Sciences, Gregor-Mendel-Straße 33, 1180 Vienna, Austria

[2] Institute of Chemical Technologies and Analytics, Division Environmental and Process Analytics, Environmental Analytics, Vienna University of Technology, Vienna, Austria

[3] Department of Atmospheric Physics, Faculty of Mathematics and Physics, Charles University, Prague, Czech Republic

[4] Zentralanstalt für Meteorologie und Geodynamik (ZAMG), Vienna, Austria

Abstract: During spring 2020, unprecedented changes in local and regional emissions have occurred around the globe due to governmental restrictions associated with COVID-19. Many European countries including Austria issued partial curfews or stay-at-home order policies, which have impacted ambient air quality through reductions in non-essential transportation and energy consumption of industrial sites and work places. Here, we analyse the effect of these measures on ambient concentrations of nitrogen oxides (NO_x), ozone (O_3) and particulate matter (PM_{10}) during the first nationwide lockdown in Austria (16.03.2020 to 14.04.2020). To ensure a robust analysis, the Austrian domain is divided into four individual subsectors contingent on regional climate. For air quality analysis a novel method is applied for filtering days with comparable weather conditions during the 2020 lockdown and spring 2017 to 2019. In general, our analysis shows decreasing pollutant concentrations, although in magnitude dependent on pollutant and regional subdomain. Largest reductions are found for NOx, reaching up to -68% at traffic sites reflecting the substantial decrease in non-essential transport. Changes in the O_3 concentrations at background sites show a rather weak response to NO_x declines varying between roughly -18 to +8% for both the median and the upper tail of the distribution. Occasional site level increases in O_3 concentrations can be attributed to comparably weak titration during night-time. PM_{10} concentrations show the smallest response among air pollutants, attributable to manifold precursor sources not affected by the lockdown measures. However, our analysis indicates also a shift of PM_{10} distributions at traffic sites closer to distributions observed at background sites.

doi: 10.1007/s11869-022-01232-w

A.2.3. Kau et al. (2022)

Thermal-optical analysis of quartz fiber filters loaded with snow samples – determination of iron based on interferences caused by mineral dust

Daniela Kau[1], Marion Greilinger[2], Bernadette Kirchsteiger[1], Aron Göndör[1], Christopher Herzig[1], Andreas Limbeck[1], Elisabeth Eitenberger[1], and Anne Kasper-Giebl[1]

[1]Institute of Technologies and Analytics, TU Wien, Vienna, 1060, Austria
[2]Zentralanstalt für Meteorologie und Geodynamik (ZAMG), Vienna, 1190, Austria
[3]X-Ray Center, TU Wien, Vienna, 1060, Austria

Abstract. The determination of mineral dust and elemental carbon in snow samples is of great interest, as both compounds are known as light absorbing snow impurities. Different analytical methods have to be used to quantify both compounds. Still, the occurrence of mineral dust, which contains hematite, leads to a bias in the quantification of elemental carbon and organic carbon via thermal-optical analysis. Here we present an approach which utilizes this interference to determine the concentration of iron via thermal-optical analysis using a Lab OC/EC Aerosol Analyzer (Sunset Laboratory Inc.) and the EUSAAR2 protocol. Therefore, the temperature dependency of the transmittance signal determined during the calibration phase, i.e. when all carbonaceous compounds are already removed, is evaluated. Converting the transmittance signal into an attenuation, a linear relationship between this attenuation and the iron loading is obtained for loadings ranging from 10 to 100 µgFe cm^{-2}. Furthermore, the evaluation of the transmittance signal during the calibration phase allows to identify samples which need to be re-evaluated, as the analysis of elemental carbon and organic carbon is biased by constituents of mineral dust. The method, initially designed for snow samples, can also be used to evaluate particulate matter samples collected within ~~from~~ the same high alpine environment. When applying the method to a new set of samples it is crucial to check whether the composition of iron compounds and the sample matrix remain comparable. If other sources than MD determine the iron concentration in particulate matter, these samples cannot be evaluated with TOA. This is shown exemplarily with data of particulate matter samples collected in a railway tunnel.

doi:10.5194/amt-2022-145

Appendix B List of conference contributions

B.1. Oral presentations

B.1.1. JAF 2022

Polycyclic aromatic hydrocarbons and where to find them: highlights and obstacles of the development of analytical methods for PAH quantification in different environmentally important matrices

Bernadette Kirchsteiger*[a], Hanne Ø. Notø[b], Dušan Materić[b], Sebastian Wöhrer[a], Karoline Rieger[a], Rupert Holzinger[b] and Anne Kasper-Giebl[a]

* Corresponding author, email: bernadette.kirchsteiger@tuwien.ac.at

[a)]TU Wien, Institute of Chemical Technologies and Analytics, 1060 Wien, Austria

[b)]Utrecht University, Institute for Marine and Atmospheric Research, Faculty of Science, 2584 CC Utrecht, The Netherlands

B.1.2. CEBC 2020

Clean Air by biomass

Bernadette Kirchsteiger [a], Thomas Steinkogler [a], Magdalena Kistler [a] and Anne Kasper – Giebl [a]

[a)]TU Wien, Institute of Chemical Technologies and Analytics, 1060 Wien, Austria

B.1.3. ICCPA 2019

PAH emission patterns from different domestic firewood combustion devices

Bernadette Kirchsteiger [a], Magdalena Kistler [a], Thomas Steinkogler [a], Florian Kubik [a], Harald Stressler[b], Rita Sturmlechner [b], Joachim Kelz [b], and Anne Kasper- Giebl [a]

[a)]TU Wien, Institute of Chemical Technologies and Analytics, Getreidemarkt 9; A-1060 Vienna, Austria

telephone: +43 1 58801 15174, email: bernadette.kirchsteiger@tuwien.ac.at

[b)]BIOENERGY 2020+ GmbH, Inffeldgasse 21b, A-8010 Graz, Austria

B.2. Poster presentations

B.2.1. Österreichische Chemietage 2022

Trace analysis of polycyclic aromatic hydrocarbons in surface snow samples

Bernadette Kirchsteiger[a], Sebastian Wöhrer[a], Gurpreet Gill[a], and Anne Kasper-Giebl[a]

[a]TU Wien, Institute of Chemical Technologies and Analytics, Getreidemarkt 9; A-1060 Vienna, Austria

B.2.2. EAC 2020

Approaches to characterize an elevated PM episode in Graz, Austria

Bernadette Kirchsteiger [1], Magdalena Kistler [1], Thomas Steinkogler [1], Christian Schmidt[2], Harald Rieder [3],and Anne Kasper- Giebl [1]

[1]TU Wien, Institute of Chemical Technologies and Analytics, Getreidemarkt 9; A-1060 Vienna, Austria

[2] University of Graz, Wegener Center for Climate and Global Change, Brandhofgasse 5; A-8010 Graz, Austria

[3] University of Natural Resources and Life Sciences (BOKU), Institute of Meteorology and Climatology, Gregor-Mendel-Strasse 33; A-1180 Vienna, Austria

B.2.3. VSS 2019

Semi-volatile organic trace quantification of emission samples with PTR-ToF-MS

Bernadette Kirchsteiger [a], Florian Kubik [a], Franziska Klauser [b], Harald Stressler [b], Rita Sturmlechner [b], Manuel Schwabl [b], and Anne Kasper- Giebl [a]

[a])E164- Institute of Chemical Technologies and Analytics, TU Wien

[b])BEST GmbH, Innfeldgasse 21b, A-8010 Graz, Austria

B.2.4. ICCPA 2019

Analysis of highly loaded emission samples using a thermal-optical method – advantages of a manual evaluation method

Bernadette Kirchsteiger [a], Magdalena Kistler [a], Franziska Klauser [b], Harald Stressler [b], Rita Sturmlechner [b] and Anne Kasper- Giebl [a]

[a])TU Wien, Institute of Chemical Technologies and Analytics, Getreidemarkt 9, A-1060 Vienna, Austria telephone: +43 1 58801 15174, email: bernadette.kirchsteiger@tuwien.ac.at

[b])BIOENERGY 2020+ GmbH, Inffeldgasse 21b, A-8010 Graz, Austria

Appendix C Co-supervised Thesis

C.1. Diploma thesis

C.1.1. Analyse von PAKs in Aerosolproben mittels GC-MS – Methodenvalidierung und Anwendung

Carried out by: Felix Happenhofer

Planed submission: November 2022

C.1.2. Characterization of the oxidative potential of nanoparticles with acellular assays

Carried out and submitted by: Thomas Rosa-Steinkogler

Submission date: April 2022

C.2. Bachelor thesis

C.2.1. Analyse von PAKs in Schneeproben – Optimierung der Probenvorbereitung

Carried out by: Gurpreet Kaur

Planned submission: November 2022

C.2.2. Trace analysis of PAHs and 1,3,5 – TPB in snow samples with GC-MS/MS

Carried out and submitted by: Sebastian Wöhrer

Submission date: March 2022

C.2.3. Determination of the oxidative potential of aerosol samples using the DTT-assay

Carried out and submitted by: Viktoria Untersulzner

Submission date: August 2020

C.2.4. PAHs in particulate matter – BaP to nitro-PAHs

Carried out and submitted by: Karoline Rieger

Submission date: October 2019

C.2.5. Analytical determination of PAHs in emission samples

Carried out and submitted by: Florian Kubik

Submission date: June 2019